IFM-GEOMAR
Leibniz-Institut für Meereswissenschaften
an der Universität Kiel

FS Sonne
Fahrtbericht / Cruise Report SO 176&179
MERAMEX I & II

Merapi Amphibious Experiment

Cilacap-Hongkong & Jakarta-Cilacap
18.05.-01.06.04 & 16.09.-07.10.04

Edited by
Heidrun Kopp & Ernst R. Flueh

Berichte aus dem Leibniz-Institut
für Meereswissenschaften an der
Christian-Albrechts-Universität zu Kiel

Nr. 1, Oktober 2004

ISSN Nr.:1614-6298

IFM-GEOMAR
Leibniz-Institut für Meereswissenschaften
an der Universität Kiel

Das Leibniz-Institut für Meereswissenschaften ist ein Institut der Wissenschaftsgemeinschaft Gottfried Wilhelm Leibniz (WGL)

The Leibniz-Institute of Marine Sciences is a member of the Leibniz Association (Wissenschaftsgemeinschaft Gottfried Wilhelm Leibniz).

Herausgeber / Editor:
Heidrun Kopp & Ernst R. Flueh

IFM-GEOMAR Report
ISSN Nr: 1614-6298

Leibniz-Institut für Meereswissenschaften / Leibniz-Institute of Marine Sciences
IFM-GEOMAR
Dienstgebäude Westufer / West Shore Building
Düsternbrooker Weg 20
D-24105 Kiel
Germany

Leibniz-Institut für Meereswissenschaften / Leibniz-Institute of Marine Sciences
IFM-GEOMAR
Dienstgebäude Ostufer / East Shore Building
Wischhofstr. 1-3
D-24148 Kiel
Germany

Tel.: ++49 431 600-0
Fax: ++49 431 600-2805
www.ifm-geomar.de

TABLE OF CONTENTS

1.1 Summary

RV SONNE cruises SO176&179 set out to collect geophysical data on the Java margin and incoming oceanic plate to better understand processes of fundamental importance related to the mechanics and the development during plate convergence. Within the scope of the BMBF/DFG special initiative GEOTECHNOLOGIEN-Continental Margins, the joint interdisciplinary SUNDAARC project was started in 2004. Within SUNDAARC, the subproject MERAMEX focusses on the well known seismic gap around 110° E in the Java subduction zone, and the Merapi volcanoe by means of geophysical studies.
During the first cruise, SO176, in May 2004, 14 Ocean Bottom Seismic Stations (OBS) were deployed to monitor the natural seismic activity, augmenting a 120 element land array. These stations were deployed from RV SONNE between 18 and 20 May 2004.
During the second cruise, SO179 from 17.09. to 06.10. altogether four seismic profiles were shot. Two were especially designed for the seismological networks (on- and offshore), while the other two were dip lines extending from the incoming oceanic plate close to the coastline to investigate the crustal structure of the Java margin. Altogether 75 OBH/S were deployed and airgun shots were fired along around 1000 profile kilometers. Gravity and bathymetry were recorded throughout the cruise, and magnetic data were collected along seismic profiles and transit lines with a total of approx. 3000 km. The data collected are generally of good quality and will allow to reach the goals envisioned.

1.2 Zusammenfassung

Die FS SONNE Fahrten SO176&179 hatten zum Ziel geophysikalische Daten vor Java am Kontinentalrand und der angrenzenden ozeanischen Platte zu gewinnen. Damit sollen Beiträge zum besseren Verständnis zu wichtigen Fragen bezüglich der Mechanik und der Entwicklung des Kontinentalrandes bei der Plattenkonvergenz geleistet werden. Im Rahmen des BMBF/DFG Sonderprogramms Geotechnologien – Kontinenträander wurde das interdisziplinäre Verbundvorhaben SUNDAARC in 2004 begonnen. Innerhalb der SUNDAARC Initiative konzentriert sich das Teilprojekt MERAMEX mit geophysikalischen Verfahren auf die bekannte seismische Lücke bei 110° Ost in der Java Subduktionszone und den Merapi Vulkan.
Während der ersten Fahrt, SO176, im Mai 2004 wurden insgesamt vierzehn Ozeanbodenseismometer abgesetzt, um die natürliche Seismizität aufzuzeichnen; diese Stationen ergänzten ein 120 Stationen umfassendes Netz an Land. Diese Stationen wurden zwischen dem 18. und 20. Mai 2004 von der SONNE abgesetzt.
Während der zweiten Fahrt, SO179, vom 17.09. bis 06.10. wurden vier seismische Profile abgeschossen. Zwei dieser Profile waren speziell auf das amphibische seismologische Netz ausgerichtet, während die beiden übrigen dazu dienten, die Krustenstruktur des Kontinentalrandes und der ozeanischen Kruste zu erfassen. Insgesamt wurden 75 OBH/S Positionen besetzt, und die Airgunschüsse entlang von ca. 1000 km abgefahren. Gravimetrie und Bathymetrie wurden kontinuierlich aufgezeichnet, magnetische Daten dagegen nur auf den seismischen Profilen und auf längeren Transitstrecken, insgesamt ca. 3000 km. Die gewonnenen Daten sind generell von guter Qualität und werden es erlauben, die gesteckten Ziele zu erreichen.

2. Introduction

Subduction zones continue to be of major interest to the Earth Science Community. This is partly due to their enormous potential for natural hazards, particularly in the form of earthquakes, tsunamis and arc volcanism. Convergent margins also serve as one end-member in a global perspective of the Earth's internal dynamics, as oceanic crust is destroyed here, whereas subduction accretion and arc magmatism are the main global processes responsible for continental crust formation. The Sunda subduction zone along the southern projection of the Indonesian archipelago (Fig. 2.1) marks the collision zone between two major lithospheric plates: the Indo-Australian plate and Eurasia. With a total length of more than 5000 km, the margin curves along the islands of Sumatra and Java and represents a prime target for investigations of the variation of forearc structures related to changes in the tectonic setting and the nature of the incoming plate. It is suited particularly well for studying some of the key questions related to the mechanics and development during plate convergence because of the significant lateral changes along the arc which also imprint the architecture of the system.

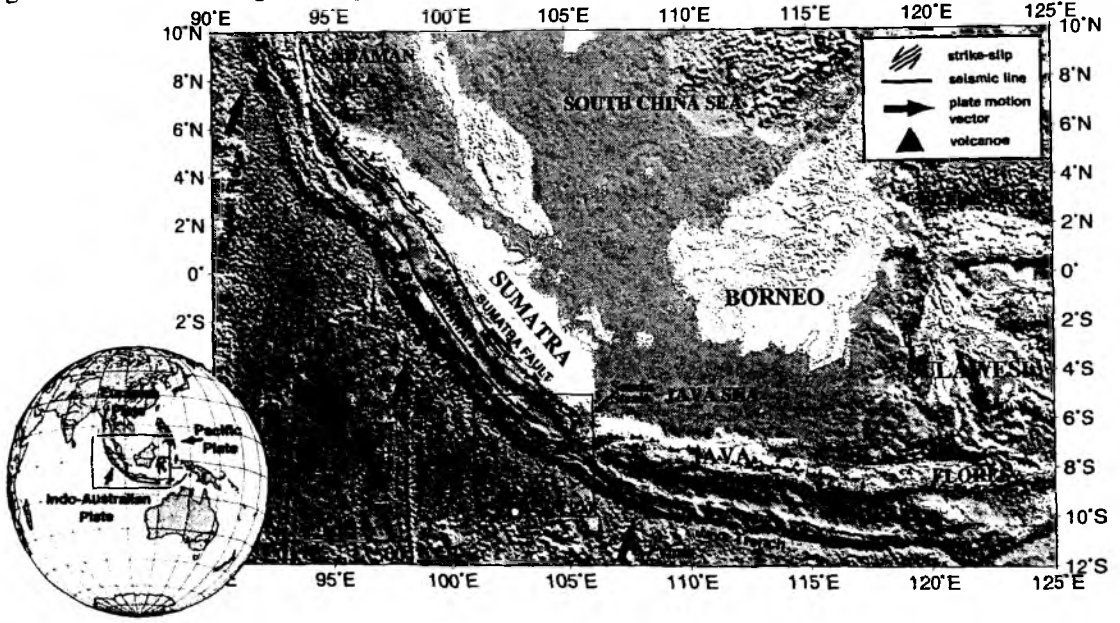

Figure 2.1: Bathymetric map of western Indonesia where the Indo-Australian plate is thrust underneath Eurasia along the Sumatra and Java trench system. The change in orientation of the Sunda margin causes an increase in subduction obliquity to the northwest. Subduction is frontal off Java and oblique off Sumatra where strain partitioning leads to the initiation of the Sumatra strike-slip fault and possibly the Mentawai transpressional fault. The study area is located at the juncture of these two subduction regimes as indicated by the box. Plate motion vectors are from the Australia-Eurasia rotation pole after DeMets (1990). Volcanic distribution is taken from the Smithonian Global Volcanism Program data set; bathymetric information is extracted from the Topex data set.

The Sunda plate boundary served as a basis for the development of the concepts of orogenesis and plate tectonics in the past century (Brouwer, 1925; Kuenen, 1935; Vening Meinesz, 1940; Van Bemmelen, 1949). The relation between the arc volcanism and the subduction zone processes in the forearc was recognized here. Studies of forearc tectonics focused on the western Sunda margin where its ‚classical' accretionary structural style advanced the models on sediment accretion and on the evolution of geological forearc structures (Karig et al., 1979, 1980; Beaudry and Moore, 1981, 1985; Curray, 1989; Huchon and Le Pichon, 1984; Samuel, 1994; Kopp and Kukowski, 2003). One of the key elements of this margin is the curvature of the trench, which results in an increasing subduction obliquity to the north. Initiation of strain

partitioning along the oblique segment is manifested in the Sumatra strike-slip fault, which partially compensates the component of arc-parallel motion (possibly in conjunction with the offshore Mentawai fault zone). The eastern portion of the margin, including the study area of the Meramex project off Java, is far less well investigated: Plate collision is orthogonal along the Java trench and sediment supply from the Ganges-Brahmaputra system is highly reduced along this sector, where an accretionary prism is not coherently developed.

2.1 Aims of the project and objectives of cruises SO176 and SO179

Within the scope of the BMBF/DFG special initiative GEOTECHNOLOGIEN-Continental Margins, the joint interdisciplinary project SUNDAARC was started in 2004 to investigate the high risk volcanism and its tectonic implications on the active Sunda subduction zone. Three volcanoes in the Indonesian region were chosen as targets (Krakatau, Merapi and Kelut). The project shall contribute to a better understanding of the potential for natural hazards of this subduction zone, which is neighboring the densely populated island of Java. Due to its enormous potential for natural hazards including earthquakes, volcanoes and tsunamis, the Sunda subduction zone holds a possible threat for the social and economic development of the region. With the increasing population density in the high risk area, a better assessment of the risk is a long-term aim of the SUNDAARC project, which shall lead to a useful early-warning system by which potential losses may be minimized.

In the course of the subproject MERAMEX (Merapi Amphibious Experiment), 120 mobile seismic land stations are deployed in a dense network around Merapi volcano and around central Java. One of the key elements within the study area is the so-called seismic ‚gap' around 110°E, where seismic activity is highly reduced while accumulations of earthquake hypocenters occur to the west and east of this 100 km wide corridor (Fig. 2.1.1). The study focusses on the relation of subduction zone processes and the arc volcanism as it is manifested in the active Merapi strato volcano. In addition to the seismicity and seismotectonics, the three-dimensional sub-bottom structure of the forearc and the activity pattern of Merapi represent the main interests of the project. It has generally been accepted that fluids released during subduction of the oceanic plate trigger partial melting in the mantle wedge. These melts are the source for the active volcanism along the arc. The knowledge of fluid pathways and the distribution of fluids and melts in the forearc is essential for the modeling of deformation processes and for a comprehensive understanding of the relation between subduction and volcanic activity. To study these relationships, 14 ocean bottom instruments are deployed during cruise SO176 offshore Java. These instruments will register the local seismicity for a period of 120 days. The registration of the seismic wave field will yield information on the seismic coupling zone and the crustal structure above the subduction earthquakes. Thus a structural image will be gained from local and teleseismic events (tomography/receiver functions). The location of the subduction earthquakes will provide information on their spatial and temporal distribution. Furthermore, dynamic information is gained from the spatial variations of the strain orientations from focal mechanisms and from the knowledge of strain reduction gained from amplitude spectra.

In addition to the passive seismic experiment, active refraction profiles shot in the offshore area during cruise SO179 are simultaneously registered onshore. These measurements will reveal the crustal structure of the forearc and underneath Merapi volcano down to the subducted slab. Seismic and tomographic investigations will map the geometry of the subduction system and the Benioff zone, including pathways of fluids and melts from their generation in the vicinity of the subducted plate to the upper crustal layers. The wide-angle seismic profiles are complemented by additional magnetic observations as well as swathmapping (conducted during SO176 and supplemented during SO179) to complete the

coverage of certain key areas and to provide a detailed base map for the geologic interpretation.

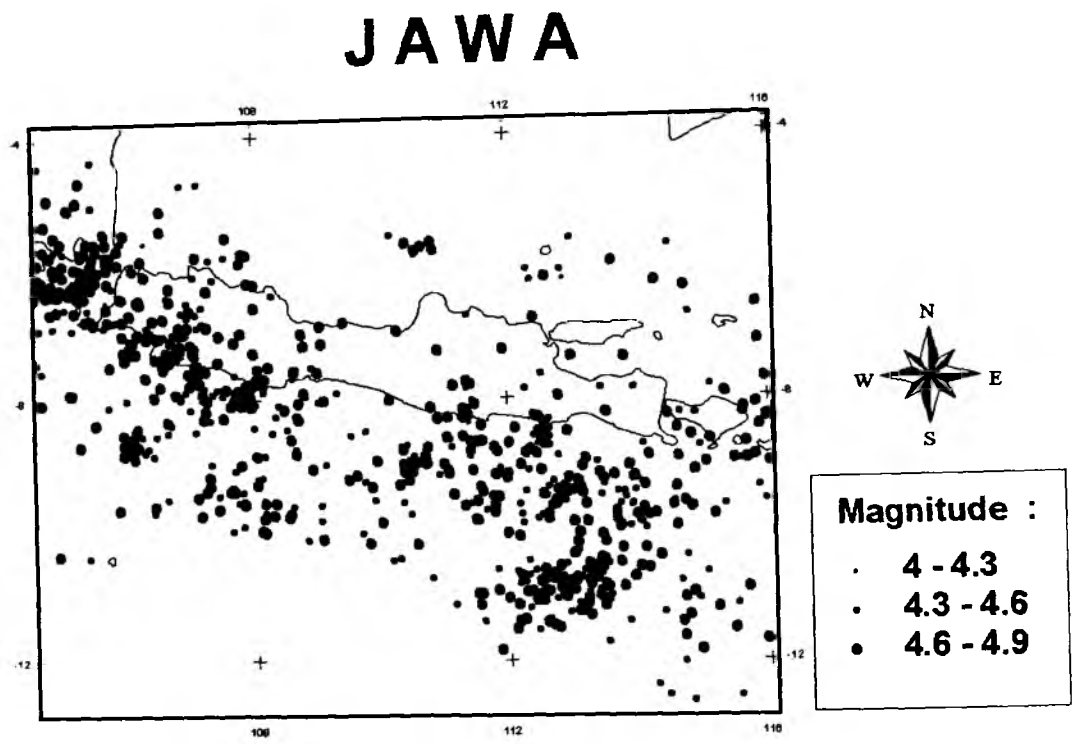

Figure 2.1.1: The seismicity distribution around Java island shows a prominent seismic gap around 110°E.

2.2 Regional background

2.2.1 Tectonic framework and evolution of the Sunda margin

The evolution of the large tectonic units of the Indian ocean is well confined by seafloor-spreading isochrons (Müller et al., 1997). Much of the Indonesian region is however characterized by the interaction of several smaller lithospheric plates, the movement of which within the complex is not well constrained. Several continental terranes were identified in SE Asia (Metcalfe, 1996), which are entirely allochthonous to central and northern Asia, although there is still some disagreement as to the number of terranes and their boundaries. Comparative studies of paleontology, paleomagnetism and stratigraphy suggest that the various pre-Cretaceous continental terranes were derived from Gondwanaland (Gasparon and Varne, 1995; Nishimura and Suparka, 1997). The evolution of Gondwanaland and Tethys during the Paleozoic and Mesozoic involved the rifting of continental slivers/fragments from northern Gondwanaland and their northwards drift and accretion, accompanied by the opening and destruction of the Tethys ocean system, to form proto-SE Asia (Fig. 2.2.1.1) (Metcalfe, 1996).

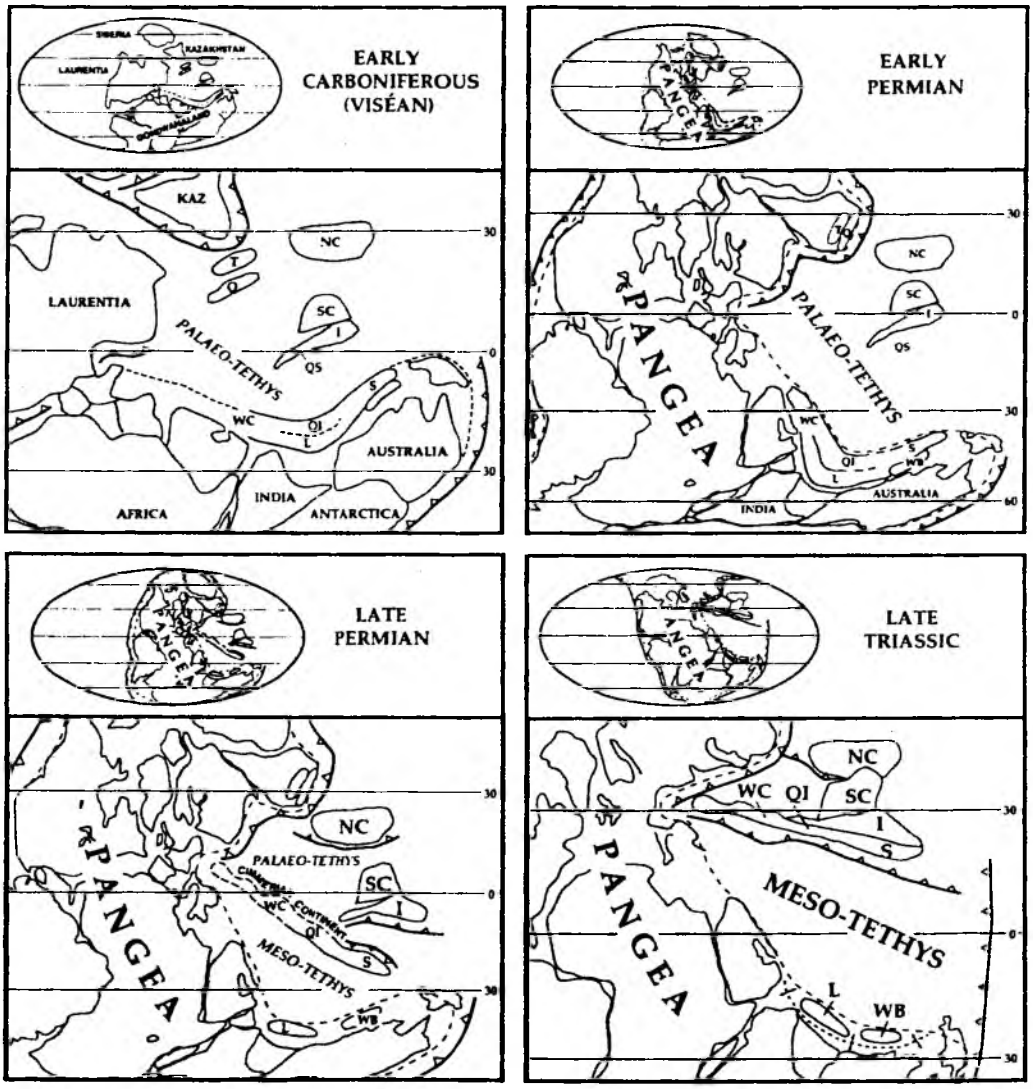

Figure 2.2.1.1: *Paleographic reconstructions of the Tethyan region for Early Carboniferous, Early Permian, Late Permian and Late Triassic showing the postulated positions of SE Asian terranes. Present day outlines are for reference only. NC: North China, SC: South China, T: Tarim, I: Indochina, Q: Qaidam, WC: Western Cimmerian Continent, Qi: Quiatang, L: Lhasa, S: Sibumasu, WB: West Burma (from Metcalfe, 1996).*

The continental terranes are bounded by sutures (representing former oceans), by narrow mobile belts or major fault zones (Fig. 2.2.1.2) (McCourt, 1996). The formation of present-day SE Asia involved the progressive suturing of terranes to each other during Late Paleozoic to Cenozoic times and their subsequent disruption, principally caused by the collision of India with Eurasia. The ages of sutures in SE Asia become younger to the south and south-east. It is generally agreed, as shown in Figure 2.2.1.2 after Metcalfe (1996), that South Tibet, Burma, western Thailand, Malaysia and Sumatra reveal strong geological correlations and formed a geological province, the Sibumasu terrane, which is bounded to the west by the Shan Boundary Fault and the Andaman Sea basin and to the south-west by the Woyla suture in Sumatra (Audley-Charles, 1988; Hutchinson, 1989; Metcalfe, 1996; McCourt, 1996). Its eastern boundary is formed by the Raub-Bentong suture in Peninsular Malaysia. The eastern boundary of Sibumasu in North Thailand and Burma is still not clear (Metcalfe, 1996). Paleomagnetic data along with Gondwanaland faunas (Cambrian to Lower Permian) with NW Australian affinities on Sibumasu strongly suggest a NW Australian origin for the Sibumasu

terrane (Metcalfe, 1996; Nishimura and Suparka, 1997). The predicted paleolatitude for Sibumasu, if placed adjacent to NW Australia, would be about 40°S in the Late Carboniferous.

A major rifting phase occurred on the northern margin of Gondwana in the Early Permian (Fig. 2.2.1.1), as is indicated by the occurrence of calc-alkaline volcanics and granitic plutons of Permo-Triassic age (248-218 Ma), (Nishimura and Suparka, 1997). Paleomagnetic data indicate that Sibumasu traveled rapidly from southern to northern paleolatitudes in Permian times (Metcalfe, 1996), followed by collision of the Sibumasu Block with East Malaya along the Raub-Bentong suture in the earliest Triassic (McCourt, 1996). Metcalfe (1996) suggested a collision time of Sibumasu with Indochina in the latest Permian or Triassic, but the exact suturing age is still controversial.

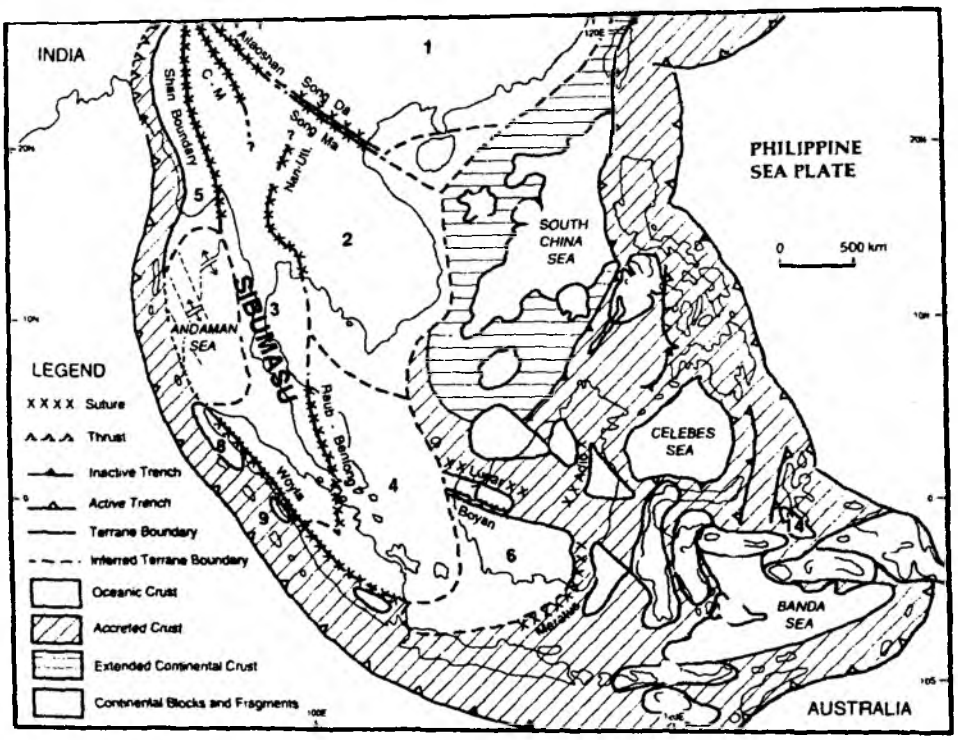

Figure 2.2.1.2: *Distribution of principal continental terranes and sutures in SE Asia: 1. South China; 2. Indochina; 3. Sibumasu, 4. East Malaya; 5. West Burma; 6. SW Borneo; 7. Semitau; 8. Sikuleh; 9. Natal (after Metcalfe, 1996).*

The Late Triassic to Late Jurassic saw renewed rifting on the north-east margin of Gondwanaland, leading to the destruction of the Meso-Tethys (Fig. 2.2.1.1). The Woyla terrane split from Gondwana in the Late Jurassic and by Late Cretaceous had accreted to proto-SE Asia. This terrane consisted of several small continental fragments, including the Sikuleh and Natal blocks, now located along the Woyla suture along the south-west margin of Sumatra, as shown in Figure 2.2.1.2, which comprises Cretaceous ophiolites and accretionary complex material (Metcalfe, 1996). Stratigraphic similarities with the Exmouth Plateau of the NW Australian shelf and paleomagnetic data from the Sikuleh block suggest paleolatitudes of 26°S for the Late Triassic and 10°S in the Late Mesozoic which is consistent with a NW Australian origin of these terranes (Metcalfe, 1996).

The time of initiation of northward subduction of the Izangi Plate, which underlay the Mesozoic Tethys Ocean along the proto-Sunda trench is still enigmatic, but magmatism and ophiolite emplacement date back to the Cretaceous (Widiyantoro and van der Hilst, 1996).

Cretaceous subduction complexes around margins of the Eurasian continent are identified in western and central Java and south-western Sulawesi (Nishimura and Suparka, 1997).

The location of these subduction complexes and paleomagnetic measurements indicate that the position of pre-Tertiary subduction was at the front of the Eurasian continent. A waning or cessation of subduction along the proto-Sunda Arc was proposed by Hamilton (1979) for the Late Cretaceous to Early Tertiary, based on the magmatic record. From middle Tertiary times on, subduction of the Indian sea plate occurred again along Sumatra and became connected to the Java Trench during the Late Miocene (10-8 Ma).

The present distribution and geometry of SE Asia is the result of the effects of the collision of India and Eurasia, i.e. indention, extrusion and strike-slip faulting. India collided with the Tethyan margin in Eocene time (Fig. 2.2.1.3), about 40 million years ago, and since then has continued to move northward at a velocity of about 5 cm/yr relative to Eurasia. The great Pakistan and Assam syntaxes at west and east corners of the Indian plate indicate northward motion of India relative to the Middle East to the west, and to South-East Asia to the east. About half the northward motion of India relative to north-west Eurasia is being accommodated by continental underthrusting of the Tibetan plateau and by compressive thickening of the entire continental crust (Hamilton, 1979). The other half is compensated primarily by the eastward motion of China, obliquely out of the way of the advancing southern continent, along a complex series of strike-slip faults and other structures. The resulting escape tectonics in southeastern Asia included clockwise rotation of tectonic units in Indochina and Indonesia, as implied by the plasticine indentation experiments of Tapponnier et al. (1982) presented in Figure 2.2.1.3a.

2.2.2 The northern and central Sunda margin: end member of accretive active margins

A wide variety of tectonic styles at subduction zones, including erosional and accretionary regimes, has been documented by seismic data. Most subduction zone histories are non-uniform and are characterized by alternate phases of subduction erosion and subduction accretion. In the past two decades numerous scientific projects investigating subduction zone margins revealed that long-term sediment accretion is exceptional among them. Only about 20% of the sectors of convergent margins thicken and advance seaward by the accumulation of ocean floor sediment and igneous masses, thus contributing to the formation of new continental crust (Scholl, 2002). The central Sunda margin south of the Indonesian archipelago off the islands of Sumatra and western Java is one of the few subduction zones worldwide where sediment accretion dominates over subduction erosion, despite the low trench input (Schlueter et al., 2002). Thus, in view of the large fraction of modern subduction zones that have been found to be erosive (von Huene and Scholl, 1991; Ranero and von Huene, 2000), Central Sunda represents one end-member of convergent margins.
This subduction system has been active since the middle Tertiary, as inferred from dating of the Sunda-system volcanism and evolved after the late Eocene collision of India with Eurasia (Hamilton, 1988). The present day kinematics of the Sunda margin (Fig. 2.1) are described to the first order by global plate motion solutions (NUVEL-1 and NUVEL-1A) (DeMets *et al.*, 1990; DeMets *et al.*, 1994). Additional GPS measurements determine the motion of Australia with respect to West Java in a direction N11°E, which is orthogonal to the trench (Tregoning *et al.*, 1994). At present, 96 Ma old oceanic crust is subducted at a rate of 6.7 cm/a along the central sector of the margin. The nature of the overriding plate changes from continental offshore Sumatra to oceanic offshore Java but this transition does not affect the evolution of the subduction complex. The extremely high ratio of accreted to subducted sediment along the

northern portion of the margin offshore Sumatra lead to the development of one of the world's largest accretionary wedges.

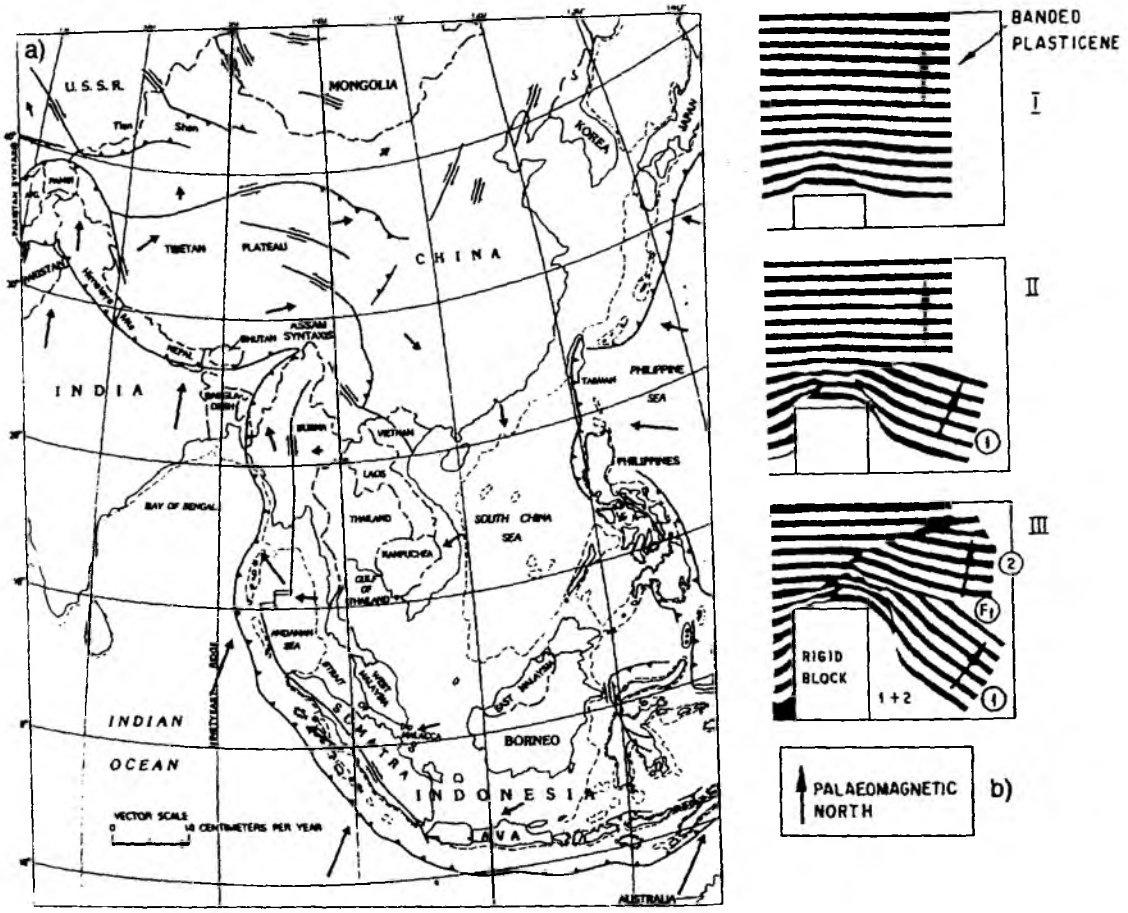

Figure 2.2.1.3: *a) Some active structures of the Chinese-Indonesian region. Perhaps half the northward motion of India relative to northwest Eurasia is being taken up by underthrusting of the Tibetan Plateau by India and by compressive thickening of the entire continental crust. The other half is compensated primarily by the eastward motion, relative to northwestern Eurasia, of China. Southeast Asia and western Indonesia are swinging clockwise, pivoted near the Assam syntaxis, over the Indian Ocean and the northern Bay of Bengal. Large arrows show direction and velocity of motion relative to northwestern Eurasia (from Hamilton, 1979).*
b) Three successive stages of an indentation experiment on plasticine (plan view). The free side is on the right. The rigid block is modeled as India. 1 is taken as the Indochina-Southeast Asian block, 2 as south China. 1 is the opening of the South China Sea and 1+2 as the Andaman Sea. F_1 is the Red River Fault (from Tapponnier, 1982).

The northern and central part of the margin, from northern Sumatra to western Java, has been the site of ongoing geophysical and geological research since the early 1970's, mainly attracted by the unique setting of an increasing subduction obliqueness to the north (Fitch, 1972; Hamilton, 1979; Huchon and Le Pichon, 1984; McCaffrey, 1992; Diament et al., 1992; Malod and Kemal, 1996; McCaffrey et al., 2000; Sieh and Natawidjaja, 2000), resulting from the convex curvature of the trench. Though the oblique collision results in the development of the lithospheric-scale Sumatra Fault (Sieh and Natawidjaja, 2000) and possibly the offshore Mentawai Fault zone (Diament et al., 1992), structural effects from the change in orientation

of the trench on the adjacent subduction complex are limited because the high degree of deformation partitioning strongly reduces the convergence obliquity for the accretionary complex of the detached forearc sliver. The central part of the Sunda margin marks the onset of oblique subduction south of the Sunda Strait (Malod et al., 1995) and was the site of the GINCO project (Flueh, 1999; Reichert, 1999), which yielded a profound data base including seismic reflection and wide-angle data, gravity data and high resolution bathymetry using RV SONNE as platform in 1998. This study is complemented by additional reflection seismic data from the RAMA cruise of RV Thomas Washington in 1980 off central western Java (Benaron, 1982; Kopp, 2002). The geophysical data sets acquired along the Central Sunda margin (Fig. 2.2.2.1) triggered a multi-scale kinematic investigation of the subduction processes (Malod and Kemal, 1996; Schlueter et al., 2002; Kopp and Kukowski, 2003) that determined the nature of the outer forearc high and the upper plate as well as the tectonic environment and the subduction geometry.

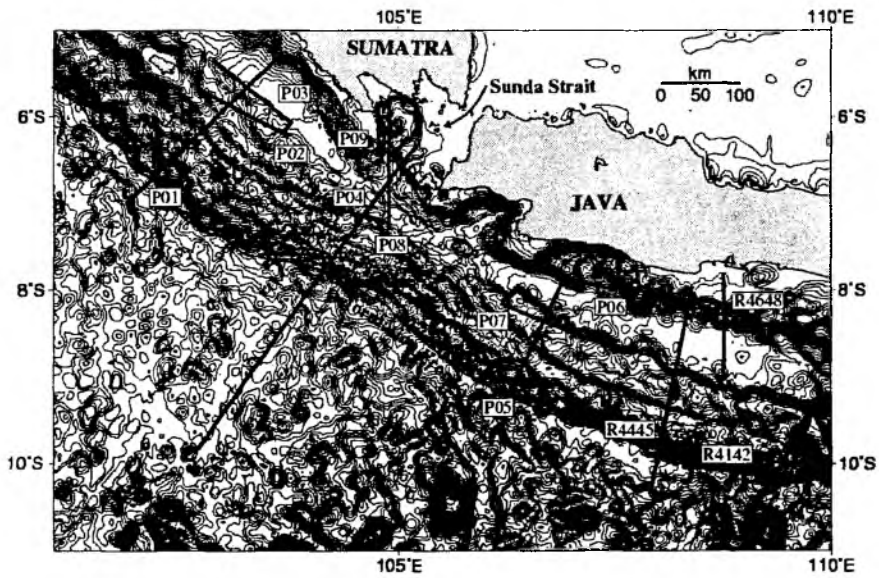

***Figure 2.2.2.1**: Refraction seismic profiles acquired during the GINCO project in 1998/1999 (P01-P07) and during the RAMA project in 1980 (R4445, R4142 & R4648).*

The integrative kinematic analysis of the various data sets focused on the identification of the different geologic-tectonic features associated with subduction accretion processes (Fig. 2.2.2.2). It allowed an exact mapping of the backstop system geometry and margin segmentation (active frontal accretionary prism, fossil accretionary prism or outer forearc high, forearc basin, subducting oceanic slab) (Fig. 2.2.2.2). One important aspect of this work is the observation that the structural elements observed along the margin are present in regimes of frontal convergence as well as in regimes of oblique convergence.

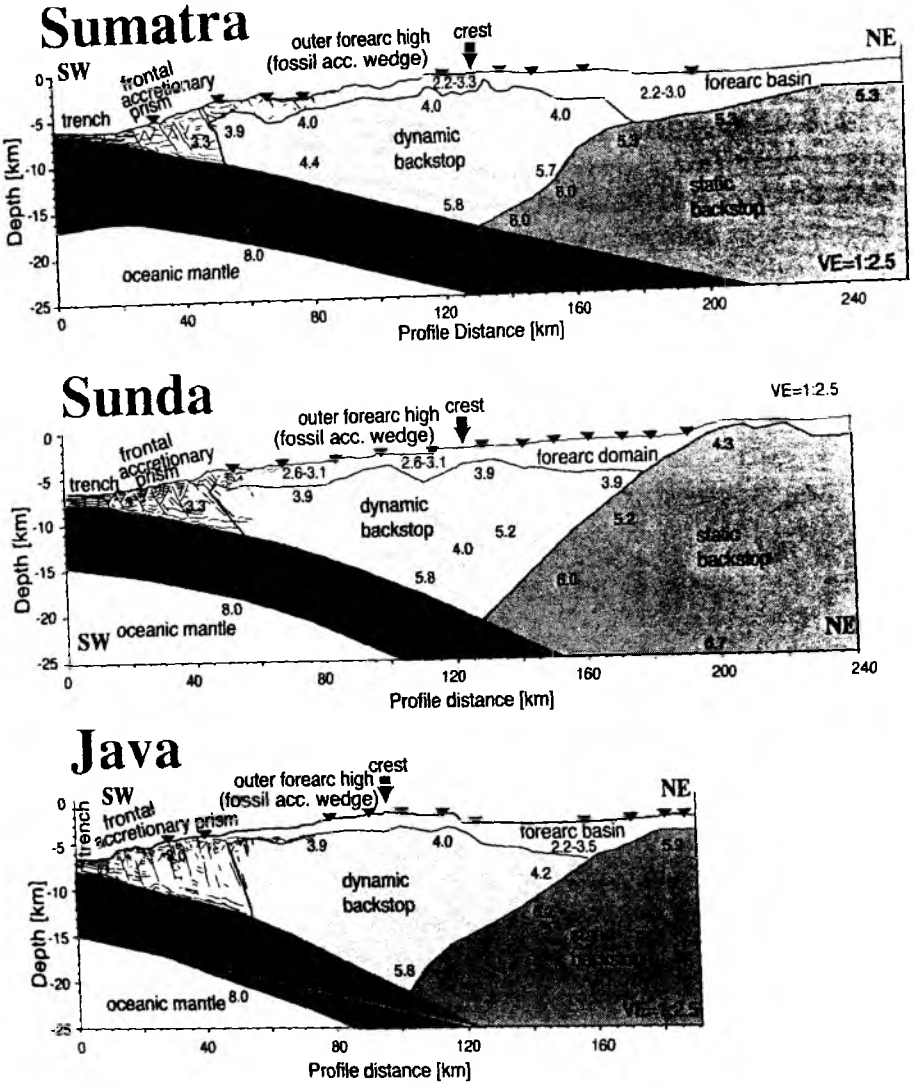

Fig. 2.2.2.2: Structural models along the central Sunda margin gained from wide-angle velocity modeling of the GINCO data. The line drawing in the accretionary prism represents main reflections of the corresponding MCS data (from Kopp and Kukowski, 2003).

Seismic refraction modeling shows that along the central portion of the Sunda margin, the subducting oceanic slab is underthrust at an angle of 5° off southern Sumatra, increasing to 7° off western Java (Kopp et al., 2002). Additional gravity modeling confirms a continental nature of the upper plate off Sumatra and an oceanic-type crust underneath the forearc basin off western Java (Fig. 2.2.2.3, bottom image). However, this variation in upper plate composition does not affect the structural evolution of the margin.

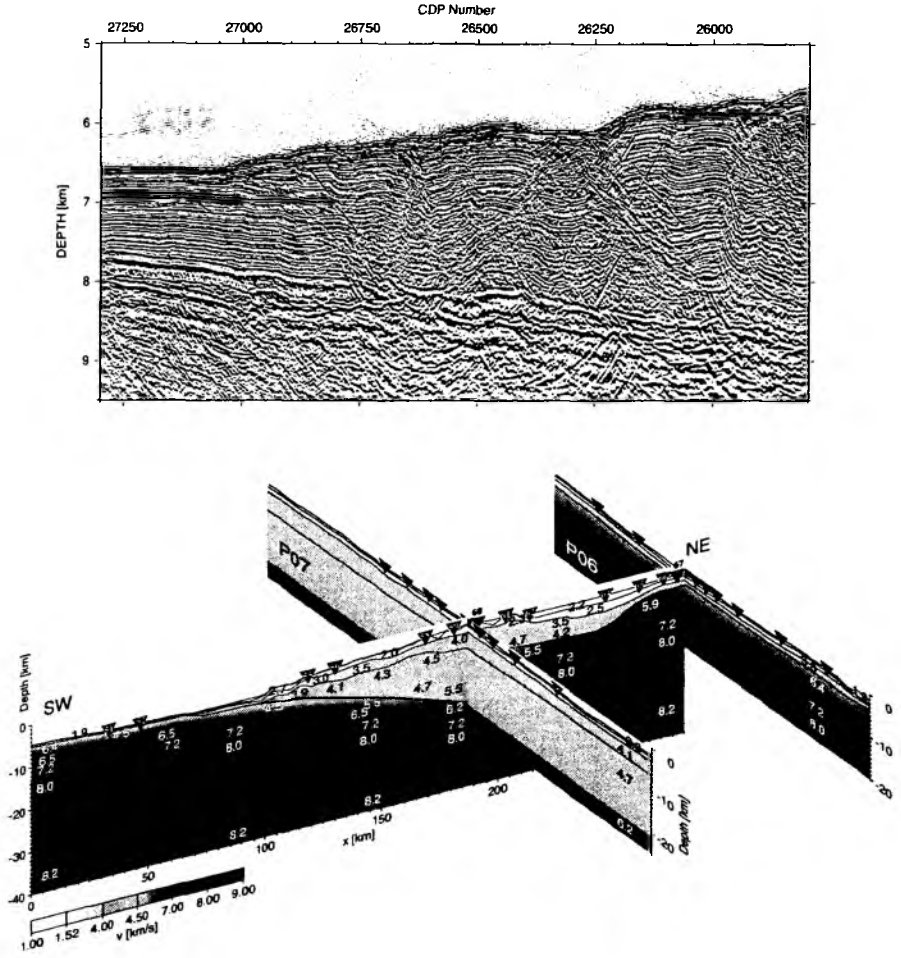

Fig. 2.2.2.3: Prestack depth migration and underlain velocity field of the deformation front and first accretionary ridges along line SO137-42 (upper image). Three-dimensional view of the velocity-depth distribution across the Sunda margin (lower image; after Kopp et al., 2002).

Underneath the frontal accretionary prism, the dip of the décollement remains constant at approximately 3°, as imaged in reflection seismic lines, whereas the surface slope of the frontal prism decreases from approximately 5.5° off Sumatra to 3° off Java (Kopp, 2001). This variation in the frontal taper is caused by minor changes in material and basal properties. At present, only about 11% to 14% of the input sediment sequence is underthrust in a subduction window (Fig. 2.2.2.3, upper image). An analysis of the structural relation of conjugate faults yielded a coefficient of internal friction of only 0.31 and showed that the accreted sedimentary sequences above the detachment are 2.3 times stronger than the décollement itself. Strain analysis studies based on the porosity-depth distribution of the frontal prism (Fig. 2.2.2.4) showed that the low basal friction does not result from fluid overpressuring, as has been found for a number of different convergent margins including Cascadia (Davis and Hyndman, 1989), but is rather due to the material properties of the sediments favoring accretive processes (Kopp and Kukowski, 2003).

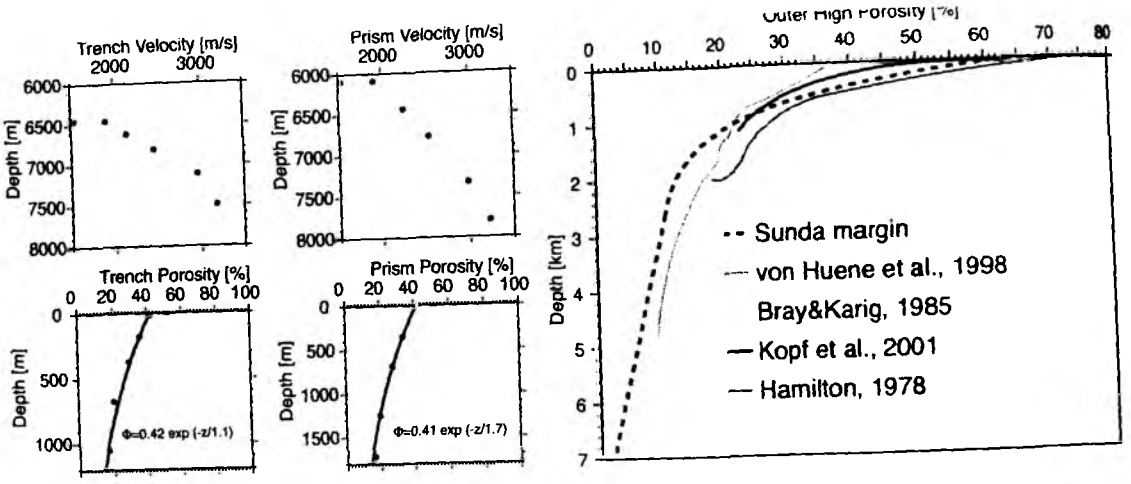

Fig. 2.2.2.4: Porosity-depth relations in the proto-thrust zone and frontal active accretionary prism.

2.2.3 Across-strike margin segmentation and dual backstop structure

The Central Sunda margin displays all characteristics of a 'classical' accretionary system and is characterized by an across-strike segmentation into distinct tectonic features (Fig. 2.2.2.2): adjacent to the deformation front a frontal prism has developed and is still active today. Accreted material, which has accumulated since the Eocene-Oligocene to a thickness of up to 20 km above the downthrusting plate, forms the outer forearc high or fossil accretionary wedge, across which pervasive tectonic deformation is evident (Schlueter et al., 2002). In contrast, the approximately 5 km of sediments trapped in the neighboring forearc basins lay mainly undeformed (Hamilton, 1979; Moore et al., 1980). The existence of the highly deformed outer forearc high (Fig. 2.2.3.1) and the seemingly paradoxical presence of undeformed sedimentary units in the adjacent forearc basin result from the influence of a static backstop or abutment which is formed by the arc framework of the upper plate's leading edge (Fig. 2.2.2.2). A dual backstop structure has for the first time been identified in nature along the Sunda margin (Kopp and Kukowski, 2003). A seaward-dipping backstop of arc material underlies the forearc basin. Its seaward tip could be resolved in the seismic data and lies underneath the crest of the outer forearc high near the downthrusting slab (Fig. 2.2.2.2). This configuration has been predicted for the Barbados accretionary wedge and by numerical modeling (Byrne et al., 1993), but has so far not been verified in nature due to a lack of data penetration. The evolution of morphological features, foremost of the outer forearc high and the forearc basin, is controlled by the backstop kinematics above the arc framework backstop. As accretionary processes dominated the margin evolution, the outer forearc high evolved as a consolidated and lithified dynamic backstop. The transition from the forearc high backstop, which is the fossil accretionary wedge, to the active accretionary prism, has been identified in the reflection data and bathymetry survey. Velocity-depth profiles gained from the wide-angle data show a clear lateral increase in seismic velocities from the unconsolidated material of the frontal prism to the more lithified outer forearc high (Fig. 2.2.2.3, bottom image). This transition corresponds to the location of an out-of-sequence thrust in the reflection data, whose surface trace could be mapped along the entire extent of the bathymetric survey (Figs. 2.2.3.1 and 2.2.3.2).

The definition as 'backstop' is independent of the composition of the upper plate (Davis, 1996), which along the Sunda margin changes from continental to oceanic (Hamilton, 1979). The material of the outer forearc high was initially pushed against this backstop during the

early stages of subduction, forming a morphological elevation. The forearc basins developed landward of the outer forearc high. It remains unclear if basin formation resulted solely from the evolution of the morphological elevated outer forearc high and simultaneous loading of the trapped sediment. Additional subcrustal basal erosion underneath the forearc basins may have enhanced subsidence. The underlying backstop casts a stress shadow over the forearc basin and prevents deformation of the sedimentary units (Byrne et al., 1993). Deformation of these units is only evident where backthrusting or strike-slip movements due to the obliqueness of convergence affect the basins (Diament et al., 1992). The forearc basins are disrupted off Sunda Strait (Malod et al., 1995), where strain partitioning due to the increasing obliquity to the north has lead to the evolution of the Sumatra strike slip fault, which accomodates the arc-parallel component of plate convergence.

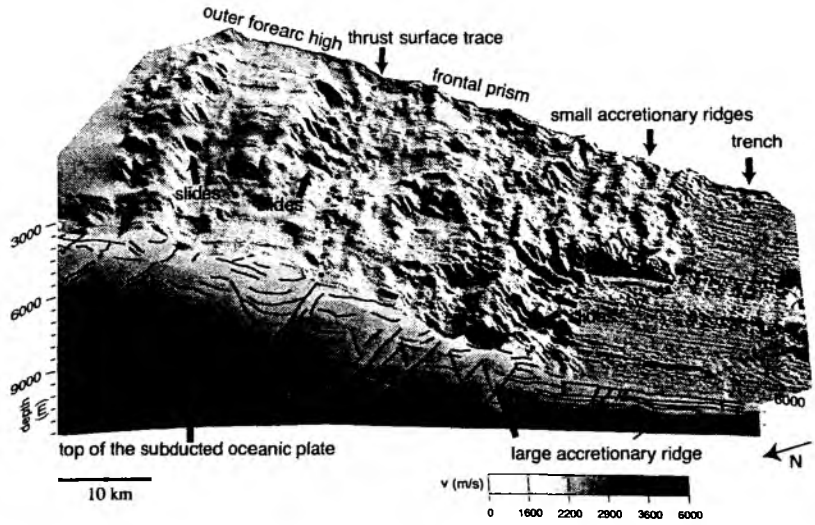

Fig. 2.2.3.1: *Three-dimensional bathymetric image of the deformation front and frontal accretionary prism off southern Sumatra with velocity-depth profile superimposed. Frontal accretion is the dominant mode of mass transfer along the northern and central Sunda margin (from Kopp and Kukowski, 2003).*

As sediment accretion progressed, the outer forearc high experienced tectonic deformation (Schlueter et al., 2002) leading to de-watering of the material and lithification. Tectonic activity decreased, while existing inherited structures are still reactivated to adjust the geometry of the forearc (Lohrmann et al., 2003). The Pliocene evolution of the active frontal accretionary prism is governed by this fossil part of the accretionary wedge, which today forms the outer forearc high. The outer forearc high may be defined as a second, seaward backstop (Fig. 2.2.2.2). As this backstop may still deform to adjust its taper, it may be regarded as transient and dynamic. Recent subduction processes at the front of the margin are controlled by this dynamic backstop. The geometry of the dual backstop structure appears to be crucial to the morphological evolution of the entire forearc.

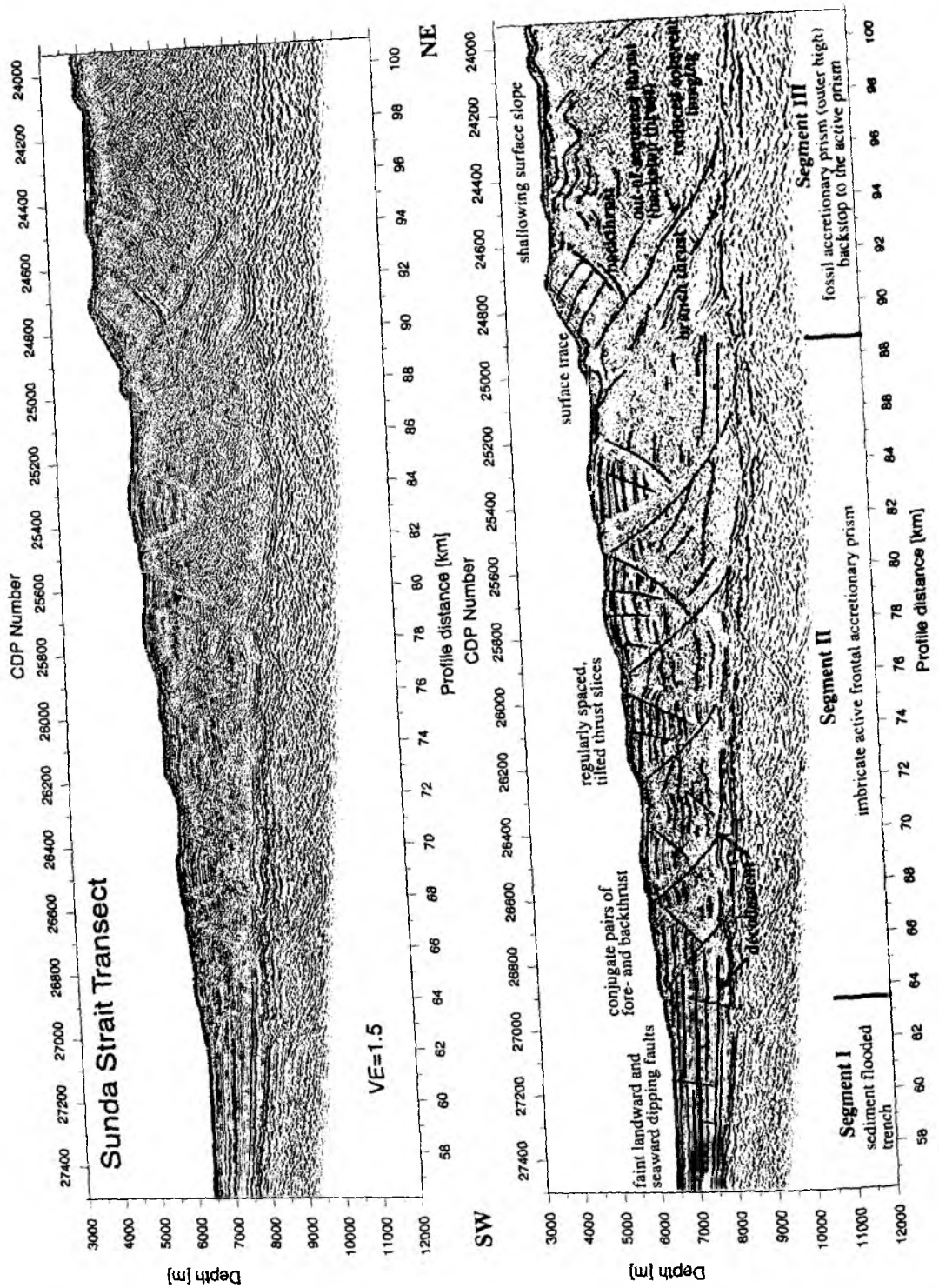

Fig. 2.2.3.2: Prestack depth migration and structural image of the front of the accretionary pr ism along line SO137-42 (from Kopp and Kukowski, 2003).

2.2.4 Accretionary mechanics

The geological framework of a subduction zone, namely the thickness and the properties of the incoming sediments, the oceanic plate roughness, and the convergence rate, control whether accretion or subduction erosion will dominate, since these features guide the amount of material necessary for accretion and subsequent growth of a wedge or prism. Factors favoring a high ratio of accreted to subducted material include a weak and deeply lying décollement in the trench sediment fill (Lallemand et al., 1994). A weak detachment may be a

consequence of either intrinsically weak material at the base showing a low coefficient of basal friction, or of a high degree of overpressuring at the base, or, as is most common, a combination of both. The stress reduction observed along the Sunda décollement most likely results from the intrinsically weak material along the base (Kopp and Kukowski, 2003). The formation of the décollement is fundamentally linked to the mechanical properties of the progressing frontal prism and is essential for the size of the subduction window. The evolution of an accretionary wedge (or, at a later subduction stage, outer forearc high) thus requires a high ratio of accreted to subducted sediment.

The growth of an accretionary wedge is described by the critical Coulomb wedge model (Davis et al., 1983; Dahlen, 1990) for ideal conditions. The critical Coulomb wedge model predicts that the material within the wedge will deform under horizontal compression until a critical taper is reached which is subsequently maintained. The wedge then grows self-similar, i.e. subsequent accretion leads to an increase in size but not to a change of shape. In nature, however, these ideal conditions, on which this model is based, are never exactly fulfilled. For example, at the Sunda margin, variations in mechanical properties enforce the segmentation of the margin across strike (Schlueter et al., 2002) and influence the progression of the décollement. The variations in internal as well as basal friction across the Sunda margin play a crucial role in the evolution of the structural characteristics associated with subduction and sediment accretion (Kopp and Kukowski, 2003). It has been shown in analogue experiments that they can be directly linked to the morphology of accretionary wedges (Lohrmann et al., 2003). An increase of the internal strength away from the deformation front can be induced by dewatering (von Huene and Klaeschen, 1999) or progressive lithification of the accreted material. Moreover, analogue experiments show that the piggy-back deformation of the existing faults, which are rotated into steeper positions and thus hardened, contribute to the increase in bulk strength of the forearc material (Lohrmann et al., 2003). The increase in internal strength from the frontal accretionary prism to the outer forearc high of the Sunda margin leads to a shallowing of the surface slope (Fig. 2.2.3.2), as the stronger material is able to support a narrower wedge while still undergoing stable sliding at its base. A shallowing of the surface slope is common in accretionary wedges, including the Nankai and Barbados accretionary wedges (Lohrmann et al., 2003, Bangs et al., 1990) and the Alaskan margin (Ryan and Scholl, 1989; Fruehn et al., 1999). Thus the evolution of the material properties that vary with the distance from the trench and the evolving strain memory of faults both control the mechanics of accretionary wedges and hence their morphology.

Furthermore, analogue experiments and natural examples show that the strength distribution is crucial not only to the overall shape of the wedge but also to the kinematic pattern of sediment accretion. The angles of friction and fluid pressure ratios of the material within the wedge, in the incipient deformation zone in front of the wedge toe and at the base of the wedge control the fault step-up angles (Davis and von Huene, 1987), the fault spacing, e.g. the slice length in the accreted sequence (Schott and Koyi, 2001), and the locus of accretion (Gutscher et al., 1996). Hence the systematic variation of these parameters in a study of accretionary wedges will yield the possible kinematic patterns of their formation.

2.2.5 Mass flux

The Sunda subduction zone is unique in that recent mass balance studies have shown that the age of the outer forearc high and the forearc basin sediments correlate with an accretive collision history, mainly governed by the evolution of the Himalayas, that must have remained fairly constant since Eocene times, even though a number of geologic and tectonic parameters show a high variability along strike of the margin, as discussed above. Frontal

accretion is the dominant mode of transfer along the Sunda margin (Moore et al., 1980), and only a low percentage of sediment is underplated or subducted, similar to the current situation along the Cascadia margin (Davis and Hyndman, 1989). At present, less than 15% of the trench material is subducted and passes the frontal accretionary prism in a subduction window (Kopp et al., 2002) (Figs. 2.2.2.3 upper image and 2.2.3.2). Distinct phases of the subduction history will have been characterized by varying sediment supply and convergence rates and by possible alternating phases of sediment accretion and sediment subduction/subduction erosion. The fossil accretionary prism or outer forearc high is of Eocene-Oligocene age (Pubellier et al., 1992; Samuel and Harbury, 1996) and most likely composed of accreted material, as suggested by refraction and gravity data (Kopp et al., 2001, 2002). To account for the Eocene age of the outer forearc high, volume balance calculations, which consider porosity changes and metamorphism, yield a fraction of less then 30% *average* of the trench fill subducted underneath the arc framework and thus 'removed' from the system (Kopp and Kukowski, 2003). Overall, accretion must have been the dominating process to explain the Eocene age of the outer forearc high which was emplaced before sedimentation filled the evolving forearc basin, where the oldest deposited strata are of Oligocene age (Beaudry and Moore, 1981; Beaudry and Moore, 1985; Izart et al., 1994; Schlueter et al., 2002).

2.2.6 The eastern Sunda margin off Java: transition to a non-accretive / erosive regime?

The character of the overriding plate changes dramatically along strike of the Sunda arc (Moore et al., 1980): oceanic lithosphere subducts off Sumatra and western Java with a steadily decreasing sedimentary cover as the distance from the Ganges-Brahmaputra-Systems increases. Only about 1.3 km of trench sediment fill is currently found off western Java. This decrease in sediment supply correlates to a decline in the size of the accretionary wedge or outer forearc high. This forearc high emerges subaerially offshore Sumatra, whereas it is found in a water depth of more than 2000 m off western Java. Along this section of the margin, a continuous and homogeneously developed outer forearc high has developed in conjunction with a well developed forearc basin. These unremitting forearc features are subject to an aprupt change in forearc structure around 110°E (Fig. 2.2.6.1), as documented by a landward displacement of the deep sea trench. An uninterrupted forearc basin has not developed here and the outer forearc high is characterized by isolated block structures. The displacement of the deformation front as well as the subducting morphological features on the oceanic plate, which are tremendously increasing the roughness of the oceanic crust, may be interpreted as indications for a non-accretive / erosive regime. This region is the site of the subduction of the Roo Rise between 110°E and 115°E (Masson et al., 1990). The Roo Rise is a little investigated oceanic plateau. Its subduction could possibly explain the uplift of the tectonic forearc structures here and may be linked to the seismic gap. This gap is the main seismological feature in the study area: out of many scattered localities of enhanced seismic activity and of relative seismic quiescence, around 110°E longitude, there is a remarkably silent zone, south off Java (Fig. 2.1.1). This seismically quiet zone of small (Mb>5.5) events is about 75-100 km in width and trends almost N-S from the trench to inland Java between 104.1°E and 116.4°E. There are few moderate to large earthquakes that are clearly associated with deformation in the forearc. Although minor seismic activity might be present here, absence of earthquakes with magnitude >5.5, even in the inner thrust zone is certainly noteworthy. Relevantly, a buoyant oceanic high--the Roo rise--is subducting just south of this locality.

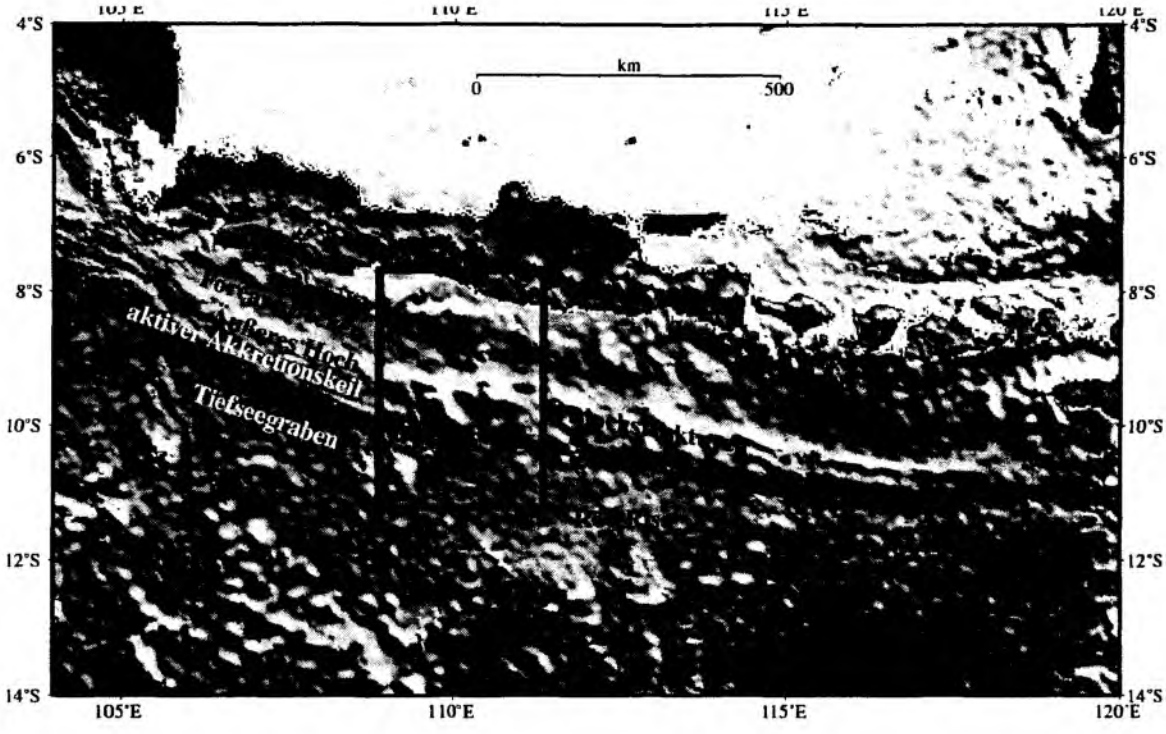

Fig. 2.2.6.1: Bathymetric map of the study area (indicated by the black box) offshore central Java. A change in tectonic style occurs around 110°E, where the outer forearc high is discontinuous and characterized by block structures and the roughness of the oceanic plate is increased by morphological features such as the Roo Rise.

The Roo Rise is a prominent bathymetric high, which appears to be interacting with the forearc. This feature was formed at a ridge crest and is more buoyant, and thus more difficult to subduct, than the surrounding seafloor. It is commonly more than 2.5 km higher than the surrounding seafloor, composed of anomalously thickened crust with an average thickness of about 11.5 km with a maximum of about 16.4 km (Ghose et al., 1990). The unusual thick layer has been interpreted as thrust faulting with a basal thrust plane possibly located at the base of the crust (Curray et al., 1977). However, thickening caused by compressional tectonism is unlikely, since the free-air gravity signature of this region shows no departure from the normal outer rise gravity high associated with bending of the lithosphere. The anomalously thick crust and the absence of a free-air expression of the relief of the Roo Rise suggest that this rise is a compensated feature supported by a low-density root, as features formed on ridge crests. Anomalously thick oceanic crust, formed after continents have rifted, is found on many of the world's passive margins (Newcomb et al., 1987).

The Roo Rise probably continues into the trench since the axis of the trench is deflected 50-60 km landward and the crust is very thick there. It also appears to be interacting with the forearc. In contrast to adjacent regions where forearc basins show undisturbed sedimentary fill, the forearc basins of Java indicate that there has been recent uplift of the trench slope break in an isolated region immediately landward of the Roo Rise. Four records by Newcomb et al., 1987, at approximately 109°E, 113°E, 114°E, and 115°E (Fig. 2.2.6.2) show this transition. The trench slope break at 109°E appears to have been more active in the past as indicated by the small compressional folds at depth in the basin strata; the shallowest strata of the basin are generally undisturbed and away from the trench slope break, deeper reflectors are only broadly warped. It is apparent in section 113°E that the seaward margin of the basin

accretion is the dominant mode of transfer along the Sunda margin (Moore et al., 1980), and only a low percentage of sediment is underplated or subducted, similar to the current situation along the Cascadia margin (Davis and Hyndman, 1989). At present, less than 15% of the trench material is subducted and passes the frontal accretionary prism in a subduction window (Kopp et al., 2002) (Figs. 2.2.2.3 upper image and 2.2.3.2). Distinct phases of the subduction history will have been characterized by varying sediment supply and convergence rates and by possible alternating phases of sediment accretion and sediment subduction/subduction erosion. The fossil accretionary prism or outer forearc high is of Eocene-Oligocene age (Pubellier et al., 1992; Samuel and Harbury, 1996) and most likely composed of accreted material, as suggested by refraction and gravity data (Kopp et al., 2001, 2002). To account for the Eocene age of the outer forearc high, volume balance calculations, which consider porosity changes and metamorphism, yield a fraction of less then 30% *average* of the trench fill subducted underneath the arc framework and thus 'removed' from the system (Kopp and Kukowski, 2003). Overall, accretion must have been the dominating process to explain the Eocene age of the outer forearc high which was emplaced before sedimentation filled the evolving forearc basin, where the oldest deposited strata are of Oligocene age (Beaudry and Moore, 1981; Beaudry and Moore, 1985; Izart et al., 1994; Schlueter et al., 2002).

2.2.6 The eastern Sunda margin off Java: transition to a non-accretive / erosive regime?

The character of the overriding plate changes dramatically along strike of the Sunda arc (Moore et al., 1980): oceanic lithosphere subducts off Sumatra and western Java with a steadily decreasing sedimentary cover as the distance from the Ganges-Brahmaputra-Systems increases. Only about 1.3 km of trench sediment fill is currently found off western Java. This decrease in sediment supply correlates to a decline in the size of the accretionary wedge or outer forearc high. This forearc high emerges subaerially offshore Sumatra, whereas it is found in a water depth of more than 2000 m off western Java. Along this section of the margin, a continuous and homogeneously developed outer forearc high has developed in conjunction with a well developed forearc basin. These unremitting forearc features are subject to an aprupt change in forearc structure around 110°E (Fig. 2.2.6.1), as documented by a landward displacement of the deep sea trench. An uninterrupted forearc basin has not developed here and the outer forearc high is characterized by isolated block structures. The displacement of the deformation front as well as the subducting morphological features on the oceanic plate, which are tremendously increasing the roughness of the oceanic crust, may be interpreted as indications for a non-accretive / erosive regime. This region is the site of the subduction of the Roo Rise between 110°E and 115°E (Masson et al., 1990). The Roo Rise is a little investigated oceanic plateau. Its subduction could possibly explain the uplift of the tectonic forearc structures here and may be linked to the seismic gap. This gap is the main seismological feature in the study area: out of many scattered localities of enhanced seismic activity and of relative seismic quiescence, around 110°E longitude, there is a remarkably silent zone, south off Java (Fig. 2.1.1). This seismically quiet zone of small (Mb>5.5) events is about 75-100 km in width and trends almost N-S from the trench to inland Java between 104.1°E and 116.4°E. There are few moderate to large earthquakes that are clearly associated with deformation in the forearc. Although minor seismic activity might be present here, absence of earthquakes with magnitude >5.5, even in the inner thrust zone is certainly noteworthy. Relevantly, a buoyant oceanic high--the Roo rise--is subducting just south of this locality.

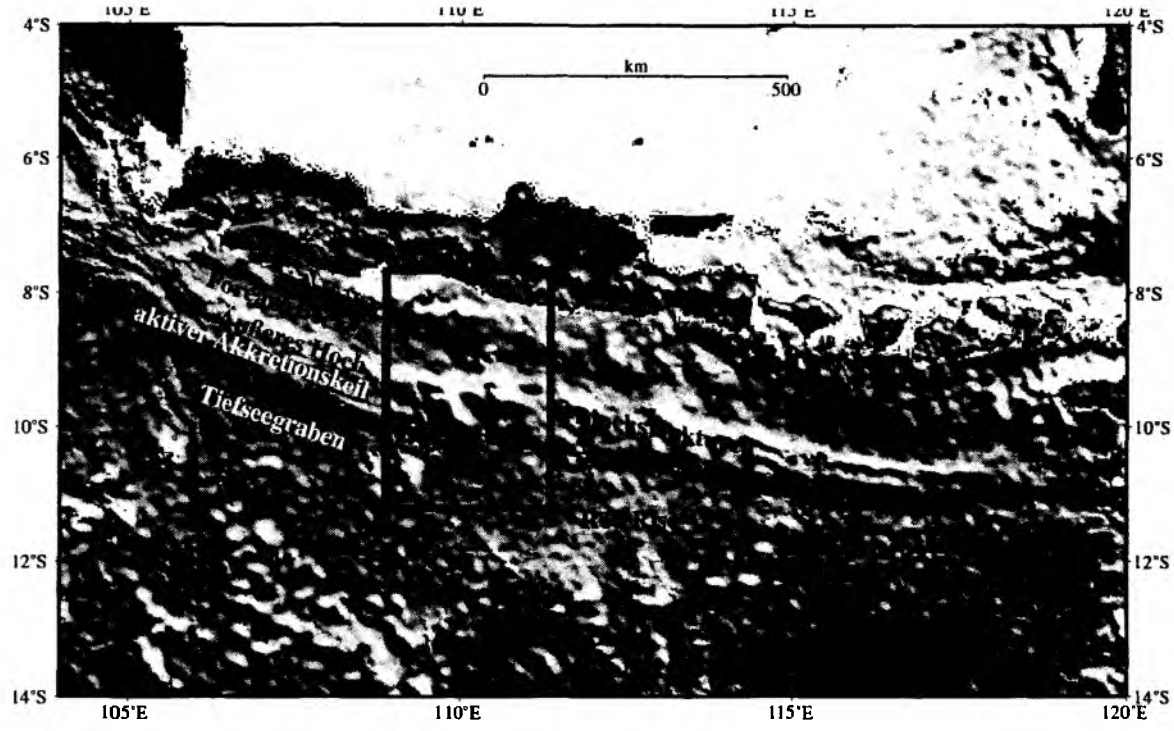

Fig. 2.2.6.1: Bathymetric map of the study area (indicated by the black box) offshore central Java. A change in tectonic style occurs around 110°E, where the outer forearc high is discontinuous and characterized by block structures and the roughness of the oceanic plate is increased by morphological features such as the Roo Rise.

The Roo Rise is a prominent bathymetric high, which appears to be interacting with the forearc. This feature was formed at a ridge crest and is more buoyant, and thus more difficult to subduct, than the surrounding seafloor. It is commonly more than 2.5 km higher than the surrounding seafloor, composed of anomalously thickened crust with an average thickness of about 11.5 km with a maximum of about 16.4 km (Ghose et al., 1990). The unusual thick layer has been interpreted as thrust faulting with a basal thrust plane possibly located at the base of the crust (Curray et al., 1977). However, thickening caused by compressional tectonism is unlikely, since the free-air gravity signature of this region shows no departure from the normal outer rise gravity high associated with bending of the lithosphere. The anomalously thick crust and the absence of a free-air expression of the relief of the Roo Rise suggest that this rise is a compensated feature supported by a low-density root, as features formed on ridge crests. Anomalously thick oceanic crust, formed after continents have rifted, is found on many of the world's passive margins (Newcomb et al., 1987).

The Roo Rise probably continues into the trench since the axis of the trench is deflected 50-60 km landward and the crust is very thick there. It also appears to be interacting with the forearc. In contrast to adjacent regions where forearc basins show undisturbed sedimentary fill, the forearc basins of Java indicate that there has been recent uplift of the trench slope break in an isolated region immediately landward of the Roo Rise. Four records by Newcomb et al., 1987, at approximately 109°E, 113°E, 114°E, and 115°E (Fig. 2.2.6.2) show this transition. The trench slope break at 109°E appears to have been more active in the past as indicated by the small compressional folds at depth in the basin strata; the shallowest strata of the basin are generally undisturbed and away from the trench slope break, deeper reflectors are only broadly warped. It is apparent in section 113°E that the seaward margin of the basin

is actively rising; basin strata that onlap the trench slope break are strongly tilted landward. The point of intersection of the along-strike extension of the Roo Rise with the fore arc is just reaching this longitude. At 114°E the forearc basin strata are discontinuous and have been severely disturbed. This section has been most recently affected. Section 115°E shows flat lying sediments in a relatively undisturbed forearc basin.

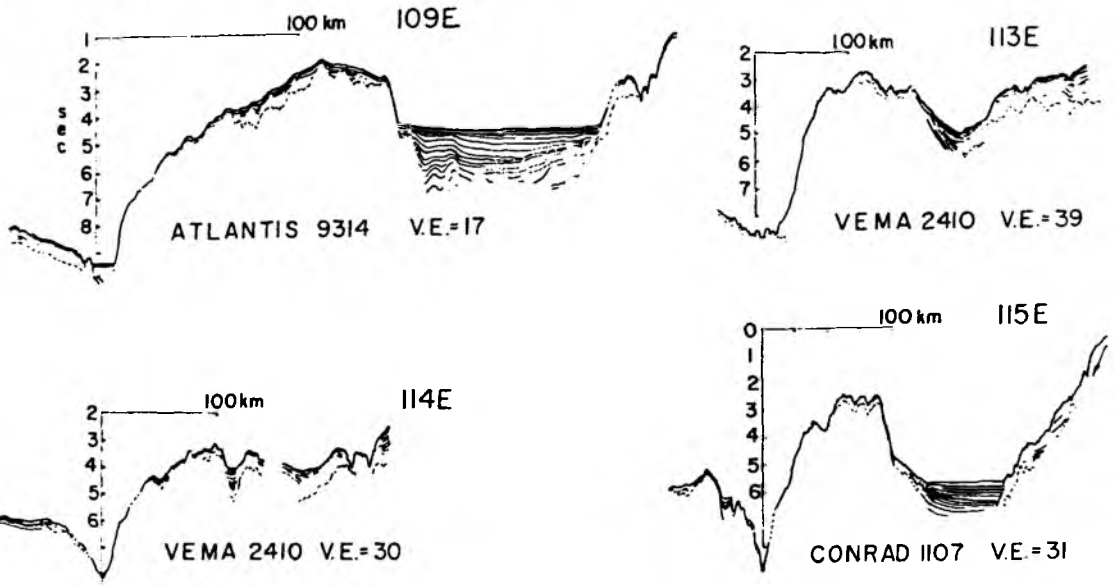

***Figure 2.2.6.2**: Line drawings from four successive seismic profiles crossing the forearc south of Java at longitudes 109°E, 113°E, 114°E and 115°E. Vertical scale is equivalent in all profiles; vertical exaggeration is indicated. Forearc basins at 109°E and 115°E are undisturbed. Profile at 113°E shows progressively onlapping horizons implying recent uplift of the trench slope break. At 114°E the forearc basin appears folded and faulted, indicating recent tectonism. Sites of disturbed forearc basins occur where the along-strike extension of the Roo Rise intersects the trench (from Newcomb et al., 1987).*

The low density root of the Roo Rise should cause this bathymetric feature to be more buoyant than the surrounding seafloor and therefore more difficult to subduct. The depth to which the Roo Rise penetrates into the thrust zone and the exact limits of the Roo Rise are still unclear. Subduction of lighter oceanic rise material has been correlated to a number of observed peculiarities in subduction zones, e.g. outer arc uplift, modification of slab dip, discontinuity in the volcanic line and lack of moderate to large earthquakes (Ghose et al., 1990, Newcomb et al., 1987). In the case of Roo Rise subduction any change in slab dip in the shallower region is not readily decipherable from the seismicity data alone. However, a clear gap in the line of active volcanoes around the north extension of the interacting Roo Rise is apparent, which coincides with the zone of scarce seismic activity around 110°E.

Ghose et al. (1990) modeled the subduction of a buoyant ridge to investigate the influence of Roo Rise on the regional stress level. Using a density contrast between the ridge and the slab of 0.42 g cm^{-3} (Ghose et al., 1990) they calculated the stress field in 75 km depth for a subducting low-density Roo Rise and found a clear rise in the stress level near the location of ridge subduction. This is quite expected since the low-density root of the Roo Rise ought to cause the rise to be more buoyant than the surrounding sea floor and therefore more difficult to subduct. When it interacts with the crystalline material of the overriding plate, the increased interplate coupling might be expected to cause enhanced seismic activity relative to adjacent areas subducting old abyssal plains. With the model parameters and the assigned material properties used by Ghose et al., (1990) it was thus not possible to justify the narrow

seismic quiescence at 110°E as to be due to the subduction of the Roo Rise. The seismic quiescence may imply that the Roo Rise is in only the initial stages of subduction.

Jurassic oceanic crust (135 Ma) is currently being subducted off eastern Java (Moore et al., 1980; Masson, 1991). The deep sea trench along the northern and central Sunda margin off Sumatra and western Java displays a flat morphology, whereas off eastern Java a V-shaped structure is found (Ganie et al., 1987), implying a reduced sediment supply into the trench (Van Weering, 1989). Side-scan sonar data acquired during the 1980's show only isolated small sediment ponds in a generally non-sedimented trench. These local sediment accumulations result from erosive processes related to the collision of seamounts with the deformation front and do not have their origin on the oceanic plate (Masson et al., 1990). Along this segment of the margin, the trench and deformation front show an irregular shape, obviously related to the subduction of the Roo Rise (Fig. 2.2.6.1). The trench is less deep here (5600-6000 m; to the east and west of the subduction site of the Roo Rise the trench reaches depths of more than 7000 m) (Masson et al., 1990). Numerous trench-parallel faults are found on the oceanic plate and result from plate-bending induced tectonic stress. This is also reflected in the local seismicity: The outer rise is characterized by normal faulting earthquake activity (Abercrombie et al., 2001). The distance between the fault zones is less only about 2-10 km; the faults have a length of 5-20 km; however, fault lengths of up to 60 km are also commonly recognized (Masson et al., 1990, 1991). The vertical throw along these faults is in the range of 100 m to 500 m in the vicinity of the trench (Beck und Lehner, 1974; Hamilton, 1979; Moore et al., 1980; Ganie et al., 1987). The faults show a trend of 30° to the magnetic anomalies and are thus not related to reactivated spreading center fabric, but originate in the near-trench setting (Masson et al., 1990). It remains unclear if and to what extent this fault pattern may contribute to a possible hydration of the oceanic lithosphere. Plate-bending induced trench-parallel faulting has been mapped along a variety of subduction zones (Masson, 1991; Kobayashi et al., 1998; Ranero et al., 2003) and a causative relationship to hydration processes in the outer rise region has been proposed (Peacock, 1990; Seno und Yamanaka, 1996; Kirby et al., 1996; Jiao et al., 2000; Peacock et al., 2001). Recent studies imply that crustal and upper mantle hydration of the oceanic lithosphere occurs in the near-trench setting of the outer rise (Ranero et al., 2003; Kopp et al., 2004), however, the required tectonic-geologic conditions (e. g. intensity of the fault pattern and depth-penetration of the faults) as well as the extent (lateral and in depth) of a possible serpentinisation of the upper lithosphere are still debated. Carlson and Miller (2003) predict 15% serpentinization for most subduction zones for which hydration processes have been postulated (Graeber and Asch, 1999; Kamiya and Kobayashi, 2000; Zhao et al., 2000; Seno et al., 2001). The fault pattern on the oceanic plate off central and eastern Java also implies hydration occurring here. Related dehydration processes of the subducted plate underneath the forearc will have a tremendous influence on the seismicity as well as the petrology of the forearc (e.g. dewatering processes, partial melting in the mantle wedge) (Peacock, 1993; Bostock et al., 2002).

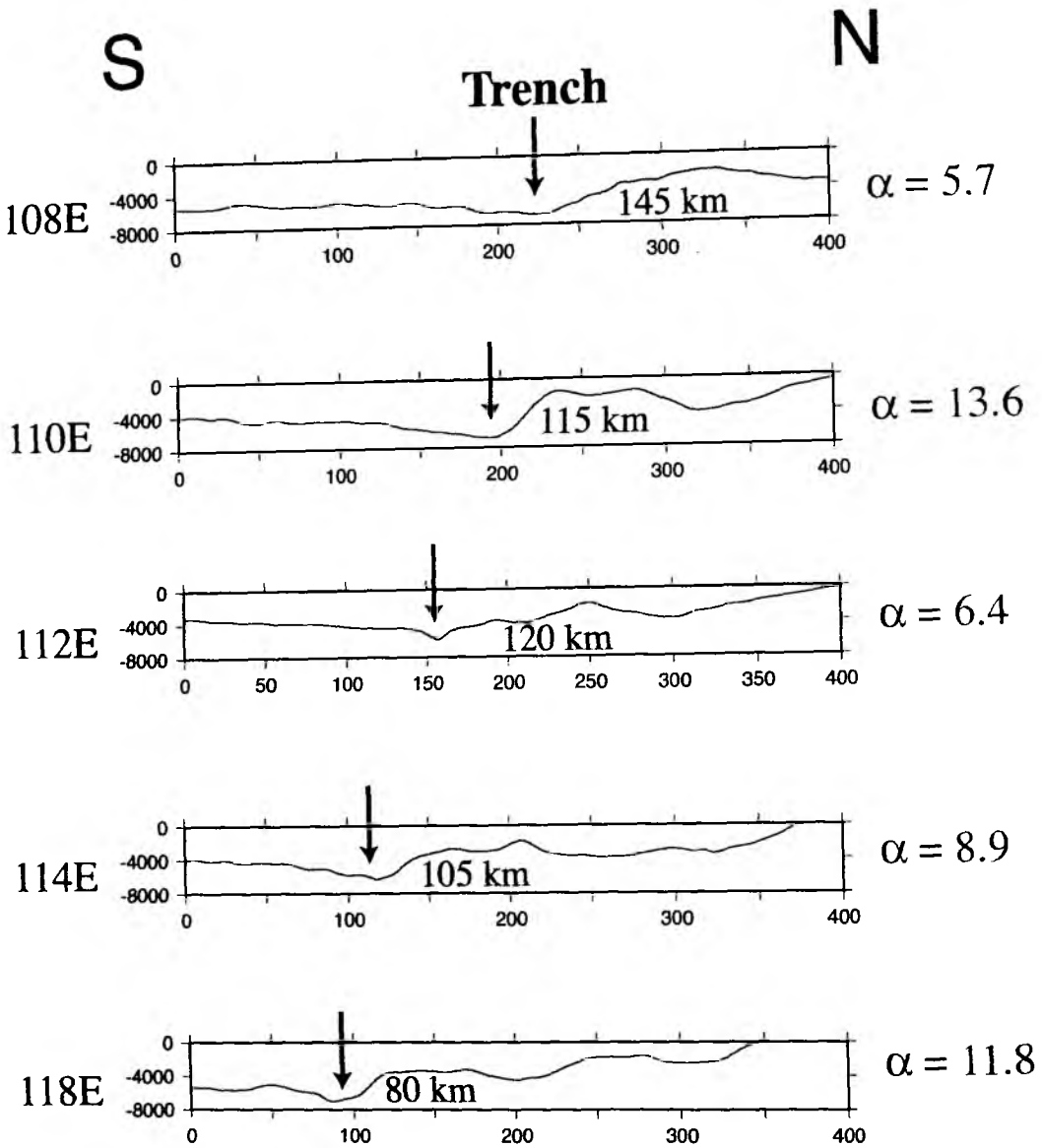

***Figure 2.2.6.3**: Bathymetric profiles across the Java trench and subduction complex. The frontal taper successively increases to the east (from _ = 5.7° to 11.8°). This increase in frontal taper may be one sign for a variation in subduction domains, changing from an accretionary regime to a non-accretive/erosive regime. This trend is interrupted around 110°E, where an anomalously large frontal angle is observed, whose origin is not clear.*

The forearc off central and eastern Java is characterized by isolated block structures (Fig. 2.2.6.1) reaching water depths of less than 1000 m. The typical morphological forearc structure found offshore Sumatra and western Java is not recognized here. A continuous accretionary wedge and landward forearc basin has not developed off central/eastern Java. The increased roughness as well as the decreasing sediment supply in this region imply a general change in the subduction processes and mechanics. This is also supported by the variation in the frontal taper at the deformation front and the corresponding reduction of the outer forearc high. The frontal taper is continuously increasing from west to east, whereas the size and volume of the outer high is decreasing in the same direction. One feature that draws attention is the anomalously large taper at 110°E within the so-called 'seismic gap' (Fig. 2.2.6.3). Its origin and related subduction zone processes here are one of the targets of the MERAMEX project.

All of the above processes suggest a change from an accretionary to a non-accretionary/erosive regime. This alteration is also supported by the large number of seamounts mapped along the eastern Sunda margin (Masson et al., 1990), which are not found along the central segment of the arc (Flueh et al., 1999; Kopp, 2001). The magnitude 7.8 earthquake on June 2, 1994 originated from the subduction of a seamount and caused a tsunami that killed 250 people on Java (Abercrombie et al., 2001). Side-scan sonar investigations off eastern Java mapped 10 seamounts with a diameter of 10 to 60 km and a height of more than 1500 m. These seamounts are in different stages of subduction (Masson et al., 1990). A collision of these bathymetric features with the forearc will result in a landward displacement of the deformation front and a deflection of the forearc (e. g. 15 km at 111°40' E, corresponding to an eroded volume of 500 km^3 (Masson et al., 1990). It remains unclear in how far these local erosive processes contribute to the regional subduction dynamics. In addition to the deflection of the deformation front, seamount subduction often results in submarine slope failure (Dominguez et al., 1998; von Huene et al., 2004). Corresponding geological features, such as large slides, are also to be expected in the study area, but have so far not been mapped here.

3. Participants

3.1 Scientists

3.1.1 Scientists - SO 176

Prof. Dr. Ernst R. Flüh	IFM-GEOMAR, chief scientist
I Ketut Gede Aryawan	P3GL
Dr. Jörg Bialas	IFM-GEOMAR
Nugroho D. Hananto	LIPI
Anne Krabbenhöft	IFM-GEOMAR
Gunardi Kusumah	BRKP-DKP
Erik Labahn	KUM
Sahudin	P3GL
Tubagus Solihuddin	BRKP-DKP
Ir. Mochamad Taufik	BPPT
Dr. Irmgard Trummer	IFM-GEOMAR
Dadan Dani Wardana	LIPI

3.1.2 Scientists - SO 179

Prof. Dr. Ernst R. Flüh	IFM-GEOMAR, chief scientist
Dr. Udo Barckhausen	BGR
Hans-Otto Bargeloh	BGR
Wiebke Brunn	IFM-GEOMAR
Maike Buddensiek	IFM-GEOMAR
Laksana Eko	NAVYSEAL
Michael Fauth	IFM-GEOMAR
Tanja Fromm	IFM-GEOMAR
Koesnadi H.S.	P3GL
Tanja Kuehler	IFM-GEOMAR
Peter Kewitsch	BGR
Thomas Lauer	IFM-GEOMAR
Cord Papenberg	IFM-GEOMAR
Carl Joerg Petersen	IFM-GEOMAR
Fajar Y. Prabowo	BRKP-DKP
Rifky Pratama Putra	ITB
Estelle Roux	IPGP
Agus Solihin	VSI
Klaus-Peter Steffen	IFM-GEOMAR
Subandriyo	BPPTK
Diana Wagner	CAU
Andreas Wittwer	IFM-GEOMAR

3.2 Crew

3.2.1 Crew - SO 176

Henning Papenhagen	Master
Lutz Mallon	Chief Mate
Walter Bascheck	1st Mate
Nils-Arne Aden	2nd Mate
Dr. Uwe Gastmann	Surgeon
Werner Guzmann-Navarrete	Chief Engineer

Klaus-Dieter Klinder	2nd Engineer
Helmuth Grund	2nd Engineer
Uwe Rieper	Electrician
Hilmar Hoffmann	Chief Electrician
Matthias Grossmann	System Operator
Michael Magiulli	System Operator
Volker Blohm	Fitter
Holger Zeitz	Motorman
Frank Tiemann	Chief Cook
Werner Slotta	Chief Steward
Guo Yong Hu	2nd Steward
Winfried Jahns	Bosum
Norbert Bosselmann	A. B.
Jürgen Kraft	A. B.
Hans-Jürgen Vor	A. B.
Christian Milhahn	Apprentice
Manfred Waldenstein	Apprentice

3.2.2 Crew - SO 179

Lutz Mallon	Master
Detlef Korte	Chief Mate
Roland Berger	1st Mate
Nils-Arne Aden	2nd Mate
Vera-Maria Dorst	Surgeon
Norman Lindhorst	Chief Engineer
Klaus-Dieter Klinder	2nd Engineer
Andreas Rex	2nd Engineer
Hilmar Hoffmann	Chief Electrician
Dariusz Zebrowski	Electrician
Wolfgang Borchert	System Operator
Nils Herrmann	RF
Michael Ippich	RF
Jacek Niewitecki	2nd Cook
Peter Mucke	Bosum
Werner Hoedl	A.B.
Torsten Bierstedt	A.B.
Detlef Etzdorf	A.B.
Dirk Dehne	A.B.
Kersten Klaevemann	A.B.
Andreas Schrapel	A.B.
Frank Sebastian	Motorman
Rainer Rosemeyer	Fitter
Waldemar Klocek	Motorman
Wilhelm Wieden	Chief Cook
Gerlinde Grübe	Chief Steward
Guo Yong Hu	2nd Steward

3.3 Addresses of Participating Institutions

IFM-GEOMAR: Leibniz-Institut für Meeresforschung
an der Christian-Albrechts-Universität zu Kiel
Wischhofstr. 1-3
24148 Kiel
Germany
Tel.: +49 – 431 – 600 – 2971
Fax: +49 – 431 – 600 – 2922
e-Mail: lname@ifm-geomar.de
Internet: www.ifm-geomar.de

BGR: Bundesanstalt für Geowissenschaften und Rohstoffe
Dienstgebäude Alfred-Bentz-Haus
Stilleweg 2
30655 Hannover
Germany
Tel.: +49 – 0511 – 643 – 0
Fax: +49 – 0511 – 643 – 2304
e-mail: Poststelle@bgr.de
Internet: www.bgr.de

BPPT: BPP Teknologi, Agency of Assessment & Application Technology
Floor 19, Building 2
Jalan M.H. Thamrin 8
Jakarta 10340
Indonesia
Tel.: +62 – 21 – 3169706
Fax: +62 – 21 – 3169720
e-mail: taufik111@hotmail.com
Internet: www.bppt.go.id

BPPTK: Volcanological Technology Research Center (VTRC)
(Former Merapi Volcano Observatory)
Jln. Cendana No. 15
Yogyakarta 55166
Tel.: +62 – 0274 – 514192
e-mail: mvopgm@yogya.wasantara.net.id
Internet: www.vsi.esdm.go.id

BRKP-DKP: Agency for Marine and Fisheries Research
Ministry of Marine Affairs & Fisheries
M.T. Haryono Kav. 52-53
Jakarta 12770
Indonesia
Fax: +62 – 21 – 79191202
Gunardi Kusumah:
Tel.: +62 – 21 – 79180303 ext. 4032
e-mail: gunardi@dkp.go.id
Fajar Y. Prabowo:
Tel.: +62 – 21 – 79180303 ext. 3113

e-mail: fajaryp@DKP.GO.ID
e-mail: jakfajar@yahoo.com
Internet: www.dkp.go.id

CAU: Christian Albrechts Universität
Institute of Geosciences/Geophysics
University of Kiel
Otto-Hahn-Platz 1
24118 Kiel
Germany
e-mail: diana@geophysik.uni-kiel.de
Internet: www.uni-kiel.de

IPGP: Laboratoire de sismologie éxpérimentale
4 place Jussieu
75005 Paris
e-mail: eroux@ipgp.jussieu.fr
Internet: www.ipgp.jussieu.fr

ITB: Bandung Institute of Technology
Seismic Laboratory, Department Geophysics & Meteorology
Labtek XI
Jl. Ganesha 10
Bandung 40123
Labtek XI
Tel.: +62 – 08157174654
e-mail: rifky_00@yahoo.com
Internet: www.itb.ac.id (University)
www.hmgm.geoph.itb.ac.id (Department)

KUM: K.U.M. Umwelt- und Meerestechnik Kiel GmbH
Wischhofstraße 1-3, Geb. D5
24148 Kiel, Germany
Tel.: 0049 – 431 – 7209 – 220
Fax: 0049 – 431 – 7209 – 244
e-mail: KUM.Umweltsmeerestechnik@t-online.de

LIPI: Research Center for Geotechnology
Indonesian Institute of Sciences
Komplek LIPI
Jl. Sangkuriang
Bandung 40135
Indonesia
Tel.: +62 – 22 – 2503654
Fax: +62 – 22 – 2504593
e-mail: nugroho@geotek.lipi.go.id
Internet: www.geotek.lipi.go.id

NAVYSEAL:

Dept. Hydro-Oceanography
Jl. Pantai Kuta Timuk No.1
Ancol – Jakarta Utara
Tel.: +62 – 21 – 54704810 ext. 3945
Tel.: +62 – 08129450253
e-mail: eko_laksana@yahoo.com
e-mail: infohid@indo.net.id
Internet: www.dishidros.or.id

P3GL:

Pusat Penelitian & Pengembangan – Geologi Kelautan
Marine Geological Institute
Ministry of Energy and Mineral Resources
Dr. Junjunan 236
Bandung 40174
Indonesia
Tel.: +62 – 22 – 6032020
Fax: +62 – 22 – 6017887
e-mail: sahudin@mgi.esdm.go.id
e-mail: koesnadi@mgi.esdm.go.id
Internet: www.mgi.esdm.go.id

RF:

RF Forschungsschiffahrt GmbH
Blumenthalstr. 15
28023 Bremen
Germany
Tel.: + 49 – 421 – 20 76 60
Fax: + 49 – 421 – 20 76 670
e-mail: info@rf-bremen.de
Internet: www.rf-bremen.com

VSI:

Volcanological Survey of Indonesia
Directorate Volcanology and Geological Hazard Mitigation
Jl. Diponegoro No. 57
Bandung – West Java
Tel.: +62 – 22 – 7271402 ext. 151
e-mail: agus@vsi.esdm.go.id
Internet: www.vsi.esdm.go.id

Figure 3.1.1.1: *Participants of cruise SO176, Cilacap-Hongkong.*

Figure 3.1.2.1: *Participants of cruise SO179, Jakarta-Cilacap.*

4. Agenda of the cruises

4.1 Agenda of the cruise SO176

Cruise SO 176 "MERAMEX I" started on May 18, 2004, in Cilacap, Indonesia. Altogether 12 scientists embarked on RV SONNE in Cilacap, comprising the international group of scientists from Austria, Indonesia and Germany. All scientific equipment had been loaded when SONNE left Germany in early April, and was installed in the laboratories upon arrival of the scientists.

At 16:00 in the afternoon of May 18 SONNE left the port of Cilacap and steamed towards the research area on the Java margin (Fig. 4.1.1). The main purpose of this less than three day long cruise was to install an array of ocean bottom seismic stations to monitor the seismicity of the Java subduction zone. In addition, during transit, high resolution bathymetric data were to be collected. The seismological array consists of 14 stations, supplementing 120 stations installed temporarily on land. Both the onshore and the offshore arrays shall be recovered in September/October 2004 after about 4 months of operation. The marine stations were deployed between 1000 and 3500 m of water, with spacing between 20 and 40 nm.

After reaching a water depth of 2000 m, first a CTD station was run to a depth of 1800 m between 21:00 and 22:30 on May 18. Following the first OBS deployment at 23:30, several short profiles were run to calibrate the Simrad EM120 system. Subsequently, instruments were deployed at intervals between 2 and 4 hours, depending on the distance between stations. Multibeam bathymetry was collected permanently with a swath width of 65°, except during the first night, when high swell reduced the quality of the outer beams.

The final station was dropped at 15:00 20. May, and the remaining hours were used for additional bathymetric data collection until 06:00 21. May, when the waterdepth was less than 200 m. SONNE met the pilot at Cilacap at 09:00 and berthed at 10:00 21. May, completing a 700 nm voyage. Scientists left the vessel, and SONNE departed 5 hours later for her transit to Hongkong, where she arrived at 15:00 on May 30.

4.2 Agenda of the cruise SO179

Cruise SO179 "MERAMEX II" started on September 16, 2004, in Jakarta, Indonesia with loading and installation of scientific equipment. Altogether 22 scientists boarded the vessel, and Sonne departed at 08:00 17. September. The working area near the south coast of Java east of 108°E was reached at 18:00 18.September. From here on bathymetric and gravity data were recorded permanently. At 108°E a CDT was lowered to 3400 m, these data were used for the water sound profile throughout the cruise. The CTD frame was also used to mount 10 releasers for a test. The magnetometer was deployed for the transit to the start of the first seismic line, P01, which was started at 06:49 on 19. September and was terminated at 08:30 on 20. September. A four-channel streamer was always deployed when shooting seismic lines, while the magnetometer was only used during long seismic profiles. An ocean bottom hydrophone (OBH) was deployed near the end of the profile (OBH15), and following a short cross line (P02) this instrument together with OBS06, deployed during SO176 were released and subsequently recovered. In the following days, the recovery of the instruments from the seismological network deployed during SO176 continued. Across each instrument two short seismic lines (about 3 nm each) were shot, and often a test OBH was deployed in addition. During transits longer than 20 nm between instruments the magnetometer was deployed, not so during shorter distances. A total of ten instruments were recovered in the morning of 23.09., when we started to deploy 20 instruments (OBH22 to OBS41) along a 160 nm long profile reaching from near the coast across Java trench onto the oceanic plate. A gap of 30 nm

had to be made, since water depths of up to 7200 m within Java trench exceed the maximum depth of instrument rating. Shooting was made along a 190 nm line using all three airguns at a speed of 4.5 kn with a trigger interval of 60 sec. Shooting started around noon 24.09 and was terminated by 06:00 26.09.. Only once one of the guns had to be stopped, because after collision with fishing lines the buoyancy of one gun had been lost.

Recovery of the instruments, incl. the remaining four from the seismological net was terminated at 22:00 on 27.09.. Unfortunately, OBH 40 could not be recovered, and also a search for several hours during daylight the following day was unsuccessful.

Deployment of 23 instruments (OBS42 to OBH64) on the second profile across the trench (P18) was made 28 and 29.9.. Again, a 30 nm gap across Java trench had to be left without instruments, due to the great waterdepth. Shooting with all three airguns at a speed of 4.5 kn and a trigger interval of 60 sec lasted until midnight 30.9.. Early on 02.10. all instruments were recovered successfully.

The final seismic profile (P19) was shot at a distance of ca. 25 nm along the coast. Eleven instruments were deployed (OBH 65 to OBH75), and shooting was done in perfect weather conditions and was finished at 13:00 on 03.10.. All instruments were recovered by 04:00 on 04.10.. The following hours were used to fill gaps in the bathymetric and magnetic coverage on the transit to OBH40, where the time release was set to 20:00 local time. Unfortunately, the instrument was not sighted, and further attempts to release it also failed.

The remaining 40 hours of the cruise were used to map the region of the trench and accretionary front between seismic profiles P16 and P18. SONNE met the pilot near Cilacap 06.10. at 15:00 and berthed at 16:00, terminating cruise SO179 after 20 days at sea with a total cruise length of approximately 3700 nm. The trackchart of SO179 is shown in Figure 4.2.1.

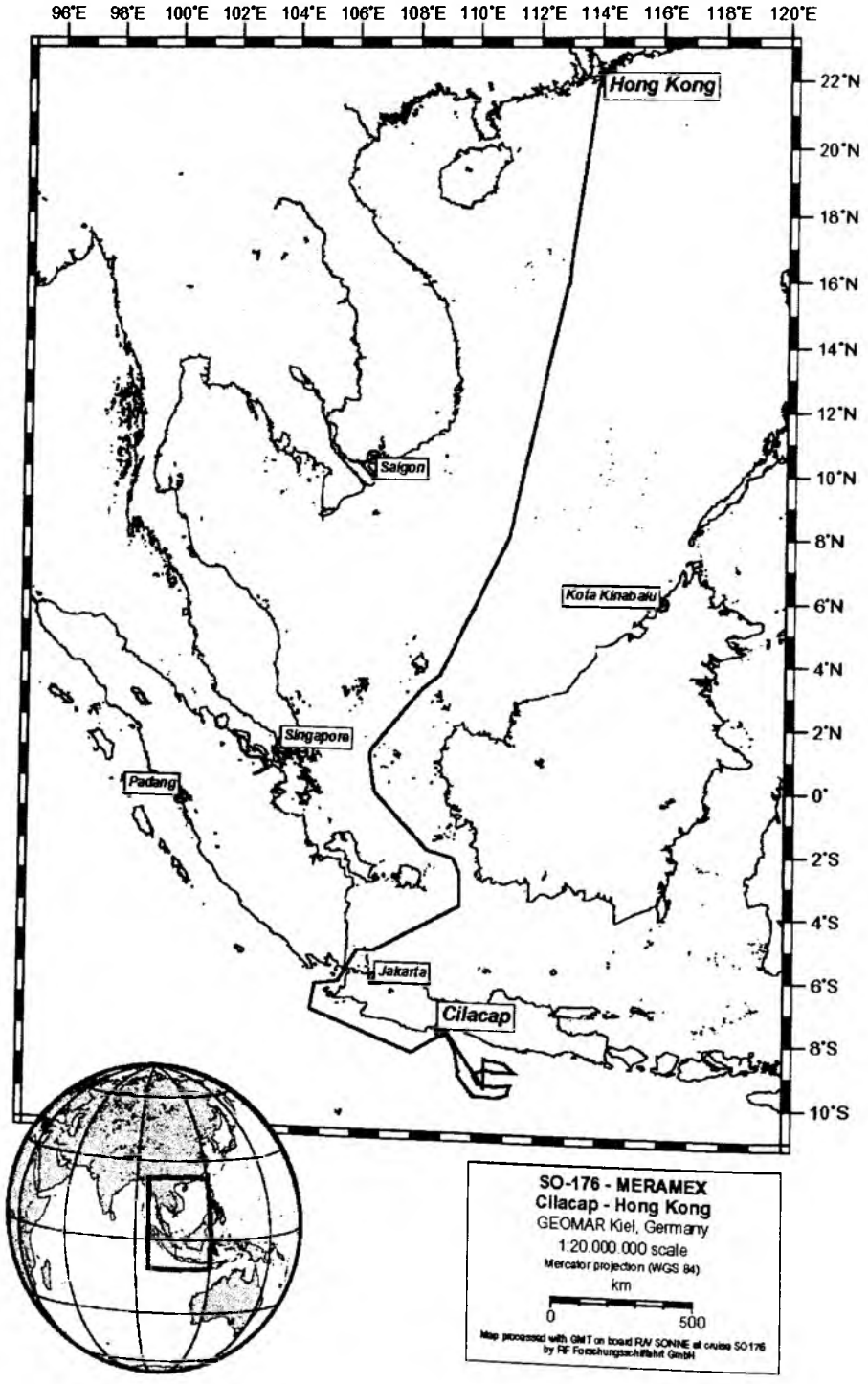

Figure 4.1.1: Track chart of cruise SO176.

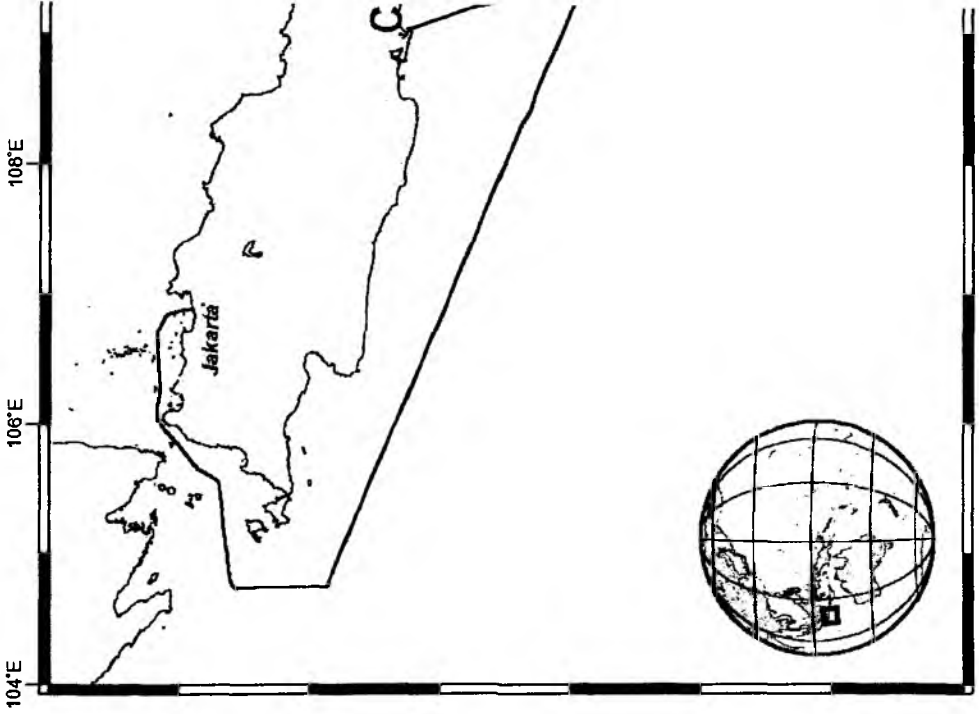

Figure 4.2.1: *Track chart of cruise SO179.*

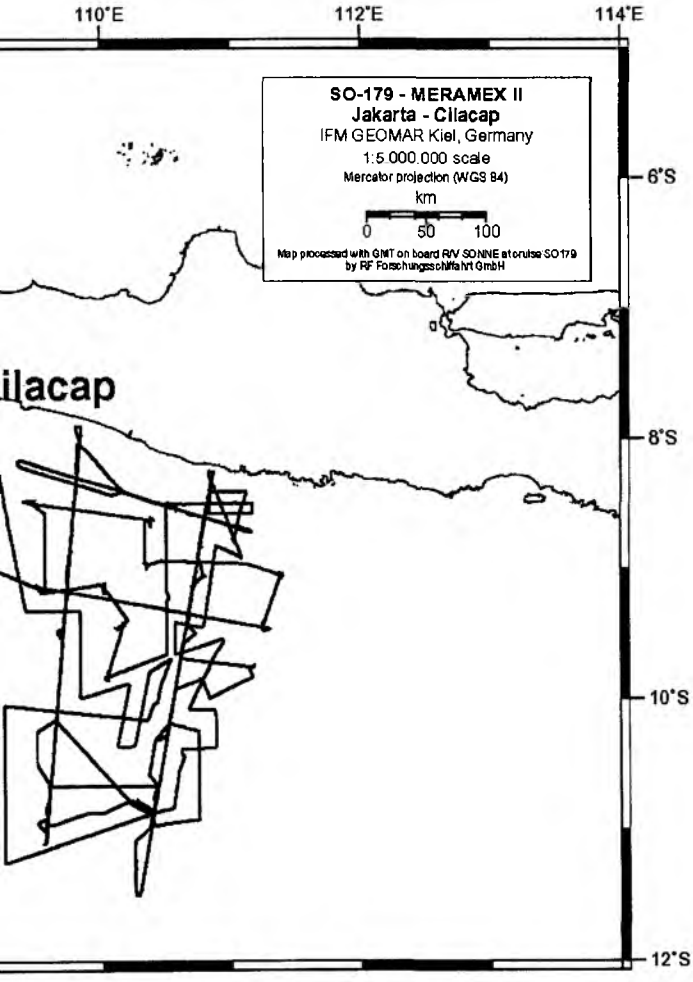
110°E
112°E
114°E
SO-179 - MERAMEX II
Jakarta - Cilacap
IFM GEOMAR Kiel, Germany
1:5.000.000 scale
Mercator projection (WGS 84)
km
0 50 100
Map processed with GMT on board R/V SONNE at cruise SO179
by RF Forschungsschiffahrt GmbH
6°S
8°S
10°S
12°S
ilacap

5. Scientific equipment

5.1 Shipboard equipment

5.1.1 Navigation

A crucial prerequisite for all kinds of marine surveys is the precise knowledge of position information (latitude, longitude, altitude above/below a reference level). Since 1993 the global positioning system (GPS) has been commercially available and widely used for marine surveys. It operates 24 satellites in synchronous orbits, thus at least 3 satellites are visible anywhere at any moment (Seeber, 1996). The full precision of this originally military service yields positioning accuracies of a few meters. In the past its use was restricted to military forces and inaccessible to commercial users (Blondel and Murton, 1997). Since about 2000 the full resolution is generally available. During the cruises SO176 and SO176 the operation of the differential (DGPS) option was not requested as standard precision coordinates were precisely enough for the work planned.

GPS-values as well as most other cruise parameters are continuously stored in the navigation database, and are distributed via the DVS- ("data distribution system") on the ship's network.

5.1.2 Simrad EM120 swathmapping bathymetry system

The EM120 system is a multibeam echosounder (with 191 beams) providing accurate bathymetric mapping up to depths exceeding 11000 m. This system is composed of two transducer arrays fixed on the hull of the ship, which send successive frequency coded acoustic signals (11.25 to 12.6 kHz). Data acquisition is based on successive emission-reception cycles of this signal. The emission beam is 150° wide across track, and 2° along track direction (Fig. 5.1.2.1). The reception is obtained from 191 overlapping beams, with widths of 2° across track and 20° along it (Fig. 5.1.2.1). The beam spacing can be defined as equidistant or equiangular, and the maximum seafloor coverage may be set to a fixed value. The echoes from the intersection area (2°*2°) between transmission and reception patterns (Fig. 5.1.2.1), produce a signal from which depth and reflectivity are extracted.

For depth measurements, 191 isolated depth values are obtained perpendicular to the track for each signal. Using the 2-way-travel-time and the beam angle known for each beam, and taking into account the ray bending due to refraction in the water column by sound speed variations, depth is estimated for each beam. A combination of phase (for the central beams) and amplitude (lateral beams) is used to provide a measurement accuracy practically independent of the beam pointing angle. The raw depth data need then to be processed to obtain depth-contour maps. In the first step, the data are merged with navigation files to compute their geographic position, and the depth values are plotted on a regular grid to obtain a digital terrain model (*DTM*). In the last stage, the grid is interpolated, and finally smoothed to obtain a better graphic representation.

Together with depth measurements, the acoustic signal is sampled every 3.2ms and processed to obtain a cartographic representation, commonly named mosaic, where grey levels are representative of backscatter amplitudes. These data provide thus information on the sea-floor nature and texture; it can be simply said that a smooth and soft seabed will backscatter little energy, whereas a rough and hard relief will return a stronger echo.

During the first night of SO 176 cruise, the Simrad EM 120 multibeam echosounder, available on R/V SONNE since June 2001, was calibrated during several dedicated profiles. This procedure was necessary to allow correction of ships motion within the beam processing. Failure of calibration would result in collected data sets that are not precise enough to be incorporated into an overall

chart compiled during various cruises in the region. The EM120 was used continuously during both cruises. Bathymetric data were processed routinely onboard during the survey, using the NEPTUNE software from Simrad, available on board and the academic software MB-System from Lamont-Doherty Earth Observatory. Data collected during SO176 and SO179 have be merged and maps were generated which are shown in Figures 5.1.2.2 to 5.1.2.6.

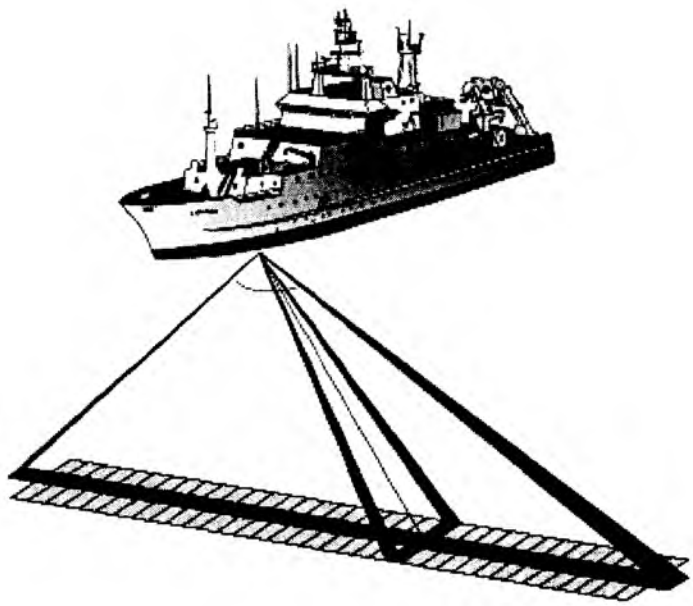

Figure 5.1.2.1: *Acquisition method for bathymetric and backscatter data from the Simrad EM120 system (crossed beams technique).*

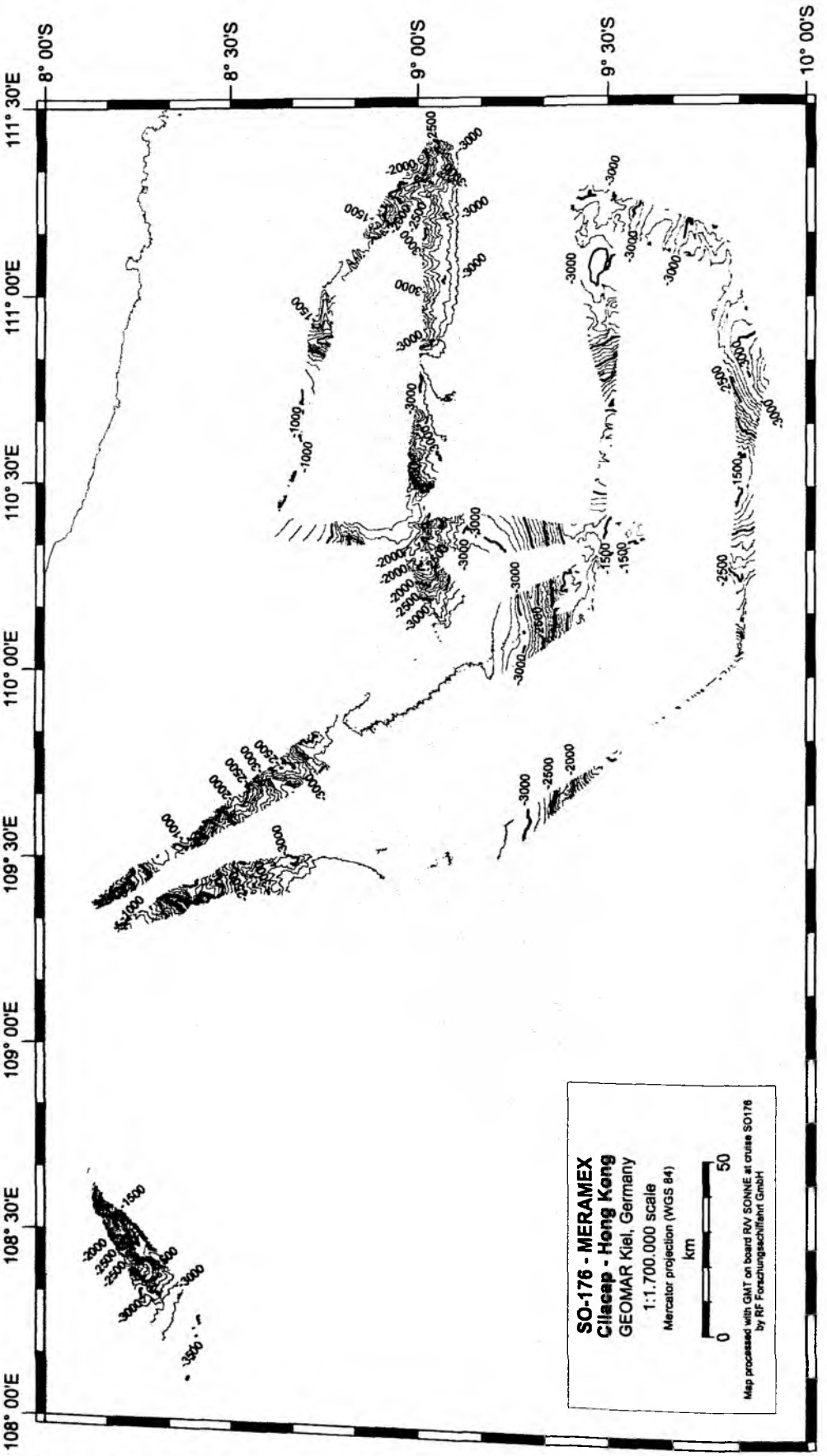

Figure 5.1.2.2: Swath bathymetric survey conducted offshore central Java.

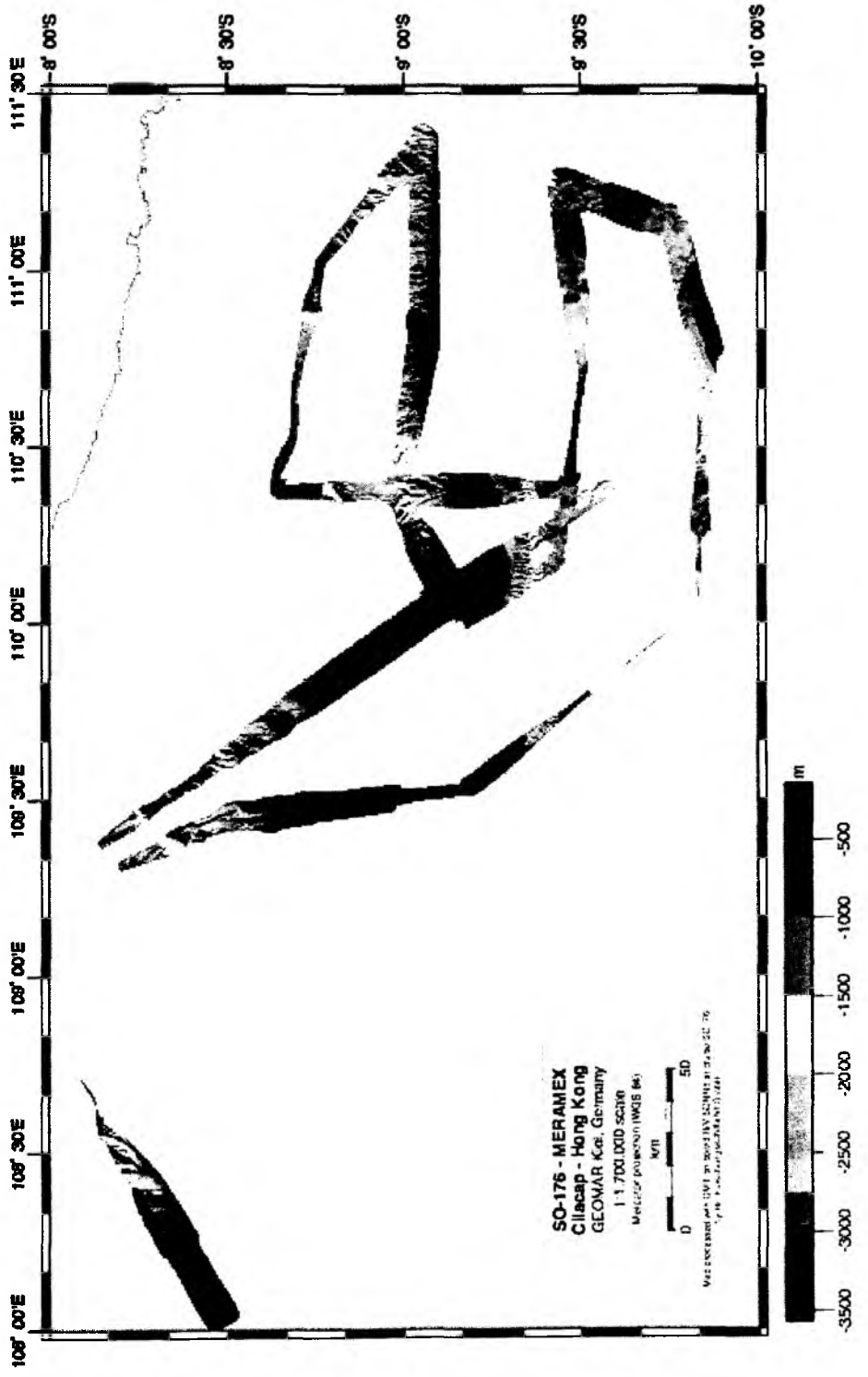

Figure 5.1.2.3: Shaded bathymetry relief of the study area

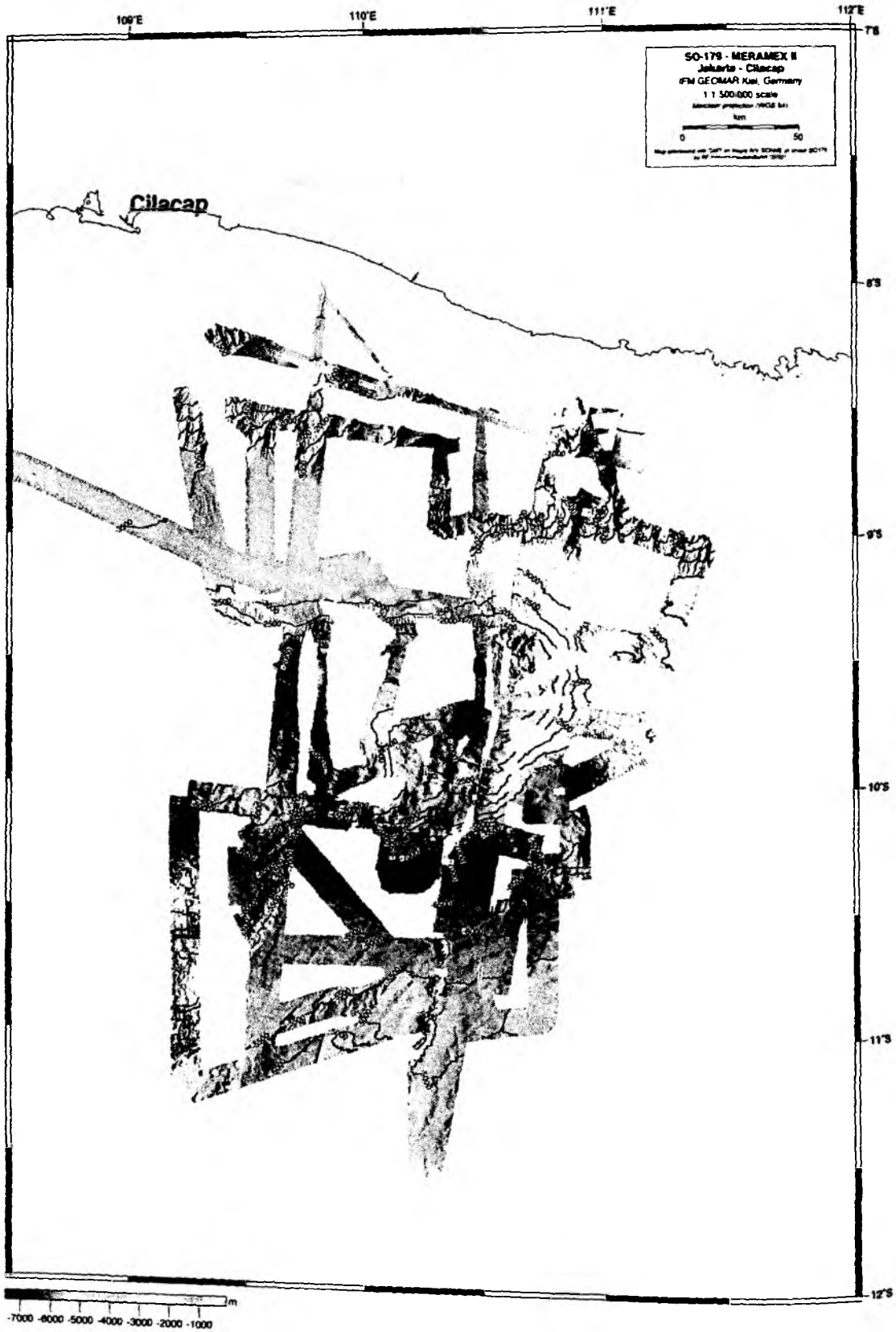

Figure 5.1.2.4 : Swath bathymetric survey conducted on the SO179 cruise

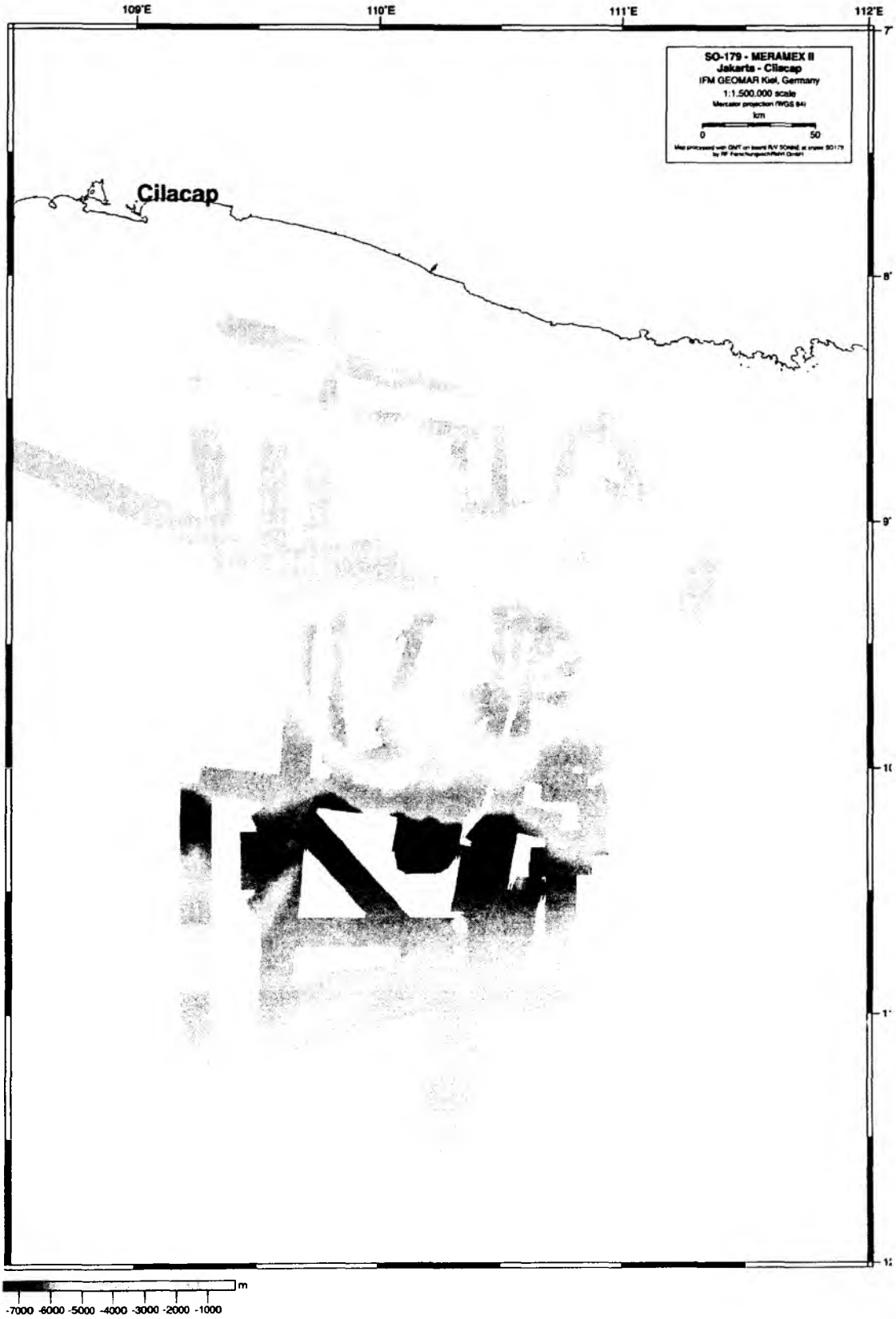

***Figure 5.1.2.5** : Shaded bathymetry relief of the study area of SO179 cruise*

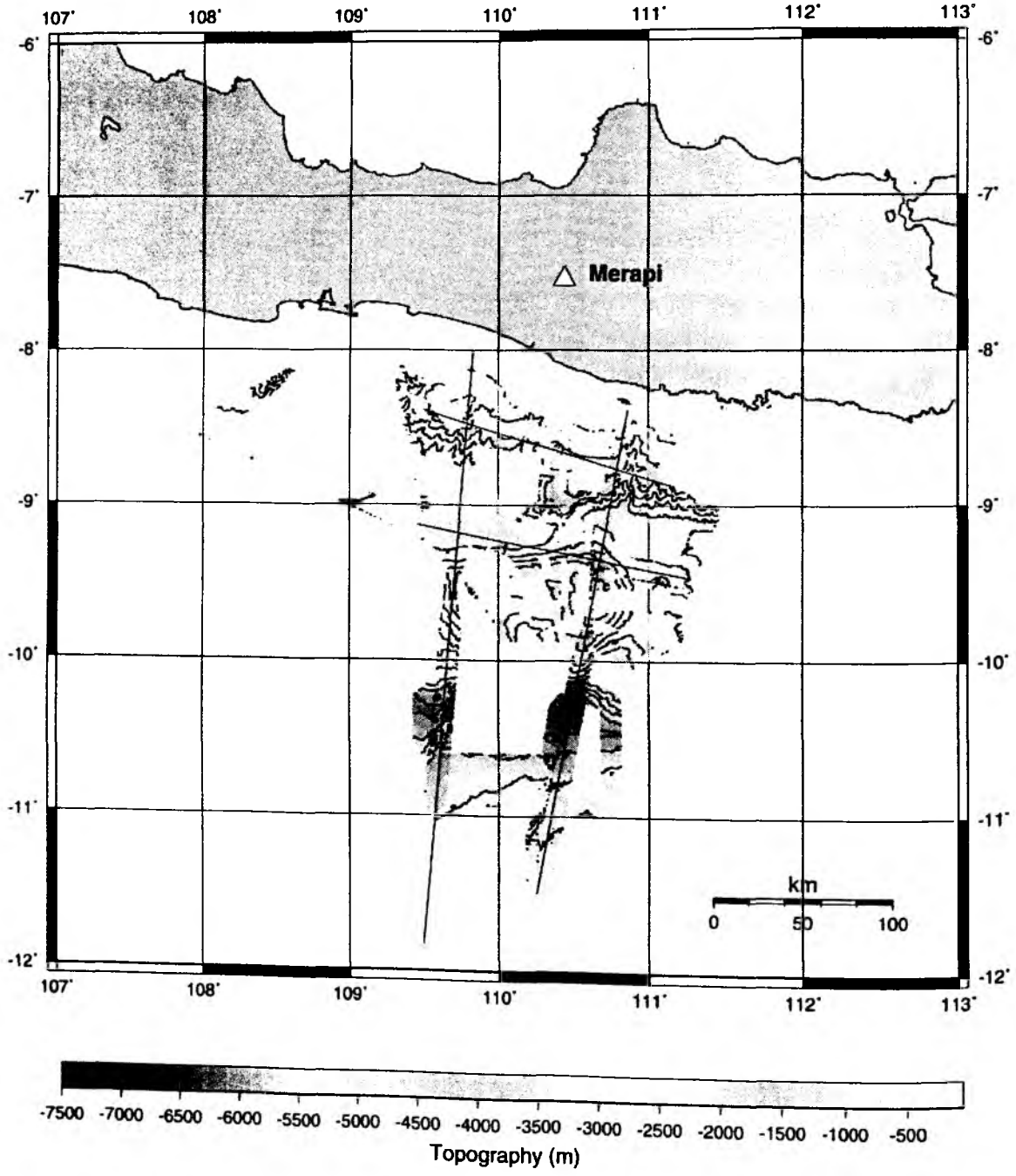

Figure 5.1.2.6: Merged bathymetric surveys of SO176 and SO179 cruises

5.1.3 Parasound

The PARASOUND system works both as a low-frequency sediment echosounder and as a high-frequency narrow beam sounder to determine the water depth. It utilizes the parametric effect, which produces additional frequencies through nonlinear acoustic interaction of finite amplitude waves. If two sound waves of similar frequencies (here 18 kHz and e.g. 22 kHz) are emitted simultaneously, a signal of the difference frequency (e.g. 4 kHz) is generated for sufficiently high primary amplitudes. The new component travels within the emission cone of the original high frequency waves, which are limited to an angle of only 4° for the equipment used. Therefore, the footprint size of 7% of the water depth is much smaller than for conventional systems and both vertical and lateral resolution are significantly improved.

The PARASOUND system is permanently installed on the ship. The hull-mounted transducer array has 128 elements within an area of 1 m^2. It requires up to 70 kW of electric power due to the low degree of efficiency of the parametric effect. In 2 electronic cabinets, beam formation, signal generation and the separation of the primary (18, 22 kHz) and secondary frequencies (4 kHz) is carried out. Using the third electronic cabinet located in the echosounder control room, the system is operated on a 24 hour watch schedule.

Since the two-way travel time in the deep sea is long compared to the length of the reception window of up to 266 ms, the PARASOUND System sends out a burst of pulses at 400 ms intervals, until the first echo returns. The coverage in this discontinuous mode is dependent on the water depth and also produces non-equidistant shot distances between bursts.

The main tasks of the operators are system and quality control and to adjust the start of the reception window. Because of the limited penetration of the echosounding signal into the sediment, only a short time window close to the sea floor is recorded.

In addition to the analog recording features with the b/w DESO 25 device, the PARASOUND System is equipped with the digital data acquisition system ParaDigMA, developed at the University of Bremen. The data is stored on removable hard disks using the standard, industry-compatible SEGY-format. The 486-processor based PC allows for buffering, transfer and storage of the digital seismograms at very high repetition rates. Of the emitted series of pulses, usually only every second pulse can be digitized and stored, resulting in recording intervals of 800 ms for a given pulse sequence. The seismograms were sampled at a frequency of 40 kHz, with a typical registration length of 266 ms for a depth window of ~200 m. The source signal was a band limited, 2-6 kHz sinusoidal wavelet with a dominant frequency of 4 kHz and duration of 1 period (250 μs total length).

During the cruises SO173 and SO179 the Parasound signals were visually inspected, but not recorded in analog nor digital form.

5.1.4 CTD data

The CTD rosette onboard RV SONNE was deployed during cruise SO176 to measure physical oceanographic parameters (Fig. 5.1.4.1.). The CTD station was run to a water depth of 1800 m at a velocity of 1 m/s measuring the sound speed in-situ continuously. The sound velocity profile is shown in Figure 5.1.4.2.

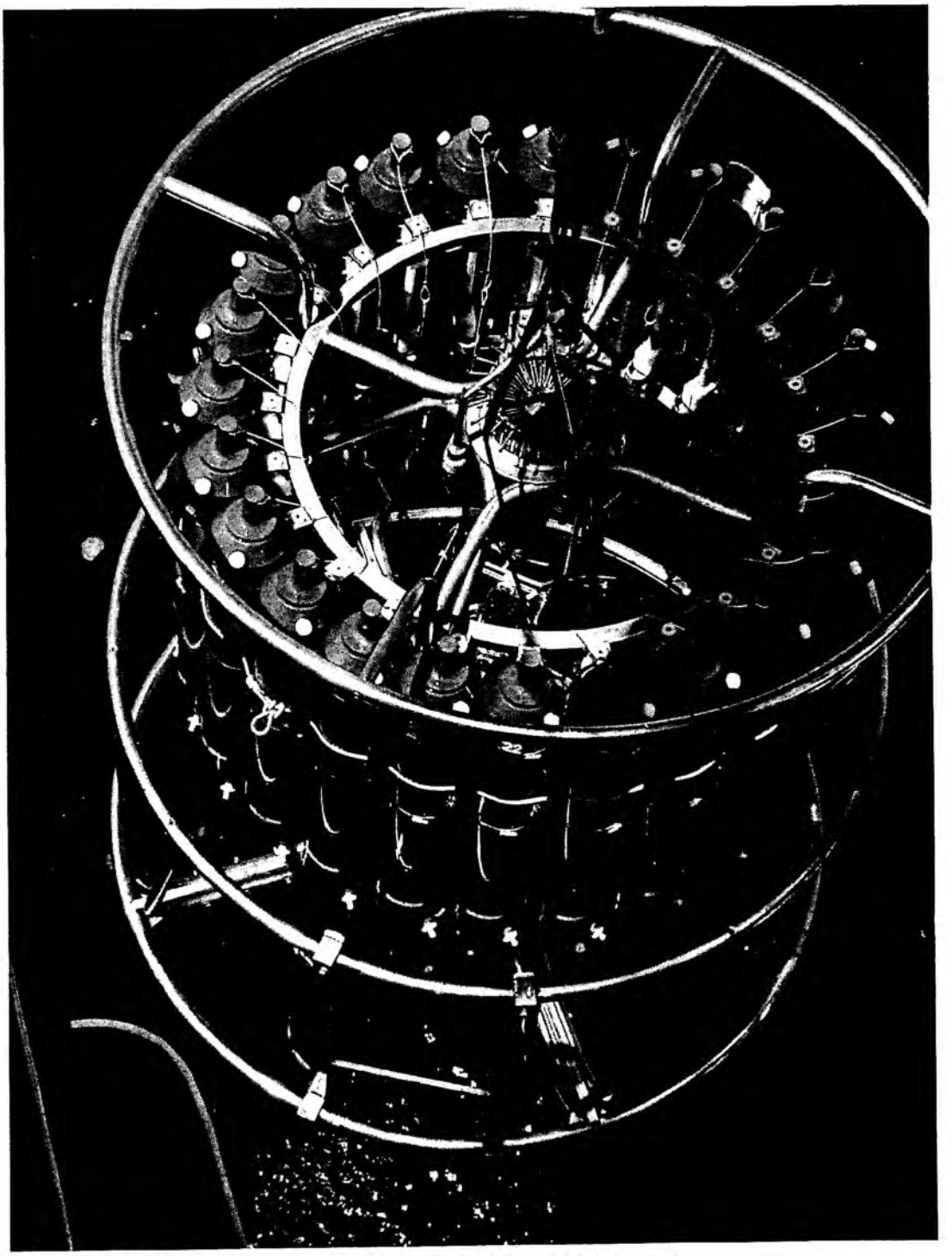

Figure 5.1.4.1: *RV SONNE's onboard CTD rosette upon deployment.*

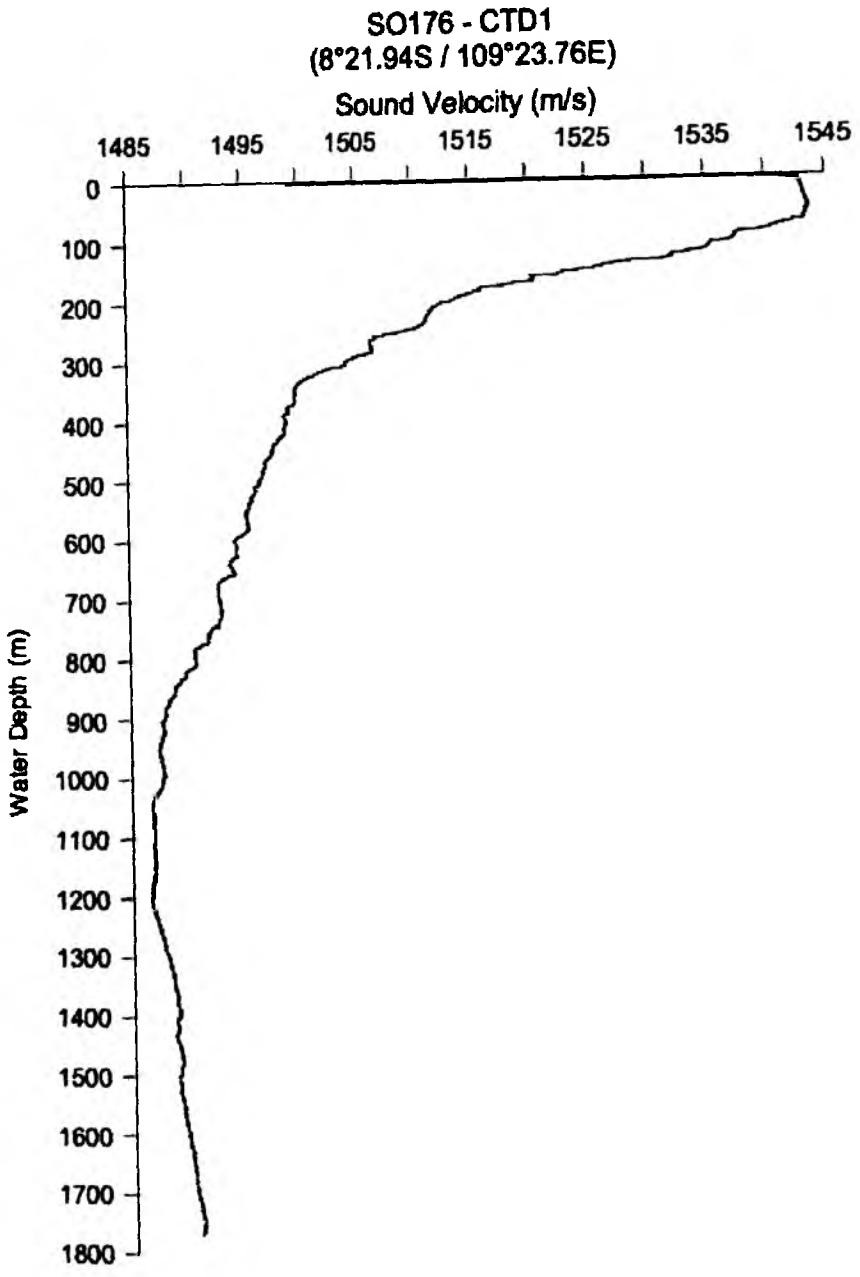

Figure 5.1.4.2: *Sound velocity profile obtained from CTD measurement during SO176.*

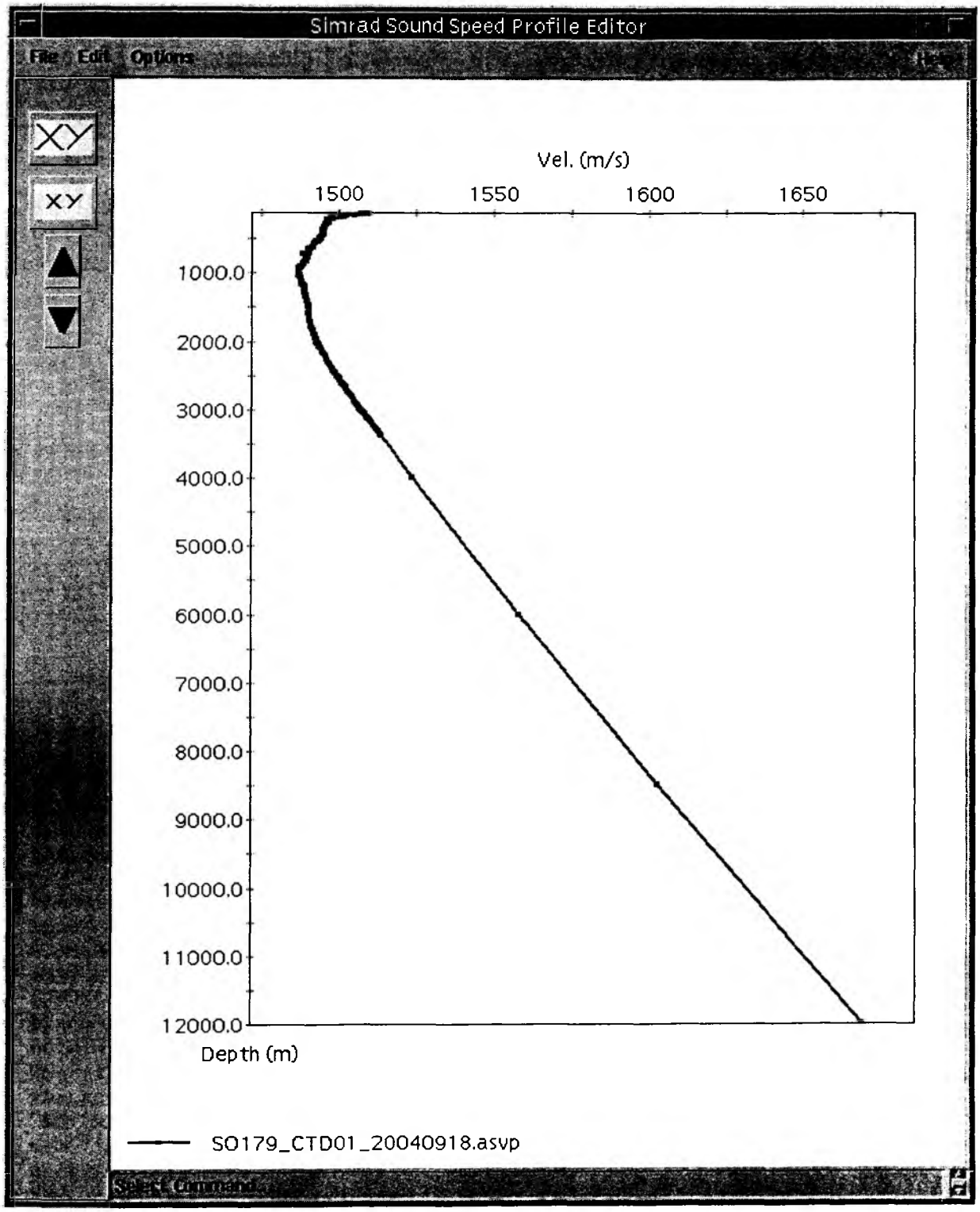

Figure 5.1.4.3: *Sound velocity profile obtained from CTD measurement during SO179*

Accurate sound velocity profiles are needed for calibration of the water sound velocity to transfer the echo times of the bathymetric swathmapping into water depth. The velocity profile exhibits the typical curvature with similar characteristics of measurements conducted elsewhere. Sound velocity in shallow water shows a very high negative gradient in the upper 300 m of the water column, decreasing to approx. 1498 m/s. Below 300 m water depth, a lesser negative gradient is observed, reaching a minimum value between 1000 m and 1200 m water depth at a sound velocity of 1487 m/s. The deeper water column is characterized by an increase in sound velocity and a positive gradient. Small excursions from the linear trend here are still observed, but less numerous and explicit as in the upper water column.

5.2 Computer facilities for bathymetry, magnetic, and seismic data processing

The experiments and investigations during SO179 required special computing facilities in addition to the existing shipboard systems. For programming of ocean bottom stations, processing and interpretation of seismic data and analysis of magnetics, several workstations and a dedicated Macintosh-laptop were installed by the wide angle and seismology groups of IfM-GEOMAR.

Due to the large amount of data transfer IfM-GEOMAR installed a workstation cluster onboard comprising the following systems:

1	"aurinacien"	Sun Ultra 1	1 CPU 768 MB memory	8.5 GB disks	Sun OS 5.8
3	"hotblack"	SUN Ultra 1	1 CPU, 128 MB memory	17.1 GB disks	Sun OS 5.8
3	"roorise"	PC	1 CPU, 512 MB memory	40 GB disk	SUSE Linux
4	"crimea"	AMD Duron 700 MHz	1 CPU, 128 MB memory	68 GB disk, 6x PCMCIA	WindowsXP Linux
5	"pinta"	AMD Duron 700 Mhz	1 CPU, 128 MB memory	68 GB disk, 6x PCMCIA	WindowsXP Linux

To read the OBH/S-data from dataloggers we used "pinta" and "crimea" with pcmcia-drives and converted the passcal-data into rsegy. The dataprocessing and modelling with Seismos was made on two X-Terminals.
In addition to these computers a Macintosh was used for modelling raypaths with MacRay. The data were backuped with a DLT-Drive on 40 GB-tapes. For plotting and printing one Postscript Laserprinter (papersize A3 and A4) as well as the shipboard color plotters were available.

The workstation cluster was placed in the Reinlabor where it was set up according to a "client-server" model, with "aurenacien" being the server. All important file systems from the main server at IfM-GEOMAR were duplicated onto a Raid-system (1.2 Tbyte). Using NFS-, NIS-, and automounter services the computing environment was nearly identical to that at IfM-GEOMAR, so every user found his/her familiar user interface. The convenience of network mounted file systems has to be paid for with a heavy network load, particularly during playback of OBH-data (c.f. SO123 cruise report, Flueh et al., 1997). This required a high-performance network, which was accomplished by a switched twisted-pair ethernet. A 12-port ethernet switching-hub (3COM-SuperstackII 1000) with an uplink connection of 100 Mbps to the server "aurinacien" and dedicated 10 Mbps ports for the client workstations maintained the necessary network performance. In order to keep the shipboard network undisturbed by the workstation cluster, but to allow for communication between them, the server "aurinacien" was equipped with two network interfaces and served as a router. This provided the additional benefit of a simplified network configuration. In addition, "hotblack" was set up as an redundant server, so in case "aurinacien" would have failed, "hotblack" could easily switched to replace "aurinacien" as a server.

This network setup showed a reliable and stable performance, and no breakdowns were observed. For data-management and processing of magnetics and gravimetry see section 5.4 and 5.5.

5.3 Seismic instrumentation

The Ocean Bottom Hydrophone

The first GEOMAR Ocean Bottom Hydrophone was built in 1991 and tested at sea in January 1992. This type of instrument has proved to have a high reliability; more than 3000 successful deployments were conducted since 1991. In total 9 OBH positions and 5 OBS positions were occupied during cruise SO176. A total of 19 OBH and 5 OBS instruments were available for SO179. Altogether 53 sites were engaged during the SO179 cruise.

The principle design and a photograph showing the instrument upon deployment are shown in Figure 5.3.1. The design is described in detail by Flueh and Bialas (1996).

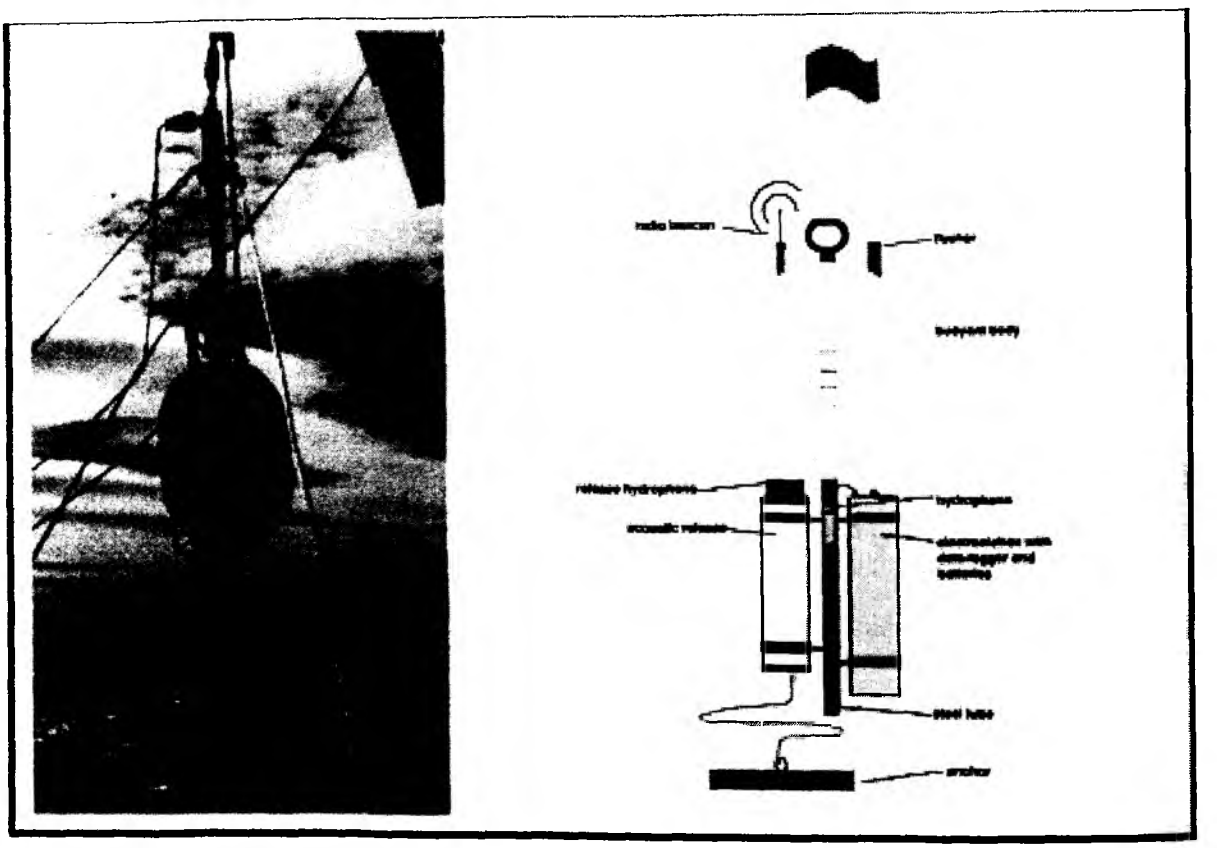

Figure 5.3.1: *Principle design of the Geomar OBH (right panel, after Flueh and Bialas, 1996) and the instrument upon deployment (left panel).*

The system components are mounted on a steel pipe which holds the buoyancy body on its top. The buoyancy is made of syntactic foam and is rated, as are all other components of the system, for a water depth of 6000 m, except for the pressure cylinders holding the recording electronics. Here, various models are available for variable depths (2500 m, 3000 m, and 6000 m). Attached to the buoyant body are a radio beacon, a flash light, a flag and a swimming line for retrieving from aboard the vessel. The hydrophone for the acoustic release is also mounted here. The release transponder is a model *RT661CE* made by *MORS Technology*. Communication with the instrument is possible through the ship's transducer system, and even at maximum speed and ranges of 4 to 5 miles release and range commands are successful. For anchors, we use pieces of railway tracks weighing about 40 kg each. The anchors are suspended 2 to 3 m below the

instrument. The sensor is an *E-2PD* hydrophone from *OAS Inc.*, or the HTI-01-PCA hydrophone from *HIGH TECH INC.* and the recording device is a *MBS* recorder of *SEND GmbH*, which is contained in its own pressure tube and mounted below the buoyant body opposite the release transponder (see Figure 5.3.1).

The GEOMAR Ocean Bottom Seismometer 2002

The GEOMAR Ocean Bottom Seismometer 2002 (OBS-2002; Fig. 5.3.2) is a new design based on experiences gained with the GEOMAR Ocean Bottom Hydrophone (OBH; Flueh and Bialas, 1996) and the GEOMAR Ocean Bottom Seismometer (OBS, Bialas and Flueh, 1999). For system compatibility the acoustic release, pressure tubes, and the hydrophone are identical to those used for the OBH and OBS. Syntactic foam was used as floatation again but this time in less expensive cylinder shape. The entire frame can be dismounted for transportation, which allows storage of more than 50 instruments in one 20" container. Upon cruise preparation onboard all parts are screwed together within 30 minutes time. Four main cylinders are fixed within the system frame, while additional disks can be added to the sides without changes. The basic system is designed to carry a hydrophone and a small seismometer for higher frequency active seismic profiling. The sensitive seismometer is deployed about 1 m to the side of the system once the OBS lands on the sea floor. At this time the only connection from the seismometer to the instrument is a cable and an attached wire, which retracts the seismometer during ascent to the sea surface. An oscillation of the instrument caused by possible currents is therefore not transmitted mechanically to the seismometer. The three component seismometer (*KUM*) is housed in a titanium tube, modified from a package built by Tim Owen (Cambridge) earlier. Geophones of 4.5 or 30 Hz natural frequency are available. In addition, a 4.5 Hz self gimballed geophone from *Geospace* was used as a prototype during the cruise, and also a short period geophone, produced by *Send GmbH*, was operated for test purposes.

By changing the frontal third of the frame (opening four screws) a broadband seismometer can be attached to the system carrier. The "Spahr Webb" type seismometer is based on *Mark-L4* sensors, which are operated with a feedback loop to enable recordings of frequencies as low as about 60 sec. As the sensors are sensitive to horizontal or vertical adjustment the complete construction is fully gimbaled. Tilt is measured at selected intervals and two electric motors are used to adjust and fix for a proper positioning. The system is mounted within a 17" glass sphere. The sensor is recorded by use of the *Marine Longtime Recorder (MLS),* which is manufactured by *SEND GmbH* and specially designed for longtime recordings of low frequency bands. The hydrophone can be replaced by a differential pressure gauge (DPG) as described by Cox et al (1984). While deployed to the seafloor the system rests horizontally on the anchor frame. After releasing its anchor weight the instrument turns 90° into the vertical and ascends to the surface with the flotation on top. This ensures maximal reduced system height and water current sensibility at the ground (during measurement). On the other hand the sensors are well protected against damage during recovery and the transponder is kept under water, allowing permanent ranging, while the instrument floats at the surface.

Marine Broadband Seismic Recorder (MBS)

The so-called *Marine Broadband Seismic recorder (MBS;* Bialas and Flueh, 1999*)*, manufactured by *SEND GmbH*, was developed based upon experience with the DAT based recording unit Methusalem (Flueh and Bialas, 1996) over previous years. This new recorder avoids a mechanically driven recording media, and the PCMCIA technology enables static flash memory cards to be used as unpowered storage media. Read/write errors due to failure in tape handling operations should not occur with this system. In addition, a data compression algorithm is implemented to increase data capacity. Redesign of the electronic layout enables a decreased power consumption (1.5 W) of about 25% compared to the *Methusalem* system. Depending on the sampling rate, data output could be in 16 to 18 bit signed data. Based on digital decimation filtering, the system was developed to serve a variety of seismic recording requirements.

Therefore, the bandwidth reaches from 0.1 Hz for seismological observations to the 50 Hz range for refraction seismic experiments and up to 10 kHz for high resolution seismic surveys. The basic system is adapted to the required frequency range by setting up the appropriate analogue front module. Alternatively, 1, 2, 3 or 4 analogue input channels may be processed. Operational handling of the recording unit is similar to the *Methusalem* system or by loading a file via command or automatically after power-on. The time base is based on a DTCXO with a 0.05 ppm accuracy over temperature. Setting and synchronizing the time as well as

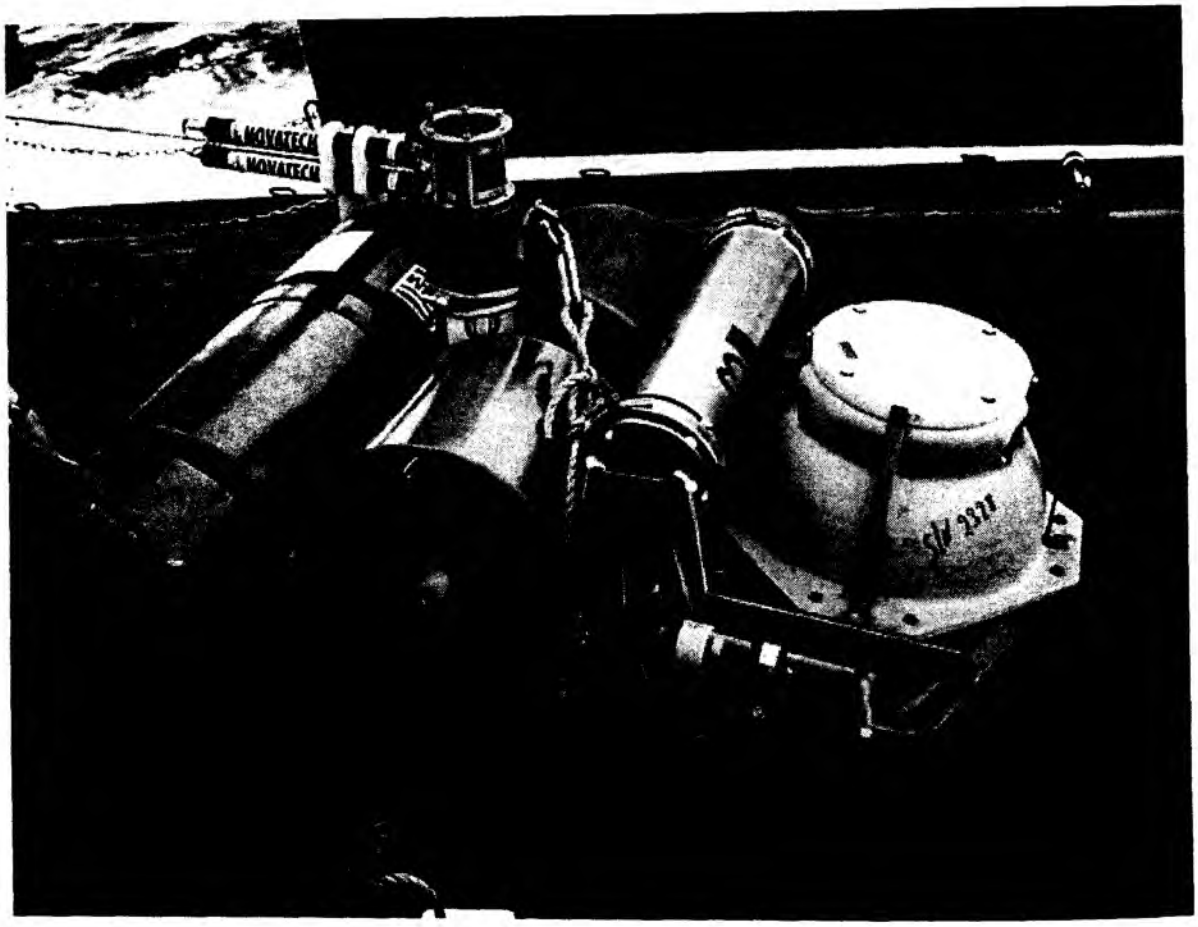

Figure 5.3.2: *Instrument setup of the Ocean Bottom Seismometer 2002.*

monitoring the drift is carried out automatically by synchronization signals (DCF77 format) from a GPS-based coded time signal generator. Clock synchronization and drift are checked after recovery and compared with the original GPS units. After software preamplification the signals are low-pass filtered using a 5-pole Bessel filter with a -3 dB corner frequency of 10 kHz. Then each channel is digitised using a sigma-delta A/D converter at a resolution of 22 bits producing 32-bit signed digital data. After delta modulation and Huffman coding the samples are saved on PCMCIA storage cards together with timing information. Up to 4 storage cards may be used. Currently, up to 640 MB per card are available. Data compression allows increase of this capacity. Recently technical specifications of flashdisks (disk drives of PCMCIA technology) have been modified to operate below 10 °C, therefore 2 GB drives are now available for data storage. After recording the flashcards need to be copied to a PC workstation. During this transcription the data are decompressed and data files from a maximum of four flash memory are combined into one data set and formatted according to the PASSCAL data scheme used by the *Methusalem* system. This

enables full compatibility with the established processing system. While the *Methusalem* system did provide 16 bit integer data, the 18 bit data resolution of the *MBS* can be fully utilized using a 32 bit data format.

The Marine Exploration Seismic Recorder (MES)
This data logger is based on the experiences with the MBS and MLS devices. It is supposed to replace the MBS system in the future. New features are a 24 bit A/D converter which provides a signal to noise ratio above 120 dB. As the development of PC cards did not allow the use of high capacity cards (2 GB and higher) in low-temperature surroundings like the ocean floor the new data logger uses an internal hard disk. From developments in laptop technology, drives are available that withstand a harsh working environment and need only a small amount of power. High data transfer through a firewire (5 GB < 10 min) ensures that the entire 20 GB disk drive can be copied within 40 min. Further features are similar to the MBS. Together with the data logger a new set of Linux-based programs allows to run the complete data transformation up to SEGY formatted trace segmentation without switching between different operating systems or computing platforms. Seven recorders were available for SO 179 and worked well.

The Marine Longtime Seismograph
For the purpose of low frequent recordings such as seismological observations of earthquakes during long term deployments of about one year time a new data logger, the Marine Longtime Seismograph (MLS) was developed by *SEND GmbH* with support from IFM-GEOMAR.

The MLS is again a four channel data logger whose input channels have been optimized for 3-component seismometers and one hydrophone channel. The modular design of the analogue front end allows to adapt different seismometers and hydrophones or pressure sensors. Currently front ends for the Spahr Webb, PMD and Guralp seismometers as well as for a differential pressure gauge (DPG) and the OAS hydrophone are available. With these sensors we are able to record events between 50 Hz and 120 s. The very low power consumption of 250 mW during recording together with a high precision internal clock (0.05 ppm drift) allows data acquisition for one year. Data storage is done on up to 12 PCMCIA type II flashcards. The instrument can be parameterized and programmed via a RS232 interface. After low pass filtering the signals of the input channels are digitized using Sigma-Delta A/D converters. A final decimating sharp digital low-pass filter is realized in software by a Digital Signal Processor. The effective signal resolution depends on the sample rate and varies between 18.5 bit at 20 ms and 22 bits at 1 s. Playback of the data is done under the same scheme as described for the MBS above. After playback and decompression the data is provided in PASSCAL format from where it could be easily transformed into standard seismological data formats.

Towed Streamer
In addition to the ocean bottom seismic recorders also a mini-streamer was used during seismic profiling. This streamer was borrowed from the University of Gent, Belgium, and manufactured by *SIG (Service et Instruments de Geophysique, France)*. The system comprises several parts: four 12.5 m long active sections with 25 hydrophones spaced at 0.5 m. The lead-in cable is 150 m long and directly connected to the lab. The individual hydrophones are omnidirectional and have a flat frequency response from 10 to 1000 Hz. The sensitivity is –90 db, re 1V/µbar, +-1 db. The hydrophones are mounted in an oilfilled polyurethane pipe of 34 mm diameter, with a nominal density of 1.12 gr/cm3. The tow depth had to be controled by visual inspection. The streamer had to be deployed and recovered manually.
The signals recorded by the streamer were stored on a four-channel MBS / MES recorder, identical to those used in the ocean bottom seismic recorders. The streamer winch was placed midships about 8 m away from aft of the vessel.

Seismic source: 32 l BOLT Airgun
Three airguns Model 800 CT *BOLT* were used during the cruise; a photo of one gun is shown in Figure 5.3.3. The guns have a volume of 32 litres (2000 inch^3), and generate a signal with a main frequency centered around 6 to 8 Hz and including higher harmonics. The guns were deployed and towed from the assistant winch and beam normally used for the piston corer recovery. Trigger cables and airhoses were deployed manually. The guns were suspended on two floats with an additional float attached to the supply lines to prevent contact between the guns and the towing wire. They were towed 60 m behind the vessel and operated at 145 bar in 7 to 8 m depth. Due to good weather conditions the handling of the guns was smooth all the time.

During cruise SO179 more than 9100 shots were fired, at a 30 or 60 s shot interval. The ship's compressor system worked smoothly and caused no delays or interruptions.

External trigger
The trigger signal was supplied from the ships *Ashtech* GG24 GPS/Glonass receiver, and was available in the Geology Lab and the Seismic Lab. The receiver can provide a one millisecond long 5 V-TTL pulse at intervals between 0.2 and 999 s. The impulse should be stable within the accuracy of the GPS Time, which is 70 nanoseconds. The impulse was delivered to the *Longshot* trigger box. The shotbreaks, necessary for subsequent data processing and instrument location, were stored on a MBS recorder and displayed in real time to double check. For this process the same time basis was used as for the OBH and the trigger signal was converted into a 5 V TTL pulse of 250 ms length by a circuit provided from the ships technical support staff (WTD). Exact position calculation for the shot time should be done by later post-processing using shot time and UTC time values stored with DGPS coordinates in the ship's data base.

Figure 5.3.3: 32 l Bolt gun upon deployment onboard RV SONNE.

5.4 Magnetometer

For the magnetic measurements on cruise SO-179 a SeaSpy Marine Gradiometer System manufactured by Marine Magnetics Corp was used. It consists of two proton precession magnetometers, enhanced with the Overhauser effect, towed in-line at distances of 650 m and 800 m astern of the ship, resp. The gradiometer principle is based on the fact that, in a uniform field, two identical and perfectly aligned and synchronized sensors will give identical outputs which can be subtracted from one another to give zero output, effectively eliminating the presence of the field. Provided the sensors remain solidly fixed in relation to one another, the assembly can be rotated in space without producing an orientational output. If, however, there is a superimposed small field gradient (from magnetic anomalies derived from rocks beneath the sea bottom) as well the uniform field (the main Earth magnetic field), the output of the sensor combination will change as a function of the magnitude and direction of that gradient.

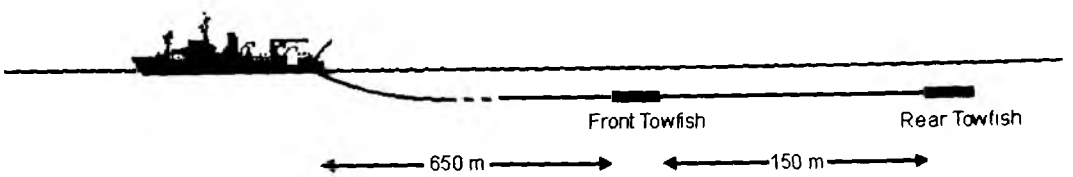

Fig. 5.4.1: Schematic sketch of the SeaSpy Gradiometer System setup

A standard proton precession magnetometer uses a strong DC magnetic field to polarize itself before each reading can be taken. An Overhauser sensor uses an AC magnetic field of radio frequency to polarize. The polarization power required is much smaller and the AC field may be left active while the sensor is producing a valid output signal. This allows the sensor to cycle much faster and produce more precise results than a standard sensor. The signal is digitized by the electronics assembly which then transmits the digital data string via the coaxial connection. The tow cable is connected to a deck leader which is in turn connected to the power supply and logging computer. As configured for this survey, the Overhauser sensors had a cycle time of one second, a sensitivity of 0.015 nT, and an absolute accuracy of 0.2 nT.

Unfortunately, ship operations did not allow the permanent deployment of the magnetometer system during the cruise. To retrieve OBH/OBS stations the ship must be completely stopped for some time and the magnetic outboard gear must be on deck while the ship is stopped. Airgun deployment and OBH/OBS deployment required a reduction of the ship's speed to 2 knots. At this speed the magnetic sensors would sink deep into the water with the risk of damage or even loss of the equipment. Therefore the magnetic outboard gear also has to be retrieved during this kind of operation, a procedure that for the complete gradiometer system needs approx. 30 minutes of time and assistance from the ship's crew to operate the boom. Neither the time nor the assistance could be provided for every maneuver. It was decided that only on longer transits (>20 nm) between OBS/OBH stations and then in most cases only standard single-sensor magnetic measurements could be carried out because the single-sensor system can be deployed and retrieved in less than 10 minutes.

In the single sensor mode, the Magnetometer was towed 300 meters aft of the stern of the vessel. During survey operations, the sensor operated at a depth of approximately 6 to 8 meters at 10 knots and 20 meters at 5 knots. During the time the three long refraction profiles were shot the full assembly of the gradiometer system was deployed. Due to a cable failure, the distance between the two sensors had to be reduced to 75 meters on two of the profiles.

5.5 Gravimeter

During the cruise SO-179 a sea gravimeter system KSS31 manufactured by the Bodenseewerk Geosystem GmbH was installed in the Gravity Laboratory one level below the main deck. The sea gravimeter was located approximately at the vessel's nominal water line, 1.5 m to portside from the centerline, and 48 m forward of the stern.

The gravimeter system KSS31 is a high performance instrument for marine gravity measurements. While the sensor is based on the Askania type GSS3 sea gravimeter designed by Prof. Graf in the 60ties, the development of the horizontal platform and the corresponding electronic devices took place at the Bodenseewerk Geosystem in the second half of the 70ties. The KSS31 system consists of two main assemblies: the gyro-stabilized platform with gravity sensor and the data handling subsystem.

The gravity sensor (Fig. 5.5.1) consists of a tube-shaped mass that is suspended on a metal spring and guided frictionless by 5 threads. It is non-astatized and particularly designed to be insensitive to horizontal accelerations. This is achieved by limiting the motion of the mass to the vertical direction. The main part of the total gravity acceleration is compensated by the mechanical spring, but gravity changes are compensated and detected by an electromagnetic system. A displacement of the spring-mass assembly with respect to the outer casing of the instrument is measured using a capacitance transducer. The output from the transducer is fed back into an electromagnetic moving coil system used for feedback control. A P-I feedback (P=Proportional, I=Integration) suppresses the accelerations of sea motion. An I-acting feedback provides a signal which drives the system to the zero position and represents an overcritical damping of the system. The current flowing through the moving coil is the measure for the gravity change.

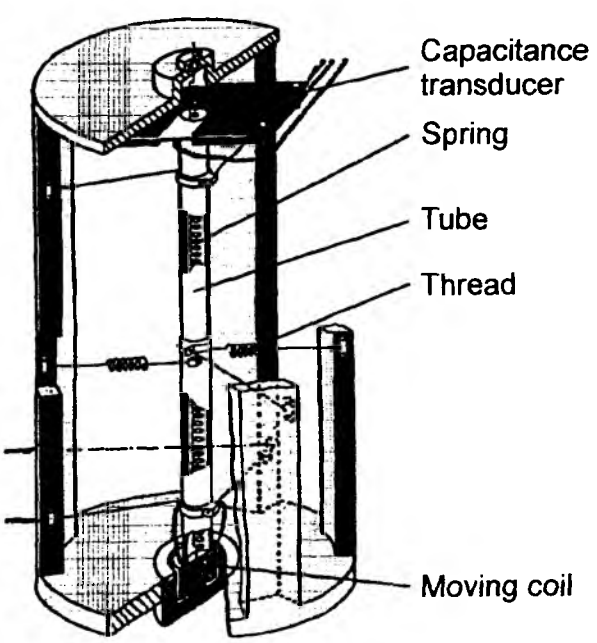

Fig. 5.5.1: Gravity Sensor GSS30 of the sea gravimeter system KSS31.

In addition to the spring-mass assembly as the gravity detector the sensor housing contains the control electronics that converts the current signal to voltage output and forwards it to the data handling subsystem. The power supply of the gravity sensor contains a sealed buffered battery unit with sufficient capacity to maintain the internal temperature stabilization of the sensor for 24 hours in case of main power loss. In case of system failure the sensor electronics activates automatically a caging mechanism preventing the spring-mass assembly from damage.

The leveling subsystem consists of a platform stabilized in two axes by a vertical electrically erected gyro. The stabilization during course changes can be improved by providing the system with online navigation data. The control electronics and the power supply of the platform are located in the data handling subsystem unit. Functions like gyro run-up and -down sequences and the automatic platform caging are performed by the system controller unit located in the data handling subsystem, too.

The stabilized platform will keep the sensor in an upright position with an accuracy of leveling in the order of 0.5 minutes of arc. This is particularly important as the sensor is very sensitive to tilting due to its very high accuracy. Vertical acceleration, however, cannot be eliminated. Luckily on a shipborne gravity system the vertical acceleration will periodically oscillate with a period of some seconds. This signal can be eliminated easily by means of electronic filtering.

6. Experiments completed and preliminary results
6.1 Magnetics and gravity
6.1.1 Magnetic data processing and first results

Onboard processing of the magnetic data included the removal of the International Geomagnetic Reference Field (IGRF2000) from the data and a thorough control of the data quality. The survey area off Java is located relatively far away from the magnetic dip equator (inclination 0°) which at this longitude lies far north of the geographic equator. Therefore the so-called equatorial electrojet and other ionospheric current systems which contribute to large daily variations and strong irregular changes during magnetic disturbances in the vicinity of the geomagnetic equator probably had no significant effect on the measurements. However, since the gradiometer could be used only during a part of the survey, a correction for daily variations will be necessary when a very high data quality with crossover-errors on the order of 10 nT is desired.

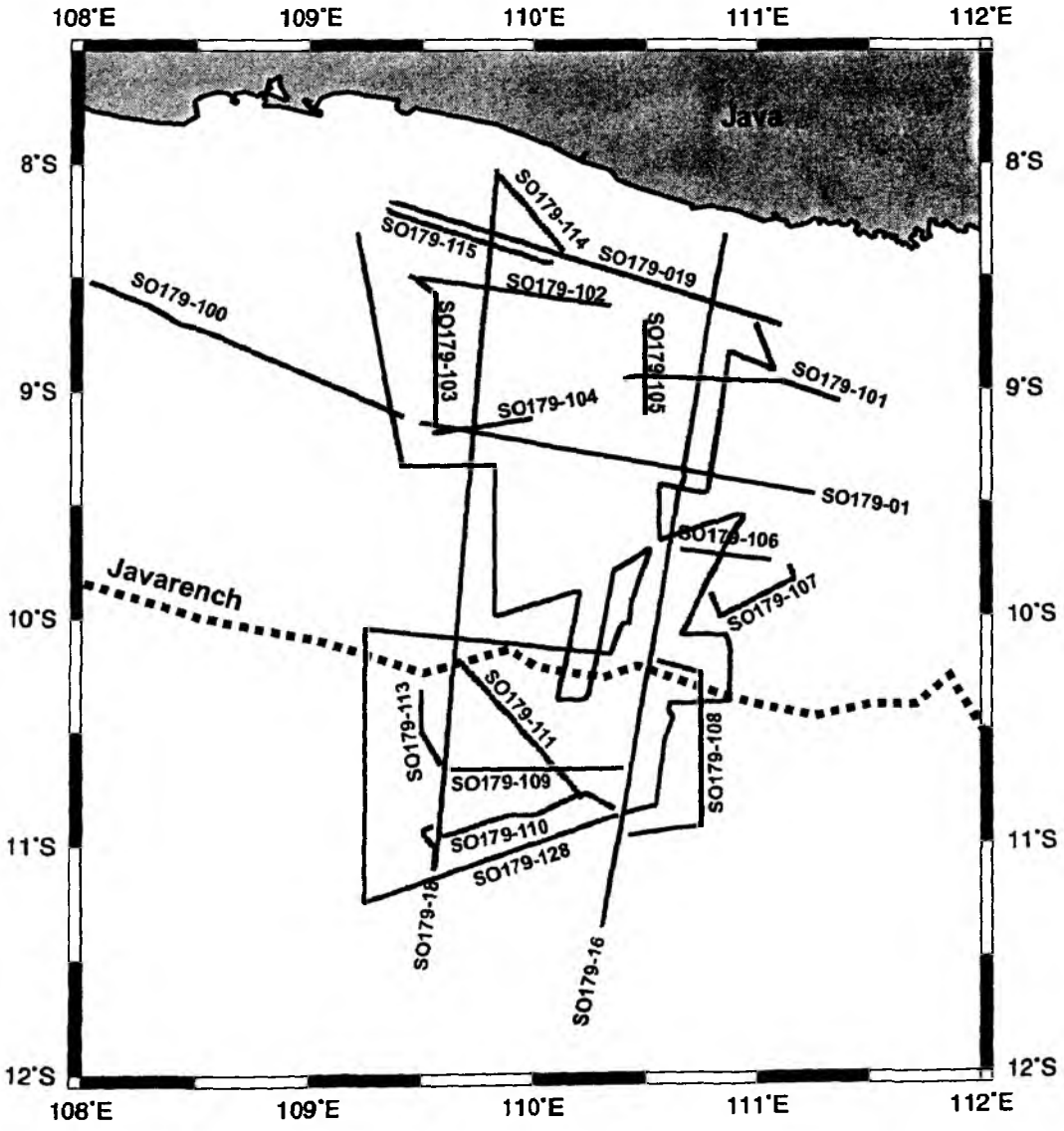

Fig. 6.1.1: Magnetic profiles of cruise SO-179

Altogether magnetic data were recorded on 35 profiles and a total of ~3700 km. The data coverage is not sufficient to compile a map of the magnetic anomalies in the survey area from these data alone. Therefore, the magnetic data from SO-179 were merged with data from two other sources: (1) The magnetic anomaly map of East Asia (Ishihara, 1996) provides gridded data for the northernmost part of the survey area and (2) the GEODAS marine geophysical data colletcion (NGDC, 2002) contains a number of magnetic profiles acquired at different times by different research vessels transiting through the survey area. Most of the GEODAS profiles are more than 20 years old. They were reprocessed by subtracting the appropriate geomagnetic reference field from the original data which are available from the CD-ROM. The resulting magnetic magnetic anomaly map is shown in Fig. 6.1.2.

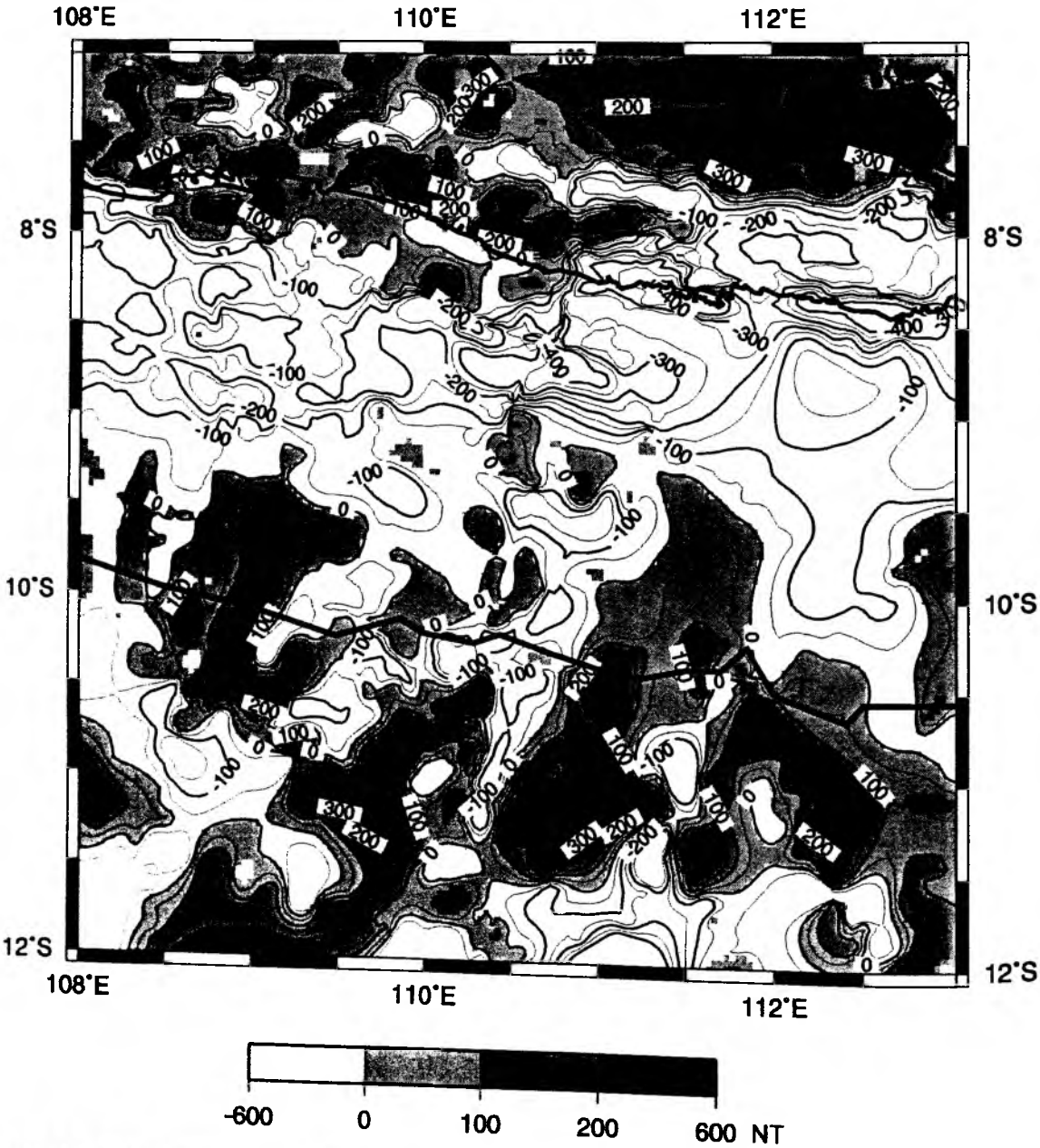

Fig. 6.1.2: Preliminary map of magnetic anomalies in the survey area of cruise SO-179. Data compiled from SO-179, National Geophysical Data Center (2002), and Ishihara (1996).

First results

North of the survey area, the island of Java is dominated by a high amplitude positive magnetic anomaly, superimposed by local anomalies which can in many cases be correlated with volcanoes. Offshore and mainly coincident with the forearc basin, a deep negative anomaly is being observed which is most probably not derived from the sedimentary fill of the basin, but rather the corresponding anomaly to the positive anomaly to the North. In the area of the forearc high, a number of short-wavelenght isolated positive anomalies indicate source rocks at shallow depth. These anomalies coincide with bathymetric and gravimetric highs. Towards the trench a series of SW-NE striking anomalies follows which continue through the trench into the oceanic crust where their amplitude increases. This clearly indicates that these anomalies are derived from the oceanic crust and fade away with the increasing subduction depth of the downgoing plate. This is a surprising result since the oceanic crust of the Australian plate in the survey area was expected to be a part of the Cretaceous Magnetic Quiet Zone (CMQZ) (Cande et al., 1989) where a very uniform magnetic field should be observed. A comparison with the seafloor topography shows that the magnetic anomalies of the oceanic crust cannot be attributed to seamounts and other topographical features. Instead it has to be assumed that the anomalies represent seafloor spreading anomalies of unknown age. One long magnetic profile from the GEODAS data source extends more than 1000 km parallel to the coast of Java and crosses the survey area. This profile gives a strong indication that seafloor anomalies extend through the survey area in western direction to a point near Christmas Island, where the amplitude of the anomalies decreases sharply, which might be interpreted as the beginning of the CMQZ (Fig 6.1.3).

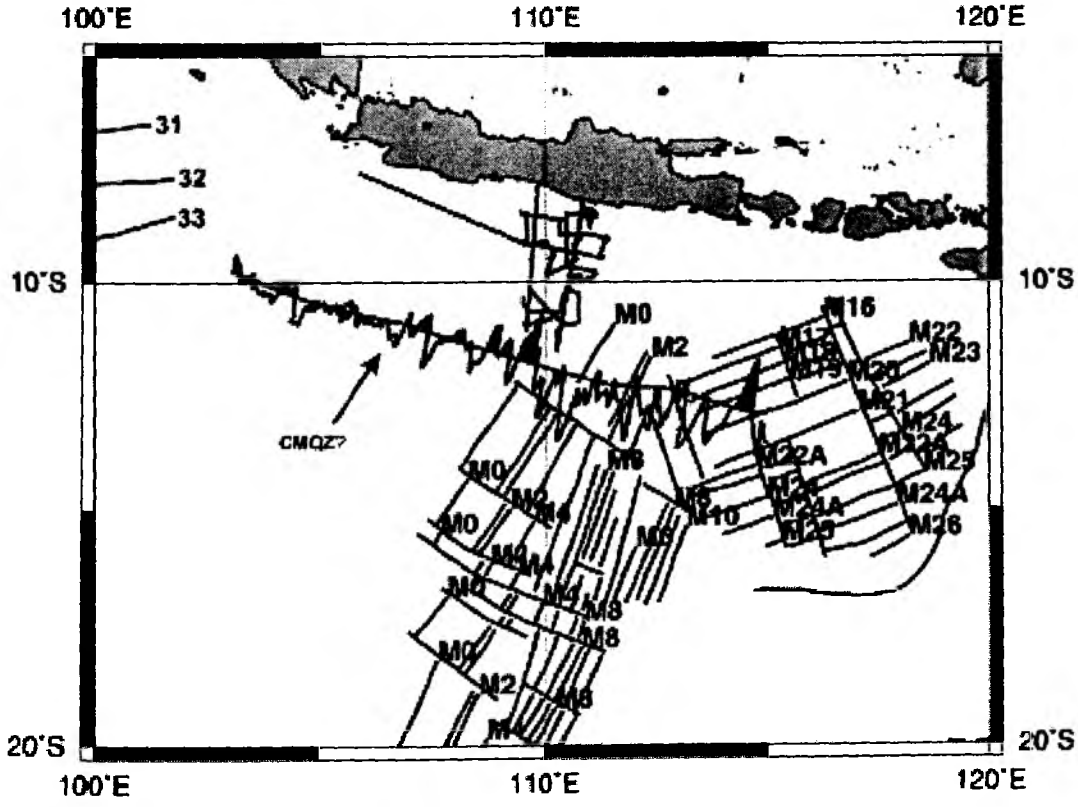

Fig. 6.1.3: Magnetic lineations around the SO-179 survey area after Cande et al. (1989) and one magnetic profile indicating that seafloor spreading anomalies probably extend further to the west

6.1.2 Gravity data processing and first results

Processing of the gravity data consists essentially of the following steps:

- a time shift of 175 seconds due to the overcritical damping of the sensor,
- conversion of the output from reading units (r.u.) to mGal by applying a conversion factor of 0.94542 mGal/r.u.; this is done internally in the gravimeter,
- connection of the harbour gravity value to the world gravity net IGSN 71,
- correction for Eötvös effect using the navigation data,
- correction for the instrumental drift,
- subtraction of the normal gravity (WGS67).

As a result, we get the so-called free-air anomaly (FAA) which in the case of marine gravity is simply the observed gravity minus the normal gravity. According to the selectable time interval of the data acquisition system, gravity values are available every second.

Gravity ties to land stations

To compare the results of different gravity surveys the measured data have to be tied in a world-wide accepted reference system. This system is represented by the International Gravity Standardization Net IGSN71 (MORELLI, 1974).

The IGSN71 was established in 1971 by the International Union of Geodesy and Geophysics IUGG as a set of world-wide distributed locations with known absolute gravity values better than a few tenths of mGal. According to the recommendations of the IUGG, every gravity survey, marine or land, should be related to the datum and to the scale of the IGSN71.

Therefore, gravity measurements at land have to be carried out to connect the gravity measurements at sea with the IGSN71. The marine geophysical group of BGR uses for the gravity connections a LaCoste&Romberg gravity meter, model G, no. 480.

The point description and gravity value of reference IGSN71 station in Jakarta was kindly provided by the Bureau of Meteorology and Geophysics (Jakarta, Indonesia).

R/V SONNE moored at the pier of Tanjung Priok (Jakarta) in the southwestern corner of „No. 3 Basin", next to storehouse 304. On September 16 and 17, tie measurements to point **A** on the pier opposite the Gravity Laboratory on R/V SONNE have been made. Point **A** is located 850 m from the northwestern end of the pier (see Fig. XX).

The connection measurements resulted in an average absolute gravity value of 978146.52 mGal (with water level –1.0 m, IGSN71) for point **A** at the water level. The reading of the KSS31 at the leaving time (September 17, 2004, 01:00 UT) from the pier was –1710.60 mGal.

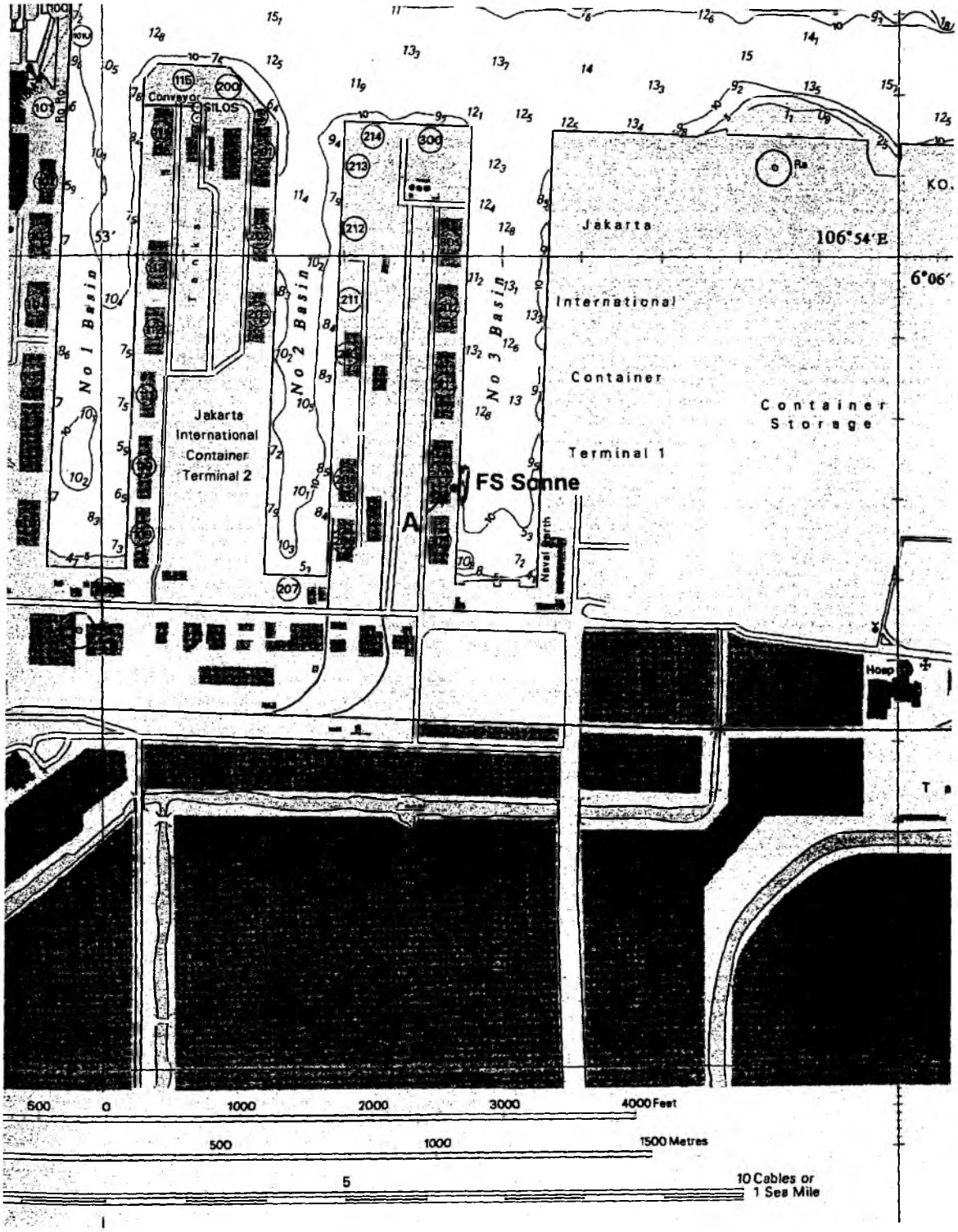

Fig. 6.1.4: Location of the mooring site of R/V SONNE at the pier of Tanjung Priok (from the Admiralty chart 932, Pelabuhan Tanjung Priok, scale 1:12500).

Table 6.1.1: Observation report of the gravity tie measurements in Jakarta and Tanjung Priok.

Station	Date	Time UT	Reading units	Measured value [mGal]	Drift correction [mGal]	Corrected gravity [mGal]
BGR / K	26.07.04	13:30	4813.20	4890.47		
01 / B	16.09.04	05:26	1751.49	1777.47		
A / K	16.09.04	08:38	1748.10	1774.03		
A / B	17.09.04	00:17	1748.17	1774.10		

Observers: K = Kewitsch, B = Barckhausen
Gravity in mGal was calculated using LCR G 480 scaling table.

Reference Stations:

BGR: Pillar, Room No. VB11 981267.73 mGal (IGSN71)
01: Bureau of Meteorology and Geophysics (BMG) 978149.68 mGal (IGSN71)
Jakarta 10720
Jl. Angkasa 1, Kemayoran
5.0 m above main sea level

Gravity station:

A: Tanjung Priok pier, 850 m from northwestern end of the pier, opposite storehouse 304

Differences between reference/gravity stations:

A – 01 = - 3.43 mGal

Absolute gravity at **A:** 978146.25 mGal

Absolute gravity for A (reduced to water level –1.0 m) 978146.52 mGal (IGSN71 system) used for the gravity tie on 17.09.2004 (00:55 UT).

BGR – 01 = + **3113.00** mGal (own measurements)
= + **3118.05** mGal (according to given IGSN71 values)

The difference between the reference points **BGR** and **01** derived from our own measurements seems to be quite far off the value calculated from the given ISGN71 values. But it has to be taken into consideration that the reading at BGR was taken two months prior to the cruise and that the gravity meter was transported to Jakarta in the meantime with the sensor heating switched off. Under these circumstances an instrumental drift of 5 mGal between the readings at **BGR** and at **01** seems possible. The absolute gravity found for point **A** differs by less than

0.1 mGal from the values derived for two points at the neighbouring pier where Sonne was moored during the cruises SO-98 (1994) and SO-137 (1998).

Reading of sea gravimeter KSS31 at 17.09.04, 00:55 UT: -1710.60 mGal (scale factor 0.94542 mGal/r.u. applied)

At the end of the cruise R/V SONNE will moore on October 06, 2004, in Chilacap. At the General Goods Wharf of Chilacap harbour, a gravity base station was established and marked by the Marine Geological Institute at Bandung in 1999 to make a gravity tie possible for a stopover of RV Sonne during cruise SO-137 (Hutagaol, 1999). This gravity base station will be reoccupied at the end of cruise SO-179 to derive the absolute gravity at the mooring site on Oct. 6, 2004.

The instrumental drift of the KSS31 can be derived from the readings at the beginning and the end of the cruise and then be applied to correct the gravity data.

First results

The sea gravimeter worked continuously and so gravity values were recorded along the complete track of the ship (Fig. 6.1.5). Thus about 4500 km of gravity profiles were measured during the cruise. The data quality is good except for times when the ship performed sharp turns. The latter is due to the fact that we could not use the active stabilization of the horizontal platform by providing it with real-time navigational data on this cruise.

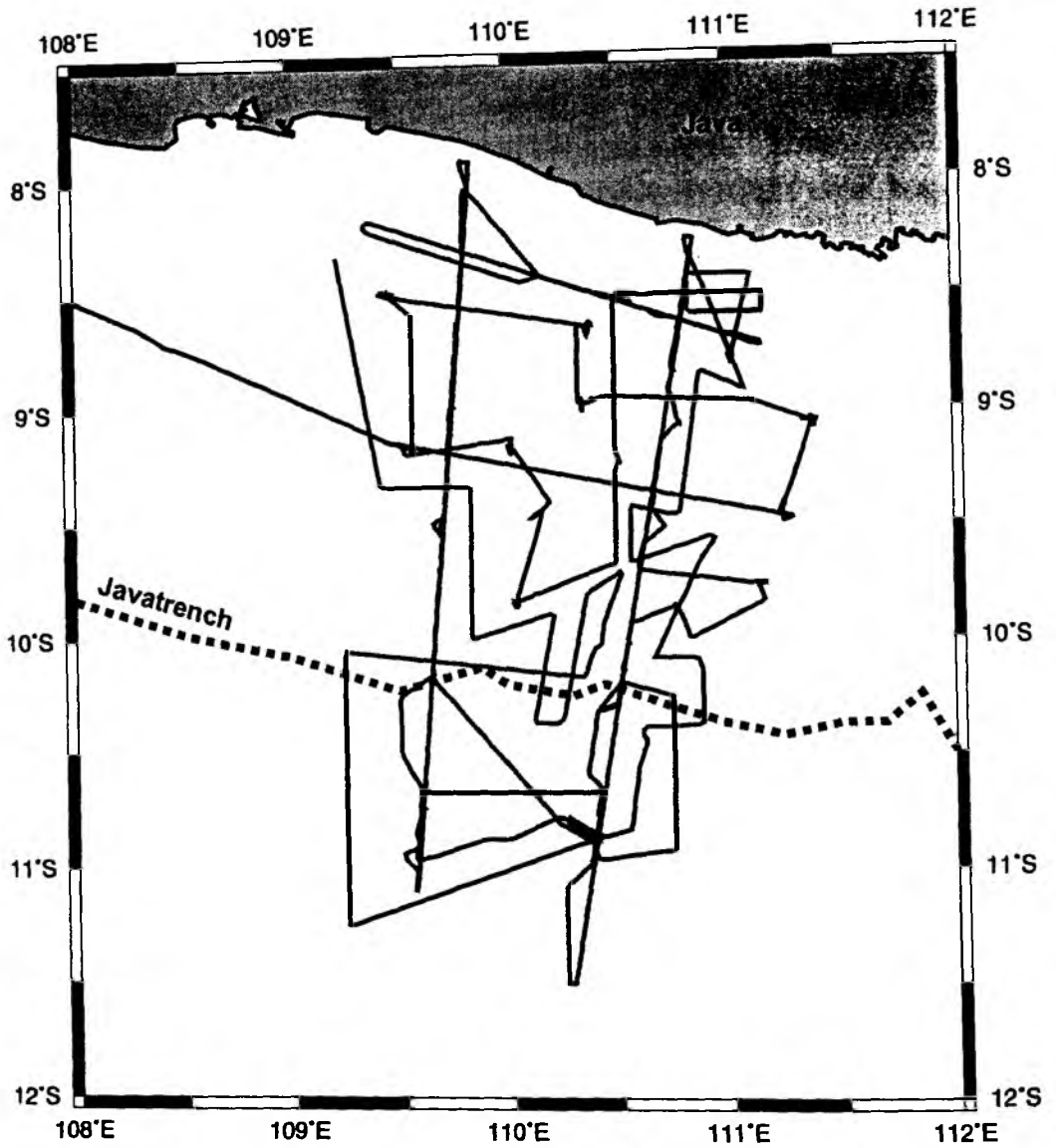

Fig. 6.1.5: Gravimetric profiles of cruise SO-179

Although the profile coverage of the survey area is not uniform, it is sufficient to compile a preliminary map of the free-air anomalies (Fig. 6.1.6). The gravity map is dominated by the anomalies derived from the main topographic features in the survey area. The oceanic crust in the South is characterized by positive values (0 to +40 mGal) and the isolated positive anomaly of a seamount. Such positive anomalies are not observed in morphologically undisturbed oceanic areas. The positive anomaly at the southern edge of the survey area results from the subduction bulge due to the downgoing lithosphere. It corresponds to a gravimetric low of -125 mGal over the up to 7500 m deep trench. Landward in the area of the outer arc high, a zone of relative maxima is being observed. In this 60 km wide zone the water depth is in places only 500 m and the gravity reaches locally positive values in a generally negative environment. Adjacent to the North, the gravity map shows an elongated minimum zone parallel to the trench which is derived from the forearc basin, filled with sediments of relatively low density. Gravity values over the forearc basin are comparable to those over the trench. Around 110°E, this minimum zone is interrupted by a small positive anomaly which almost bridges from the strong positive anomaly area close to the coast to the forearc high.

This structure can only partly be explained with the seafloor topography, a rock unit of higher density must be present in that area beneath the seafloor. In general, the typical situation of convergent margins is being observed where the plate driving forces hold up the arc and force down the trench out of the isostatic equilibrium.

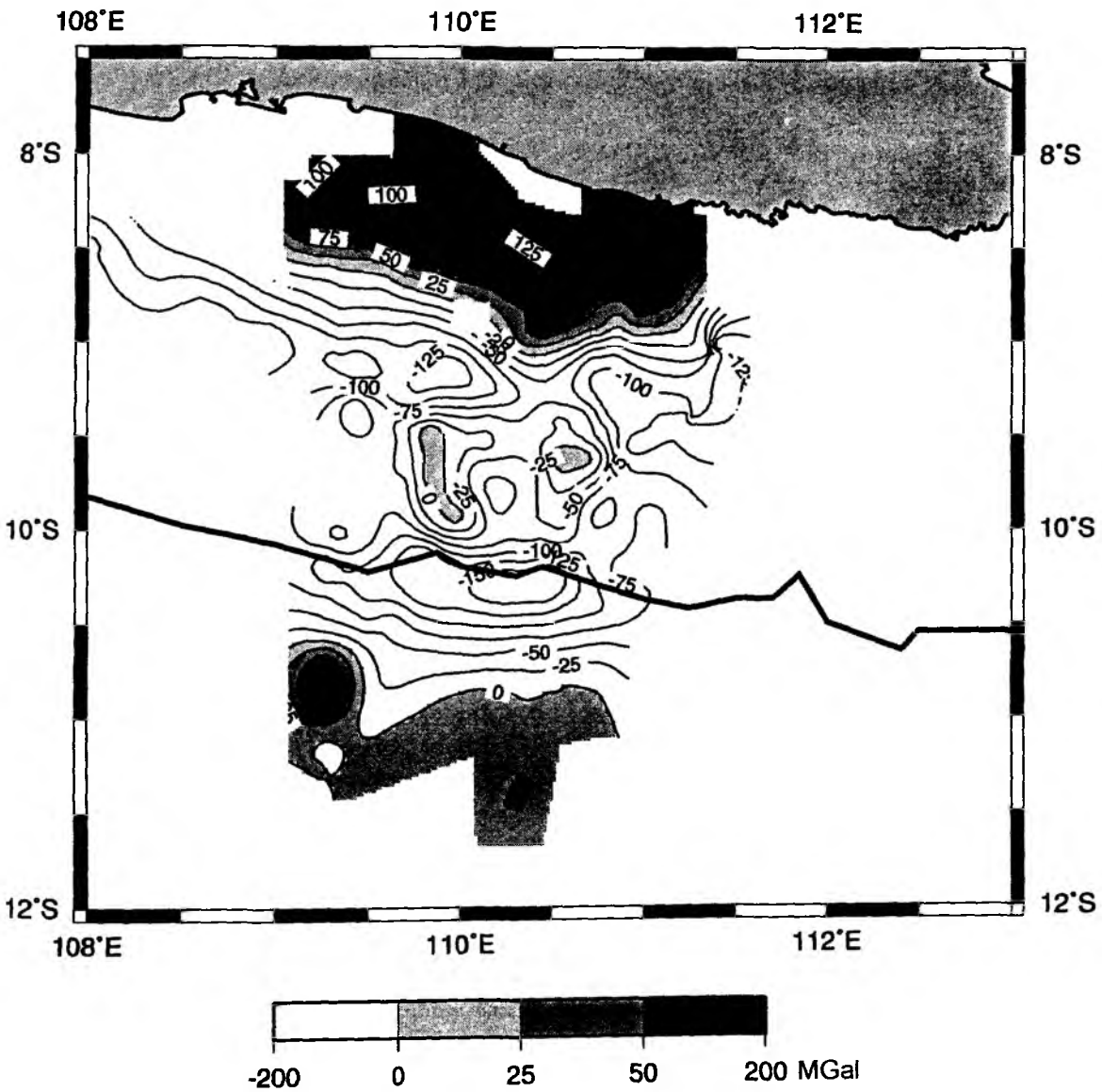

Fig. 6.1.6: Preliminary map of free-air gravity anomalies in the survey area of cruise SO-179

6.2 Seismology

Seismological aspects of the MERAMEX- project

The MERAMEX-project comprises several subtopics; one of them is the operation and later interpretation of a temporary seismological network. The main objectives of this network are:

- The seismic gap south of Java at 100° east seems to characterize the seismogenic zone along the Sunda subduction zone. The seismogenic zone in extension of the gap under the Java Sea in the north shows a pronounced accumulation of hypocentres in much greater depth. The monitoring of the earthquake wavefields provides information about the seismic coupling zone offshore Java and the crustal region above subduction earthquakes.
- Resolving a structural image from local and teleseismic events (tomography).
- The seismic observation network is an important support for the determination of the local and regional stress distribution and for the definition of the position and importance of the Merapi complex in the convergence zone between oceanic and continental plates.
- The determination of the regional stress orientation due to focal mechanisms, moment tensor inversions and determination of the stress drop via adjustment of amplitude spectra.
- Determination of Qp
- Different tomographic methods and seismic velocity determination shall reveal the internal structures of the Merapi volcanic system down to the source area at the Wadati Benioff zone.

A temporal seismological network consisting of 115 mobile seismic stations, was installed in a dense grid of about 10-20 km station distance around the Merapi volcano in Central Java (200* 125km) in Mai 2004. Onshore, both short periodic, three component Mark seismometers (L4-3D) in combination with a data logger called EDL and 16 broadband stations are used.
Since most events have their source in the coupling zone in the subduction zone offshore Java, 14 OBH/S stations were deployed south of Java with 20 – 50 nm station distance and depths between 990 – 3300m during SO176 in May 2004 to better resolve events down to 300 km depth. They comprise five OBS stations with four components (one hydrophone and the Webb seismometer) and nine OBH-stations. Data were recorded on MLS recorders with a sampling intervall of 50 msec. On two instruments the hydrophone was replaced by a Differential Pressure Gauge (DPG). The location is shown in Figure 6.2.1.
The operating life of the stations offshore is about 4-4.5 months, the ones onshore were in operation for about 4 months.

Processing

The data were transferred from datalogger to pc and converted with SEND2PAS into Passcal format. In the next step the REF2SEGY program converts the Passcal output to a pseudo SEGY trace. For each channel one file is created with the name derived from the start time, the serial number of the datalogger and the channel number. REF2SEGY will create a so-called `R`-directory containing the pseudo-SEGY data files. In the following step it is possible to convert the pseudo-SEGY format into SAC with SEGY2SAC or GSE format. After picking phases in SAC2000 one can locate hypocenters for example with HYPOSAT (Schweitzer, 2001).

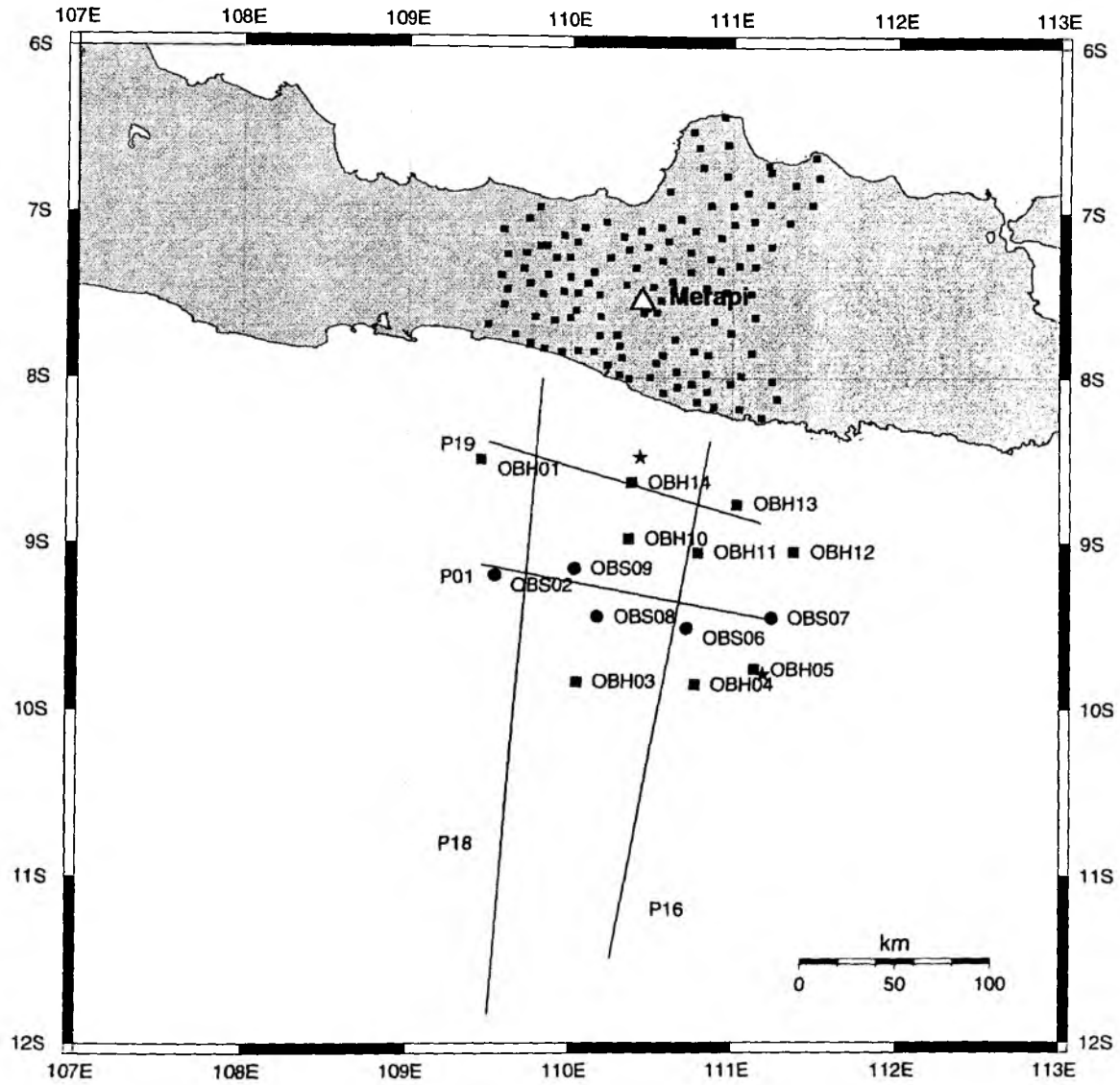

Figure 6.2.1: *Overview map showing refraction seismic profiles (P01, P16, P18, P19) and location of OBS-stations type: WEBB with 4 components (circles) and OBH-stations with hydrophones type: HTI (squares) deployed in May 2004 on SO176 cruise. Offshore, 115 short periodic and 16 broadband seismometers were installed. Profile P01 was shot before the network was recovered, during shooting of P16 only four stations (OBH04, OBH05, OBS07 and OBH11) remained active. One can also see the locations of two earthquakes (stars) next to OBH14 and OBH05, which will be shown in the following examples.*

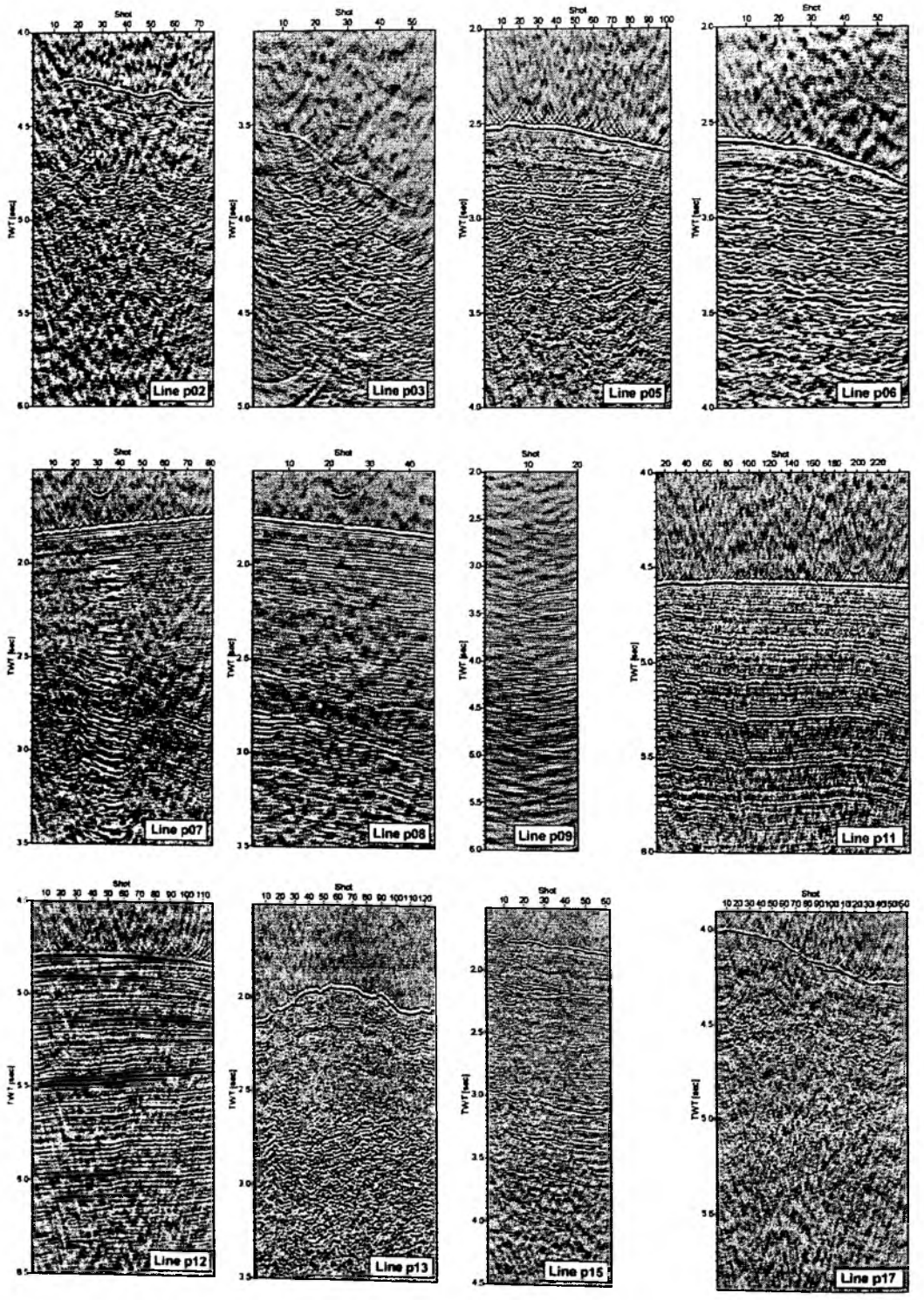

Figure 6.2.2: Streamer sections of cross profiles for exact relocation of a station

Due to the drifting of the OBH and OBS instruments during sinking and recovering, the OBH positions may be dislocated by up to several 100 m. Two short cross (see Figure 6.2.2) profiles were shot over the stations to calculate exactly their position on the seafloor. Since an assumed incorrect location leads to asymmetry of the direct wave, this can be corrected using the program RELOBS. For input, the assumed OBH location, shot locations and the picked traveltimes of the direct wave near to its apex are needed. Also, the true orientation of the two horizontal components can be determined.

Recorded data and local earthquake examples

The four component stations (OBS02, OBS06, OBS07, OBS08 and OBS09) registered the local seismicity in a quite good data quality, showing many local events. OBS07 recorded only till August 2004 due to an early closing of the cards storing the data.
Most hydrophones have a worse signal to noise ratio than the OBS-instruments. Some of them are overamplified (clipped). Sometimes the hydrophone recordings are interrupted due to gaps in the recorded data. OBH10 provided continuously a better data quality compared with the other hydrophones (see Figure 6.2.7b)
In the following figures we show plots made by using PQL-plot (Pascal Quick Look).
The filename on the left side of the seismograms can be read like the following example: obs09_04_205_21.01hrs.1
obs09 = instrument
04 = year
205 = julday
21.01 = the start time of the displayed section
hrs = the length of the file, here one hour
1 = the channel (can be either 1: hydrophone, 2: vertical, 3 or 4: horizontal)

The coordinate systems of the PQL-plots consist of three different axes. The y-axis illustrates the number of registered counts, the x-axis at the bottom of the figures shows both the whole length of the file and the displayed zoomed section (thick black lines). And finally, the upper x-axis shows the actual length of the displayed section. The data has to be read from the RSEGY format used by PQL-plots.

In the following we show the data quality of two local events:
The data of these local events can be found in Indonesian earthquake lists in the world wide web. In both examples we show the data recorded on station OBS09, which generally has a good data quality throughout the recording period. The OBS09 provides all four components for both local events. The events were also recorded on OBS02, OBS06 and OBS08. But the data quality on these three stations is not as good as that of station OBS09- worse signal to noise ratio and sometimes one of the four components is missing. Unfortunately, OBS07 did not record this event due to the closed flash cards.

Figure 6.2.3. shows seismograms of a local earthquake (see asteriks in Figure 6.2.1 next to OBH14, 8.48°S / 110,43° E). The event took place on July 23, 2004 (Julian day 205) at 21:46:49 in approximately 15 km depth and has a magnitude of 4.87 Ml. The traces in Figure 6.2.3. are filtered using a bandpass filter of 5- 20 Hz. Figure 6.2.3.a illustrates the whole coda (120 s) and Figure 6.2.3.b a 30 s section of the event. Figure 6.2.4 shows the frequency spectra of each component of the seismogram sections.

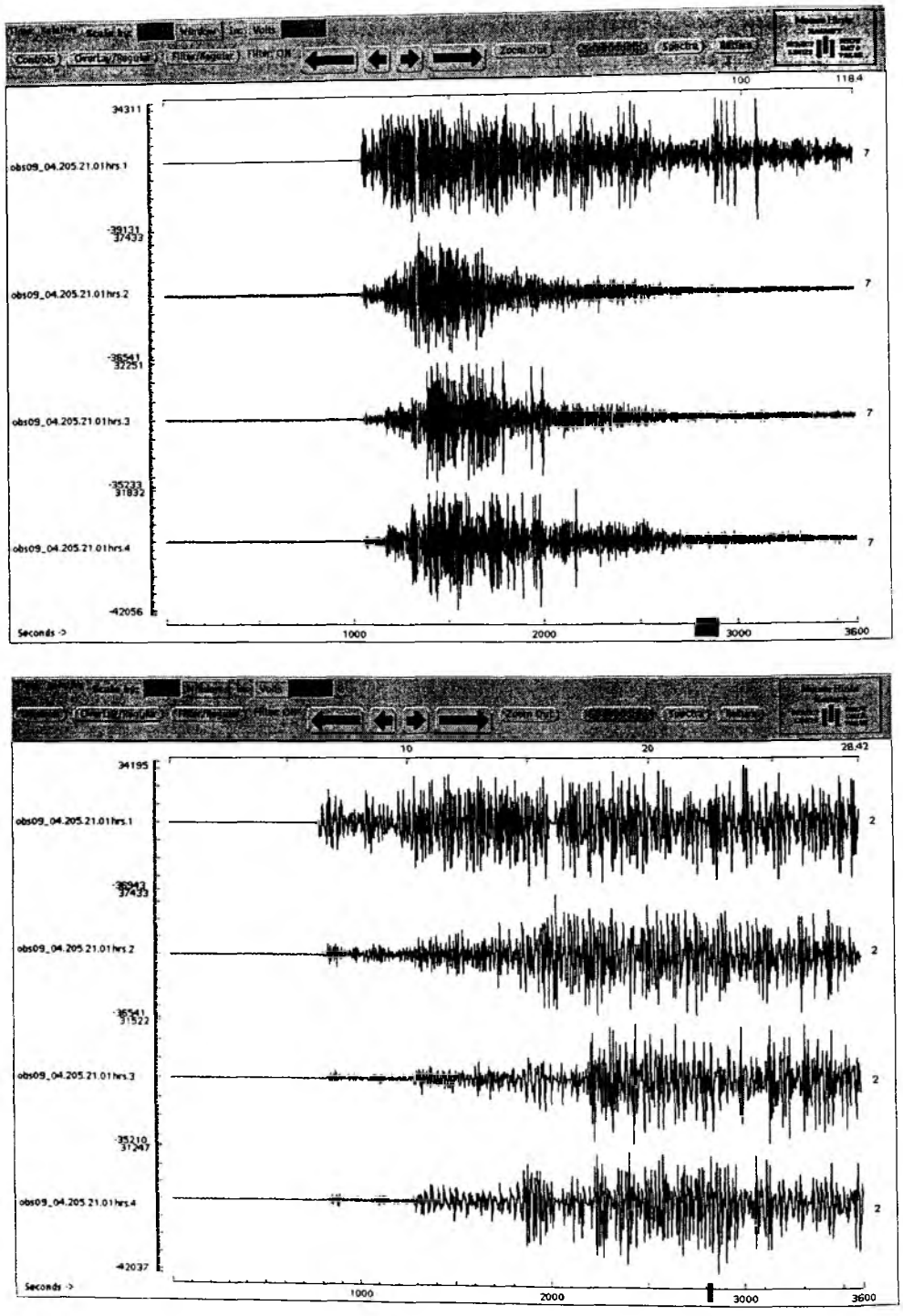

Figure 6.2.3a/b: *Local event on July 23, 2004 (Julian day 205) at 21:46:49 in 15 km depth: 8.48° S, 110,43° E; 158 km south of Wonosari. Magnitude: 4.87 Ml. Both diagrams show filtered data of OBS09 using a bandpass filter of 5- 20 Hz. Figure 6.2.3.a illustrates the whole coda (120s) and figure 6.2.2b only a 30 s section of the event. The seismograms provide a clear p-phase onset and a PwP-Phase after 3 sec.*

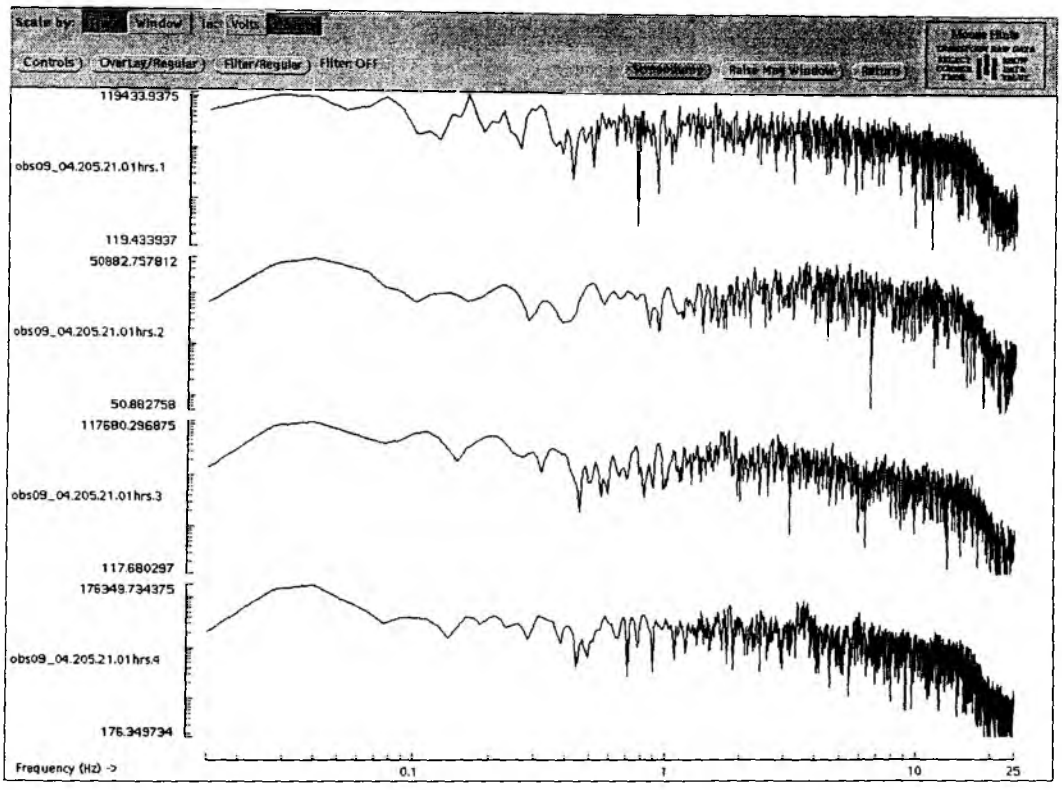

Figure 6.2.4: *Frequency spectra (from raw data) of event shown in Figure 6.2.3. The x-axis shows the frequency in a logarithmic scale [Hz]. The y-axis illustrates the counts/frequency. There is no significant gap over the whole frequency band. Over a wide range energy is registered.*

The second example of a local earthquake is illustrated in Figure 6.2.5. The epicenter location is at 9.79°S / 111,19° E (location in Figure 6.2.1 next to OBH05). The event took place on August 3rd, 2004 (Julian day 216) at 16:30:04 in approximately 15 km depth and has a magnitude of 4.92 Md.

The seismograms in Figure 6.2.5 are filtered using a bandpass filter of 5- 20 Hz. Figure 6.2.5.a illustrates the whole coda (120 s) and figure 6.2.5.b a 30 s section of the event. Figure 6.2.6 shows the frequency spectra of each component of the seismogram sections.

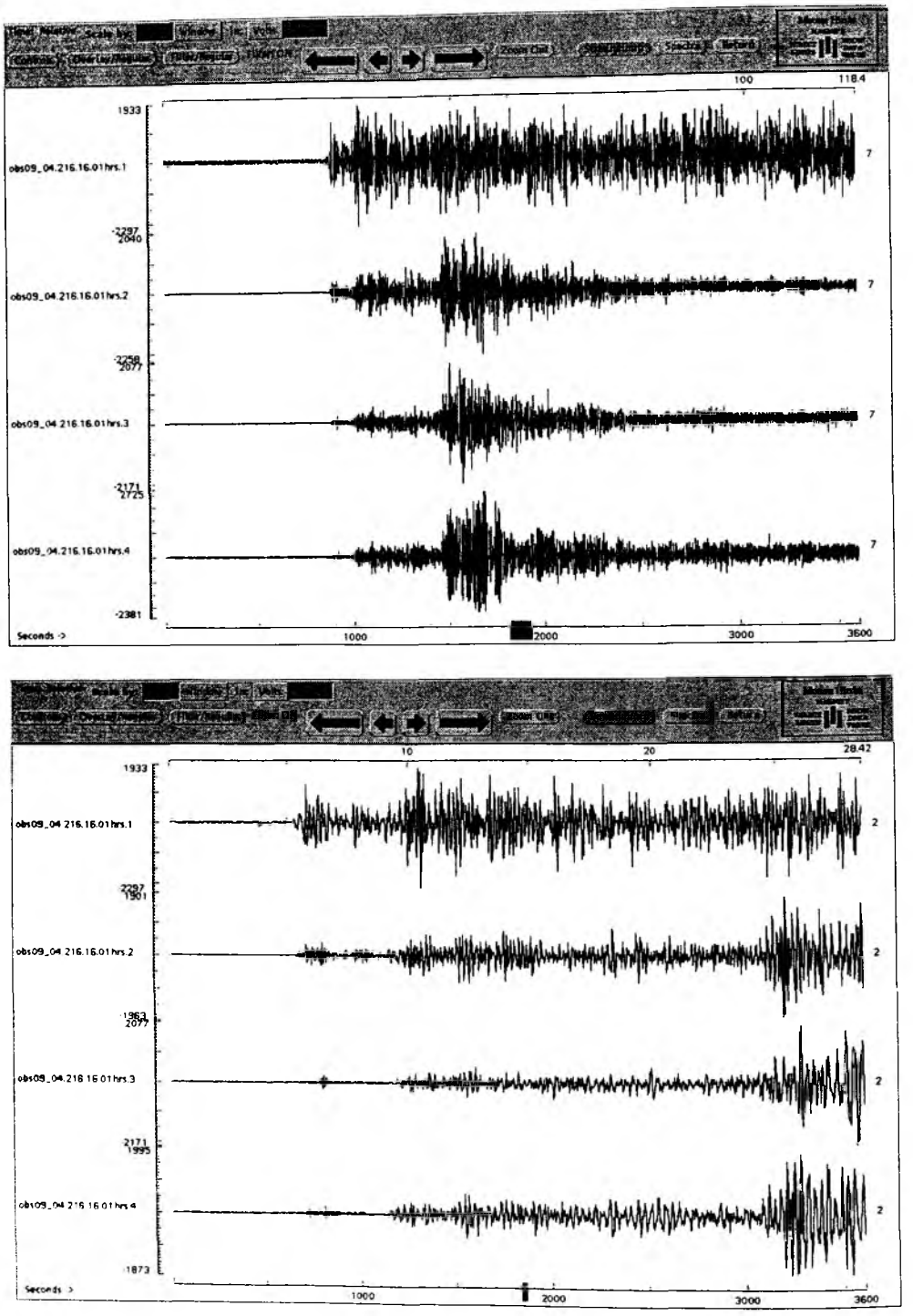

Figure 6.2.5a/b: *Local event recorded on August 3rd, 2004 (Julian day 216) at 16:30:04 in 15 km depth at station OBS09: 9.79°S , 111,19° E; 177 km south of Pacitan. Magnitude of 4.92 Md. Both seismograms are filtered using a bandpass filter of 5- 20 Hz. Figure 6.2.5.a illustrates the whole coda (120 s) and figure 6.2.5.b a 30 s section of the event. On every channel a clear p-phase onset is provided and a s-phase after 20 sec.*

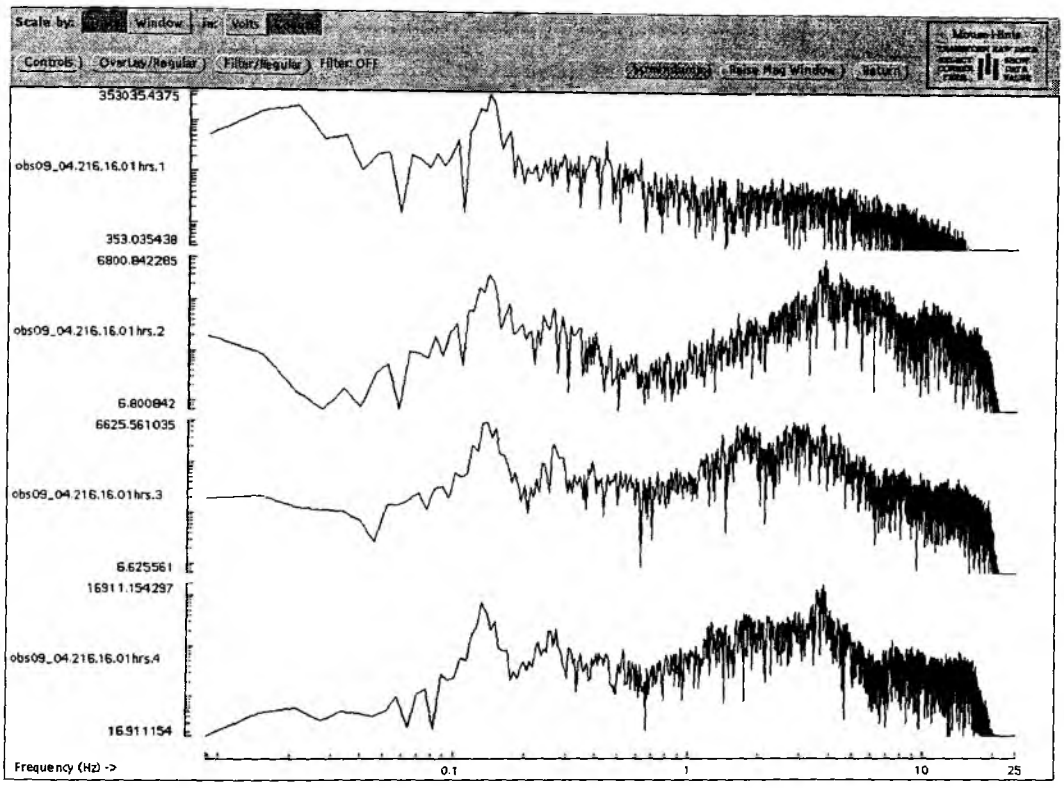

Figure 6.2.6: *Frequency spectra of the event recorded on August 3rd. The x-axis shows the frequency in a logarithmic scale [Hz]. The y-axis illustrates the counts/frequency. These spectra show a energy gap between 0.3 and 2 sec. There is a maximum between 0.1 and 0.2 sec due to the ocean microseismicity.*

We plotted some seismogram sections of a local earthquake to show the data quality of every hydrophone- component of each station. The traces in Figure 6.2.7a/b are sorted by onset-time of p-wave respectively s-wave. One can see the time-delayed s-wave onset due to the increasing distance from the first trace with respect to the epicenter of the earthquke. The upper part of Figure 6.2.7.a/b is filtered with a bandpass of 5 – 20 Hz compared with the raw data in the lower part. The unfiltered traces show that OBH10 has a quite good data quality. Most stations are noisy due to the typical ocean noise.

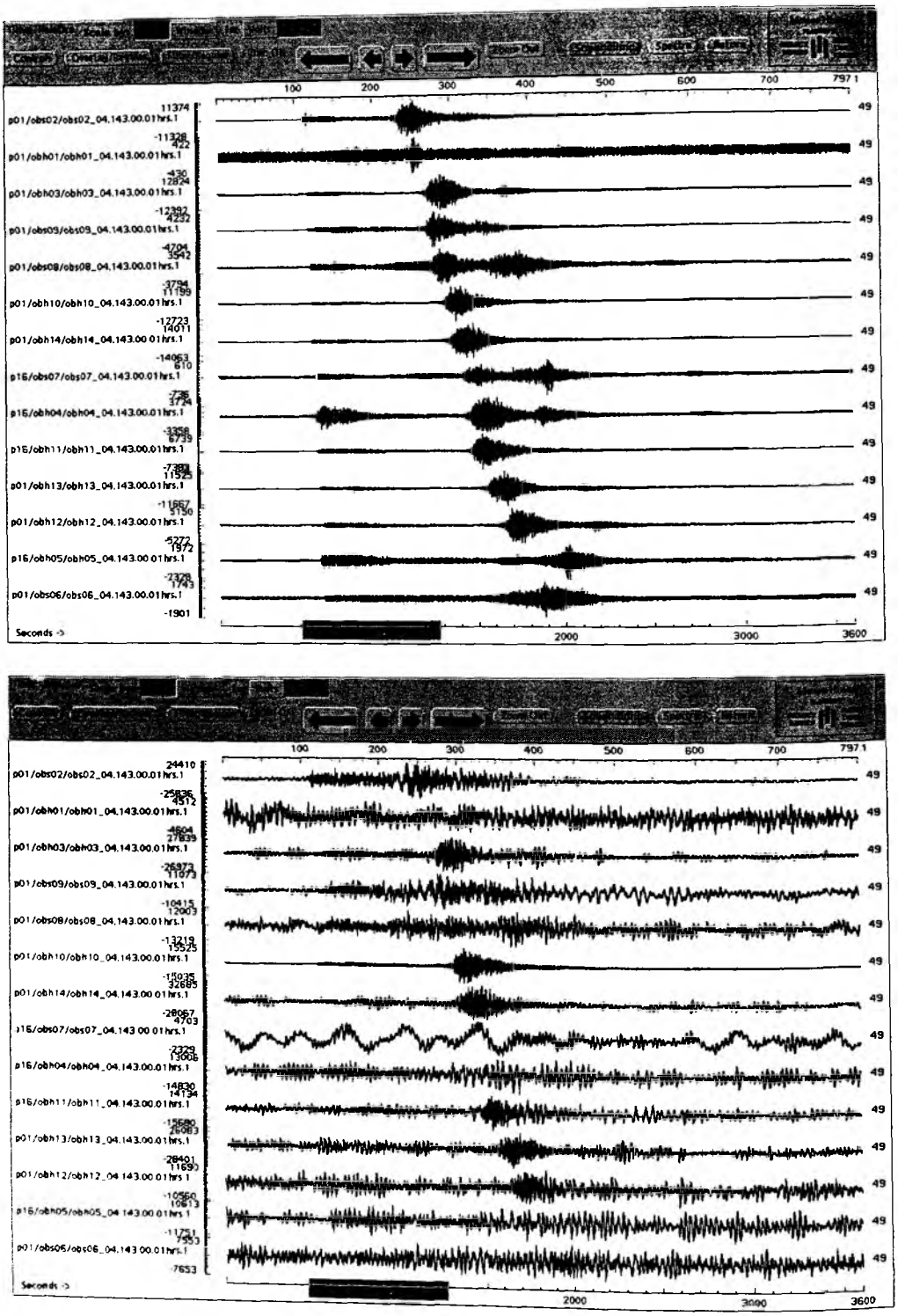

Figure 6.2.7a/b: Seismogram section of a local event recorded at the beginning of the experiment. The traces are sorted by onset time of p- and s-waves. The upper diagram shows filtered data using a bandpass filter (5 – 20 Hz) and the lower diagram shows the raw data.

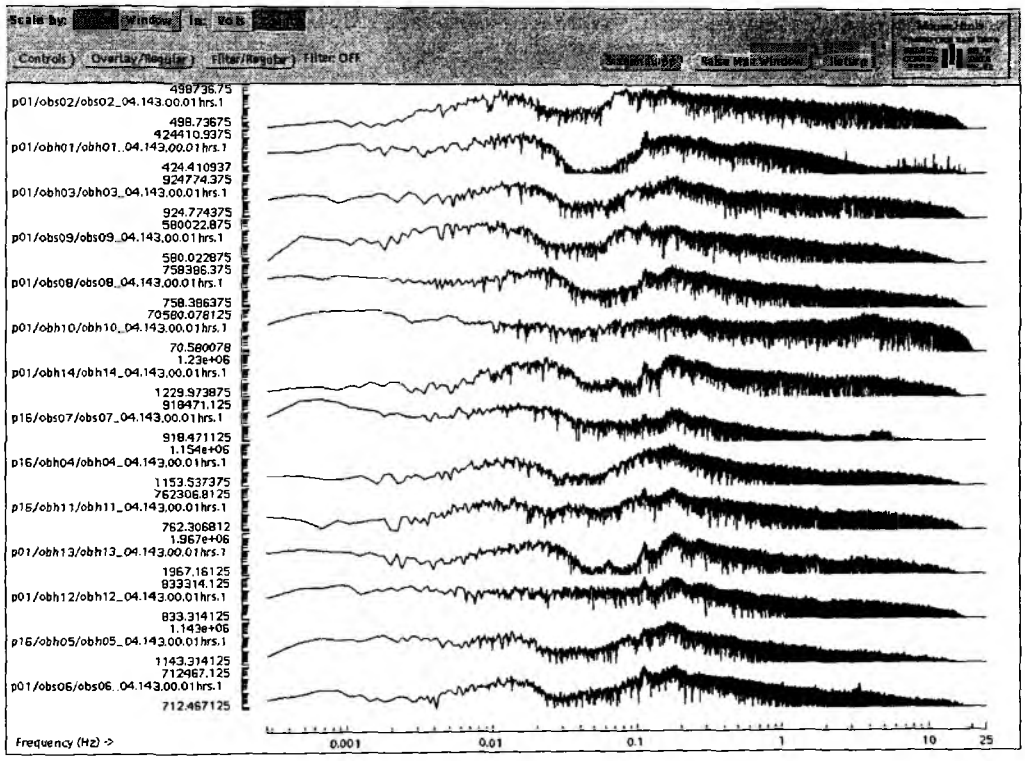

Figure 6.2.8: *Frequency spectra of event shown in Figure 6.2.7b. The x-axis shows the frequency in a logarithmic scale [Hz]. The y-axis illustrates the counts/frequency. Compared with Figure 6.2.6 these spectra provide an energy gap at lower frequencies between 0.02 and 0.1 Hz. The peak near 0.1 Hz is a typical noise peak on the ocean floor.*

6.3 Seismic processing: OBH/OBS wide-angle data

• The processing scheme

The OBH/S data recorded in continuous mode on the MLS and MBS units have to be converted into standard trace-based SEG-Y format for further processing. The necessary program structure was mainly taken from the existing REFTEK routines and modified for the OBH requirements and IFM-GEOMAR´s hardware platforms.
The flow chart shown in Figure 6.3.1 illustrates the processing scheme applied to the raw data. A detailed description of the main programs follows below:

send2pas
For the PC-cards used with the MBS and MLS recorders, data expansion and format conversion into REFTEK data format is performed using a DOS/Windows based PC. The program send2pas reads data from the flashcards used during recording. Decompressed data are written onto the PC's hard disk using PASSCAL data format. Either 16 or 32 bit storage is available. After ftp transmission to a SUN workstation, ref2segy and all other software can be used to handle and process the data files and store them as SEG-Y traces.

While processing the MLS recordings many time slips of one sampling interval were detected by the send2pas software, typically at a rate of one time slip every 1-2 hours. The time slips are caused by mismatch of the actual sampling rate of the MLS recorder compared to the desired sampling rate. This mismatch arises because the clock rate of the crystal oscillator in the MLS recorder is temperature dependent (Klaus Schleisiek, SEND GmbH, pers. comm.). The temperature dependence is known and corrected for in the determination of the system time, but for performance reasons the sampling pulses are directly generated from the oscillator signal without any time correction. The send2pas routine detects when the accumulated inaccuracies of the sample rate cause an effective timing error of one sample, but only reports and does not correct the "time slip".

The resulting total time error was on average 200 to 400 ms for the wide-angle profiles and up to several tens of seconds for the seismology network, showing clearly the necessity of a special time slip correction for the MLS data. After careful analysis of the problem, we concluded that the best way to address the time slip timing error in the wide-angle data is to add the time slips reported in the send2pas logfile, and regard the time slip total as an extra skew contribution which later in the processing flow is corrected within the dat2segy program (see below, note that the sign of skew and time slips are opposite, i.e., a negative sum of time slips corresponds to a positive skew). As each trace is at most a few tens of seconds long (vs. 1 hour and more between non-cancelling time slips), the corrected time is expected to be highly accurate with uncertainties well below one sample length.

ref2segy
The ref2segy program converts the output of send2pas to a pseudo SEG-Y trace consisting of one header and a continuous data trace containing all samples, as used by the PASSCAL suite of seismic utility programs. For each channel (normally pressure, vertical velocity, and velocity along two mutually perpendicular horizontal directions for OBS; pressure for OBH) one file is created with the name derived from the start time, the serial number of the Methusalem system, and the channel number. The file size of the pseudo-SEGY file is directly related to the recording time. For instance, a recording time of one hour sampled at 200 Hz (16 Bit) will produce a file size of 1.44 MB per channel. A record with two channels and a recording time of two days will produce a total data volume of 70 MB.

Send2x
The program library SEND2X converts the compressed recordings of GEOLON-MES into different formats. Send2x is available for the operating system Linux. The current version allows

the conversion of raw data into a binary file, an audio-wave file, or into the SEG-Y format if an appropriate shot file is available. Furthermore, the log data includes the parameter settings such as the sample rate and the amplifier gain for each channel. The internal temperature and humidity as well as the battery voltage will be stored together with the recorded seismic data on the internal disk.

- **meslog**

All control, status, and identification information of the current experiment are stored on GEOLON's harddisk. Furthermore, the log data includes the parameter settings such as the sample rate and the amplifier gain for each channel. Normally the program meslog displays these data on the screen. Through the assignment of the standard output to the harddisk on the connected external PC, these data can alternatively be stored in a text-file.

- **mescopy**

Via an IEEE-1394 Firewire interface the raw data is copied to a Linux-PC.

- **mesread**

The program mesread converts the raw and compressed data to a s2x-format and provides the extraction of the engineering data out of the recorded data stream.

- **segywrite**

Segywrite converts the data stored in s2x format to standard SEG-Y format. The option --reftek is used for a pseudo SEG-Y output format.

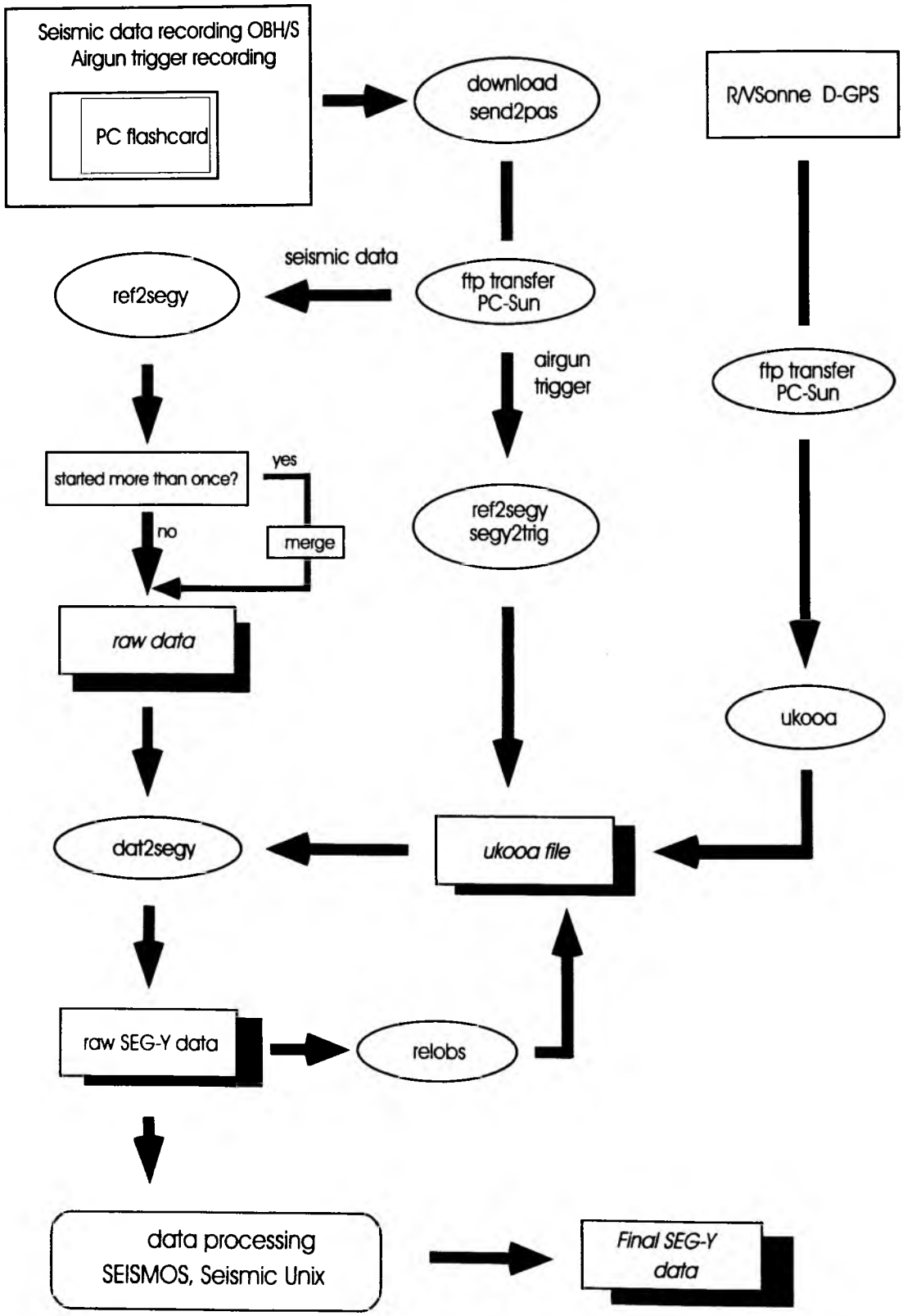

Figure 6.3.1: *Processing flow of seismic refraction data (OBS/OBH) from raw data to SEG-Y records.*

merge
If an error occurs during the download process, the ref2segy program has to be restarted. This may lead to several data files with different start times. Merging these files into a single file is performed by the merge program. Gaps between the last sample and the first sample of the consecutive data traces are filled with zeros. Overlapping parts are cut out.

pql
pql (Passcal Quick Look) is a simple display program for continuous seismic data. Its interactive zooming capability allows a rapid inspection of data quality.

segy2trig
The trigger signal, provided by the airgun control system, is recorded on an additional MBS unit during the shooting period. The trigger data are treated similarly to regular seismic data and downloaded to the hard disk via the send2pas and ref2segy programs. Then, the segy2trig program detects the shot times in the data stream by identifying the trigger signal through a given slope steepness, duration and threshold of the trigger pulse. The output is an ASCII table consisting of the shot number and the shot time. Accuracy of the shot time is one of the most crucial matters in seismic wide-angle work, and must be reproduced with a precision of a few ms. Due to this demand the shot times have to be corrected with the shift of the internal recorder clock. Additionally, the trigger file contains the profile number, the start/end time of the profile and the trigger recording. The shot times are part of the ukooa file, which links them with the coordinates of the source and the hydrophones.

ukooa
The ukooa program is used to establish the geometric database by calculating the positions of sources at any given shot time and offset from the ship. The source is placed on the ship track using simple degree/meter conversions and then written to a file in UKOOA-P84/1 format. Corrections for offsets between antenna and airguns as well as consistency checks are included. This file will be used when creating a SEG-Y section via the dat2segy program. The program requires the trigger file to contain the shot times, the ship's navigation (see Chapter 5.1.1), and a Parameter file containing information for the UKOOA file header as basic input information.

dat2segy
The dat2segy program produces standard SEG-Y records either in a 16 or 32 bit integer format by cutting the single SEG-Y trace (the ref2segy output) into traces with a defined time length based on the geometry and shooting time information in the ukooa file In addition, the user can set several parameters for controlling the output. These parameters are information about the profile and the receiver station, number of shots to be used, trace length, time offset of the trace and reduction velocity (to determine the time of the first sample within a record). Also the clock drift of the recorder (skew) is taken into account and corrected for. For the MLS data the total time error resulting from the observed time slips described above was subtracted from the clock drift value. The final SEG-Y format consists of the file header followed by the traces. Each trace is built up by a trace header followed by the data samples. The output of the dat2segy program can be used as input for further processing with GEOSYS, SEISMOS or Seismic Unix (SU).

relobs
Because of drifting of the OBH and OBS instruments during deployment and errors in the ship's GPS navigation system, the OBH positions may be mislocated by up to several 100 m. Since this error leads to asymmetry and incorrect traveltime information in the record section, it has to be corrected. This is accomplished with the program relobs.

For input, the assumed OBH location, shot locations and the picked traveltimes of the direct wave near to its apex are needed. To simplify the picking a static correction with a hyperbolic equation was performed to flatten the direct wave. This yields a much more coherent direct arrival which would normally suffer from strong spatial aliasing in the uncorrected section making it difficult to

track. By shifting the OBH position, relobs minimizes the deviation between computed and real travel times using a least mean square fitting algorithm (assuming a constant water velocity). Fortunately, wide-angle profile 2 was shot forth and back during the cruise giving us the opportunity to adjust the source offset, i.e. the distance from the research vessel's GPS position to the center of the airgun array, which was calculated to be 80 m. Thus, an accuracy in receiver position determination of about 10 m was possible.

Beside these main programs for the regular processing sometimes additional features are needed for special handling of the raw data:

divide
The program divide cuts the raw data stream into traces of a given length without offset and time information, storing the output in SEG-Y format. The routine is useful for a quick scan of the raw data or if a timing error has occurred.

segyhdr
The routine segyhdr prints all the header values of the raw data on the screen.

segyshift
Segyshift modifies the time of the first sample, such that the whole raw data trace can be shifted by a given value. This is very useful when shifting the time base from Middle European Time to Greenwich Mean Time or any local time. Because of recording problems, the data sometimes show a constant time shift, which can be corrected as well with segyshift.

castout
The program castout allows the user to remove a specified time window from the raw data stream. When the shooting window is much smaller than the recording time, one can reduce the data volume by cutting out only the useful information. This will reduce the demand on disk space.

- **OBH/OBS-Data analysis and processing with source signals of 32 liter Bolt-Guns**

As an example, the OBH record section obh36 for profile 16 is shown in Figure 6.3.2. A standard band-pass frequency filter was applied to the data.

The source configuration was similar to the setup used on previous cruises (e.g. SO161, SO173), therefore the same processing was applied to the data. A detailed analysis of the filter and deconvolution parameters is described in the cruise reports of SO161 and SO173.

To improve the temporal resolution of the seismic data a deconvolution is applied to compress the basic seismic wavelet. The recorded wavelet has many components, including the source signature. recording filter, and hydrophone/geophone response. Ideally, deconvolution should compress the wavelet components and leaving only the earth's reflectivity in the seismic trace. We applied Wiener deconvolution in successive trace segments, based on the following assumptions:

1. The earth's reflectivity is 'white'.
2. The wavelet shows the minimum-delay phase behavior.

As in this wide-angle data the amplitude spectra of the seismic traces vary with time and offset (e.g. reflected, refracted pp phases and reflected ps and ss phases), the deconvolution must be able to follow these time and offset variations. For the single trace deconvolution each trace is therefore divided into 3-s data gates with 1-s overlaps, in which time-invariant deconvolution operators are computed from the

autocorrelation function of the data segment and applied to account for the nonstationarity of the seismic signals. The overall deconvolved trace results from a weighted merging of the independently deconvolved gates.
Input for the deconvolution process is raw data. As several recordings were influenced by a DC shift, a 1-3-Hz high-pass minimum delay Kaiser frequency filter with 60 dB attenuation between the pass and reject zone was applied prior to deconvolution in order to center the amplitudes around zero. A predictive length of 140 ms and a multi-trace deconvolution was chosen for this data set which is a compromise between temporal resolution and signal-to-noise ratio.

After deconvolution an offset- and time-variant Ormsby filter with minimum delay characteristic was applied. As the seafloor depth changes along the seismic lines, each trace was statically corrected to a fixed seafloor travel time of 11 s based on the water depth before filtering. This information is available in the trace headers. After this filter was applied, the data were shifted back to their original travel times.

Comparison of the preprocessed data in Figure 6.3.3 to the unprocessed data in Figure 6.3.2 shows a clear reduction of the low and mono-frequency noise in the near and far offset traces and moderate compression of the wavelet signal. For the picking of events and model building by raytracing both sections were used to keep all available seismic information.

Final processing sequence

- Input: SEGY-data, 4 ms or 5ms sampling rate with complete geometry information.
- Tapering the first 0.5 s to zero to reduce the response of the debias filter operator.
- Kaiser highpass (debias).
- Gated Wiener deconvolution: gate length 3 s, overlap 1 s, length of merge region 1 s, operator length 300 ms (prediction interval included), prediction interval 140 ms.
- Static correction to a fixed seafloor traveltime of 11 s.
- Time and offset-dependent Ormsby frequency filter.

On time-shifted traces with a reduced time scale of 6 km/s the following filter parameters were used:

lower stop/pass	upper pass/stop (Hz)	offset(m)	beginfull(s)	endfull(s)
3/5	28/48	0	0	12.8
		8000	0	12.6
		48000	0	0
3/5	23/38	0	13.7	14.3
		8800	13.5	14.4
		13200	13.0	13.9
		52000	1.0	2.0
		107000	0	0
3/5	18/28	0	15.3	16.8
		11700	15.1	16.6
		19200	14.8	16.3
		61700	7.0	10.1
		114000	2.0	3.0
		152000	0	0
3/5	13/18	0	19.0	trace length
		20000	18.4	trace length
		130000	3.5	trace length

• **Data archiving**
Data recorded with the MBS/MLS recorder on flash discs were transferred via a PC to a SUN workstation. On the workstation they were transformed into a so-called PSEUDO-SEGY format. After navigation data had been merged and SEGY formatted traces with the appropriate header words had been created, the data were also archived. Finally, a third set was stored and archived after the shipboard processing, as described above, had been applied. All final processed SEGY data were archived on tapes.

• **Data exchange**
For the exchange of the OBH/OBS data, the SEGY-format on disk with a Sun tar-format was chosen. The raw segy data is in Integer2 format with trailer bytes between the record structure of SEGY. The processed data is in IBM-floating point without trailer bytes between the records. For UTM transformation into Cartesian coordinates use: WGS84 spheroid, central meridian 73 0. 0. W, southern hemisphere.

This is the definition of the segy trace header for the GEOMAR OBS wide-angle reflection data. The extension of the standard SEGY header from 181 to 240 byte is a layout in order to process the data on the GEOSYS/SEISMOS software system. Reading bytes directly into this header will allow access to all of the fields.

BytePos	Bytes	Information	Comments (note: not all headers available in processed data)
1-8	(2x4)	lineSeq, reelSeq;	/* Sequence numbers within line and reel, resp.*/ /* here station and shot number Def: 1, 1 */
9-12	(4)	profNumber;	/* Original field record number */ /* Here profile number */
13-16	(4)	traceNumber;	/* Trace number within the original field record.*/ /* Here station (receiver) Number */
17-20	(4)	energySourcePt;	/* Energy source (shot) point number */ /* Def: 0 */
21-24	(4)	cdpEns;	/* CDP ensemble number: shot number */ /* Def: 0 */
25-28	(4)	traceInEnsemble;	/* Trace number within CDP ensemble */ /* Here azimuth in seconds of arc for unprocessed data*/
29-30	(2)	traceID;	/* Trace identification code: 1=seismic data (Def) 4=time break 7=timing 2=dead 5=uphole 8=water break 3=dummy 6=sweep 9..., optional use */
31-34	(2x2)	vertSum, horSum;	/* Def: 1, 1 */
35-36	(2)	dataUse;	/* 1=production (Def), 2=test */
37-40	(4)	sourceToRecDist;	/* Distance in (m) */
41-44	(4)	recElevation;	/* Elevation in (m), Def: 0 */
45-48	(4)	sourceSurfaceElevation;	/* Def: 0 (m) */
49-52	(4)	sourceDepth;	/* Def: 0 (m) */
53-60	(2x4)	datumElevRec, datumElemSource;	/* Def: 0, 0 (m) */
61-68	(2x4)	sourceWaterDepth, recWaterDepth;	/* Def: 0, 0 (m) */
69-70	(2)	elevationScale;	/* Scale elevations Def: 0 (10**0) */
71-72	(2)	coordScale;	/* Scale coordinates Def: -2, means coordinates multiplied by 10**(-2) to get real value for unprocessed data. NOTE: for processed data -100 means to divide by 100 to get the real value */
73-80	(2x4)	sourceLongOrX, sourceLatOrY;	/* Either Cartesian or geographic */
81-88	(2x4)	recLongOrX, recLatOrY;	

```
89-90   (2)     coordUnits;                 /* 1= meter or feet; 2=sec of arc */

91-92   (2)     weatheringVelocity;         /* Def: 0 (m/s) */
93-94   (2)     subWeatheringVelocity;      /* Reduction velocity, Def: 6000 (m/s) */
95-96   (2)     sourceUpholeTime;           /* Def: 0 (ms) */
97-98   (2)     recUpholeTime;              /* Def: 0 (ms) */
99-102  (2x2)   sourceStaticCor, recStaticCor;      /* Def: 0, 0  (ms ) */
103-104         (2)     totalStatic;                /* Def: 0 (ms) */
105-106         (2)     lagTimeA;                       /* T(shottime) - T(first sample) */
107-108         (2)     lagTimeB;                       /* Def: 0 (ms) */
109-110         (2)     delay;                  /* Def: 0 (ms) */
111-114         (2x2)   muteStart, muteEnd;     /* Def: 0, 0 (ms) */
115-116         (2)     sampleLength;           /* Number of samples in this trace */
                                /* ( > 32767 )? = 32767
                                set long samp_rate in 185-188 byte */
117-118         (2)     deltaSample;            /* Sampling interval in microseconds. */
119-120         (2)     gainType;               /* 1=fixed (Def), 2=binary,
                                3=floating, 4... opt.*/
121-122         (2)     gainConst;              /* Gain of recording channel  */
123-124         (2)     initialGain;            /* Gain of preamplifier in db */
125-126         (2)     correlated;             /* 1=no (Def), 2=yes */
127-130         (2x2)   sweepStart, sweepEnd;   /* min. and max. amplitude of trace */
131-132         (2)     sweepLength;            /* Here defined as
                                fraction of second of shot time  */
133-134         (29)    sweepType;              /* Source type:
                                1=linear, 2=parabolic, 3=exponential, 4=others
                                5=bohrhole explosive, 6=water explosive, 7=airgun (Def)
                                or fraction of microsecond of shot time for high resolution data */

135-138         (2x2)   sweepTaperAtStart, sweepTaperAtEnd;     /* Start and end of trace (ms)
                                                                   relative to Tred(0) */
139-140         (2)     taperType;              /* scaling factor for last two values Def: 1 (x10) */
141-144         (2x2)   aliasFreq, aliasSlope;  /* Def: 0, 0  */
145-148         (2x2)   notchFreq, notchSlope;  /* Def: 0, 0  */
149-152         (2x2)   lowCutFreq, hiCutFreq;  /* Def: 0, 0  */
153-156         (2x2)   lowCutSlope, hiCutSlope;/* Def: 0, 0  */
157-166         (5x2)   year, day, hour,        /* Source (shot) time, the fraction of sec */
                minute, second;         /* is set in millisec between 131-132 byte
                                is set in microsec between 133-134 */

167-168         (2)     timeBasisCode;          /* 1=local, 2=GMT, 3=MET (GMT + 1 hour)
(Def) */

169-170         (2)     traceWeightingFactor;   /*  */

171-172         (2)     phoneRollPos1;          /* Component: 1=time code, 2=radial,
3=transverse
                                4=vertical, 5=hydrophone (Def)  */
173-174         (2)     phoneFirstTrace;                /* Methusalem instrument number in
YYNN */
175-176         (2)     phoneLastTrace;         /* Channel number */
177-178         (2)     gapSize;                /* Source charge in cubic inches (airgun)
                                or kg (explosives) */

179-180         (2)     taperOvertravel;        /* Def: 0=meaningless  1=up, 2=down    */
/* !!! Following is extension !!! */

181-182         (2)     compNo;                 /* 1=time code, 2=radial, 3=transverse
                                4=vertical, 5=hydrophone (Def)  */
183-184         (2)     samplingRate;           /* samples/sec */
185-188         (4)     numberSamples;          /* ( <= 32767) ? sampleLength | ( > 32767) */
```

```
189-190     (2)     shotPointNo;
191-192     (2)     ADCoeff;            /* Coefficient of A/D converter in mv/digit */
193-194     (2)     receiverCoeff;      /* Conversion coefficient of receiver,
                                        pascal/cm2 for hydrophone,
                                        velocity(m/s)/volt for geophone */
195-196     (2)     receiverType;       /* 1=hydrophone (Def), 2=geophone, 3...*/
197-200     (4)     lengthData;         /* Def: 0 (ms), not used here */
201-204     (4)     distance;           /* Source to receiver distance in (m) */
205-208     (4)     (float) scaleFactor;  /* Scale factor same as in <segy.h>
                                        Here azimuth in second of arc for processed data */
209-210     (2)     azimuth;            /* Orientation of the component in min */
211-212     (2)     eigenperiod;        /* Eigenperiod of geo- or hydrophone in (ms) */
213-216     (4)     minAmpl;            /* Min. peak amplitude within trace    */
217-220     (4)     maxAmpl;            /* Max. peak amplitude within trace */
221-222     (2)     stationNo;          /* Station number */
223-224     (2)     channelNo;          /* Channel number (Default: 1) */
225-228     (4)     sourceCharge;       /* Charge in kg (explosive) or cc (airgun) */
229-230     (2)     redVelocity;        /* reduction velocity in (m/s);
                                        Def: 0 if no reduction velocity se */
231-232     (2)     timeOffset;         /* Time offset in (ms) of first sample
                                        relative to reduced source time:
                                        positive if earlier than reduced time */
233-236     (4)     redTime;            /* Reduced time in (ms) = distance/redVel */
237-238     (2)     unused2;
239-240     (2)     instNo;             /* Methusalem instrument number */
```

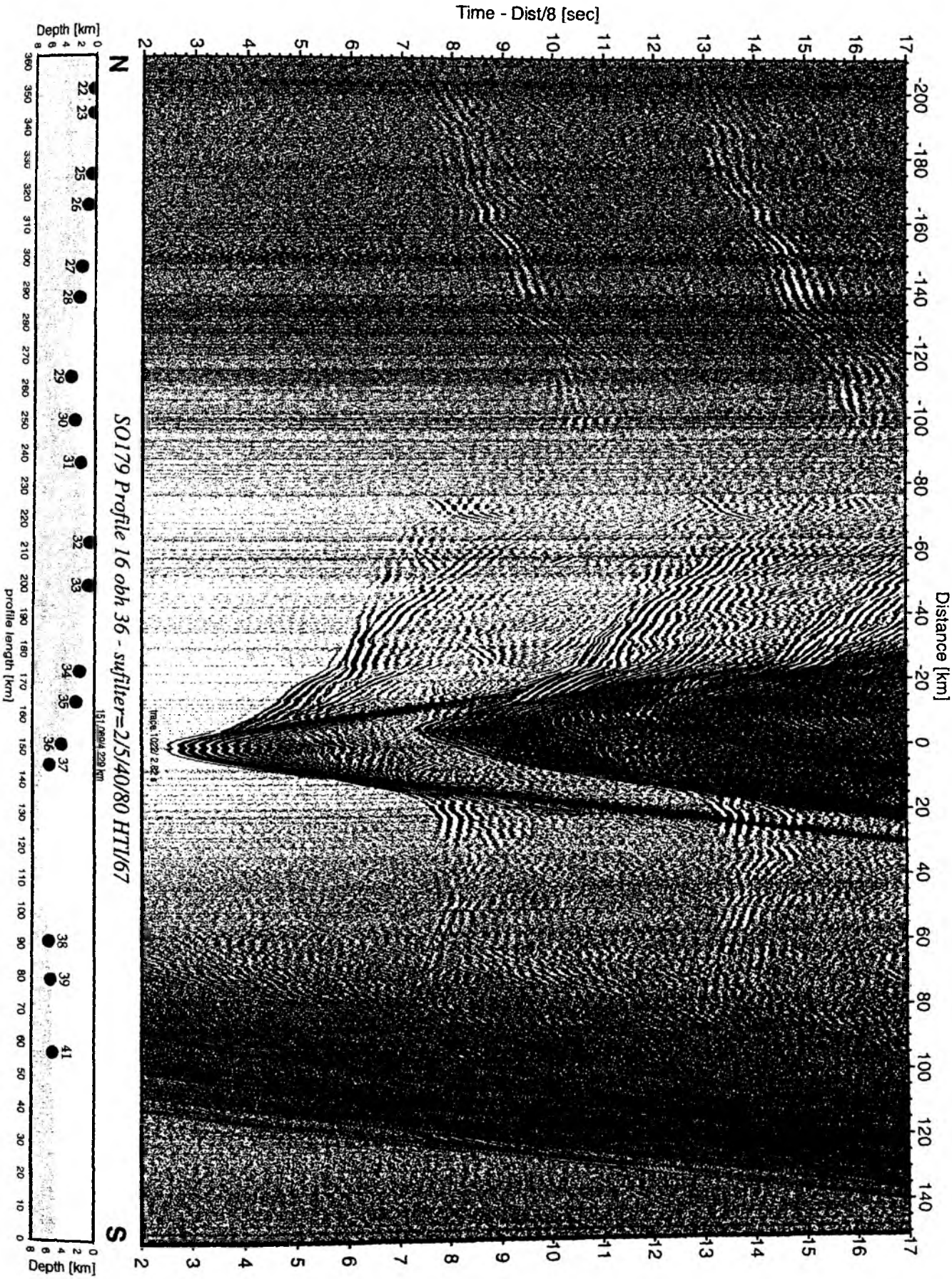

Figure 6.3.2: Record section from obh 36 HTI/67, Profile 16.

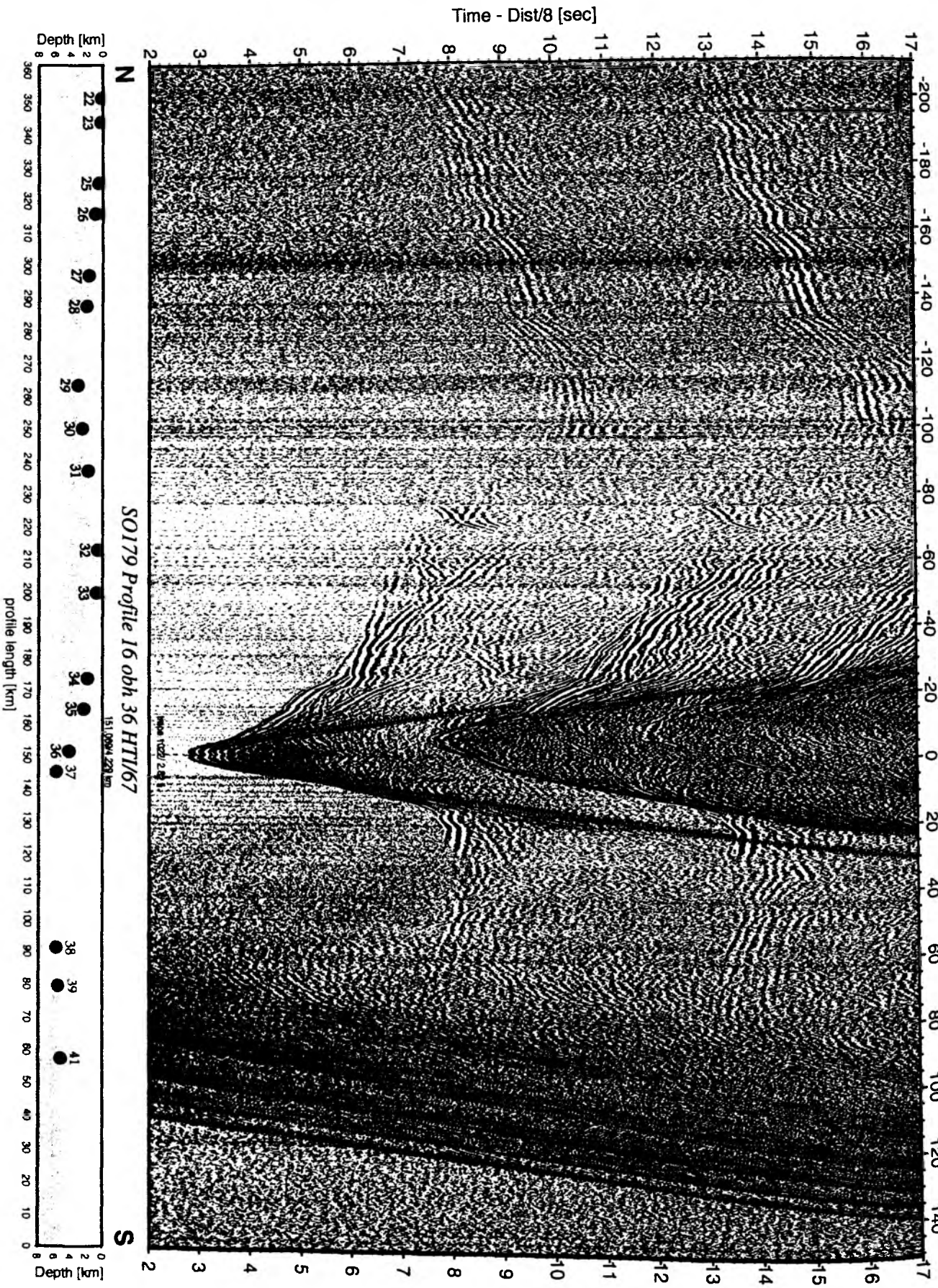

Figure 6.3.3: Record section from obh 36 HTI/67, Profile 16.

6.4 Wide-angle seismic work
6.4.1 Profile 01

Profil 01 of SO179 is intended to provide three dimensional information for the seismological network. It was shot in the center of the network, starting near OBS02 and ending near OBS06. Its location is shown in Figure 6.4.1.1. It was shot with 2 or three airguns on 19. and 20.09., see Appendix 9.3. During shooting, the four channel streamer was also deployed and the sedimentary structure can in parts be resolved. The processed section is shown in Figure 6.4.1.2. As an example of the recordings data from station OBS09 are shown in Figures 6.4.1.3 and 6.4.1.4.

The streamer section shows a thick sedimentary sequence in the west, where the profile is located in the flat forearc basin. Starting at around 80 km, a basement reflection is seen about 1 s twt below seafloor, and it nearly reaches the seafloor at 130 km, where the profile is closest to the forearc high.

Record sections from the instruments of the network show a disappointingly low signal to noise ratio. This may in part be due to the swell that was persistent when shooting the line, and in parts also due to the low sampling rate of 50 Hz, so that the high frequency part of the source is not recorded.

The signal to noise ratio is better on the seismometer than on the hydrophone, and first arrivals can be traced to about 70 km distance with a high apparent velocity. The horizontal components also show considerable energy to about the same range with identical apparent velocities. The data shall later be used to improve the tomographic inversion of the earthquake data recorded and described in section 6.2.

Profil P01

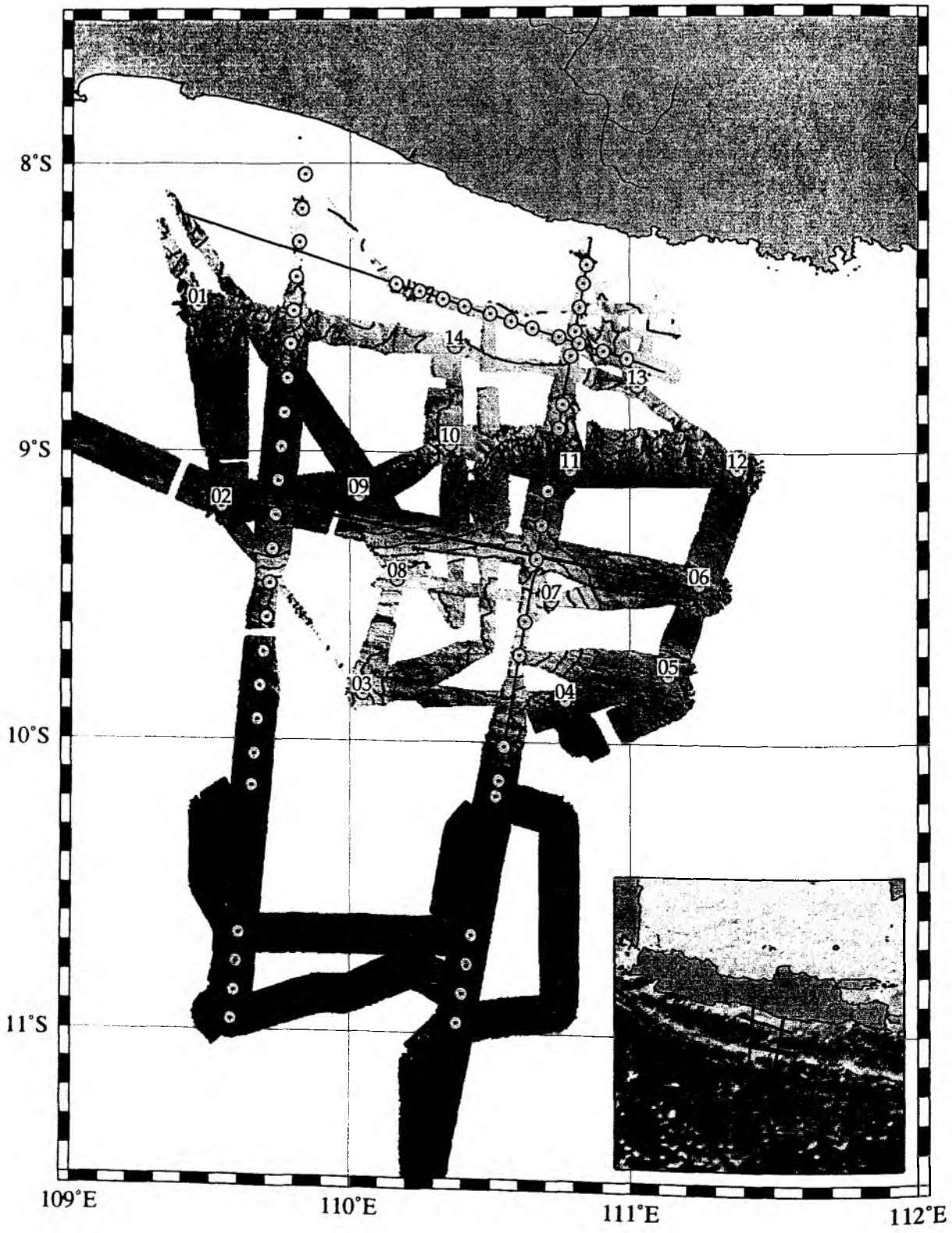

Figure 6.4.1.1: location map of profile 01.

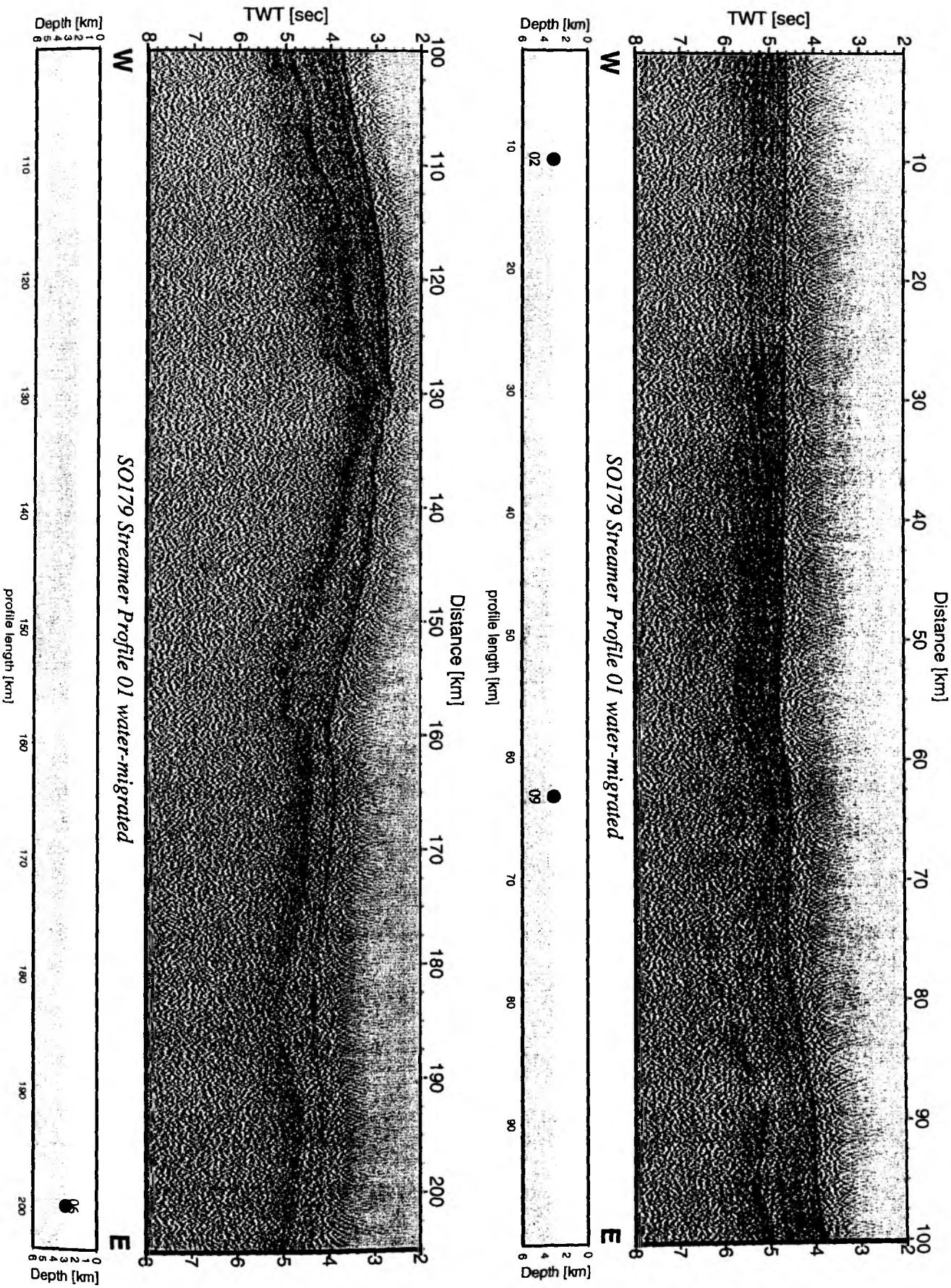

Figure 6.4.1.2: Record section from Streamer Profile 01 water-migrated.

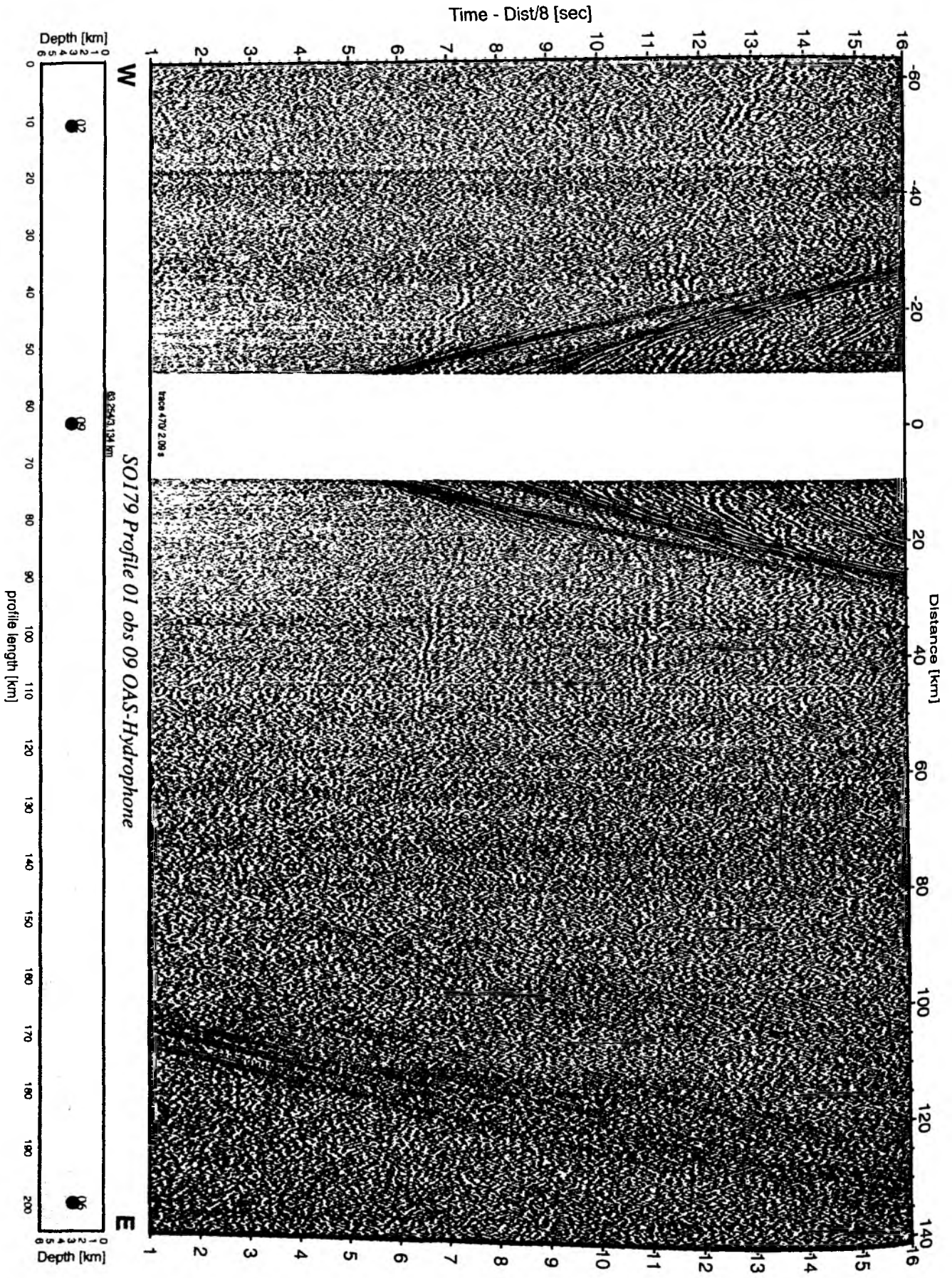

Figure 6.4.1.3: Record section from obs 09 OAS-Hydrophone, Profile 01.

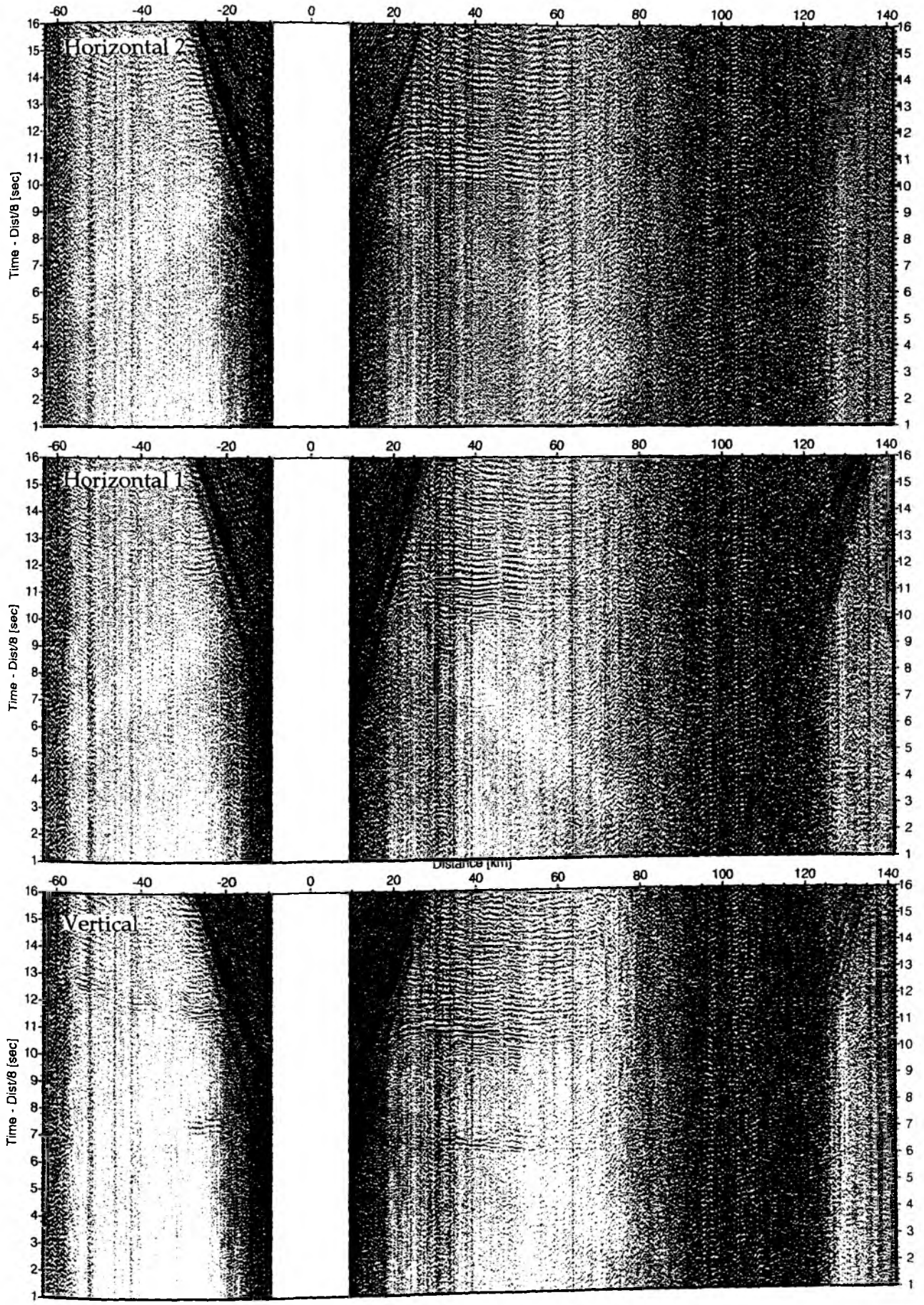

Figure 6.4.1.4: Record sections from obs 09 WEBB, SO179 Profile 01.

6.4.2 Profile P16

This profile is the eastern one of two dip lines acquired during SO179 acors the Java margin and trench. It is 190 nm long and reaches from close to the coast across the trench and onto the downgoing oceanic plate. In total 20 OBH/S were deployed on 23/24.09, and in addition 4 instruments from the seismological network were still in operation, three of them close to the line (see Figure 6.4.2.1).
Shooting started at noon 24.09 seeward from the trench and was terminated 06:00 26.09 close to shore. All three guns were in operation, except for a few interruptions, when the buoyancy bodies of one gun were lost (for details see Appendix 9.3). Instruments were recovered subsequently, incl. those from the network, see Appendix 9.2). Unfortunately, OBH 40 did not respond when we tried to release it, and despite a search for several hours, it could not be recovered.
During shooting the magnetometer and the streamer were also deployed, the streamer section is shown in Figure 6.4.2.2. All data were processed according to the dataflow described in section 6.3, the resulting record sections are shown in Figures 6.4.2.3 to 6.4.2.23.

The three OBH/S 38, 39 and 41 are situated on the southern part of profile 16, on the oceanic crust.A modelling technique is used to reveal the structure of the crust in this area.

First arrivals of the OBH data, including refracted waves in the upper and the lower oceanic crust, could be identified. Refracted waves in the oceanic mantle were also recorded by stations 38 and 41 (figures 6.4.2.24 and 6.4.2.26).After picking these traveltimes on OBH data, we can try to model them, by establishing a layered model for the oceanic crust (figure 6.4.2.30).

The results of the modelisation for OBH 38, 39 and 41are shown in figures 6.4.2.24 to 6.4.2.26.

The figures 6.4.2.27 to 6.4.2.29 are showing the velocity model at the position of the three OBH/S which are studied here.

The vertical incidence reflexion on MCS data helped us to establish the thickness of the first sedimentary layer. Indeed, refracted waves in this layer, displaying a velocity of 1600m/s and a thickness of 400m, cannot be seen on OBH data.
Then, the upper oceanic crust of 2km thickness was modelled with a velocity depth gradient from 4.0km/s to 6.3km/s.
The lower oceanic crust was also modelled with a vertical velocity gradient (from 6.35km/s to 6.9km/s) and has a thickness of about 6km.
Finally, the oceanic crust is underlain by an oceanic mantle displaying velocities increasing from 7.8km/s to 8.2km/s at a depth of 14km. Thus, the oceanis crust is slightly thicker than the global average.

Profil P16

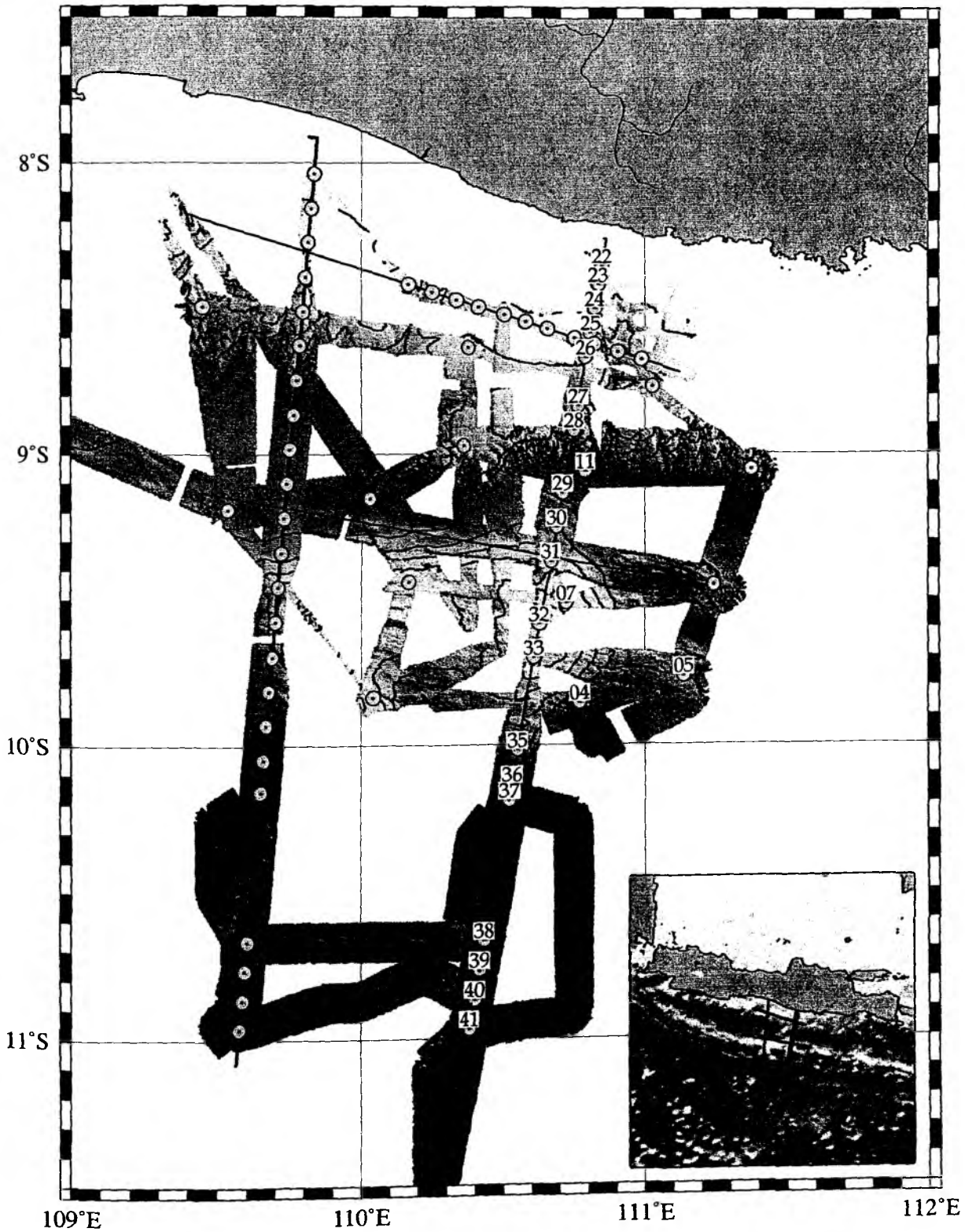

Figure 6.4.2.1: location map of profile 16.

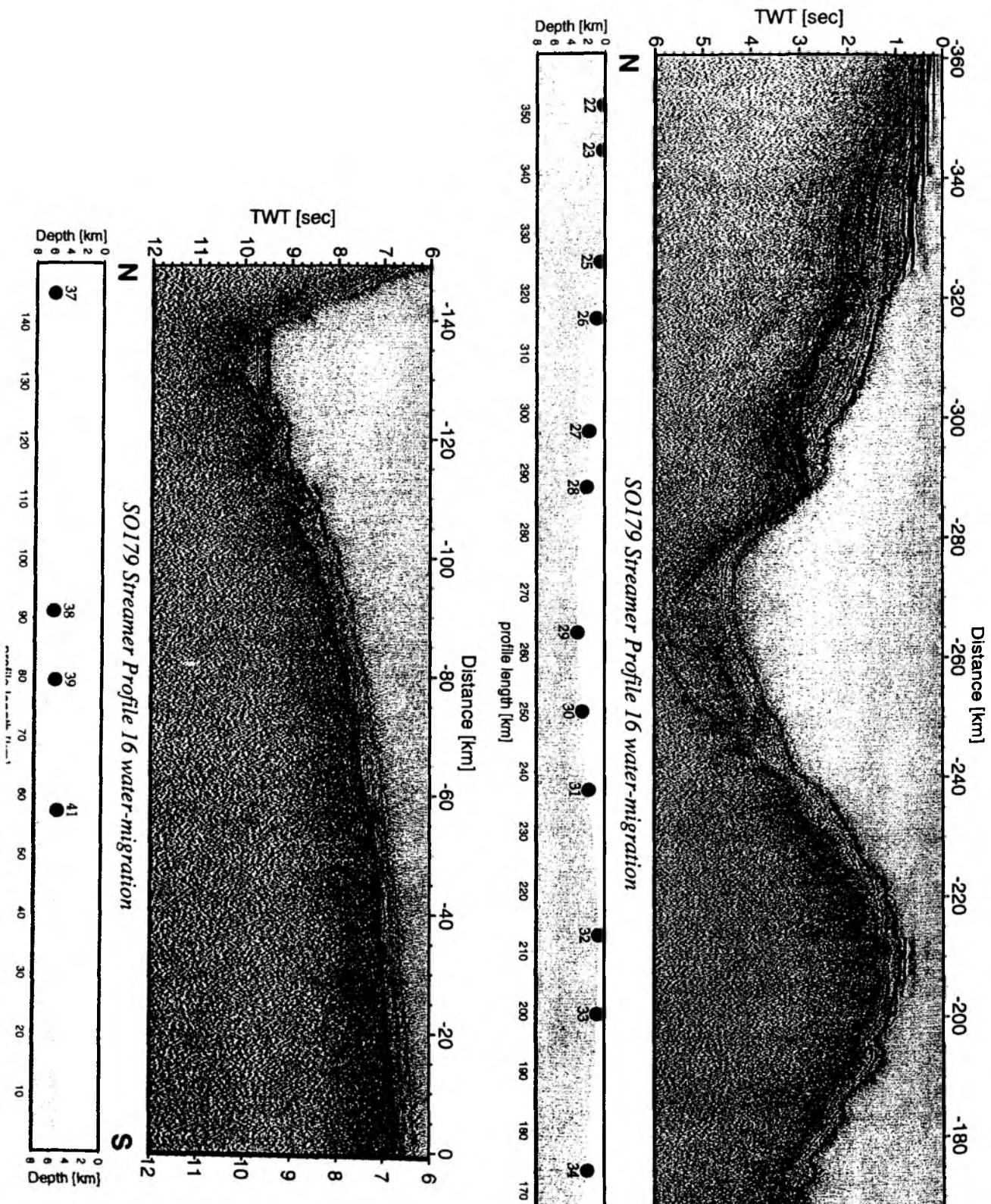

Figure 6.4.2.2: Record section from Streamer Profile 16 water-migration.

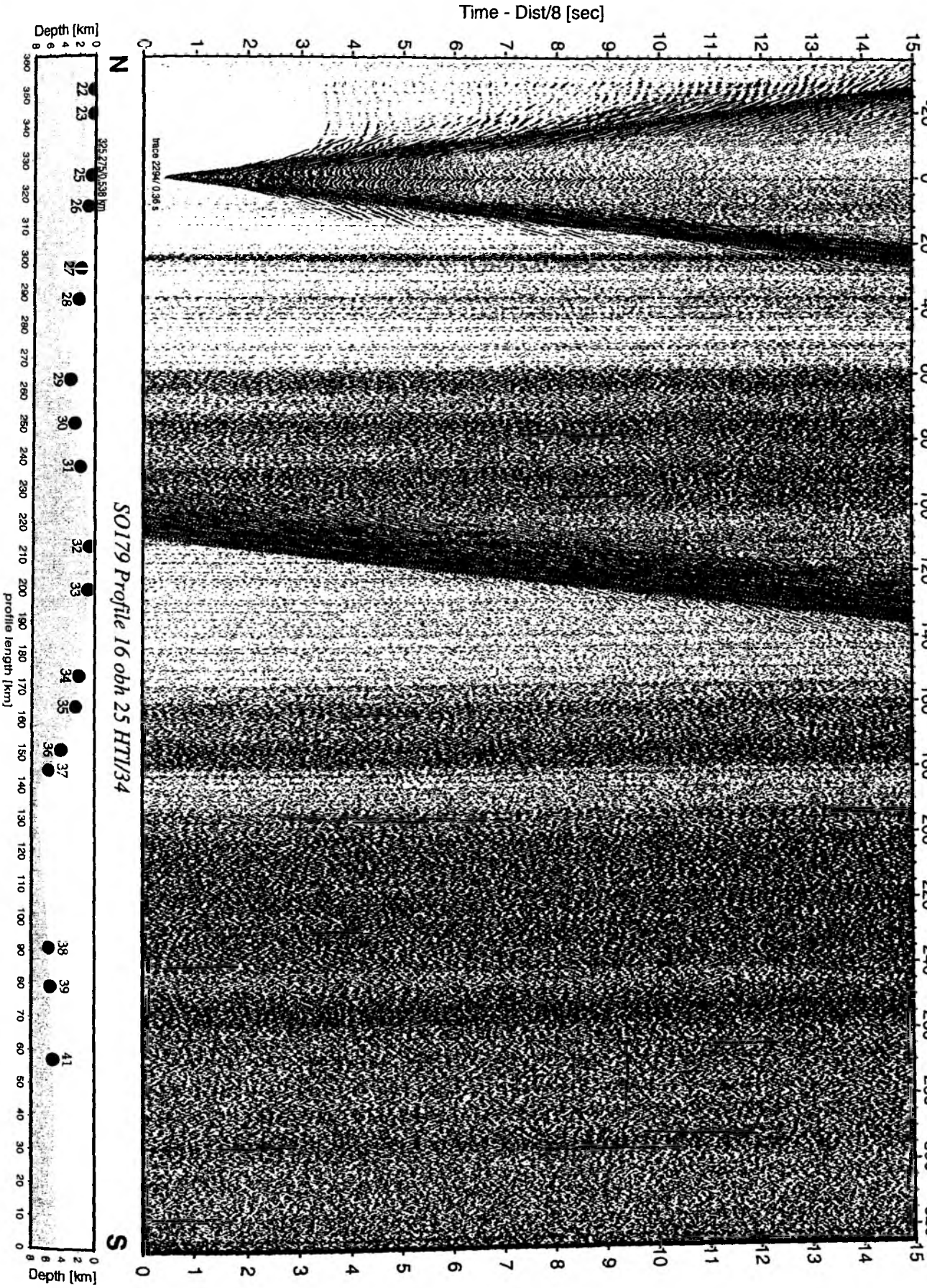

Figure 6.4.2.3: Record section from obh 25 HTI/34, Profile 16.

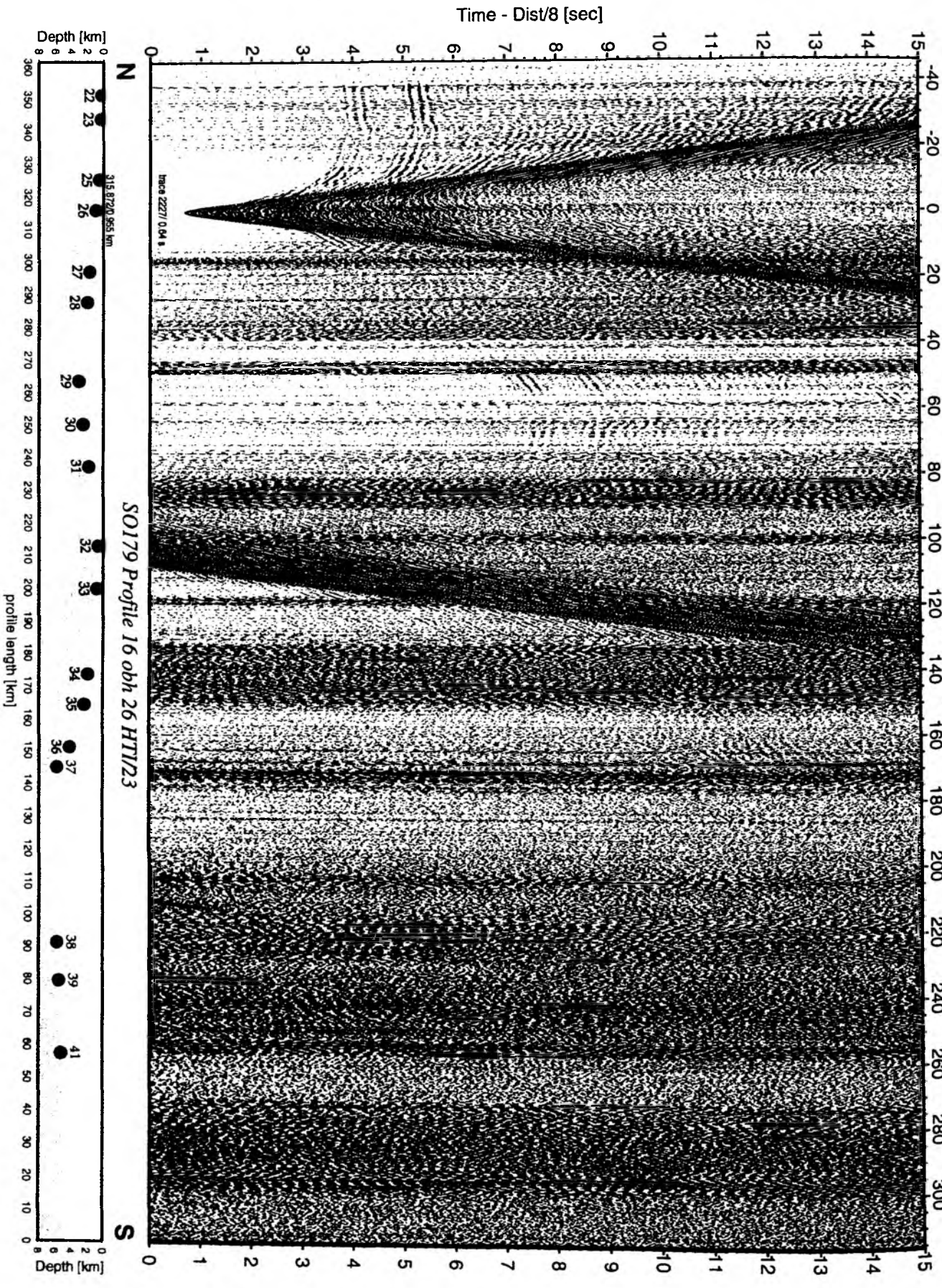

Figure 6.4.2.4: Record section from obh 26 HTI/23, Profile 16.

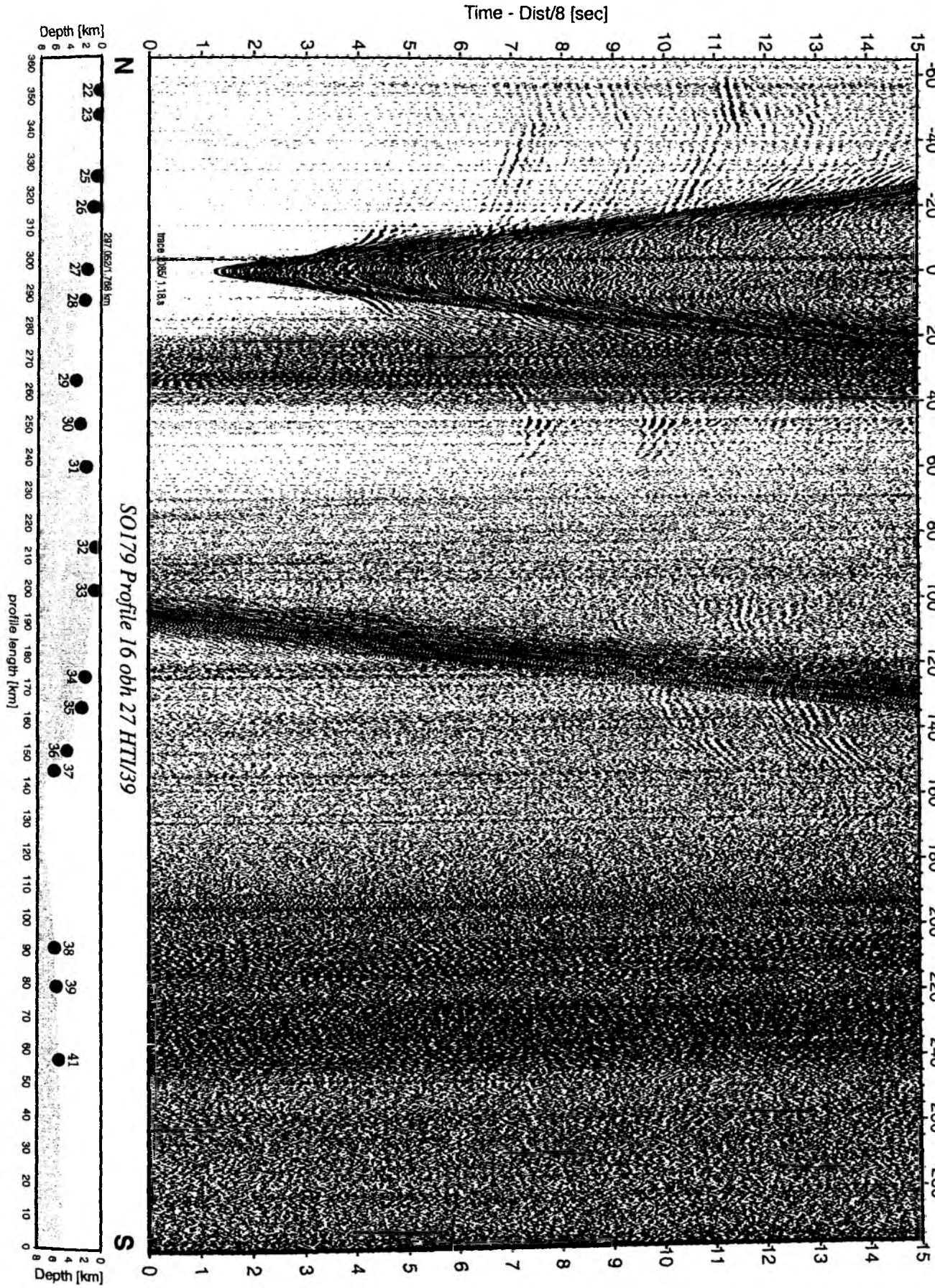

Figure 6.4.2.5: Record section from obh 27 HTI/39, Profile 16.

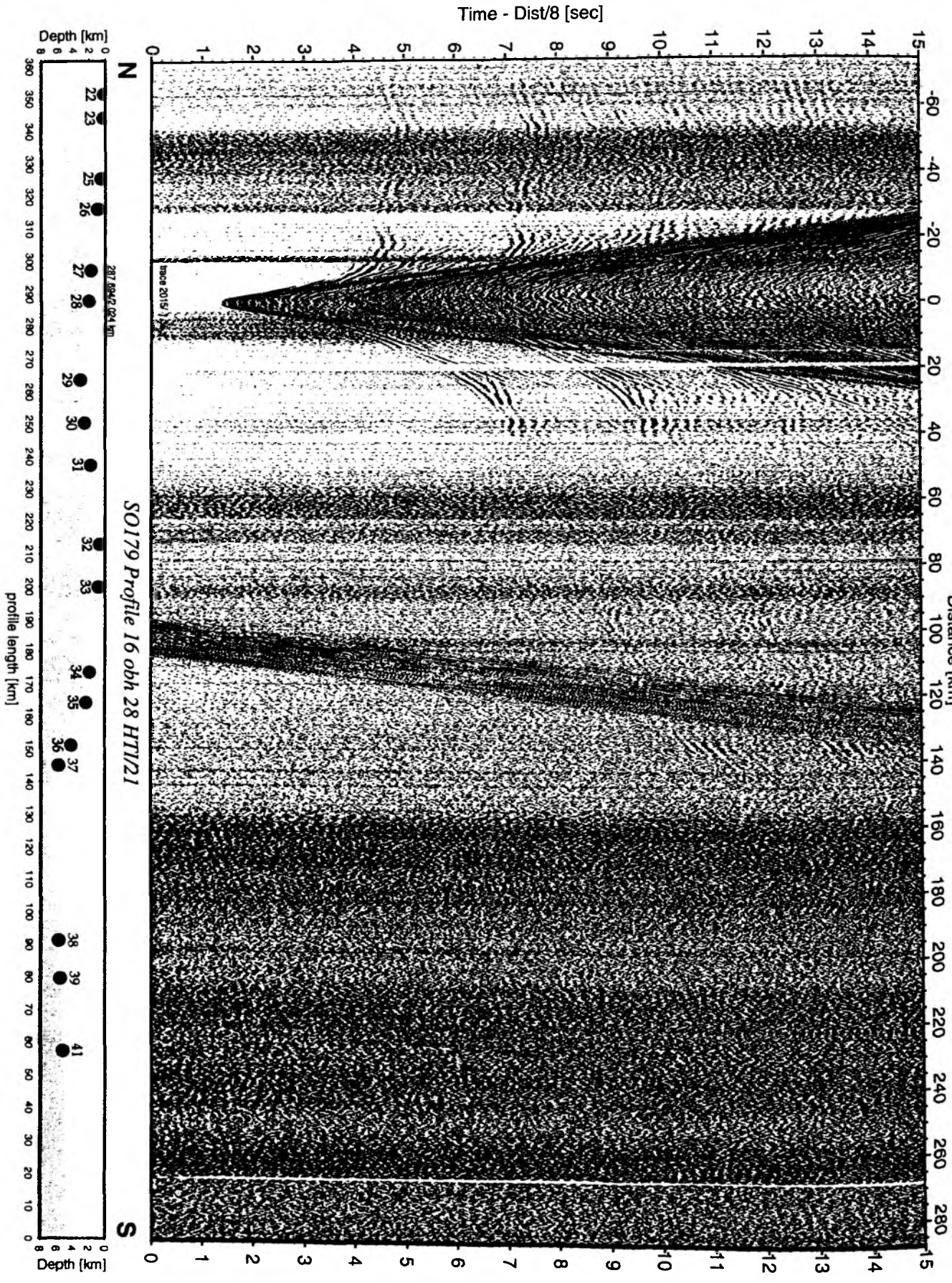

Figure 6.4.2.6: Record section from obh 28 HTI/21, Profile 16.

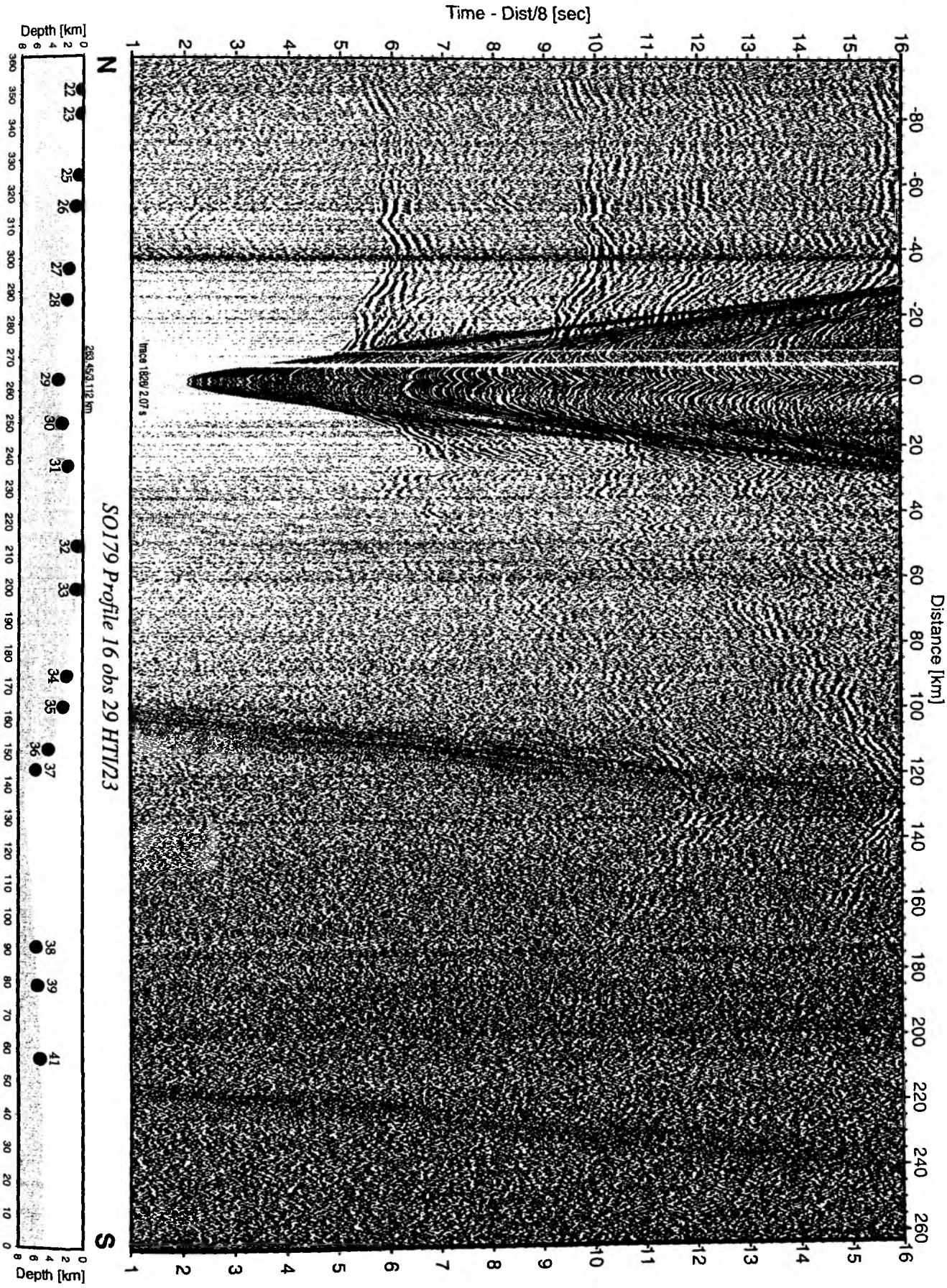

Figure 6.4.2.7: Record section from obs 29 HTI/23, Profile 16.

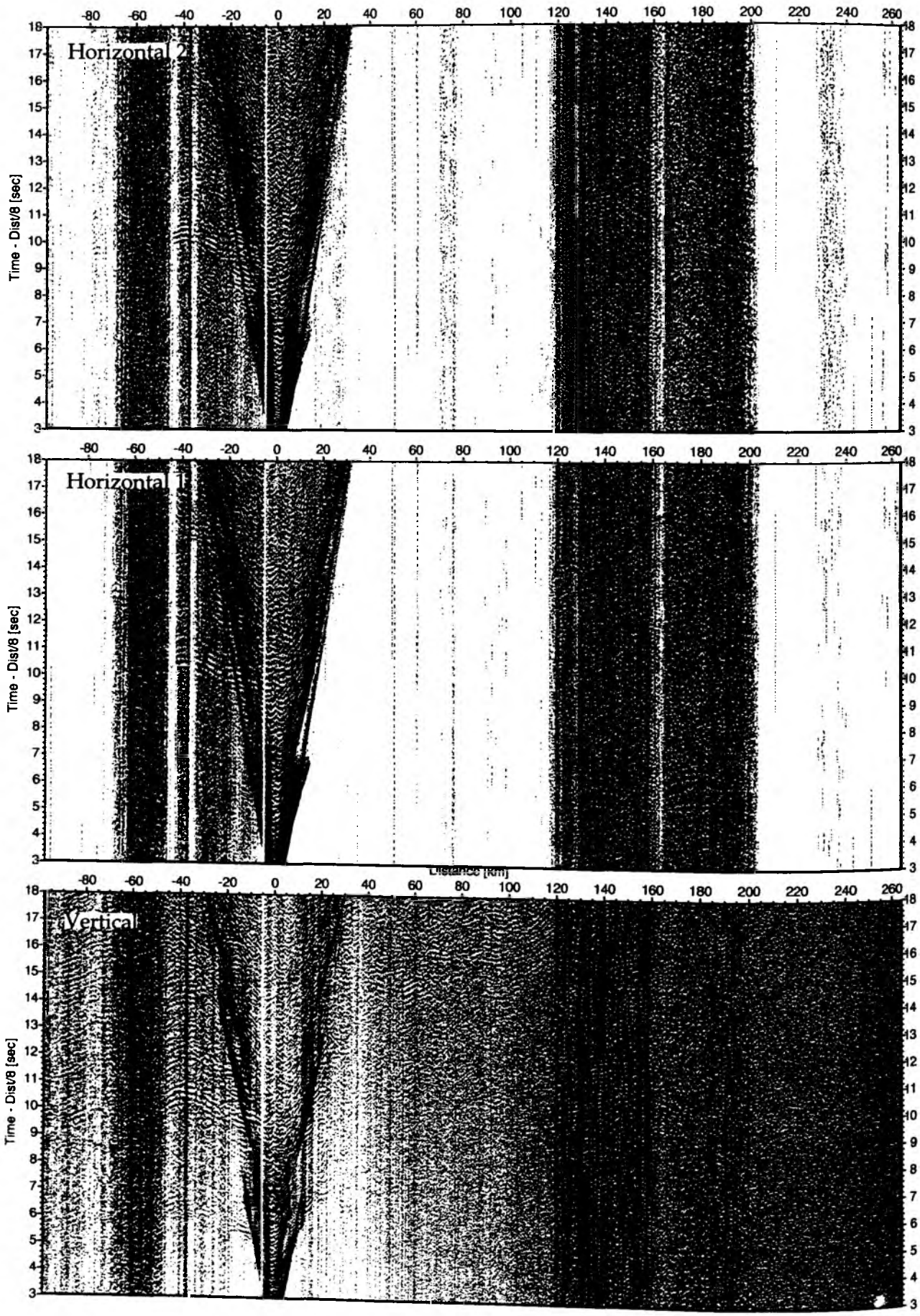

Figure 6.4.2.8: Record sections from obs 29 Geospace-Geophone, SO179 Profile 16.

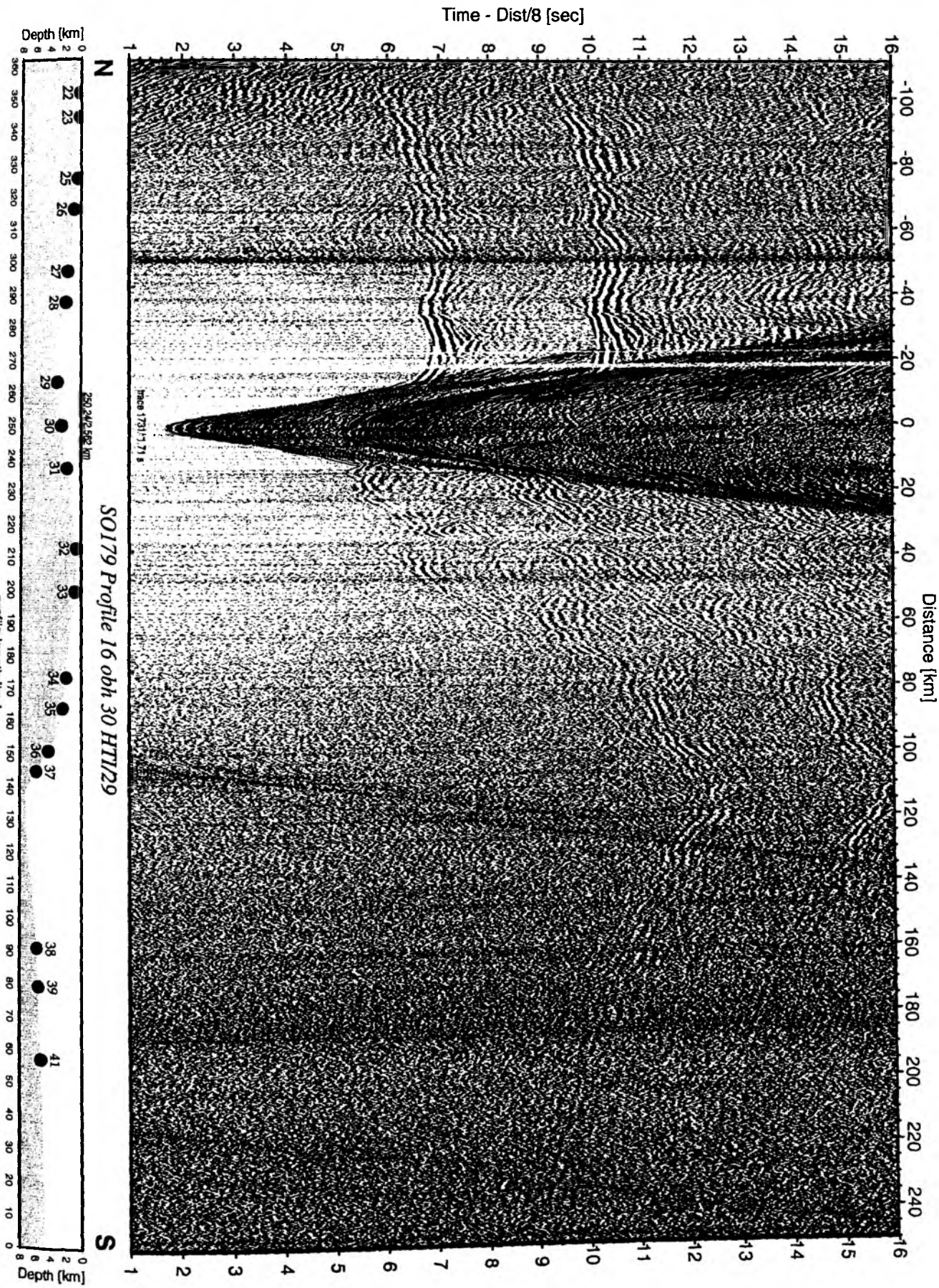

Figure 6.4.2.9: Record section from obh 30 HTI/29, Profile 16.

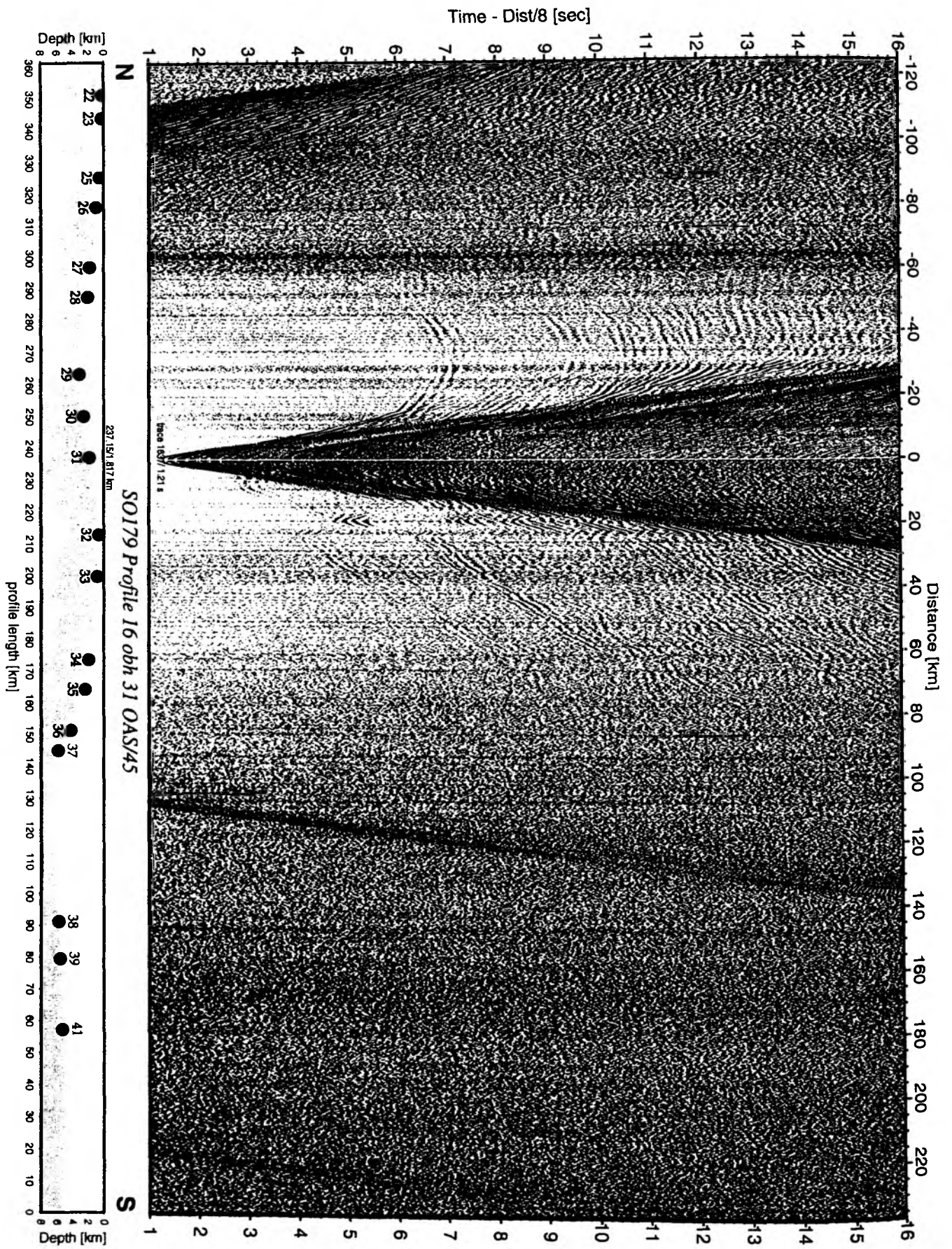

Figure 6.4.2.10: Record section from obh 31 OAS/45, Profile 16.

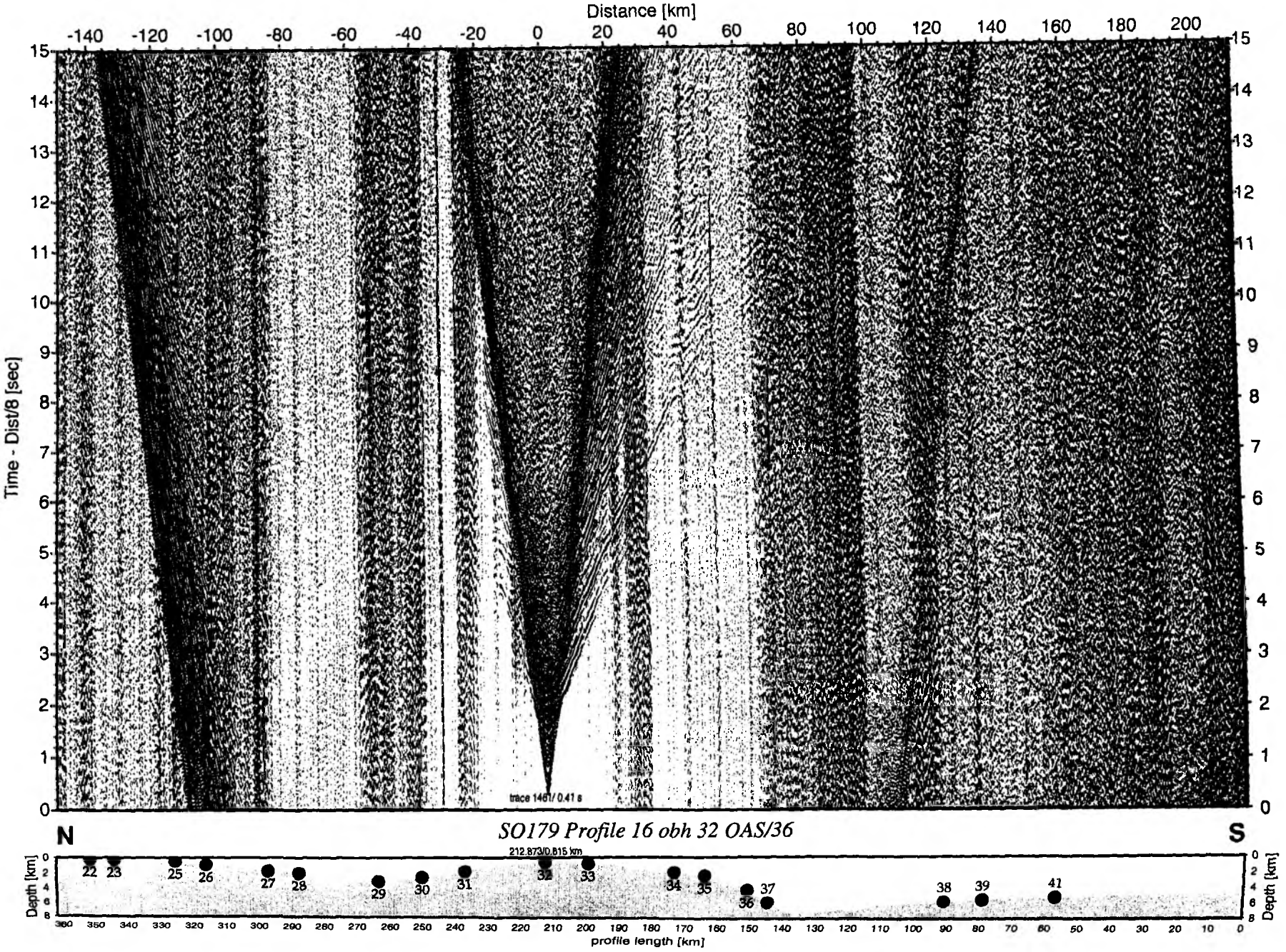

Figure 6.4.2.11: Record section from obh 32 OAS/36, Profile 16.

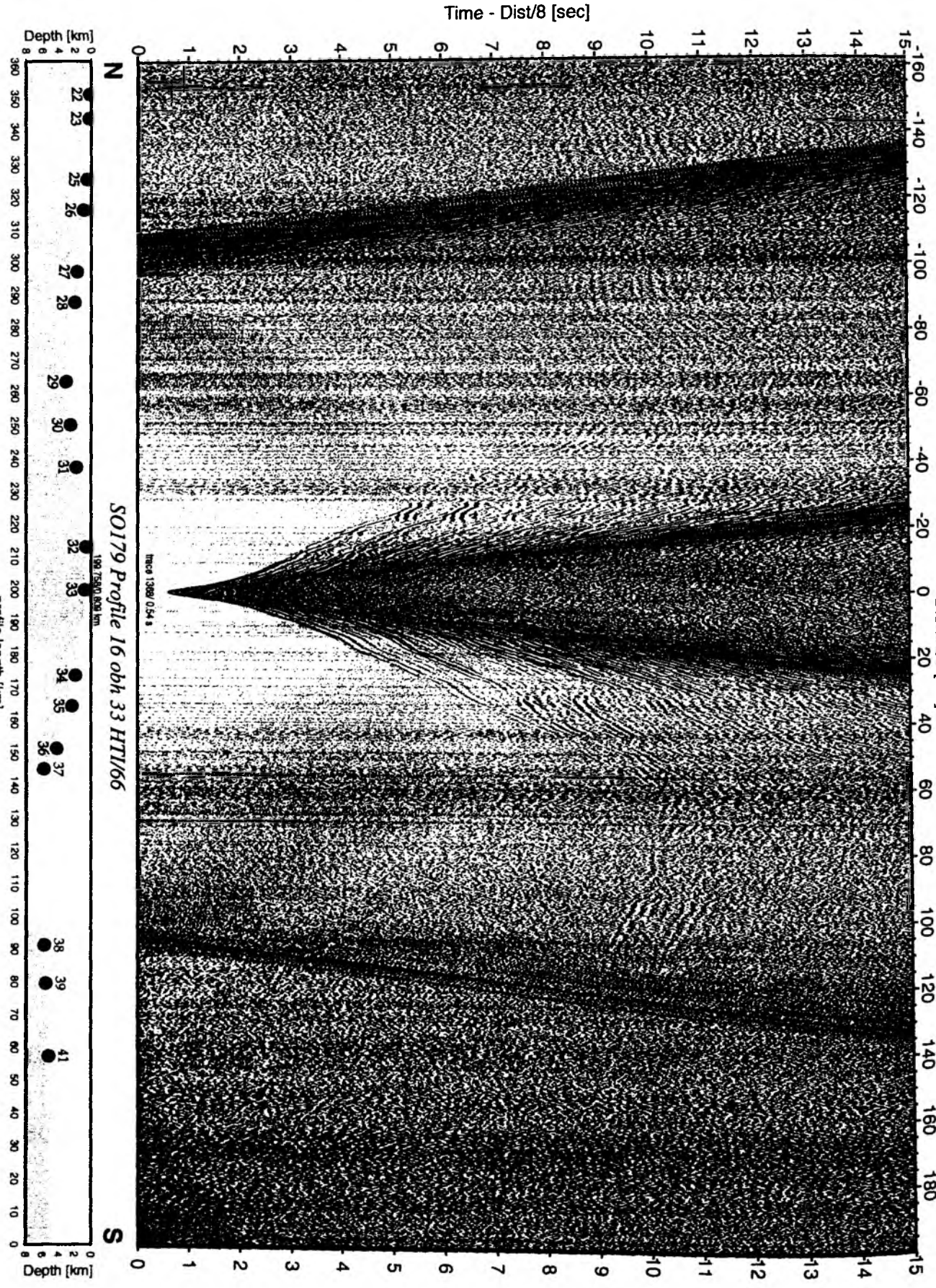

Figure 6.4.2.12: Record section from obh 33 HTI/66, Profile 16.

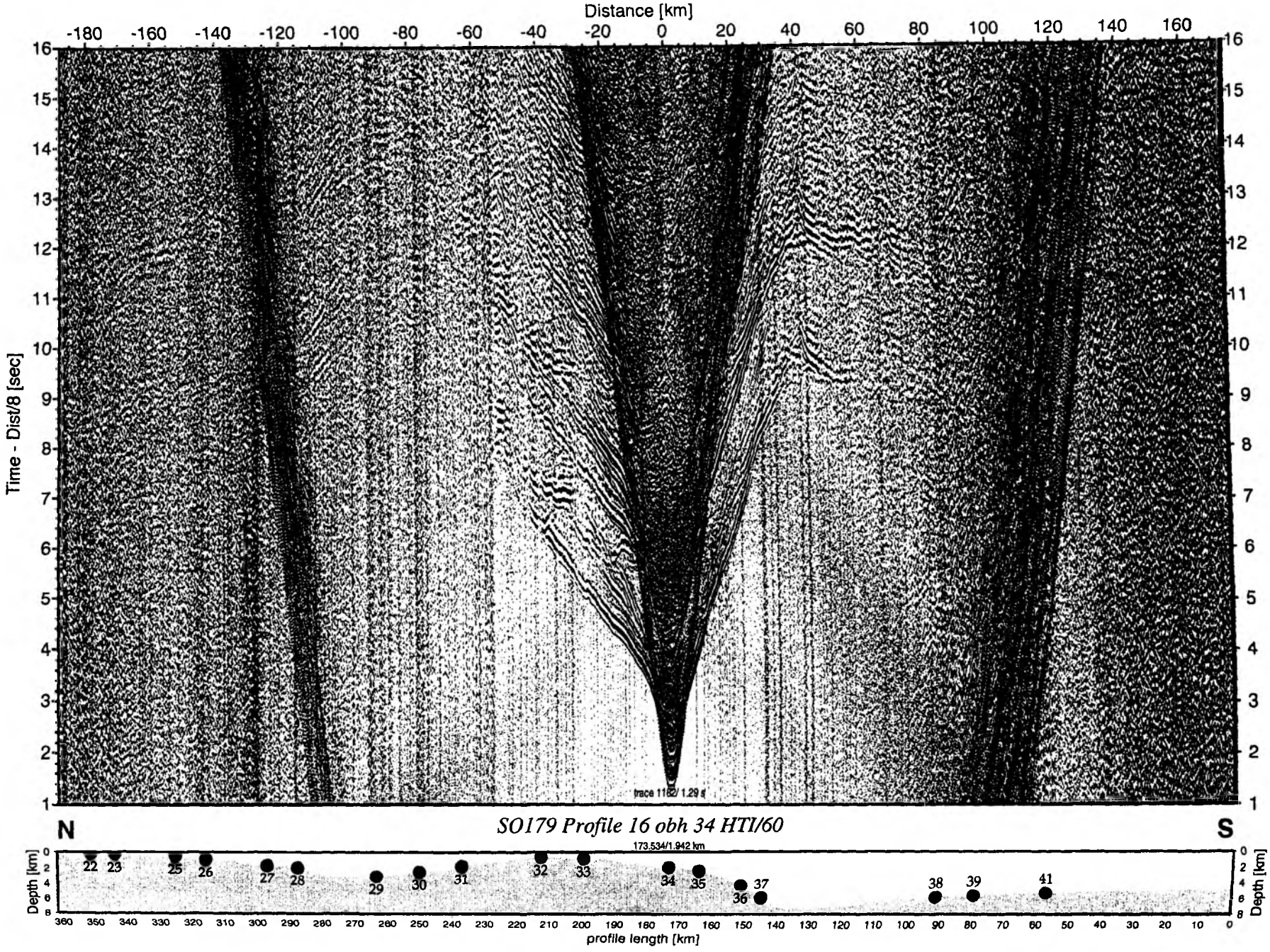

Figure 6.4.2.13: Record section from obh 34 HTI/60, Profile 16.

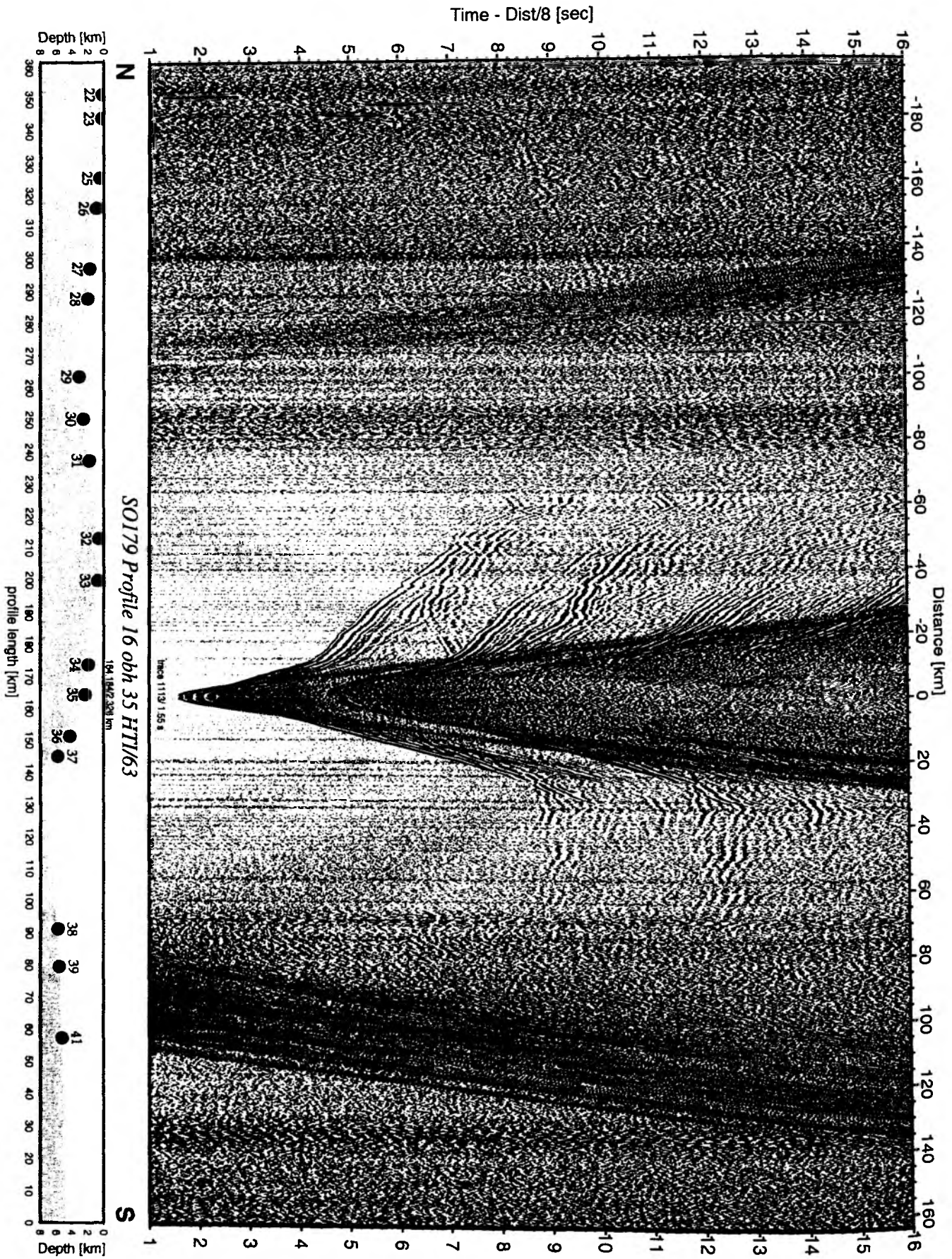

Figure 6.4.2.14: Record section from obh 35 HTI/63, Profile 16.

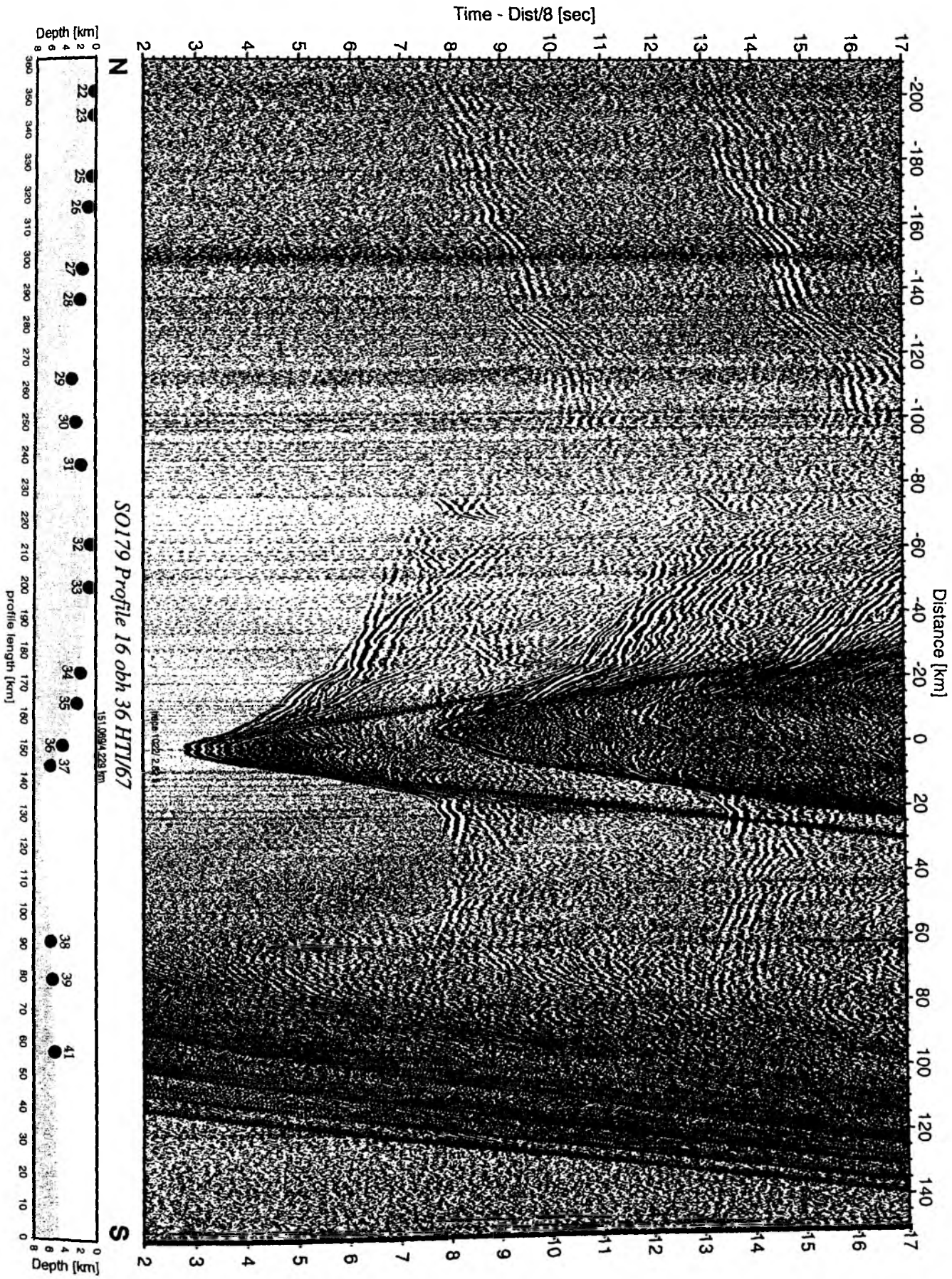

Figure 6.4.2.15: Record section from obh 36 HTI/67, Profile 16.

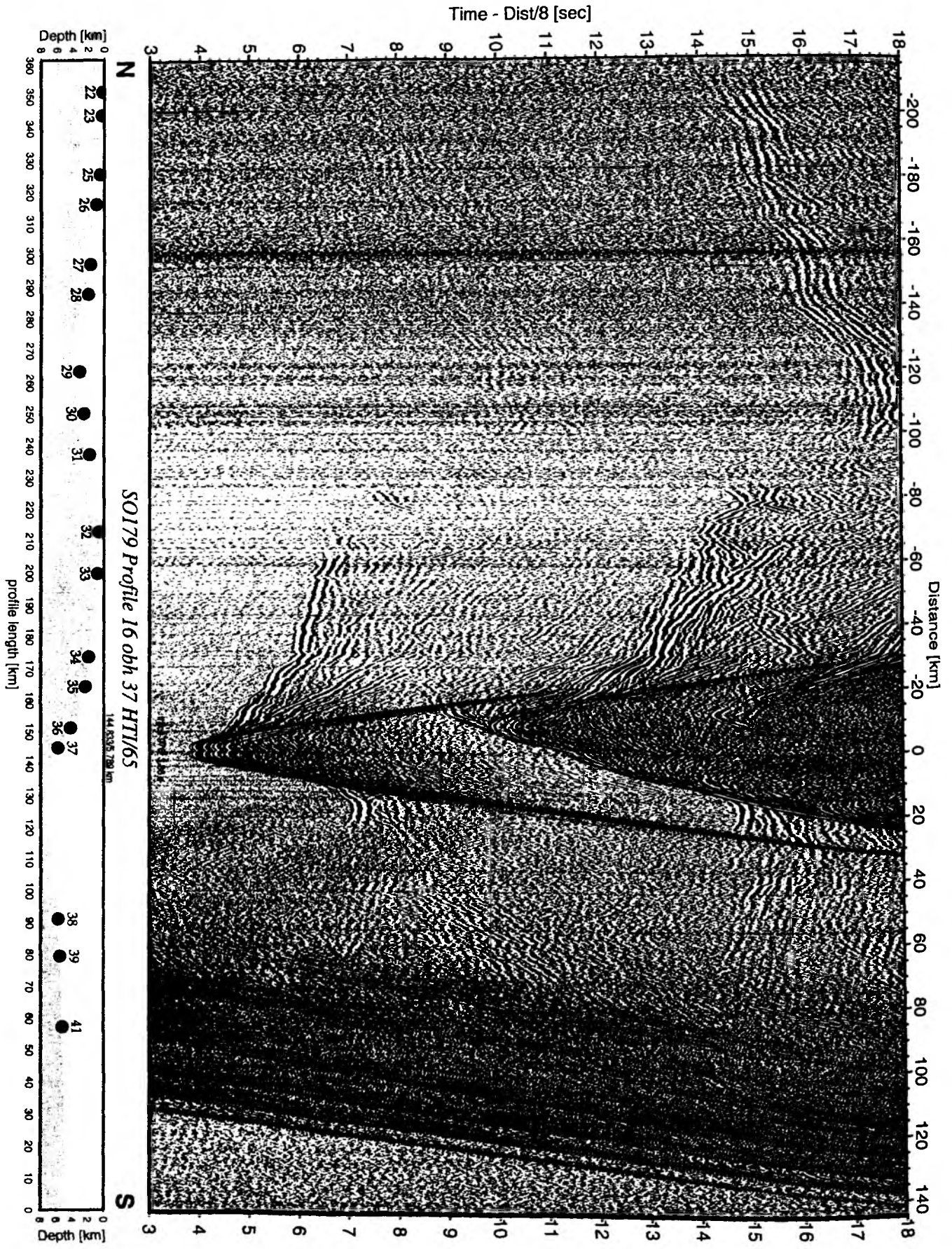

Figure 6.4.2.16: Record section from obh 37 HTI/65, Profile 16.

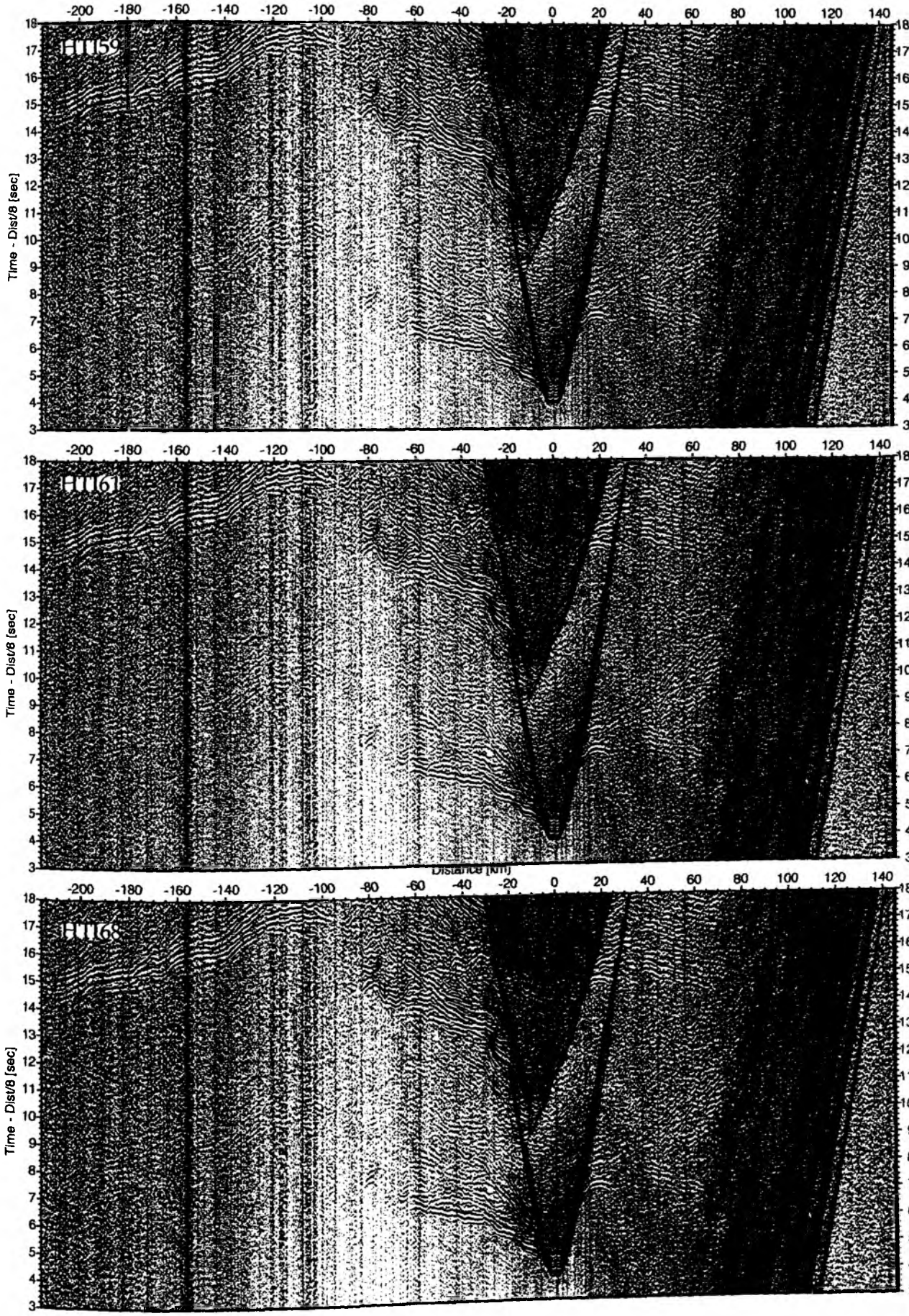

Figure 6.4.2.17: Record sections from obh 37 HTI/Test-hydrophones, SO179 Profile 16.

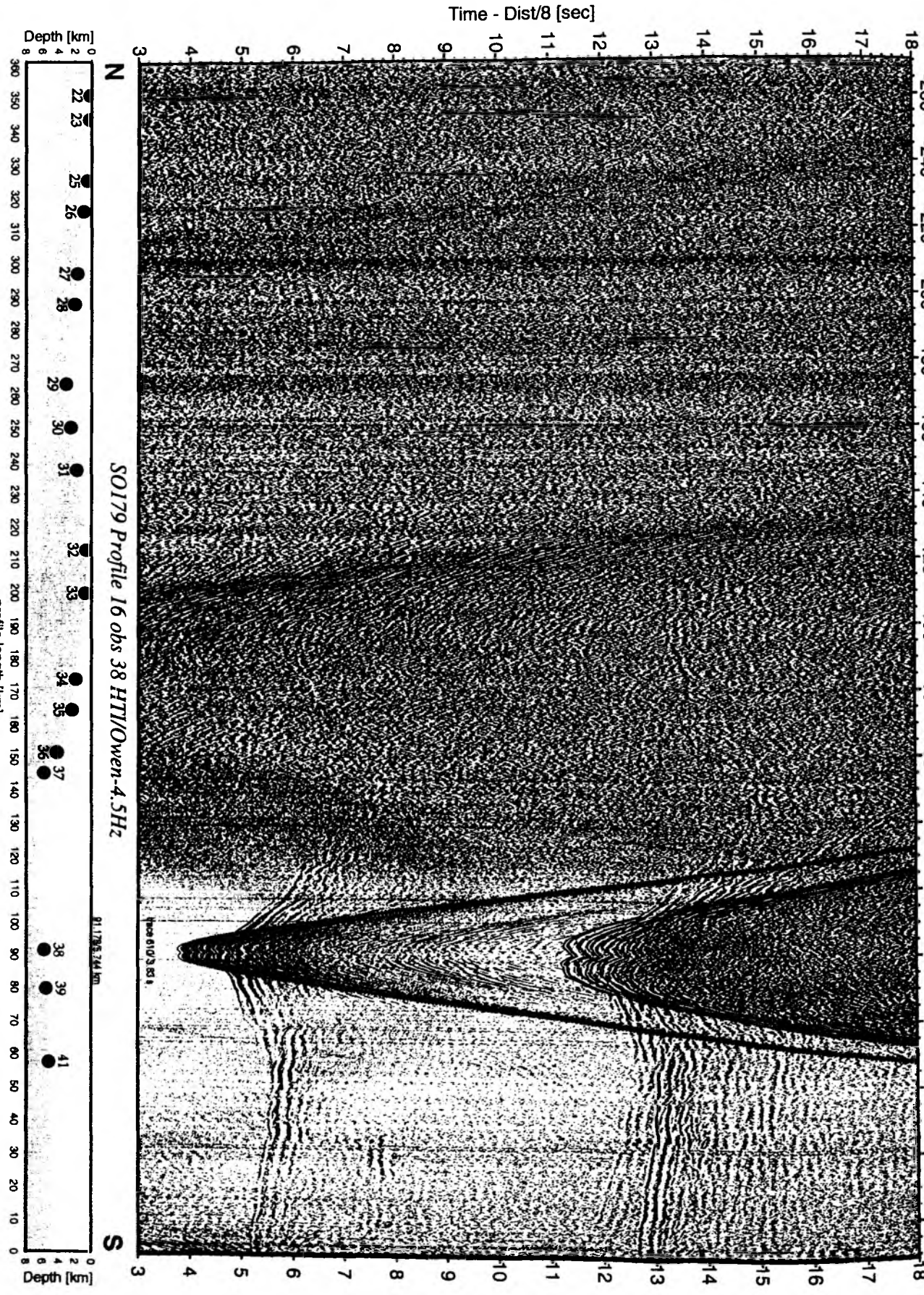

Figure 6.4.2.18: Record section from obs 38 HTI/Owen-4.5Hz, Profile 16.

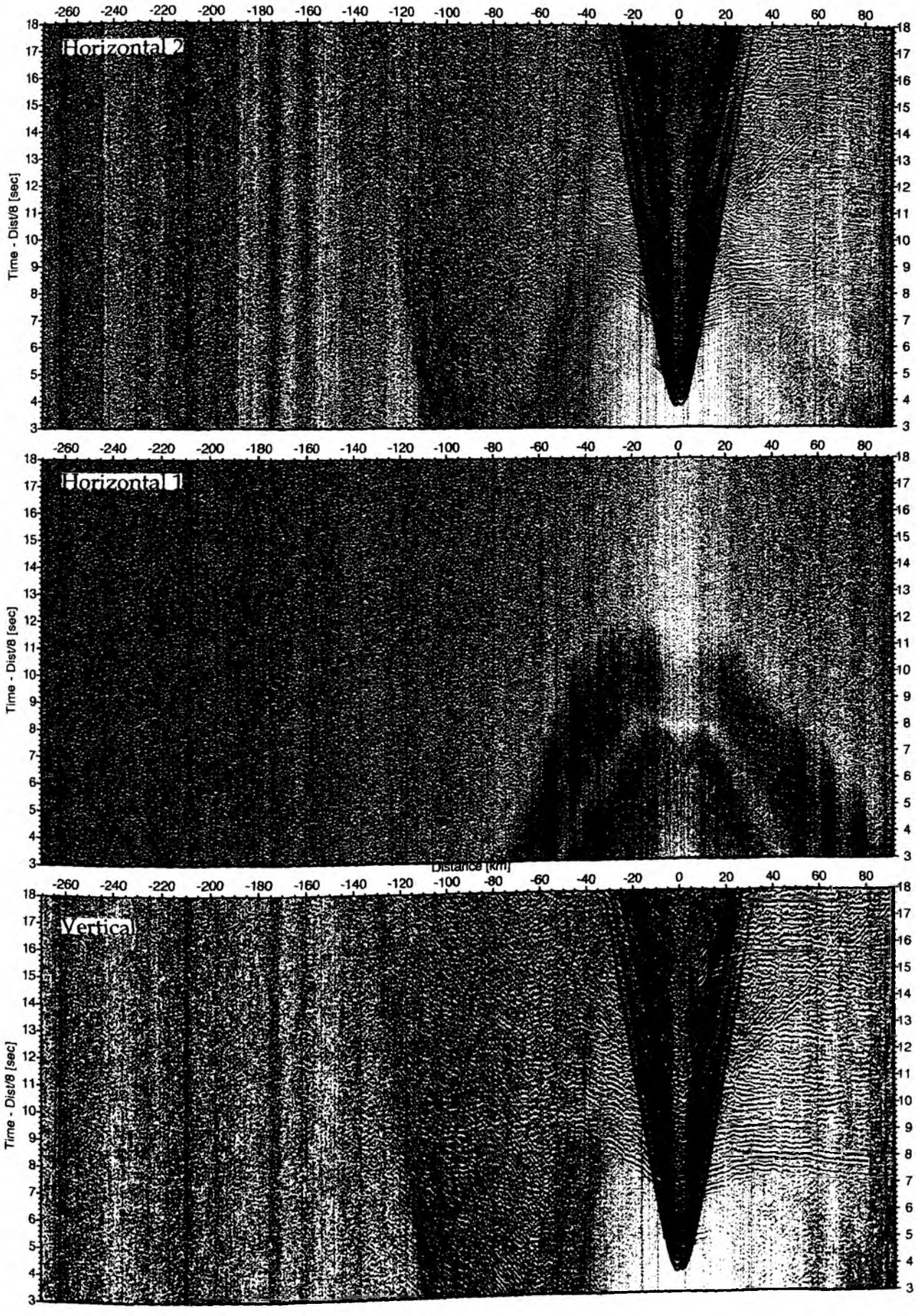

Figure 6.4.2.19: Record sections from obs 38 Owen-4.5Hz, SO179 Profile 16.

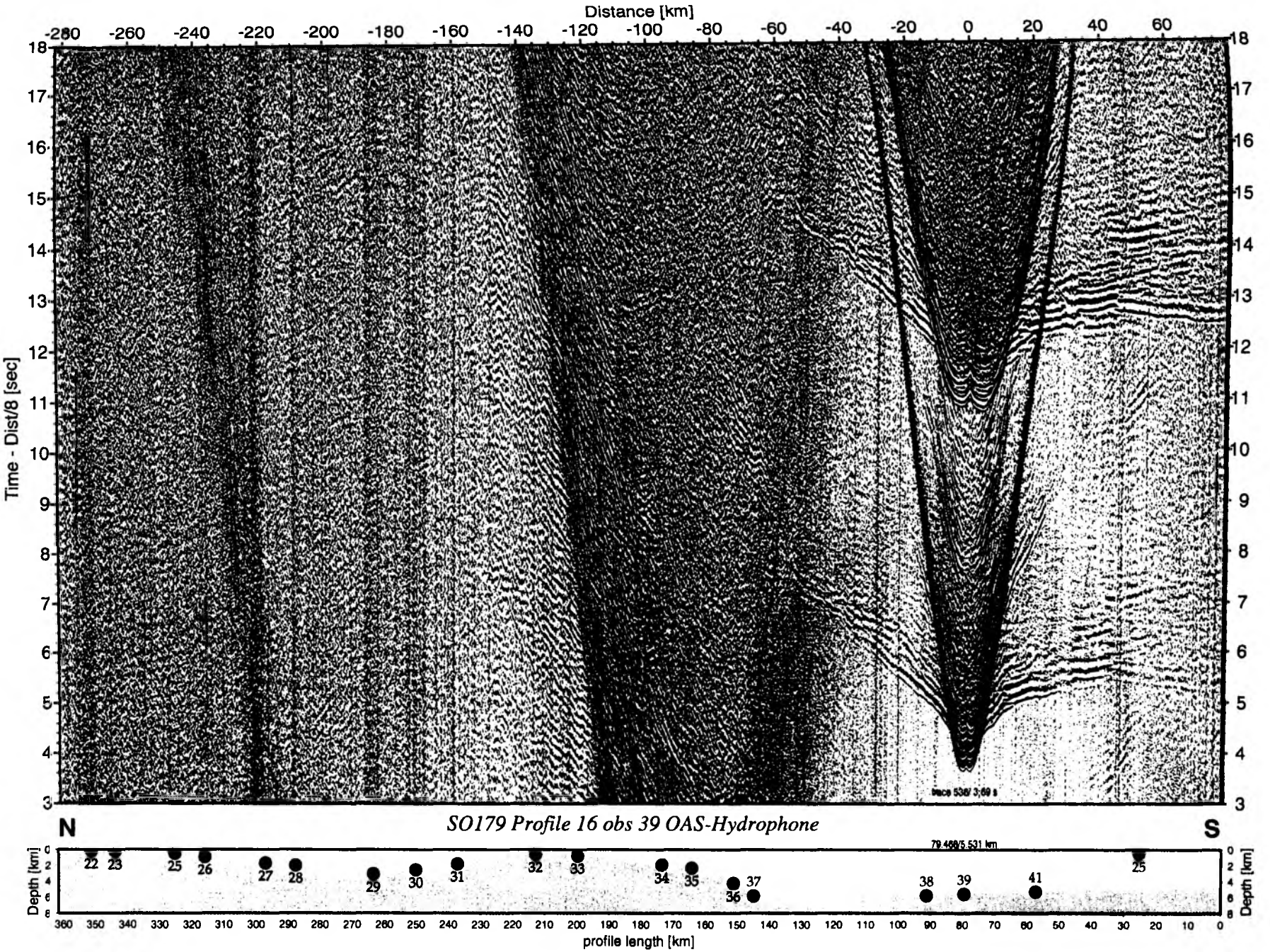

Figure 6.4.2.20: Record section from obs 39 OAS-Hydrophone, Profile 16.

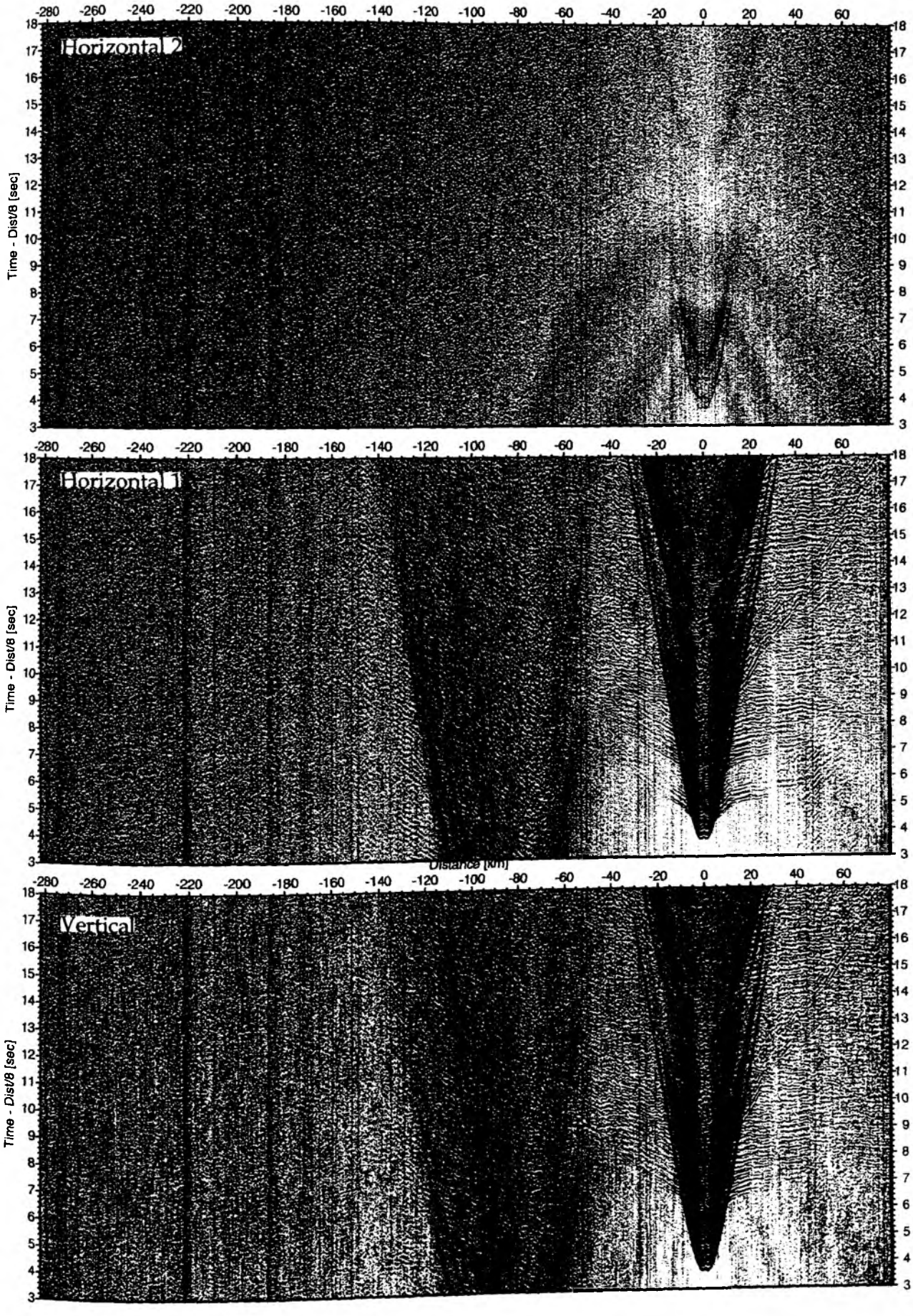

Figure 6.4.2.21: Record sections from obs 39 Owen-4.5Hz, SO179 Profile 16.

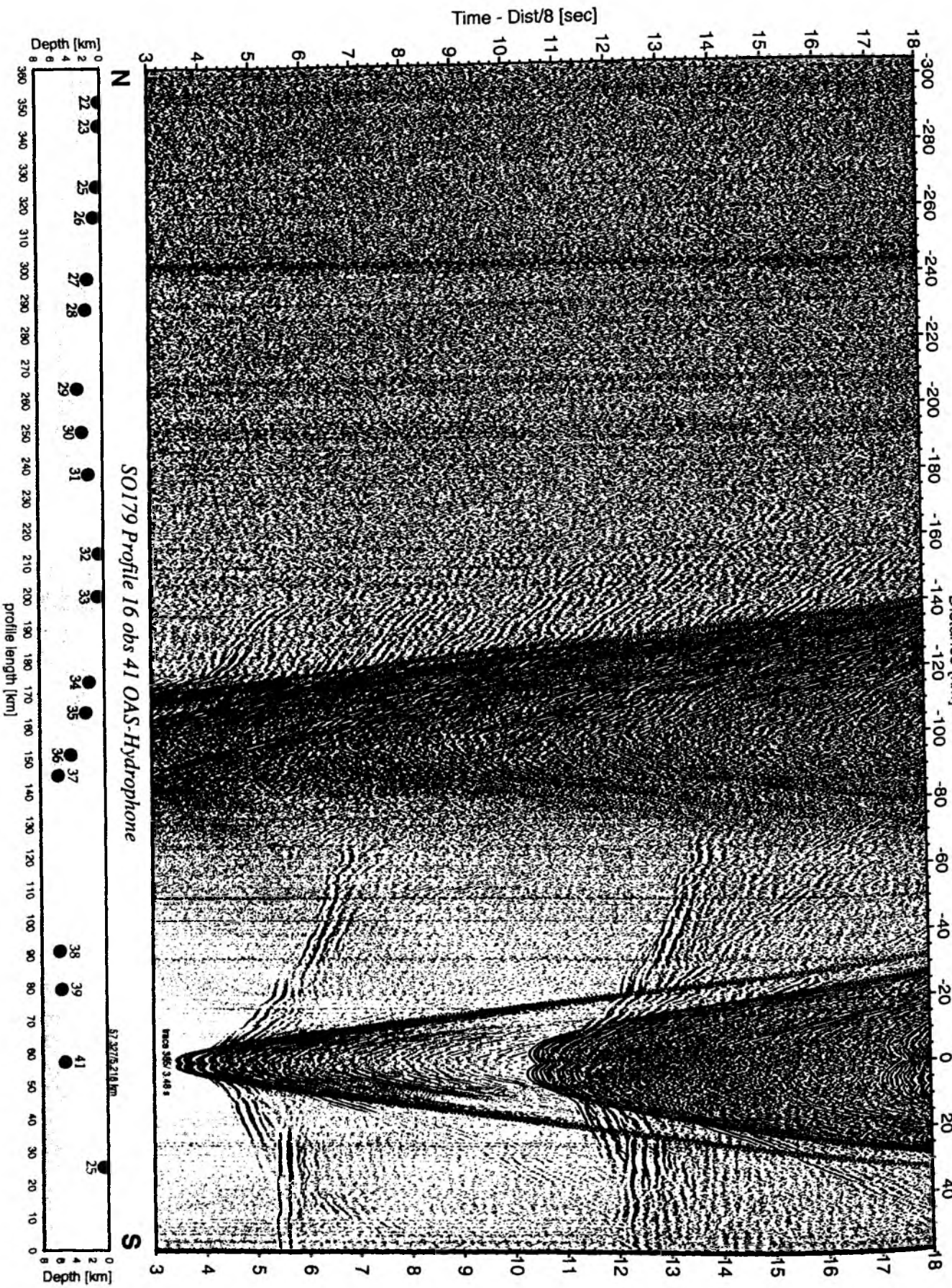

Figure 6.4.2.22: Record section from obs 41 OAS-Hydrophone, Profile 16.

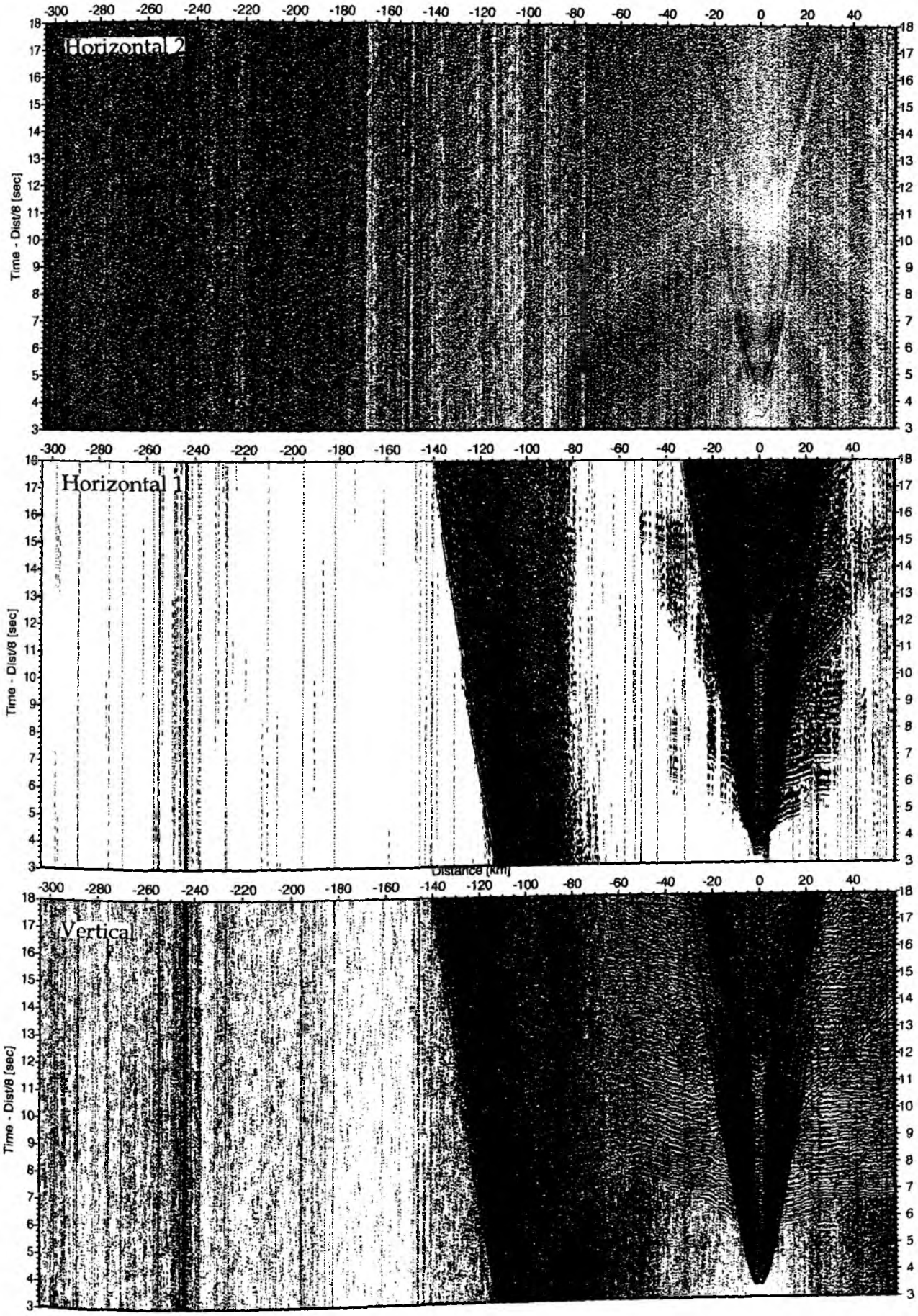

Figure 6.4.2.23: Record sections from obs 41 Owen-4.5Hz, SO179 Profile 16.

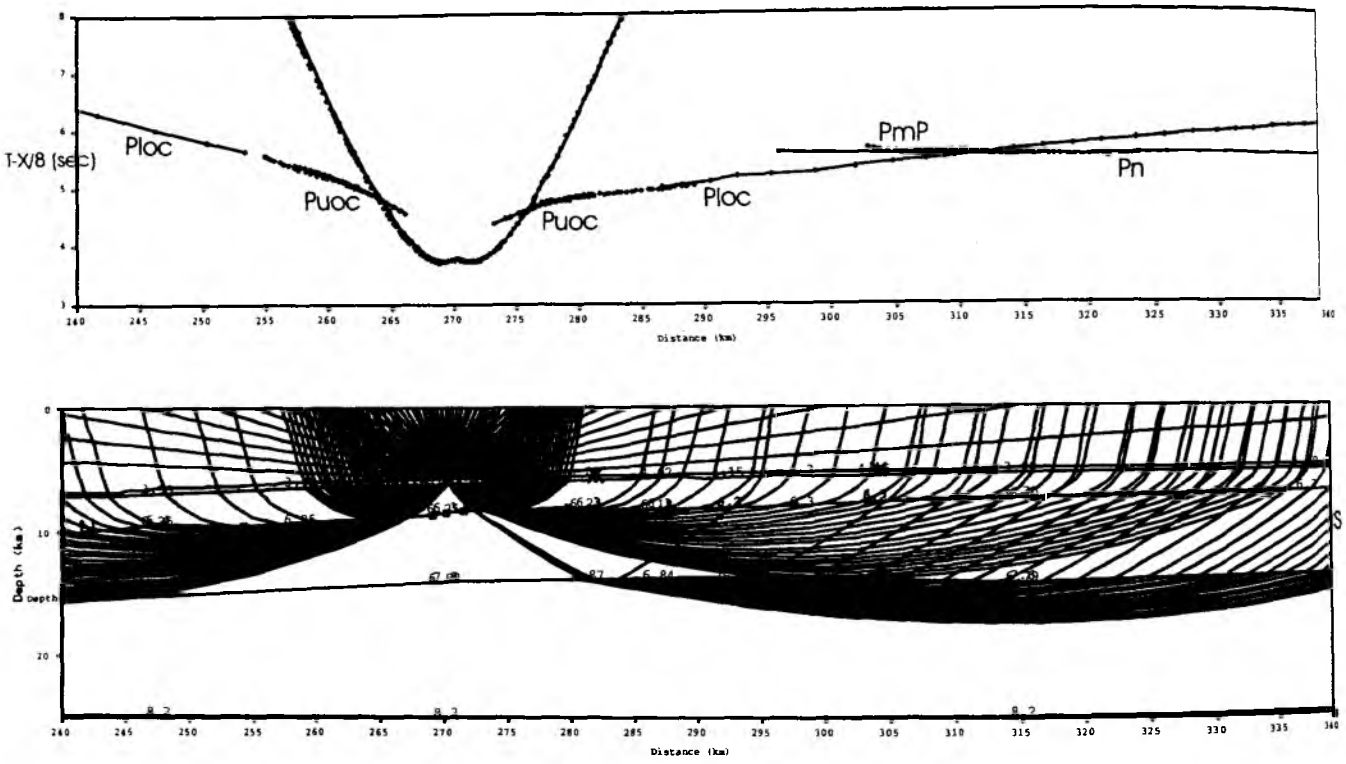

***Figure 6.4.2.24**: traveltimes picks (upper image) and raypaths of OBH 38. This OBH recorded refracted waves in upper and lower crust (Puoc and Ploc) and in oceanic mantle (PmP and Pn).*

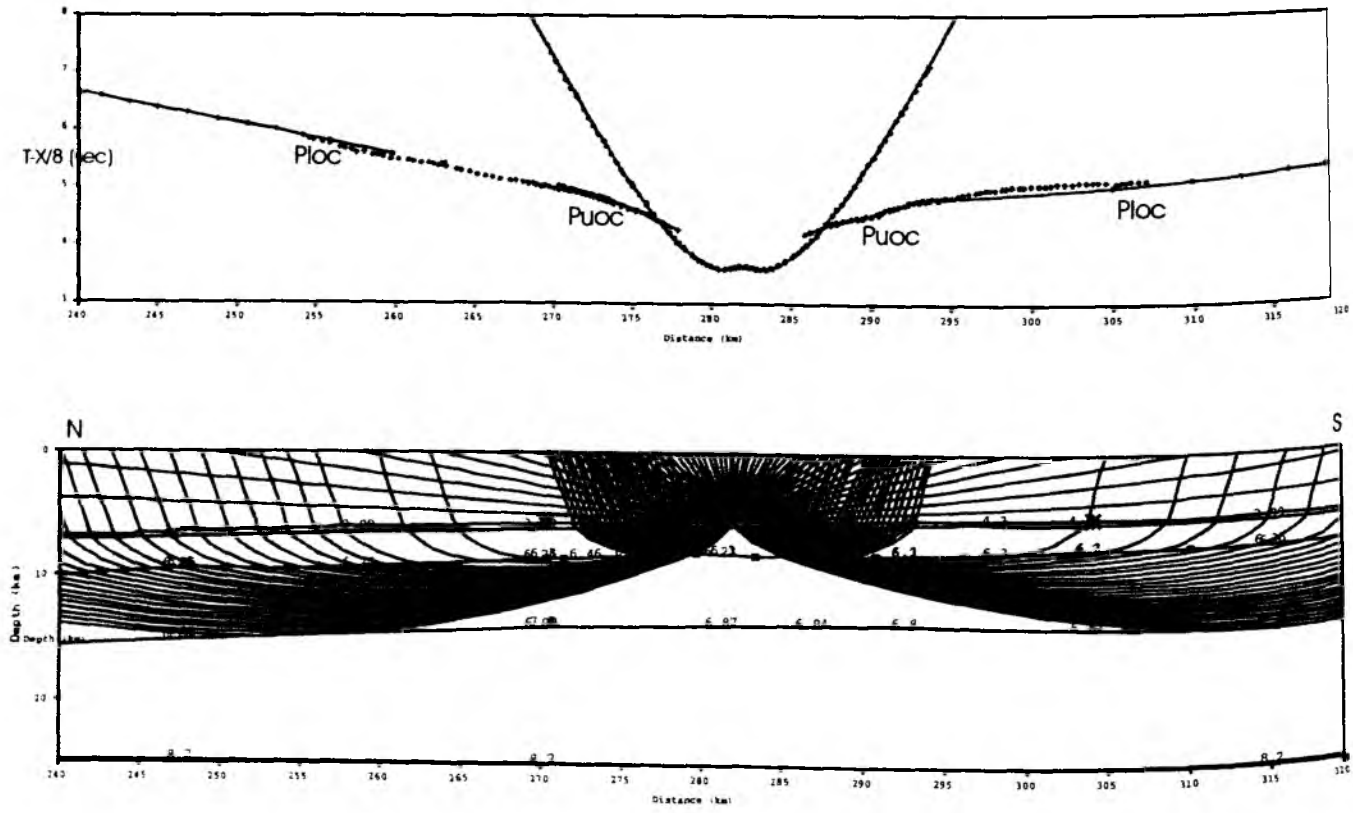

***Figure 6.4.2.25**: traveltimes picks (upper image) and raypaths of OBH 39. This OBH recorded refracted waves in upper and lower crust (Puoc and Ploc).*

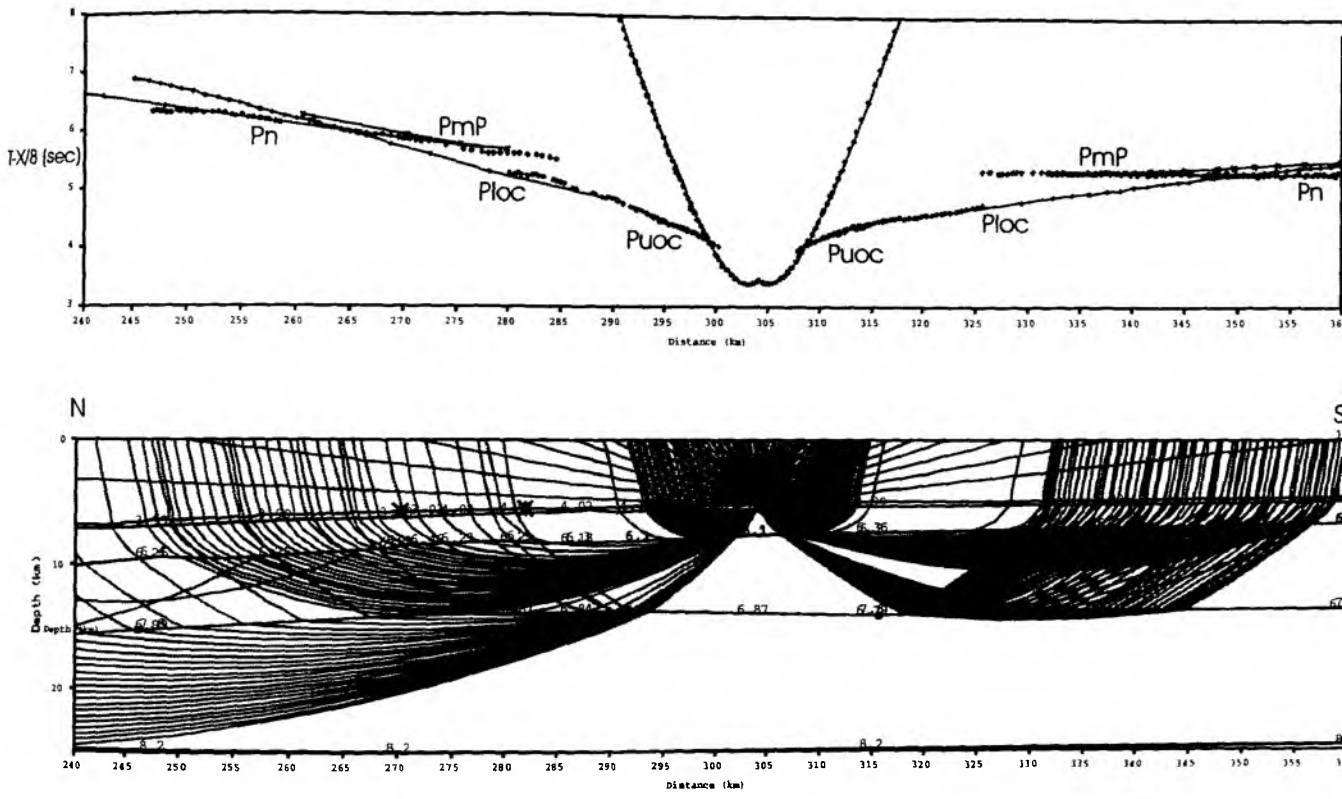

Figure 6.4.2.26: *traveltimes picks (upper image) and raypaths of OBH 41. This OBH recorded refracted waves in upper and lower crust (Puoc and Ploc) and in oceanic mantle (PmP indicates the wide-angle reflexion on the Moho and Pn, the refracted waves in oceanic mantle).*

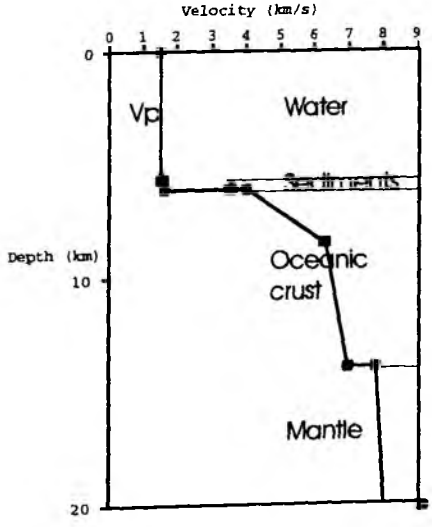

Figure 6.4.2.27: *1D velocity model at the OBH 38*

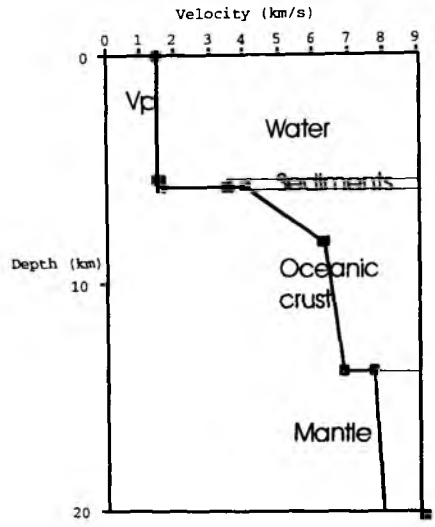

Figure 6.4.2.28: *1D velocity model at the OBH 39*

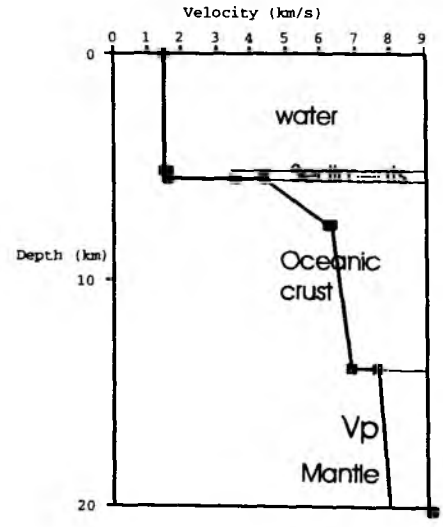

Figure 6.4.2.29: *1D velocity model at the OBH 41*

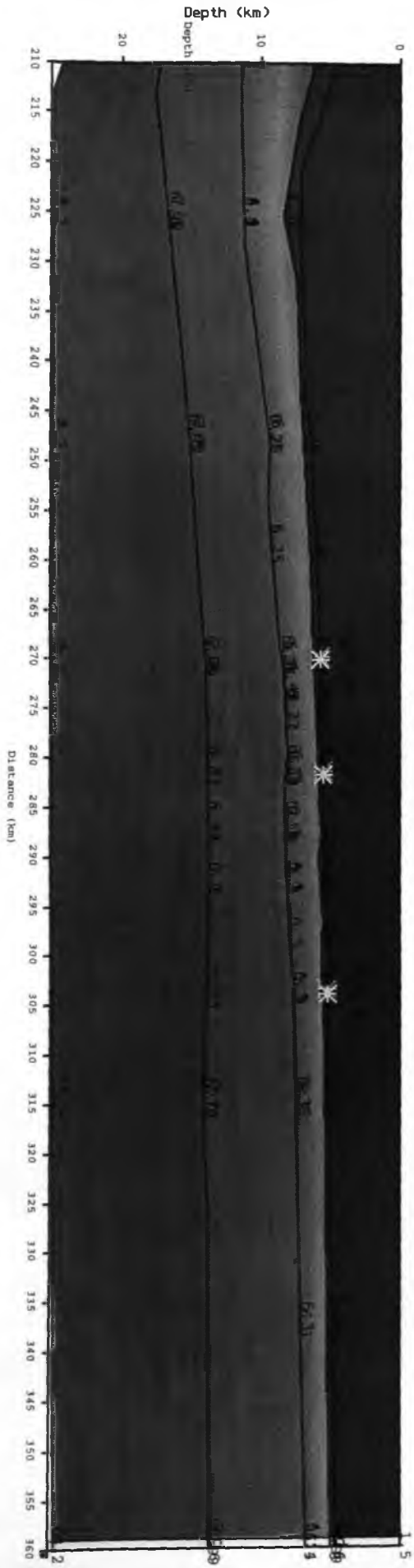

***Figure 6.4.2.30**: velocity model of the oceanic crust in the southern part of profile 16*

6.4.3 Profile P18

This profile is the western dip line across the Java margin and trench. It is 189 nm long and reaches from close to the coast across the trench and onto the oceanic plate. In total 23 OBH/S (OBS42 to OBH64) were deployed on 28/29.09, with an average spacing of 7 nm, leaving a 30 nm gap across the 7200 m Java trench (see Figure 6.4.3.1).

Shooting started at 05:00 29.09 close to the shore and was terminated around midnight 30.9/1.10. All three guns were in operation, but again a few interruptions occurred, when the buoyancy bodies of one gun were lost (for details see Appendix 9.3). Instruments were recovered successfully by 05:30 on 2. October. During shooting the magnetometer and the streamer were also deployed, but the streamer data were totally corrupted due to leakage. All data were processed according the the dataflow described in section 6.3, the resulting record sections are shown in Figures 6.4.3.3 to 6.4.3.25

The record sections of the OBH/S stations are generally of good quality, but also variable. In most cases one can see the crustal and mantle phases up to an offset range from 80 - 100 km. On the oceanic plate, the recordings from OBS42 can be followed to a distance of 160 km across the lower slope, while on the neighboring three instruments first arrivals are rather weak.
On the record sections from OBS56 to OBH58 a later reflection can be identified easily towards the north with a critical distance of about 80 km. This could well be associated with the plate boundary.

One of the most spectacular section is from OBH62, despite its deployment in shallow water energy can be followed throughout the section to distances of 300 km.

OBH63 had a power failure soon after shooting had started, and data from OBH50 could not be retrieved onboard, but will be available after repair of the flashdisc in the lab.

No attempt was made onboard to start an interpretation of the data.

Profil P18

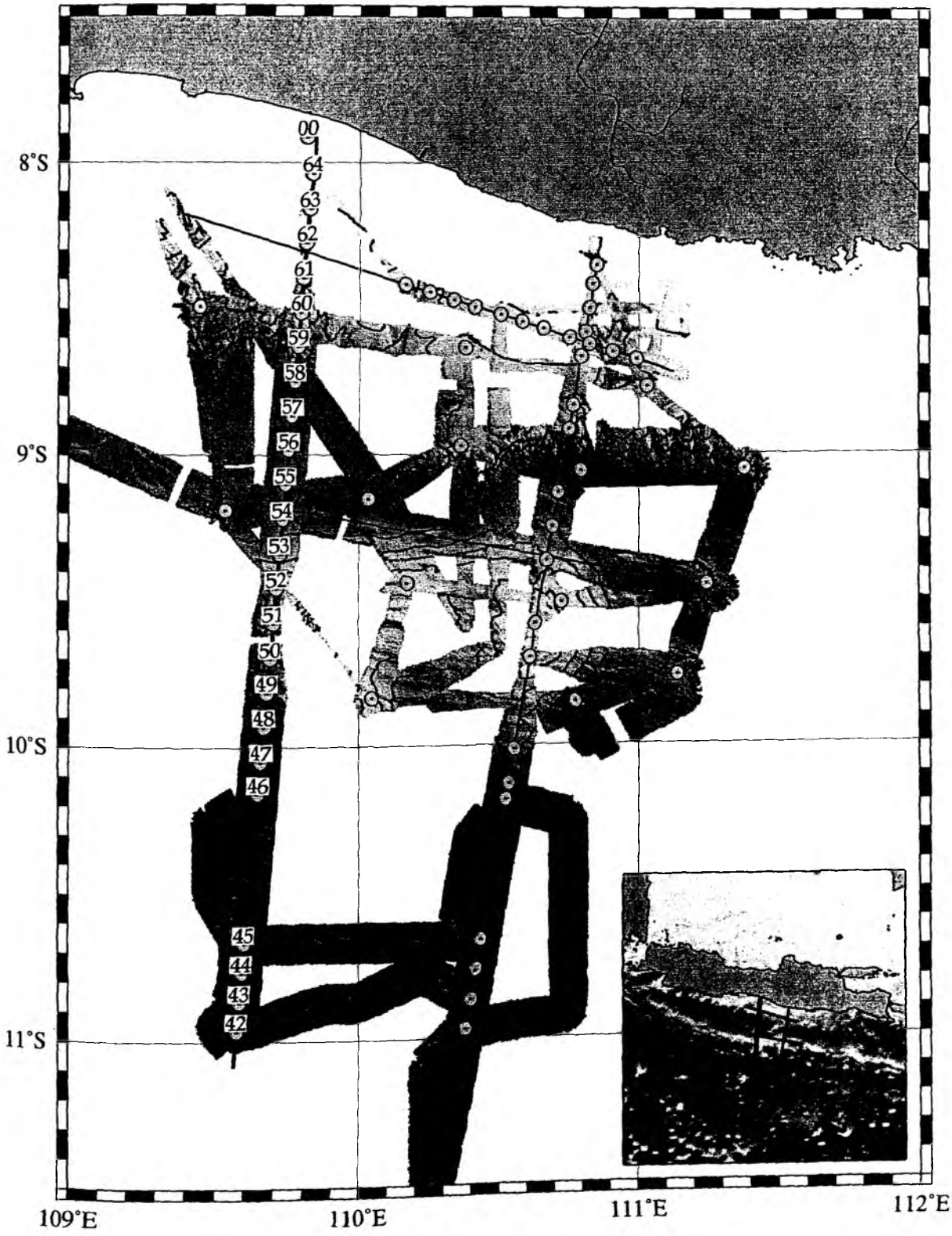

Figure 6.4.3.1: *location map of profile 18.*

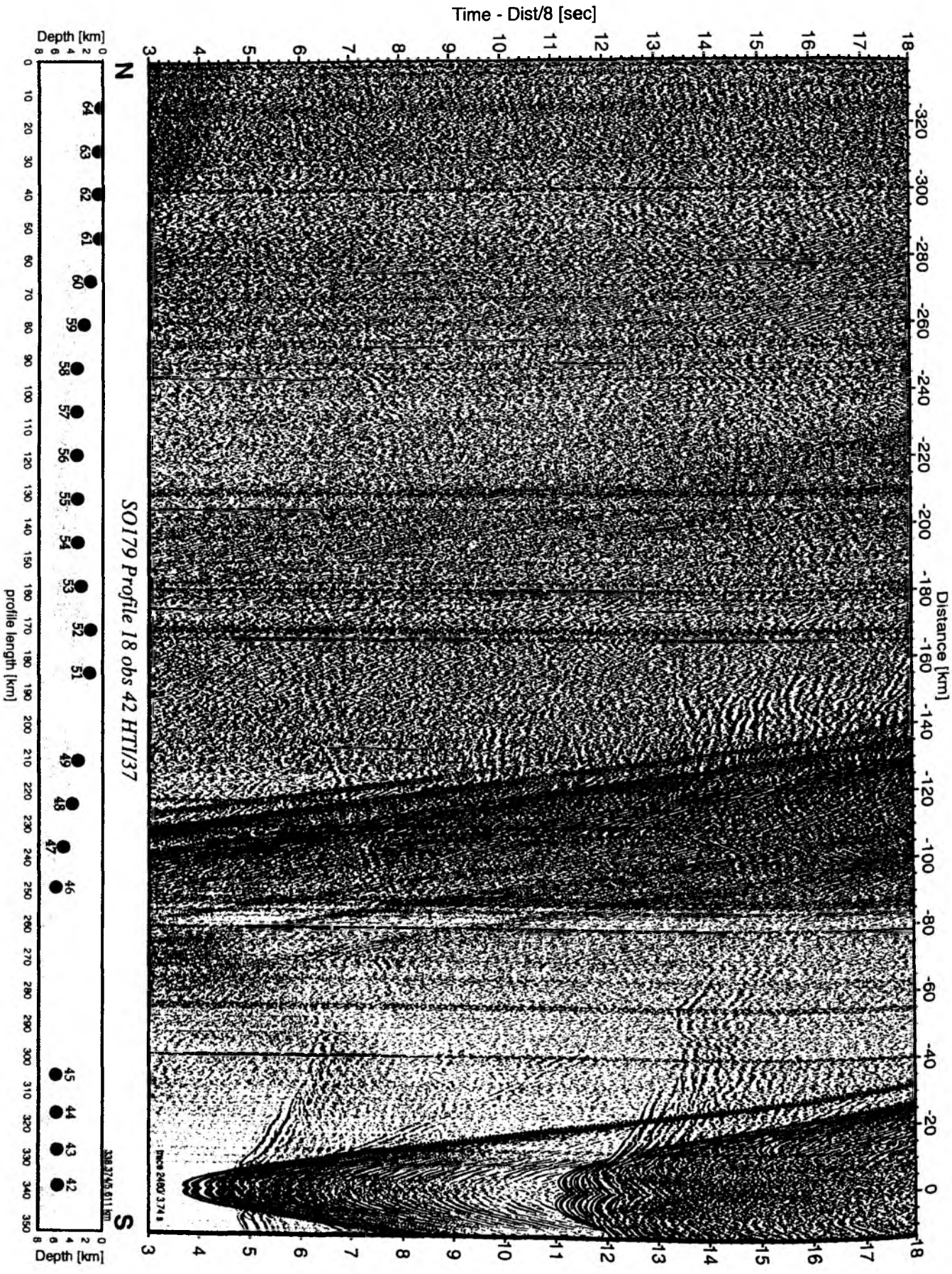

Figure 6.4.3.2: Record section from obs 42 HTI/37, Profile 18.

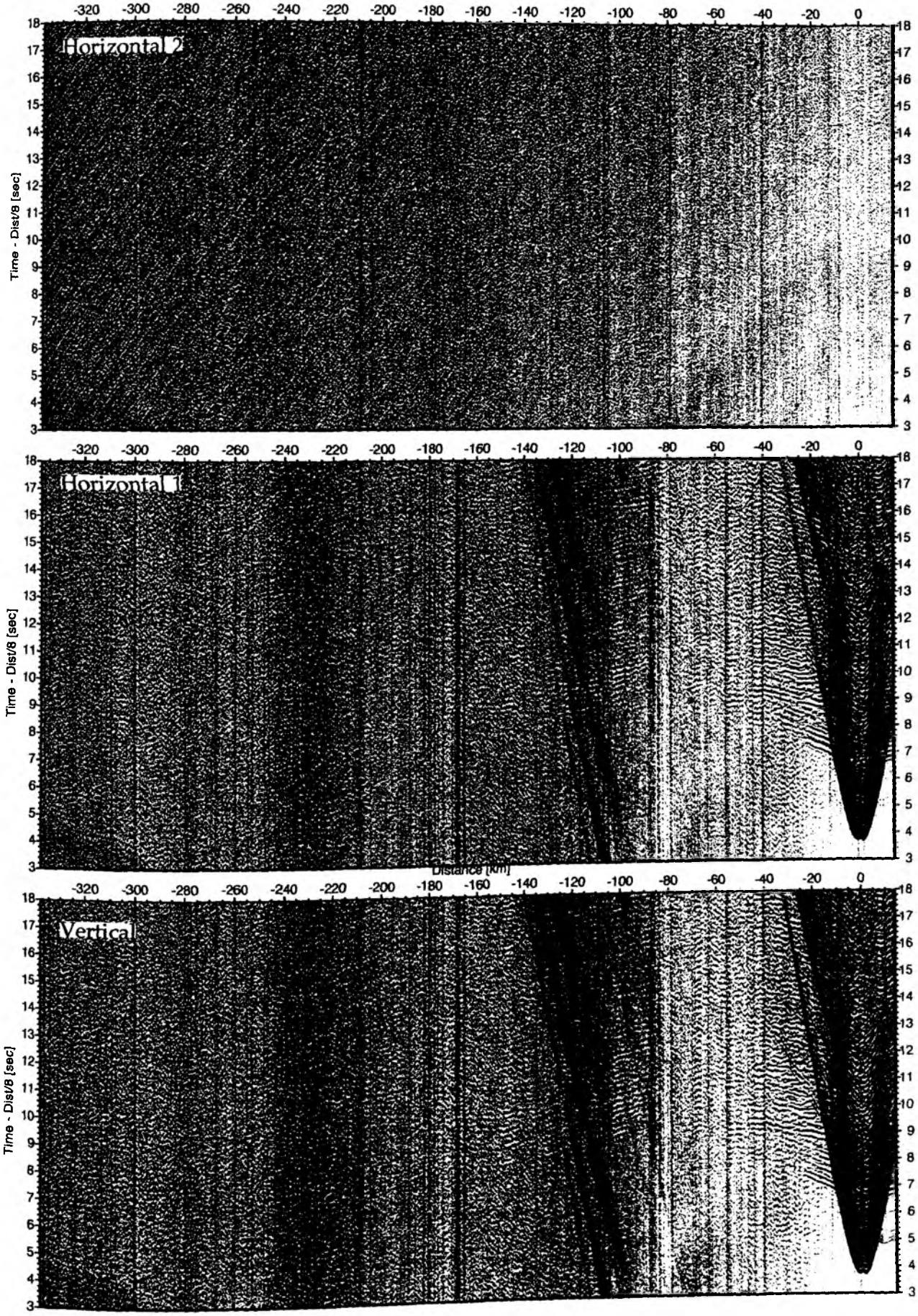

Figure 6.4.3.3: Record sections from obs 42 Owen-4.5Hz, SO179 Profile 18.

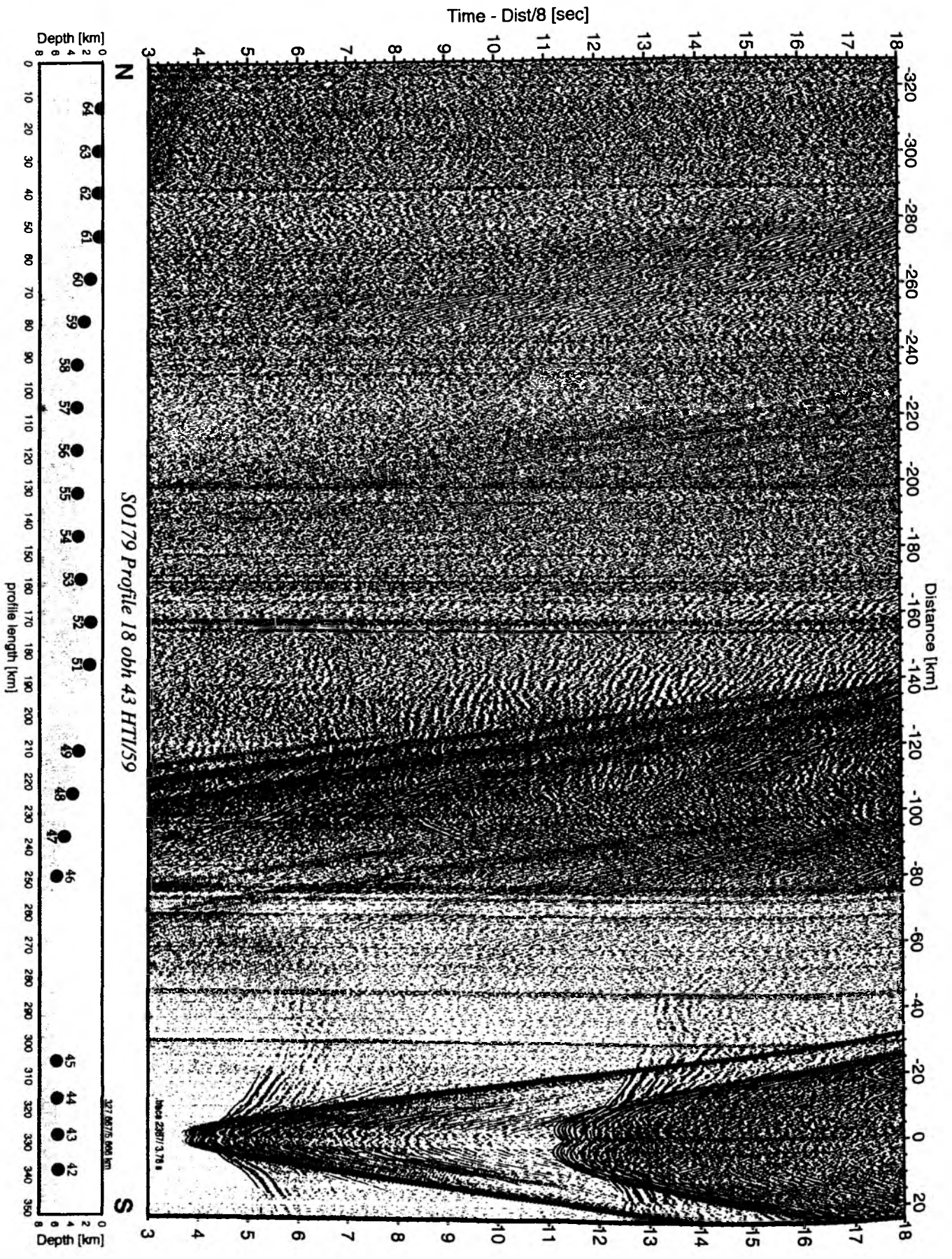

Figure 6.4.3.4: Record section from obh 43 HTI/59, Profile 18.

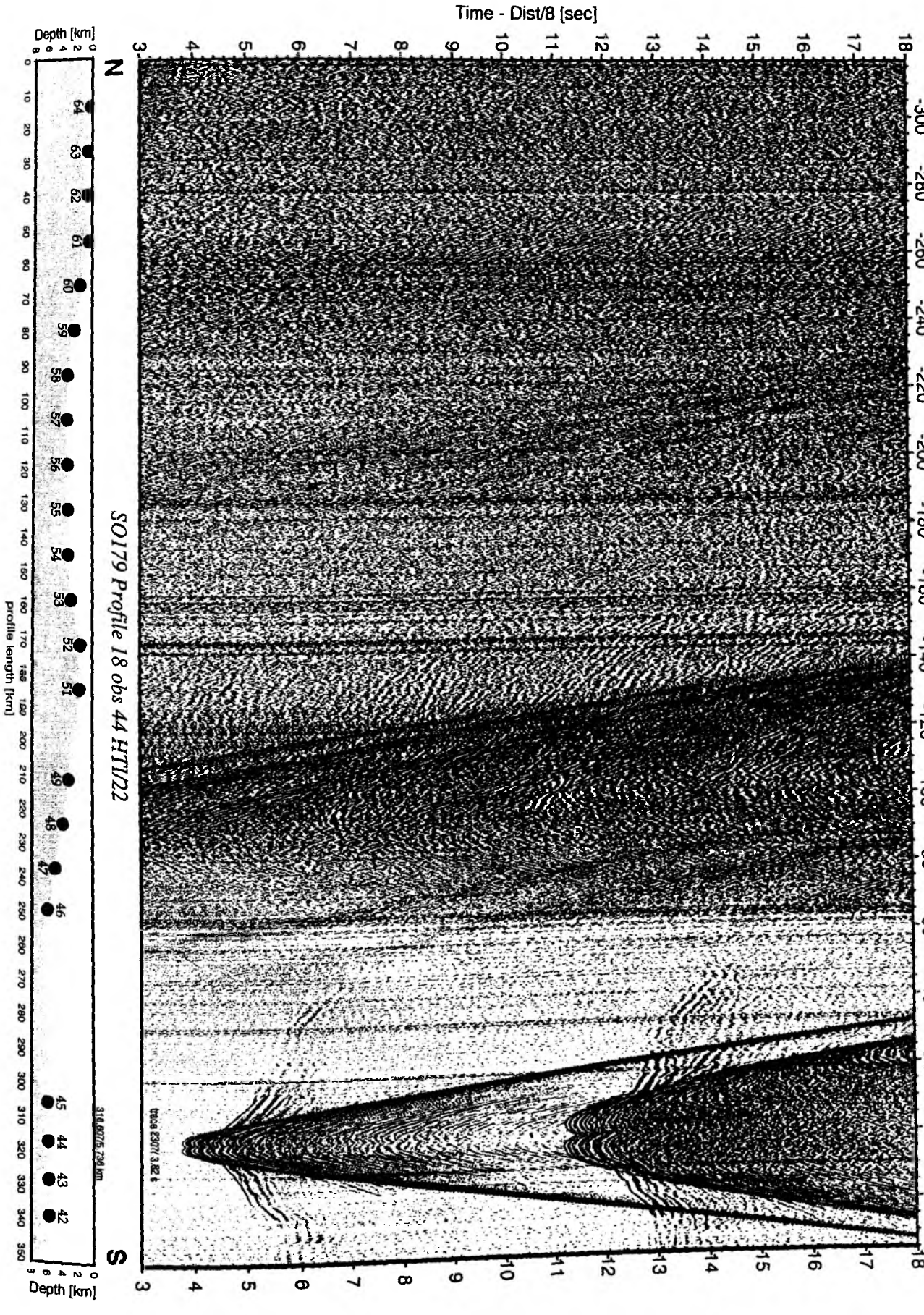

Figure 6.4.3.5: Record section from obs 44 HTI/22, Profile 18.

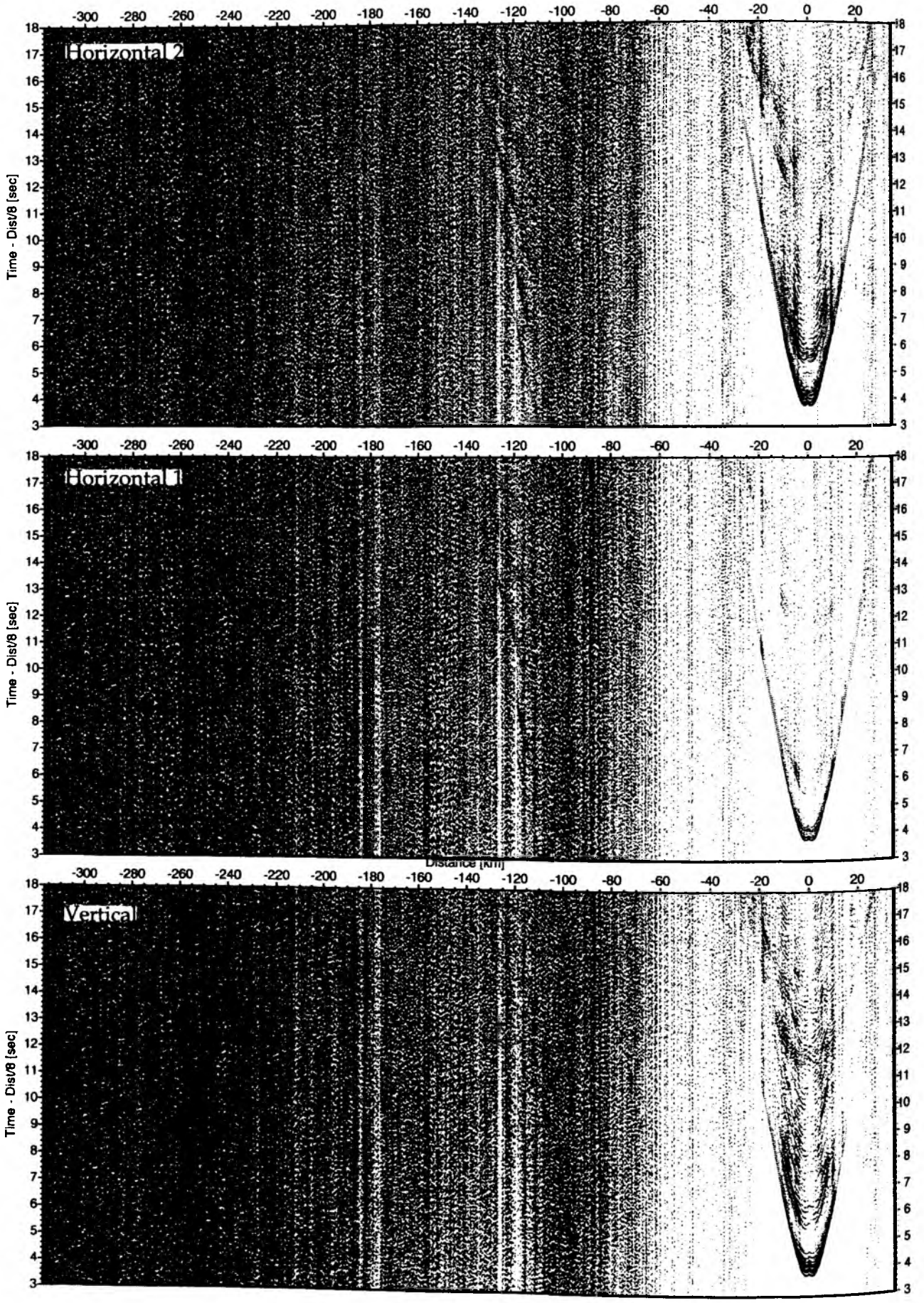

Figure 6.4.3.6: Record sections from obs 44 Geospace-Geophone, SO179 Profile 18.

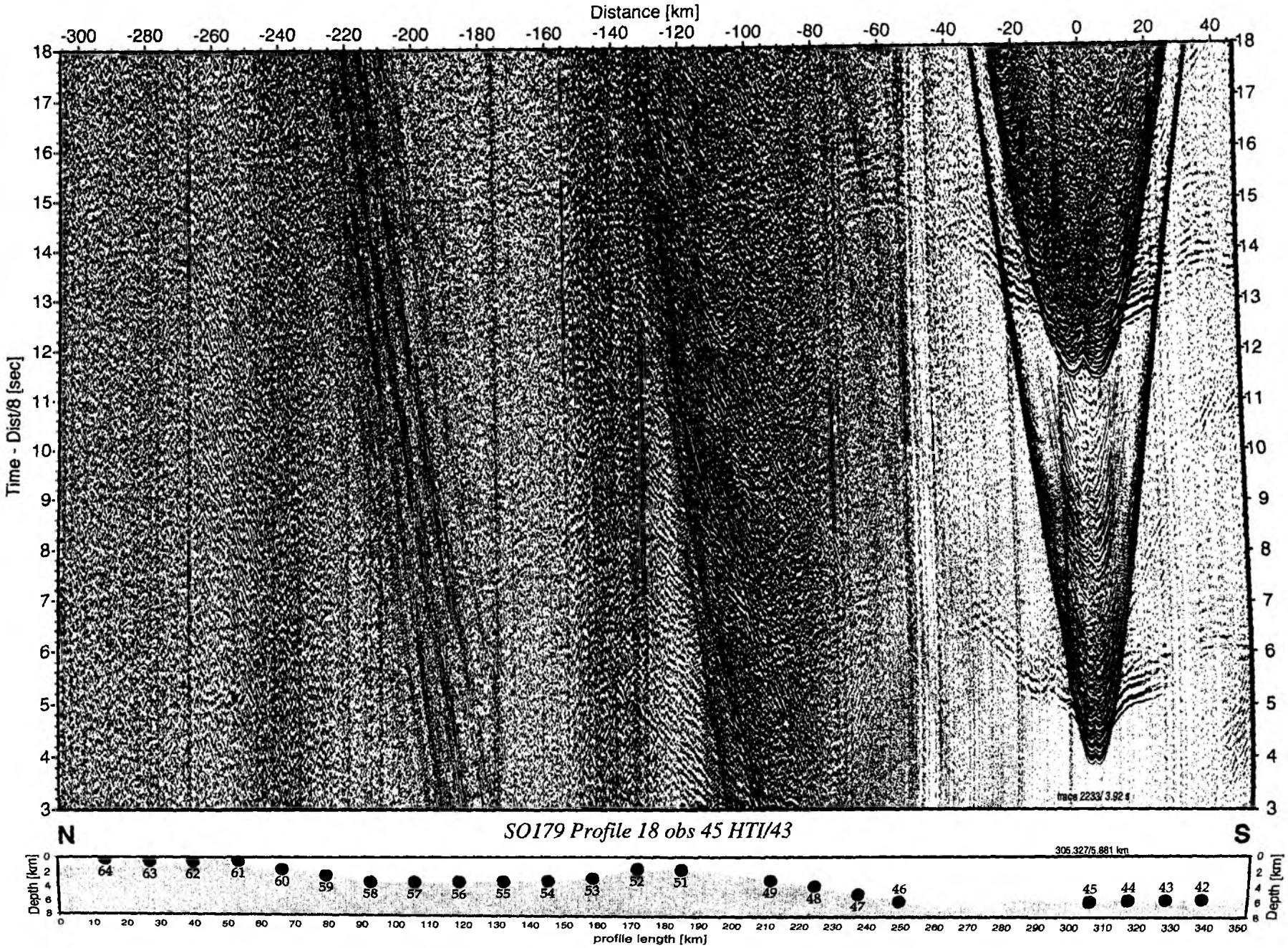

Figure 6.4.3.7: Record section from obs 45 HTI/43, Profile 18.

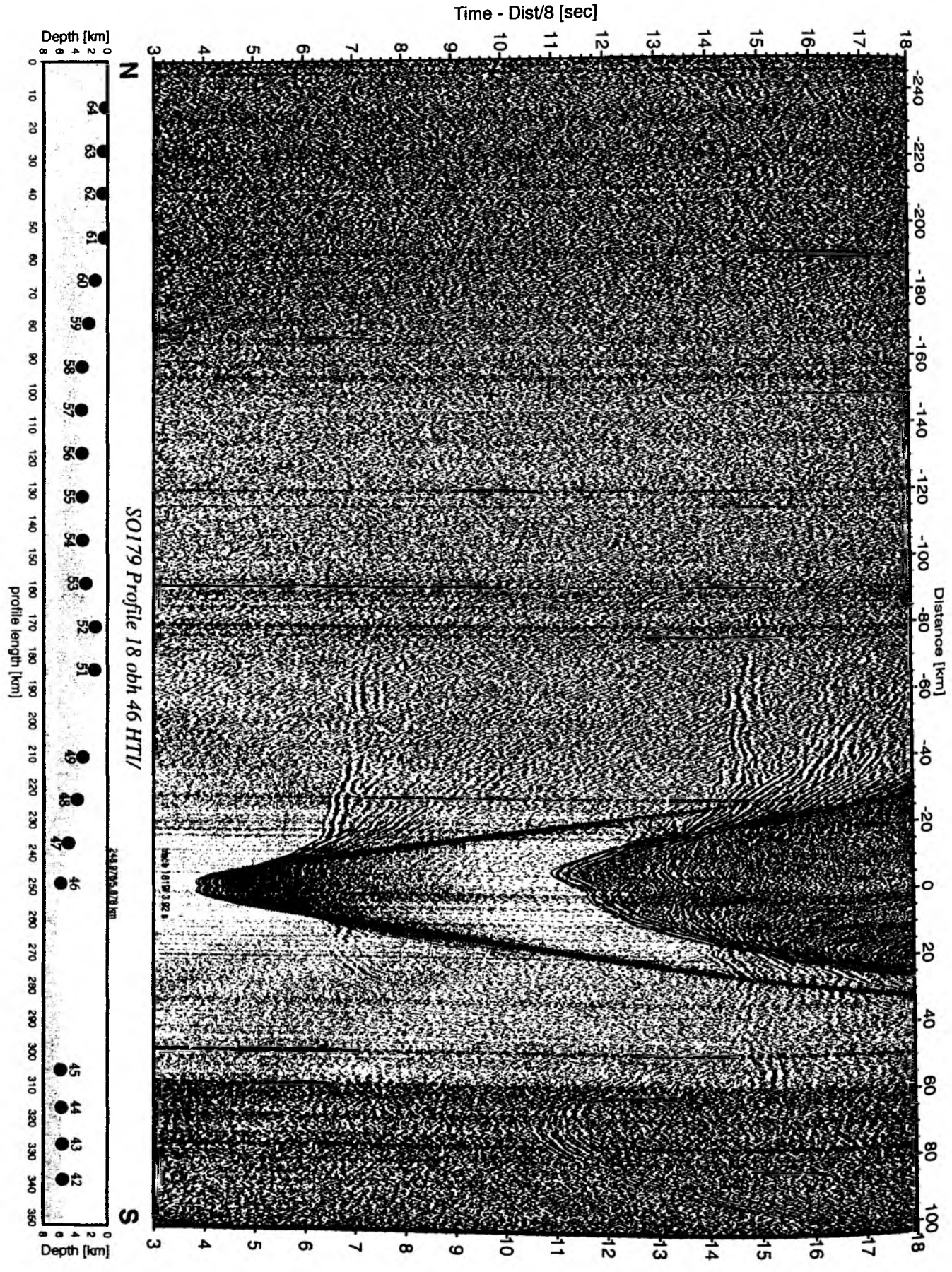

Figure 6.4.3.8: Record section from obh 46 HTI/, Profile 18.

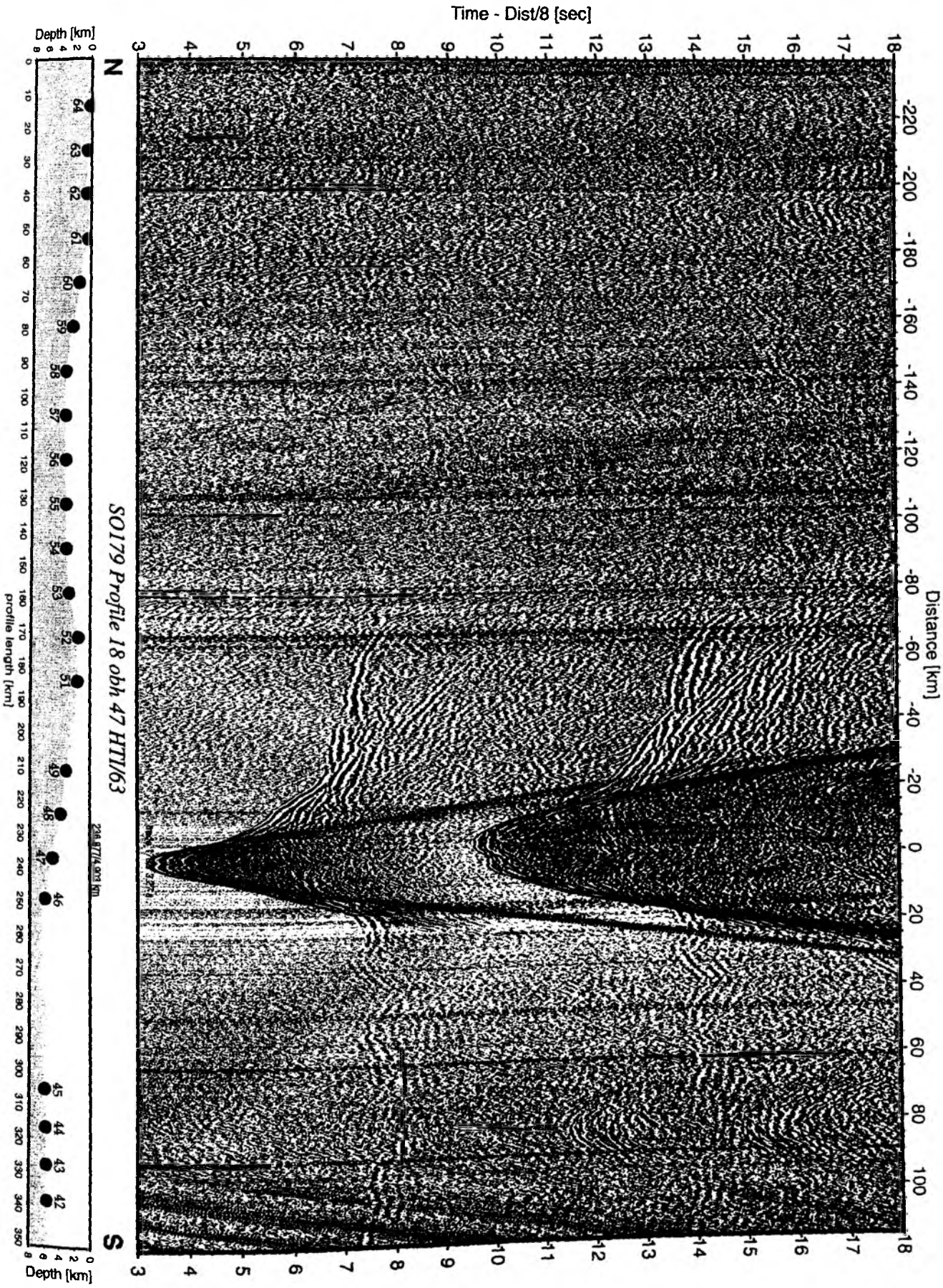

Figure 6.4.3.9: Record section from obh 47 HTI/63, Profile 18.

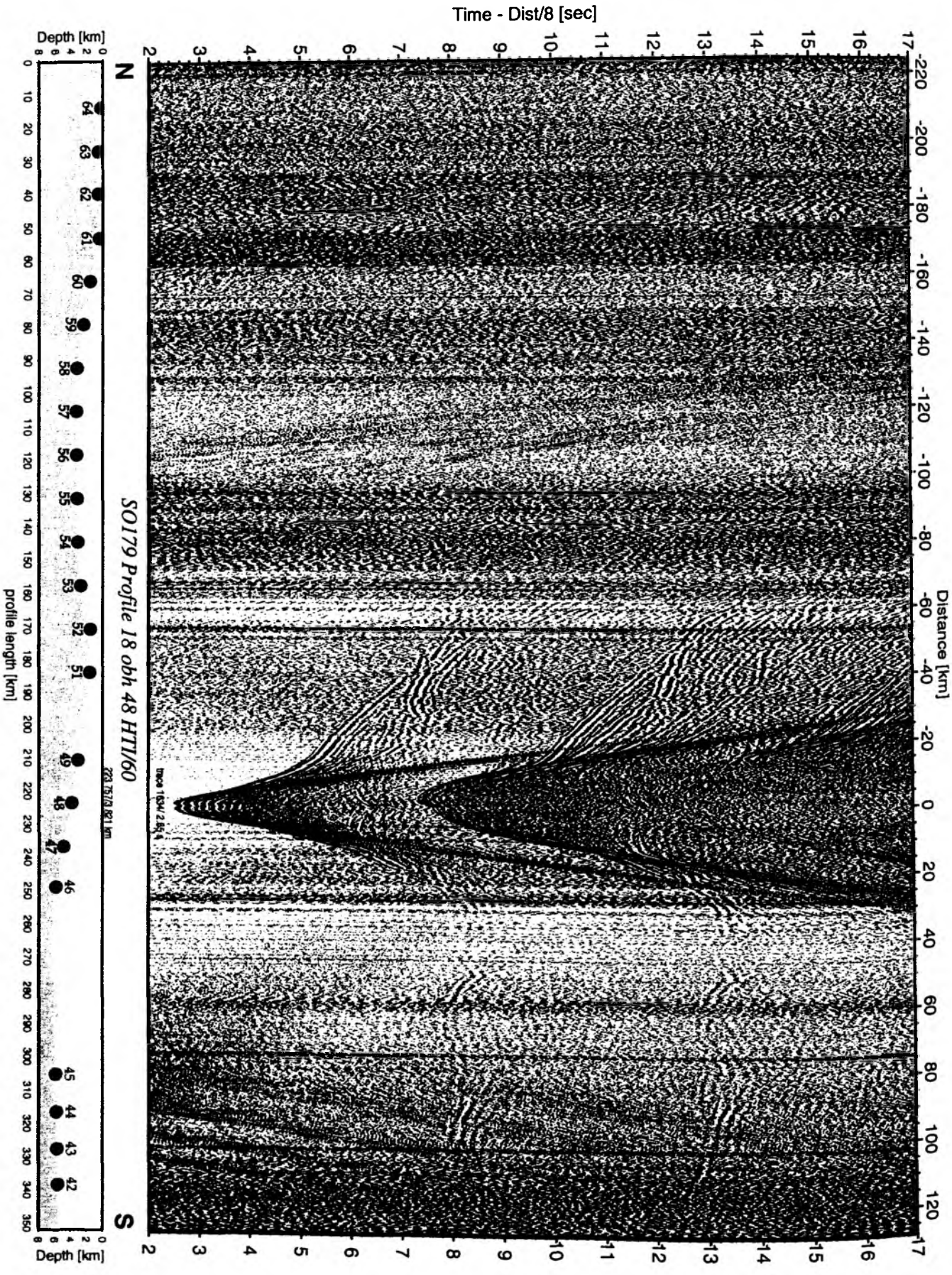

Figure 6.4.3.10: Record section from obh 48 HTI/60, Profile 18.

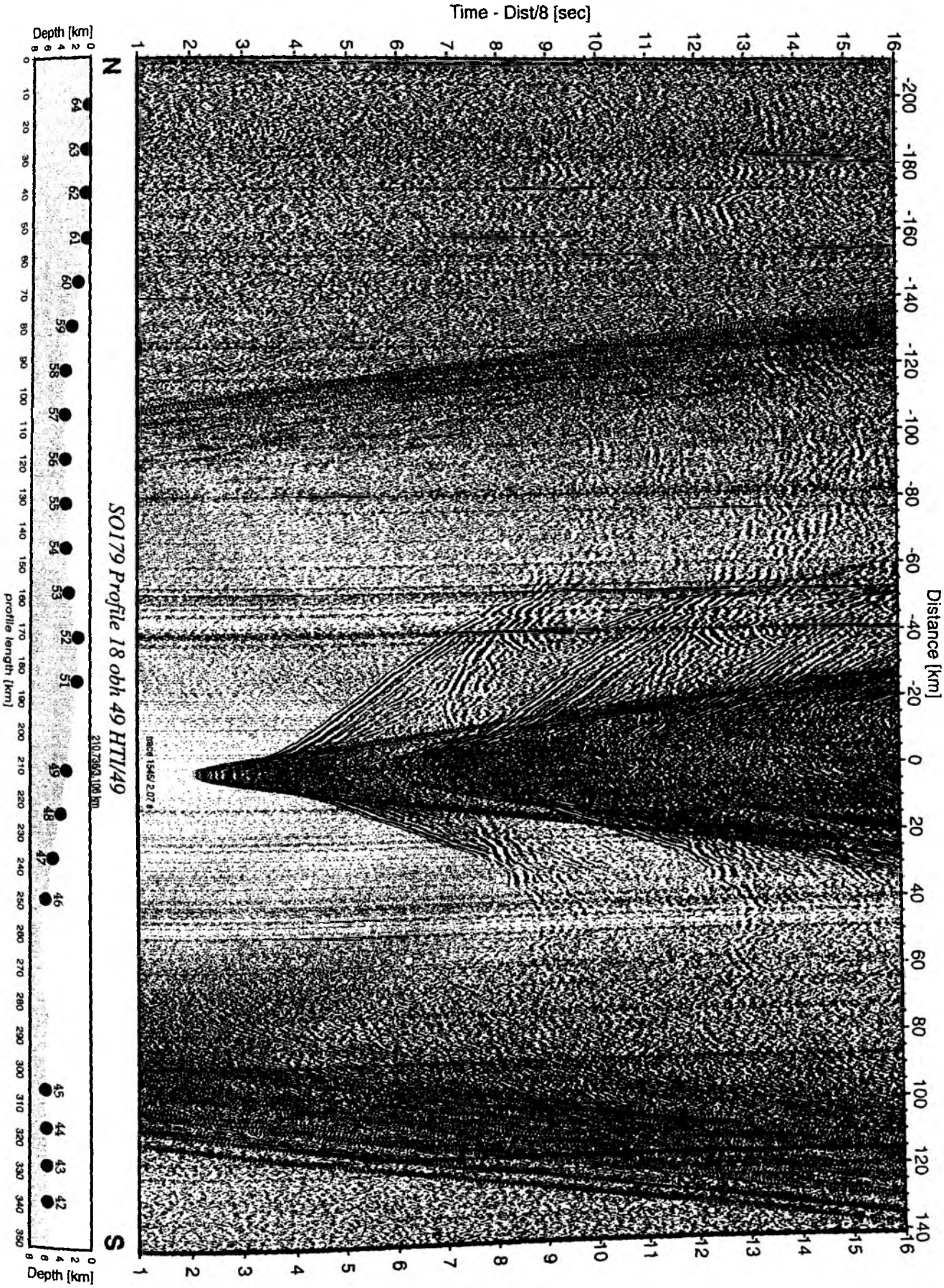

Figure 6.4.3.11: Record section from obh 49 HTI/49, Profile 18.

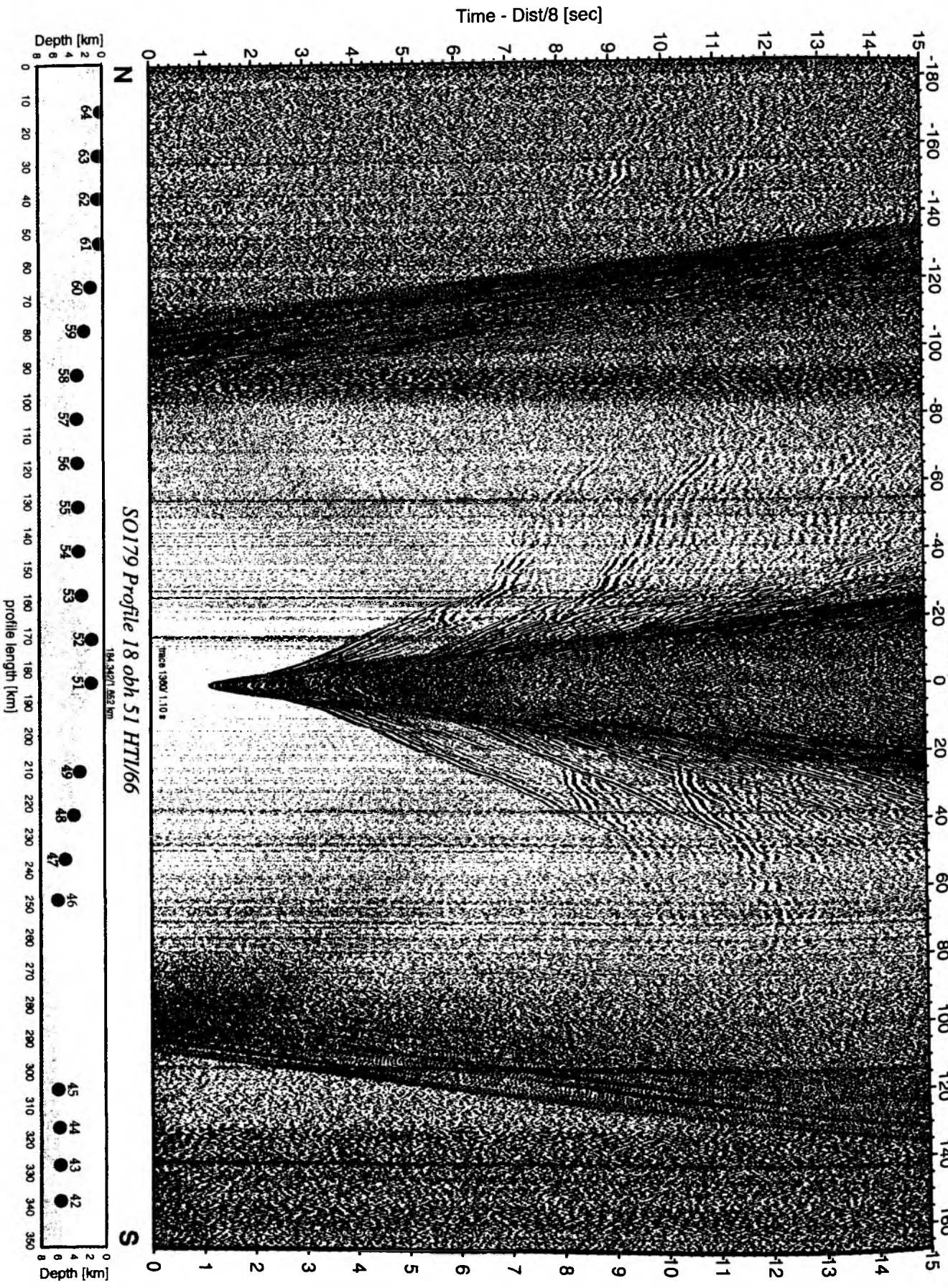

Figure 6.4.3.12: Record section from obh 51 HTI/66, Profile 18.

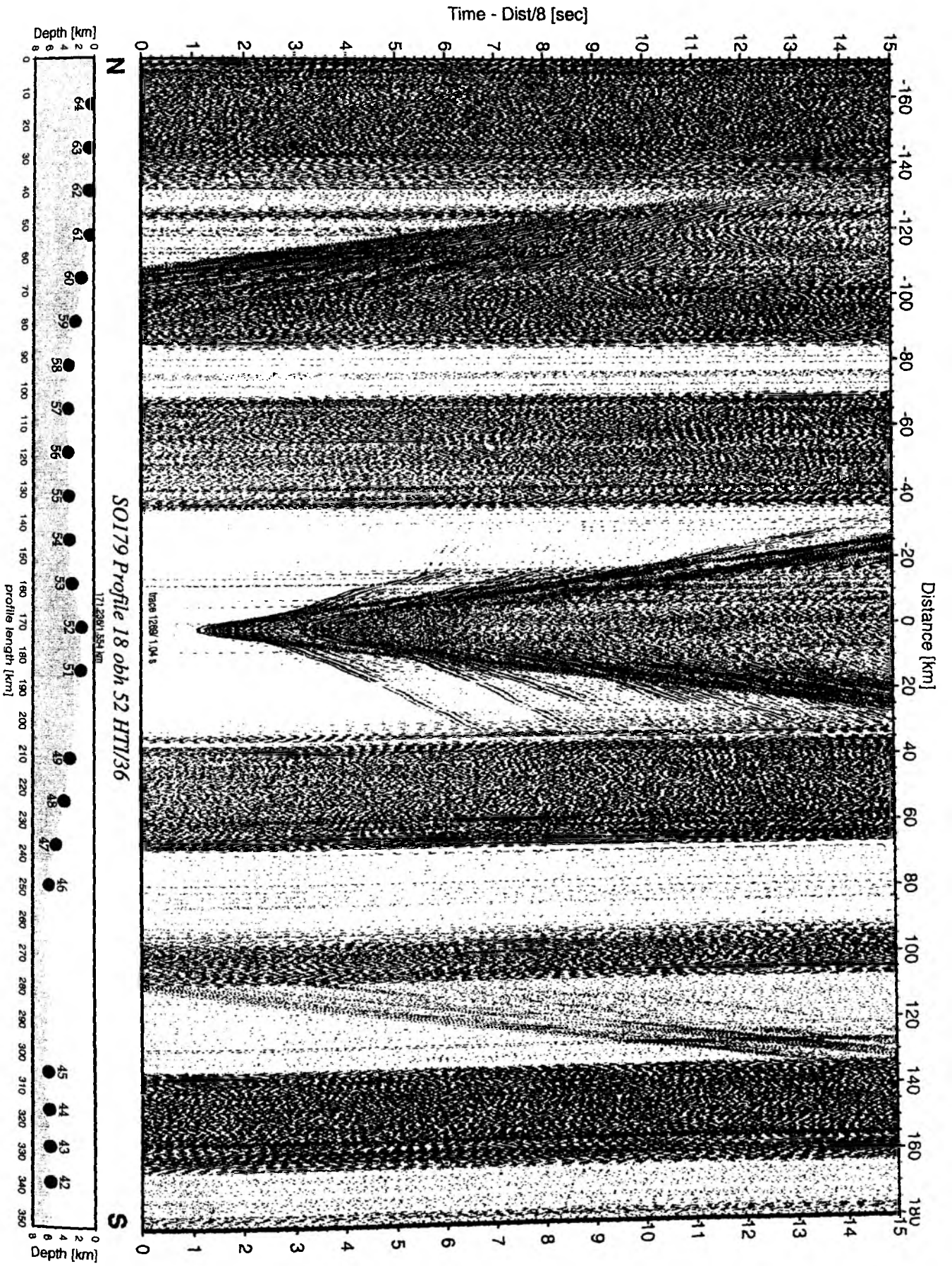

Figure 6.4.3.13: Record section from obh 52 HTI/36, Profile 18.

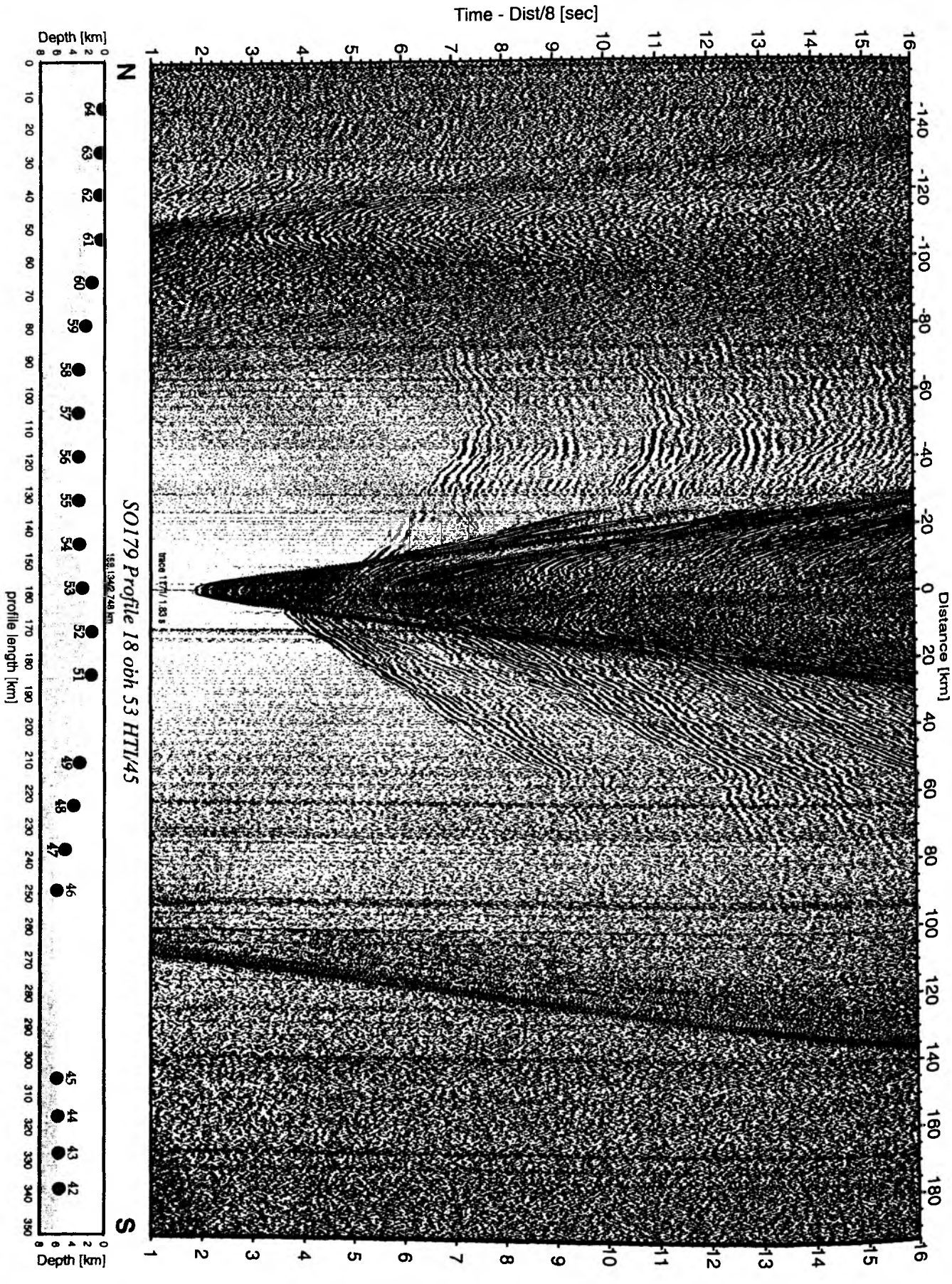

Figure 6.4.3.14: Record section from obh 53 HTI/45, Profile 18.

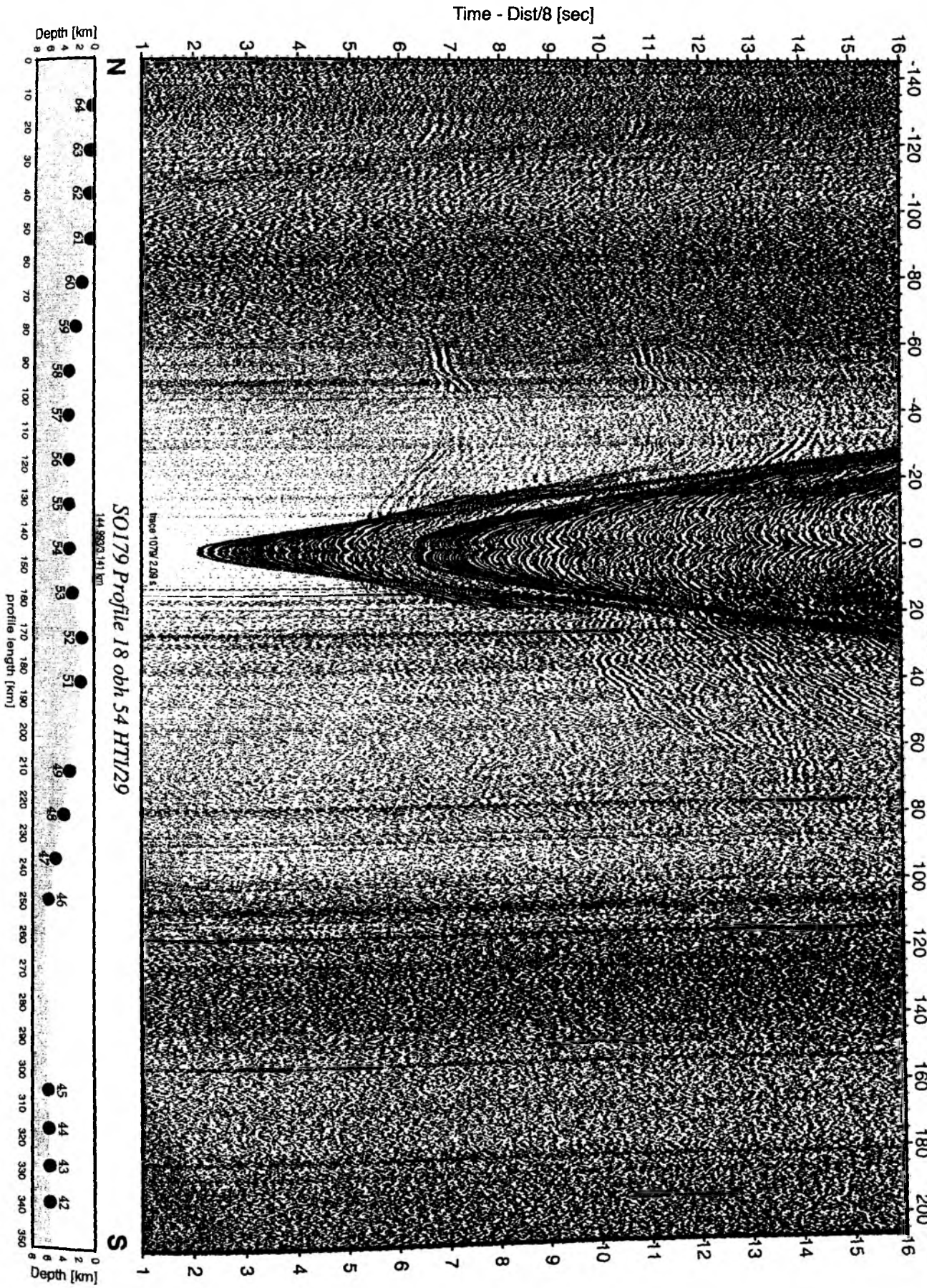

Figure 6.4.3.15: Record section from obh 54 HTI/29, Profile 18.

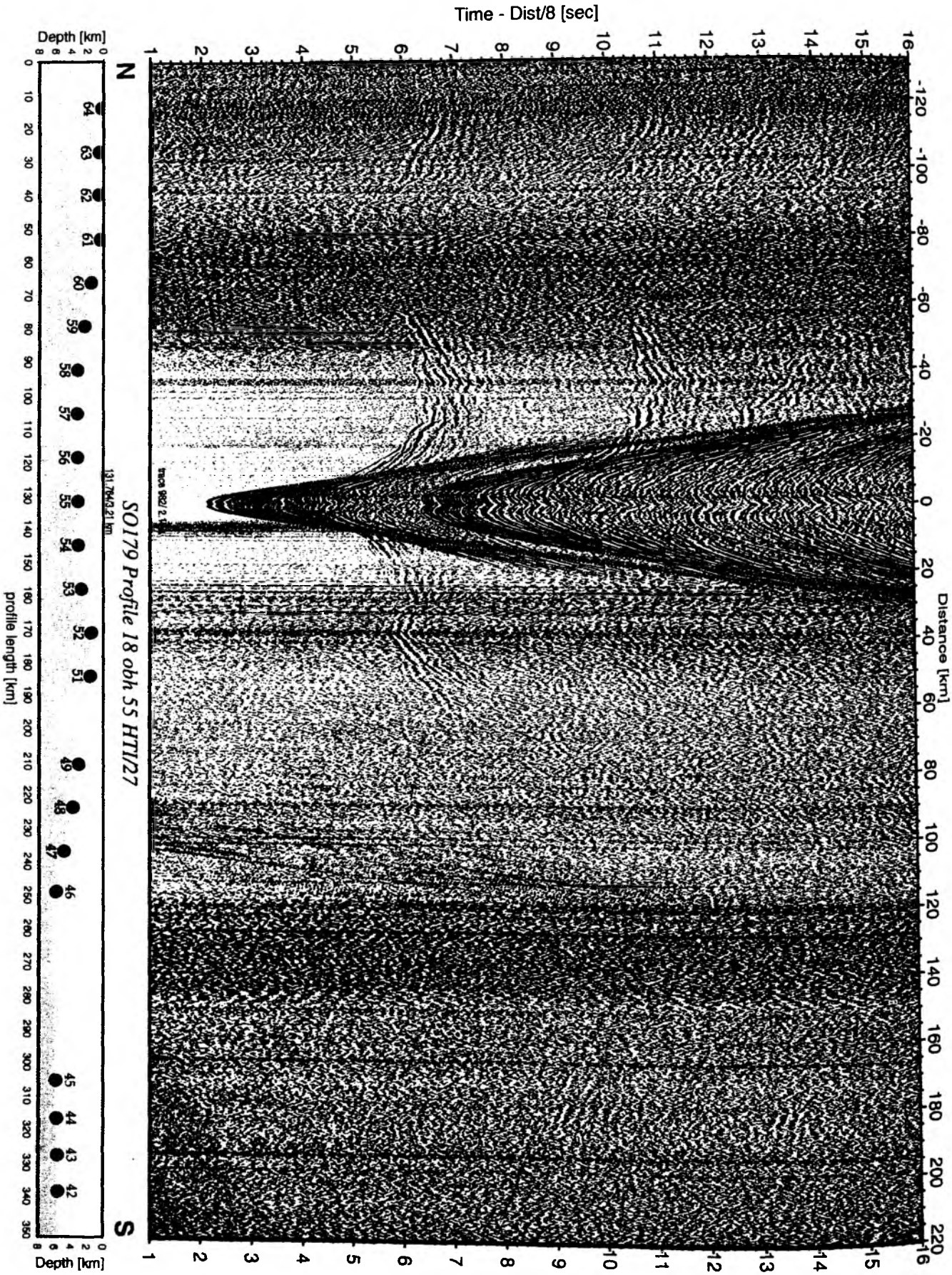

Figure 6.4.3.16: Record section from obh 55 HTI/27, Profile 18.

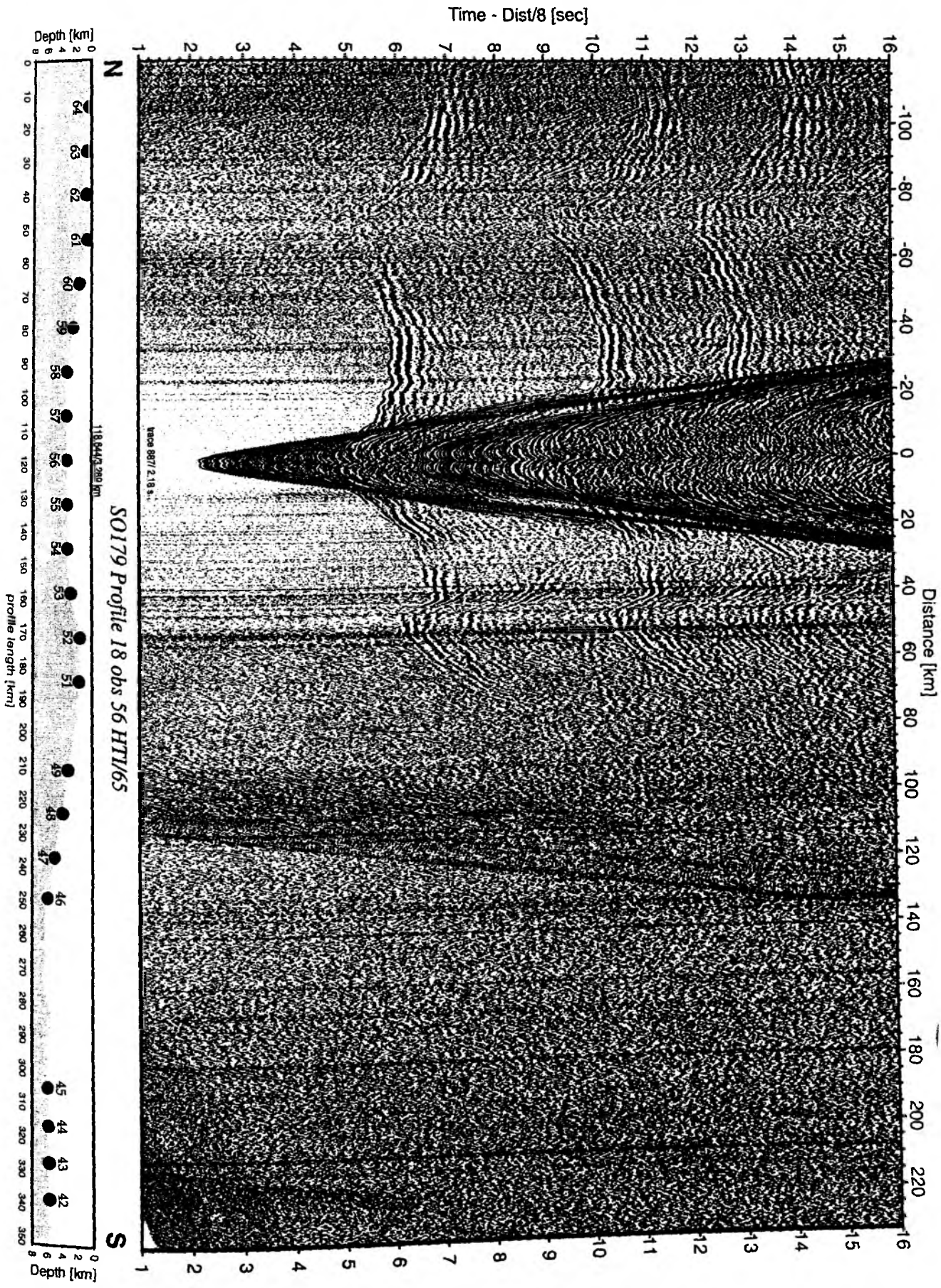

Figure 6.4.3.17: Record section from obs 56 HTI/65, Profile 18.

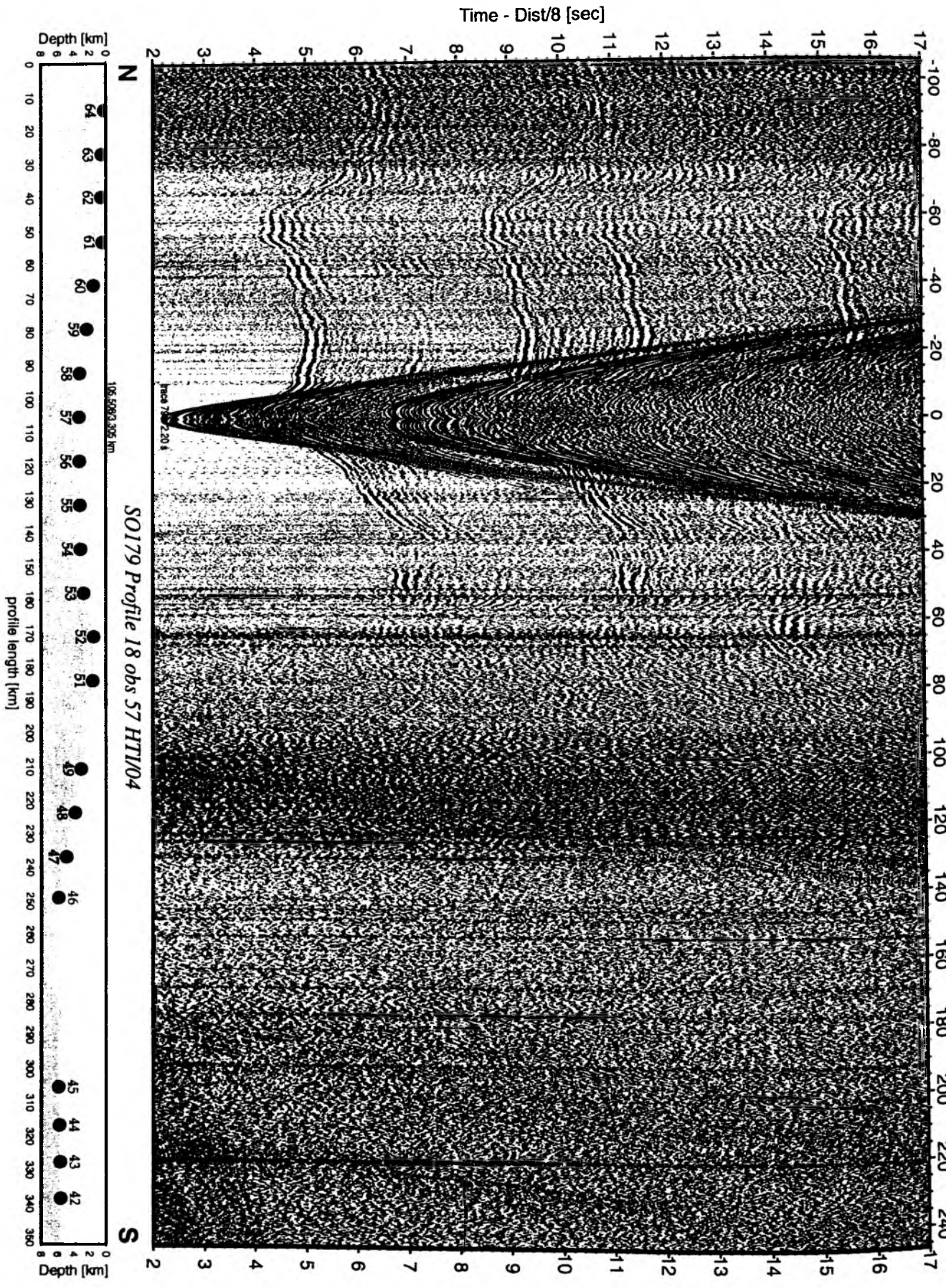

Figure 6.4.3.18: Record section from obs 57 HTI/04, Profile 18.

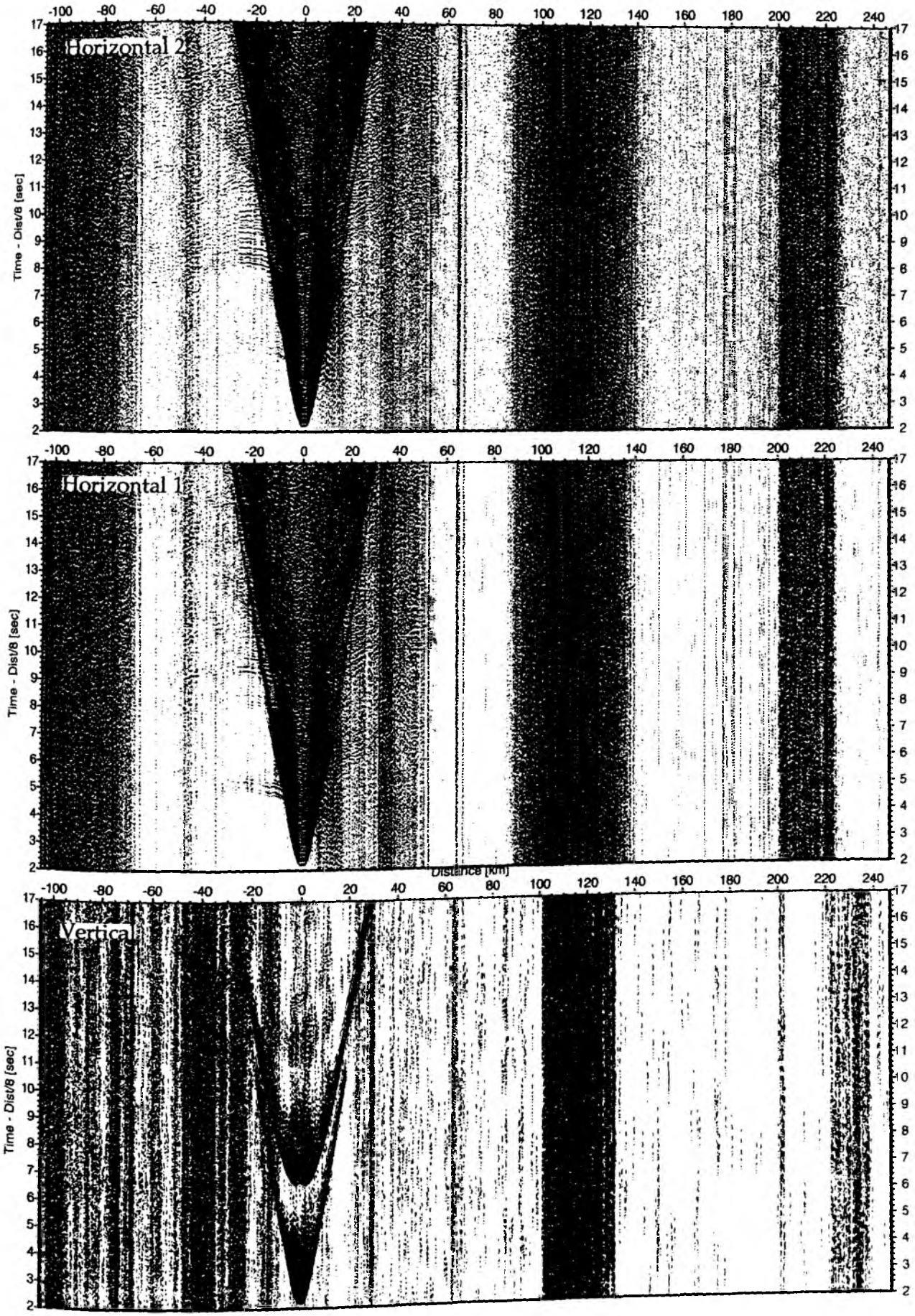

Figure 6.4.3.19: Record sections from obs 57 Owen-4.5Hz, SO179 Profile 18.

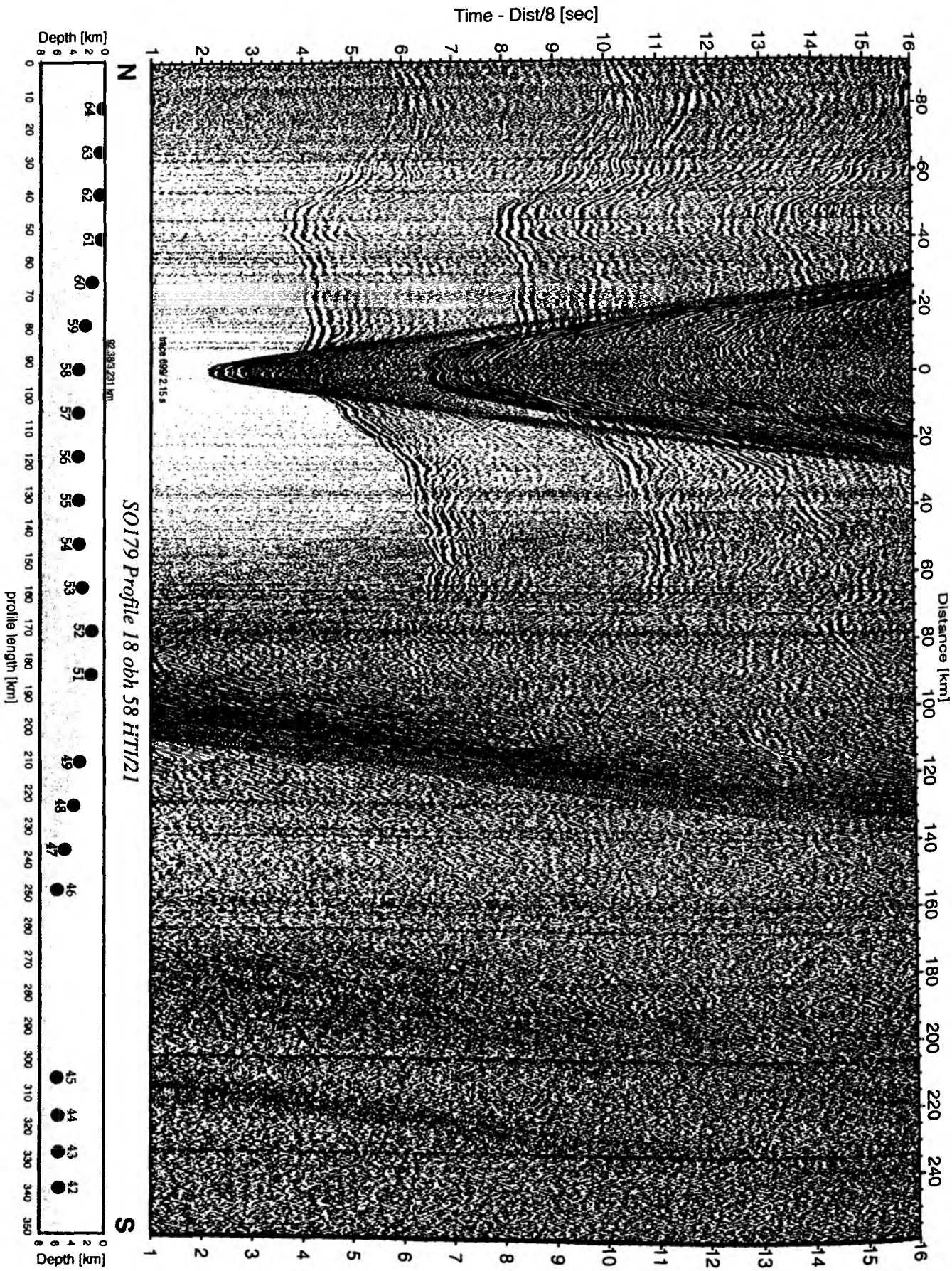

Figure 6.4.3.20: Record section from obh 58 HTI/21, Profile 18.

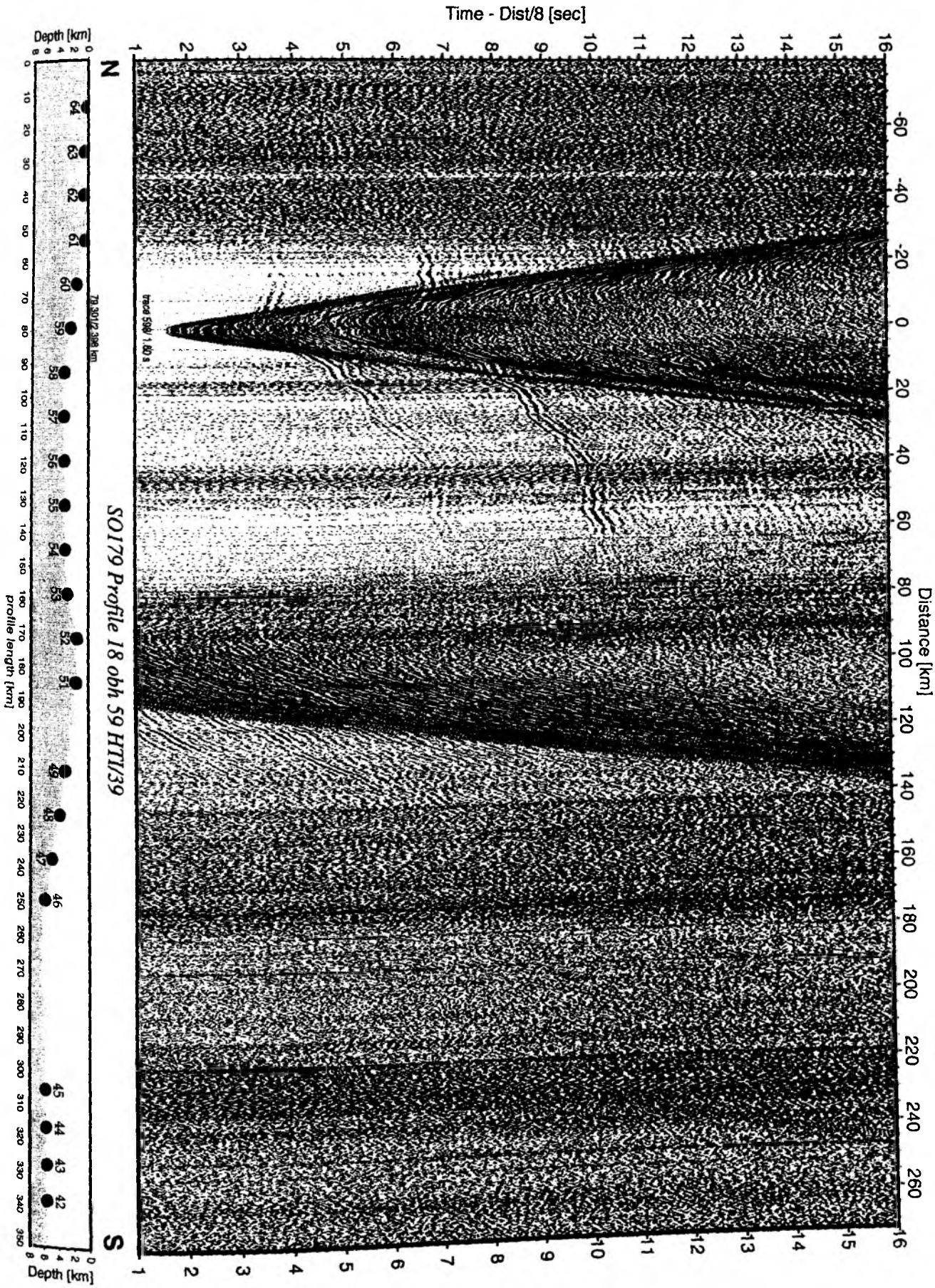

Figure 6.4.3.21: Record section from obh 59 HTI/39, Profile 18.

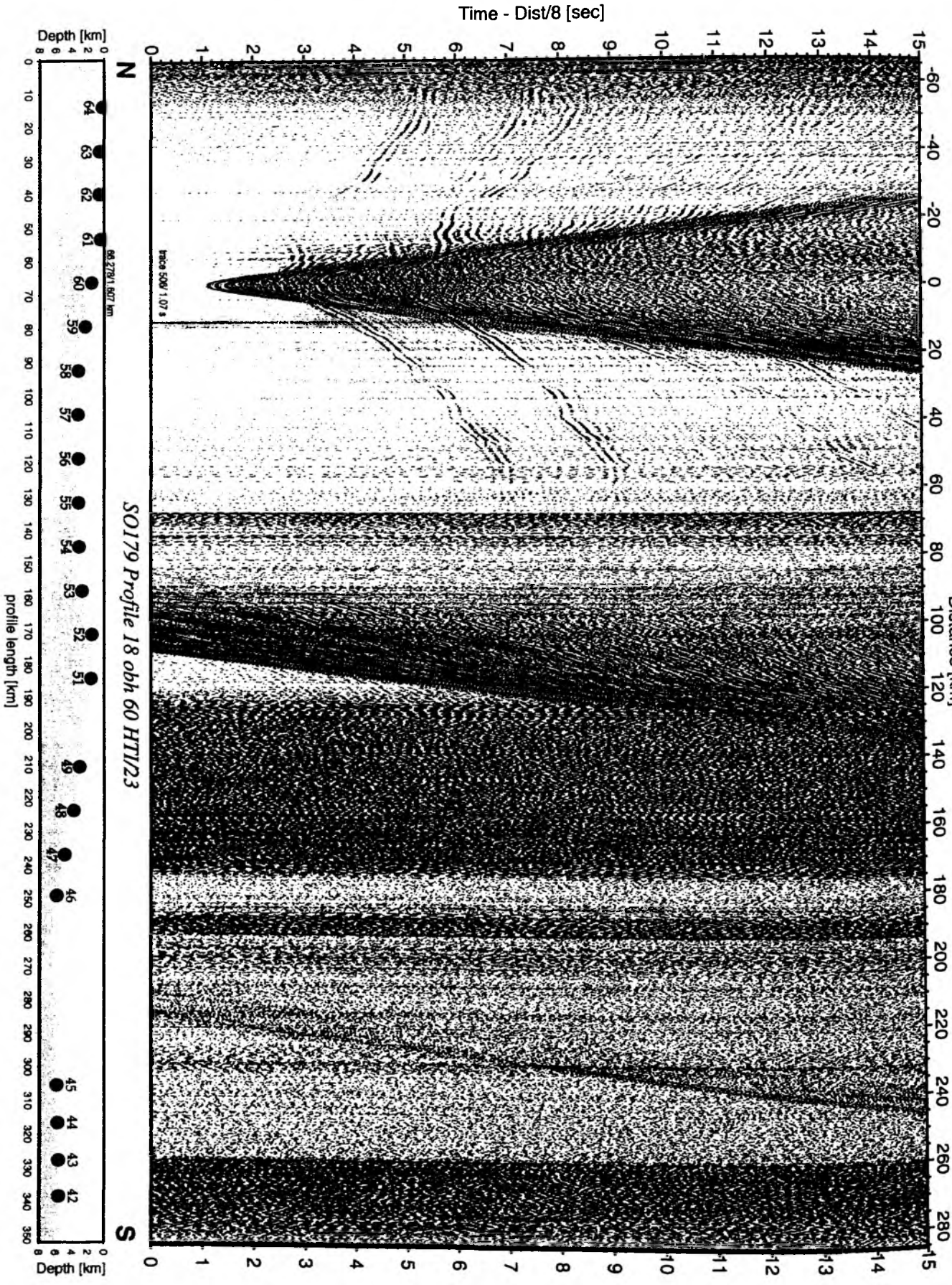

Figure 6.4.3.22: Record section from obh 60 HTI/23, Profile 18.

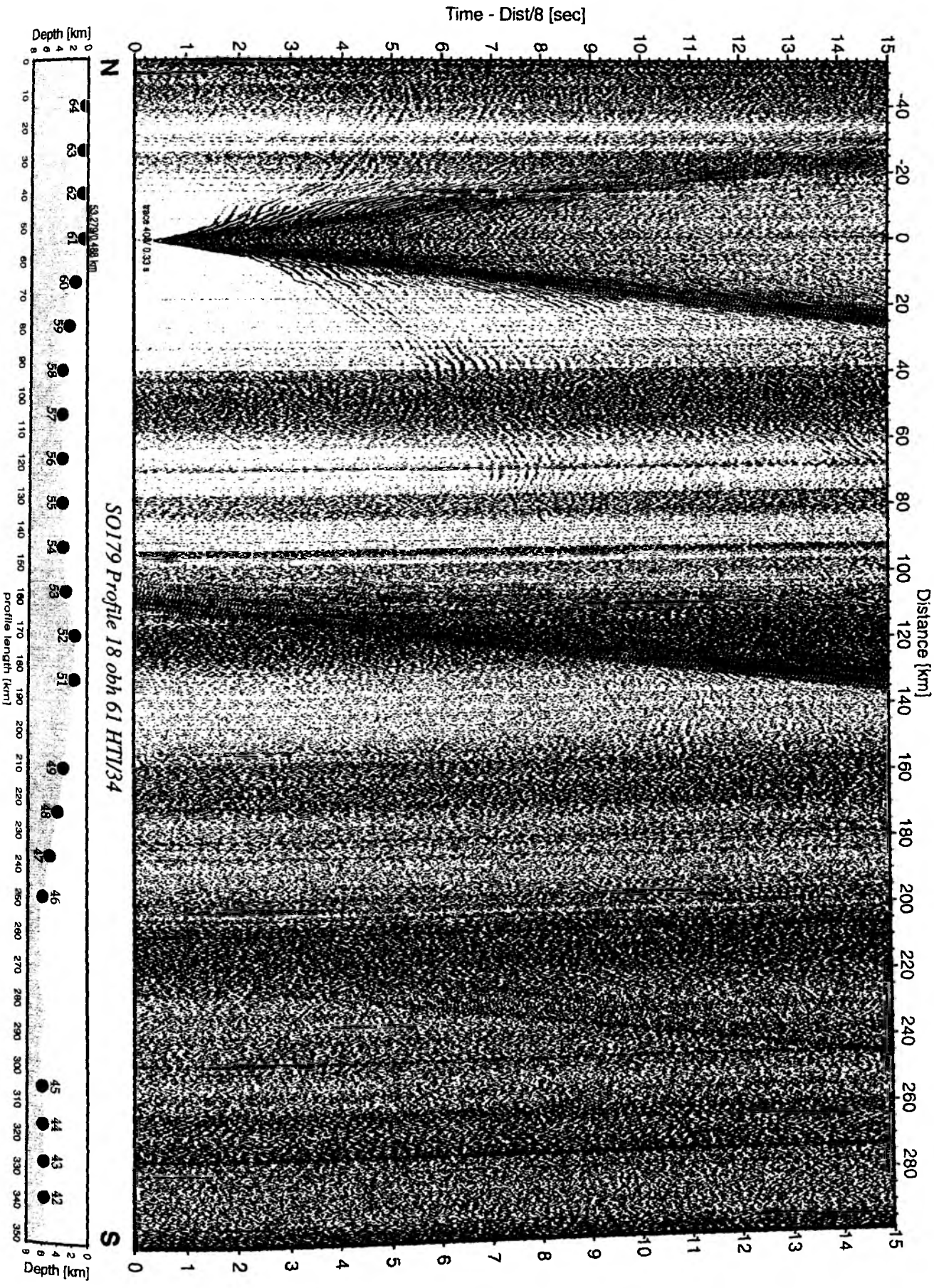

Figure 6.4.3.23: Record section from obh 61 HTI/34, Profile 18.

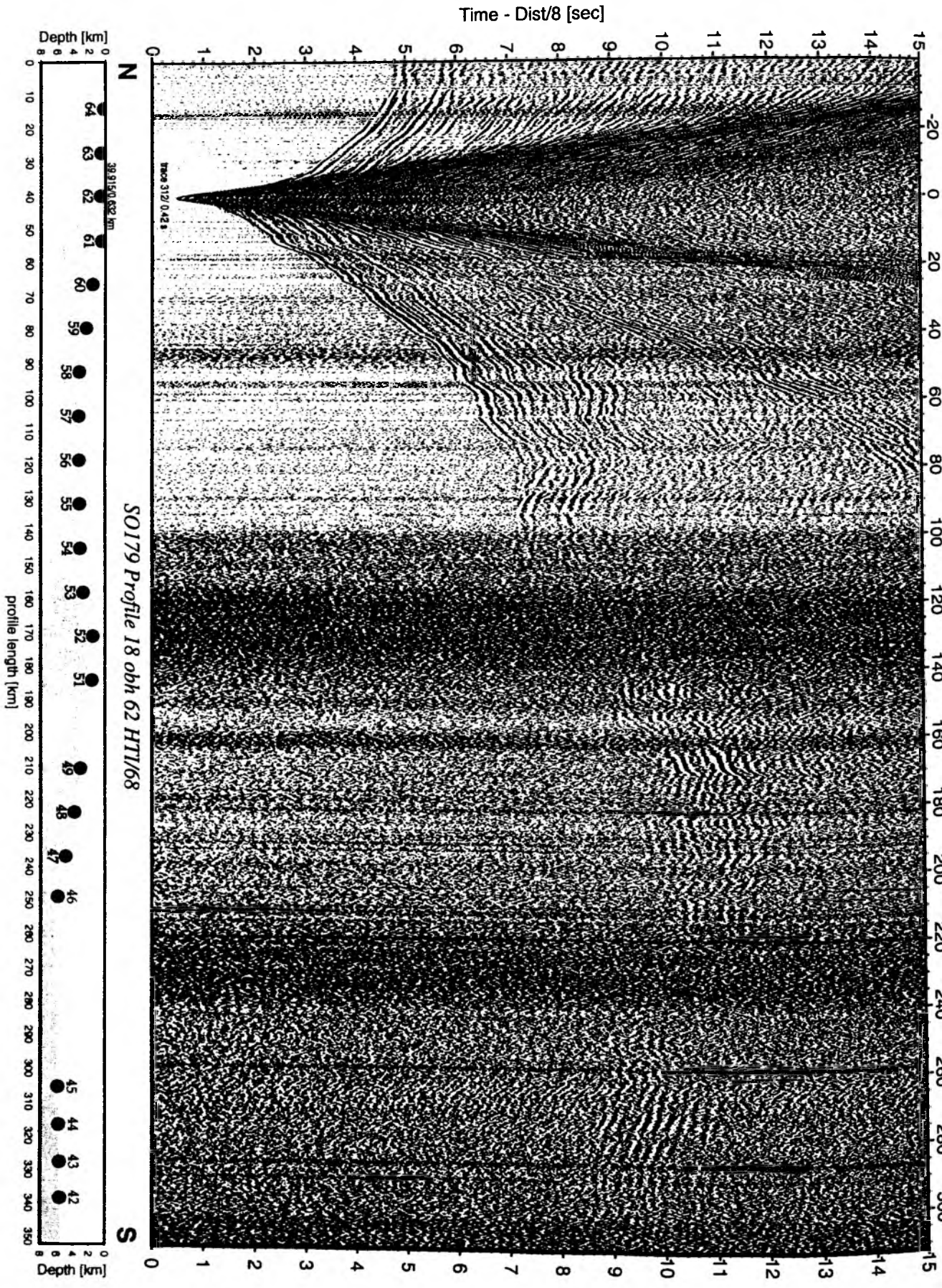

Figure 6.4.3.24: Record section from obh 62 HTI/68, Profile 18.

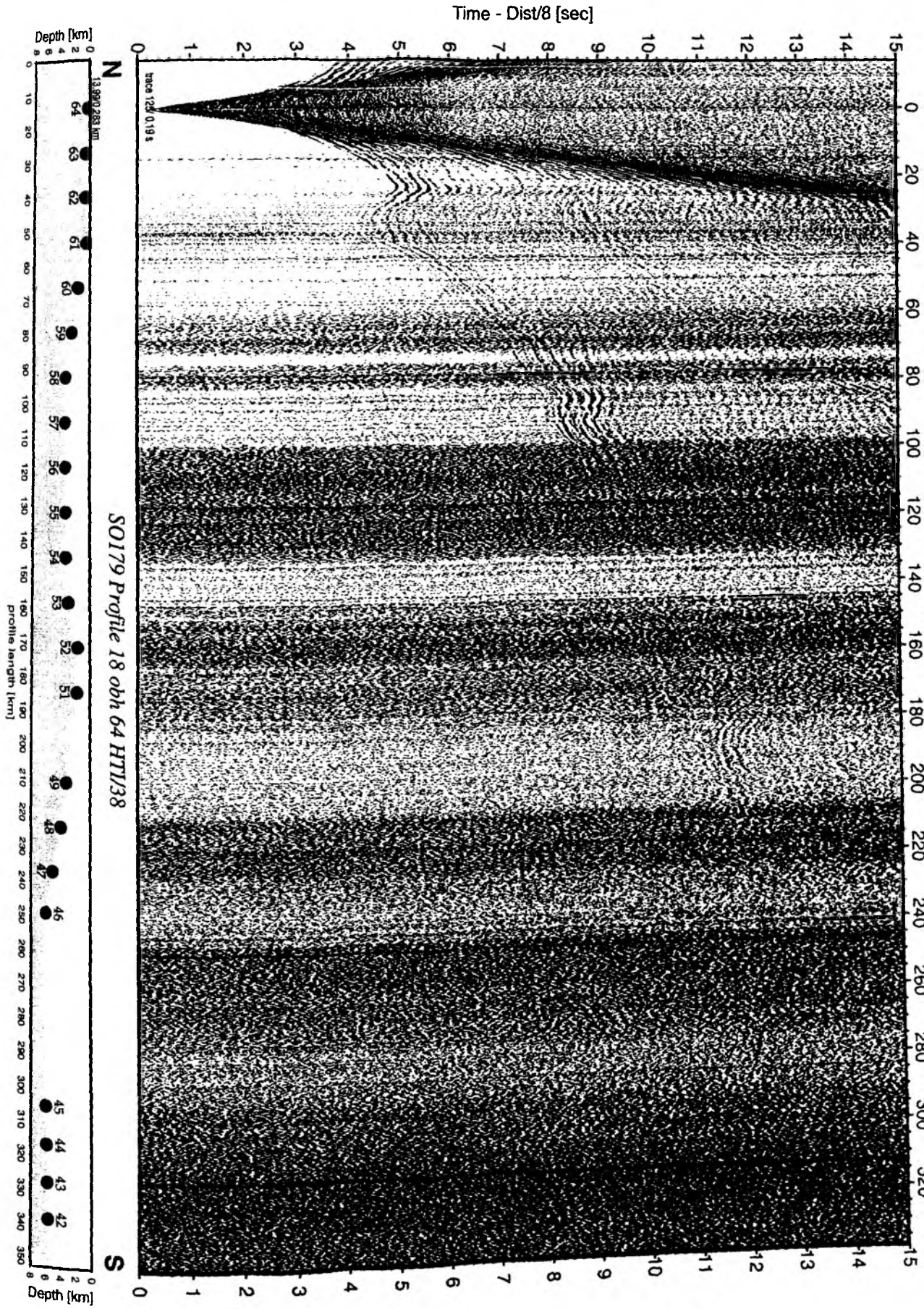

Figure 6.4.3.25: Record section from obh 64 HTI/38, Profile 18.

6.4.4 Profile P19

Profile P19 is approximately 100 nm long, located about 25 nm off the coast of Java. The main aim of this line was to shot into the landarray, to allow for some 3-D control of the plate interface. Due to time constrains only in the eastern half of the profile ocean bottom instruments could be deployed. In total eleven OBH (OBH65 to 75) were deployed in the morning of October 2nd. Shooting was performed under ideal weather conditions with all three guns working without interruption. All instruments were recovered on October 4th.
For details on instruments see Appendices 9.2 and 9.3. In Figure 6.4.4.1 the location map of the profile is shown. The record section for the streamer is shown in Figure 6.4.4.2, and the record sections from the OBH are given in Figures 6.4.4.3 to 6.4.4.13.

Figure 6.4.4.2 shows the water migrated stack of the recorded streamer data. The bathymetry along the profile including the locations of the deployed OBH is displayed below the seismic data. Basic processing including frequency filtering and deconvolution was applied to the streamer data. However, the bubble pulses of the airguns are still visible. Multiples and a distinct reflection pattern from the basement can be determined. This reflection pattern is overlain by a sedimentary cover varying in thicknesses (e.g. at profile km 100 and 120). Between profile km 130 and 143, two strong reflections can be seen indicating a sedimentary infill of a basin.

After observing the record sections of the deployed OBH (see Figure 6.4.4.3 to 6.4.4.13), two sections provided good data and were chosen to pick first arrivals to develop preliminary 1D-models using the R1D-software.
The models of the record sections OBH66 and OBH73 are shown in Figure 6.4.4.14 and 6.4.4.15 and illustrate the P-wave velocity over depth. The small x in the diagrams displays the position of the OBH. Below the model diagrams, the bathymetry along the interesting parts of profile P19 including the positions of the OBH are shown.

The modelling process for data obtained from each OBH was divided into two parts: we modelled the eastern and western part of the profile independently and combined the two velocity over depth diagrams to resolve Figures 6.4.4.14 and 6.4.4.15.

Figure 6.4.4.14 shows the 1D-modell of OBH66, located at profile km 101 in a depth of 1.047 km. On the eastern part, one can recognise a sedimentary layer down to a depth of 2 km. The second layer consists of consolidated sediments up to 5 km depth with a velocity increase from 3 to 6 km/s. The data indicates, that this section is followed by a layer with a small velocity gradient down to the Moho located at 17 km depth.
The western part shows higher velocity gradients, but almost the same thickness of the sedimentary layers as in the eastern part. The data indicates here a Moho depth in approximately 19 km providing a larger velocity step.

Figure 6.4.4.15 shows the 1D-model of OBH73, located in a depth of 1064 km at profile km 38.849. The eastern part of the model shows sedimentary layers of a thickness of about 2-3 km. Between 4 and 10 km depth, velocity increases from 4.8 to 6.2 km/s at the Moho. At 12 km depth a velocity of 7.2 km/s is obtained. The observed reflections at 140 to 160 km offset indicates the presence of a velocity inversion from 7.2 to 6.8 km /s in 21 km depth.
The western part is dominated by two layers with continuously increasing velocities.
15: 1-D velocity model of OBH73.

Profil P19

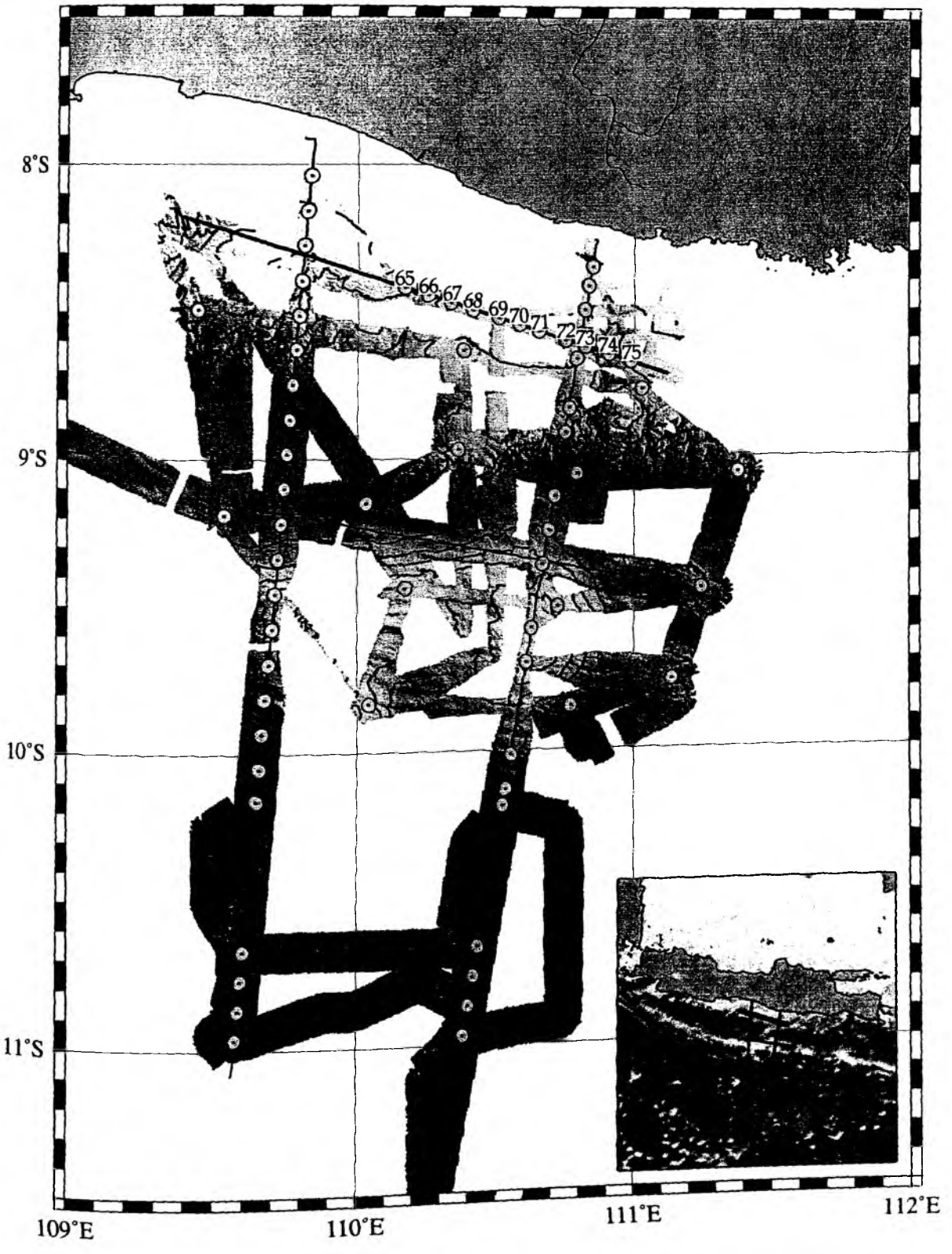

Figure 6.4.4.1: location map of profile 19.

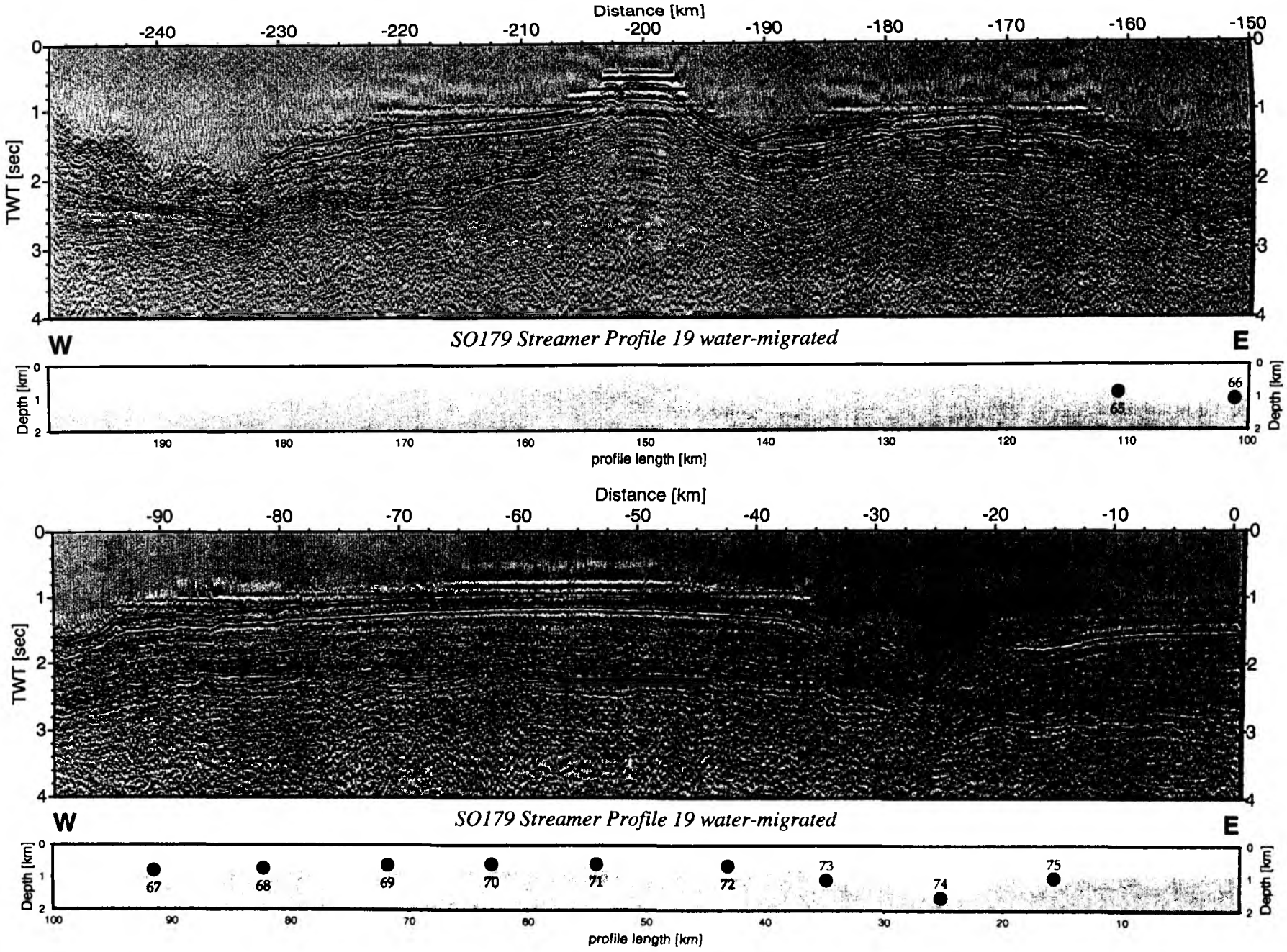

Figure 6.4.4.2: Record section from Streamer Profile 19 water-migrated.

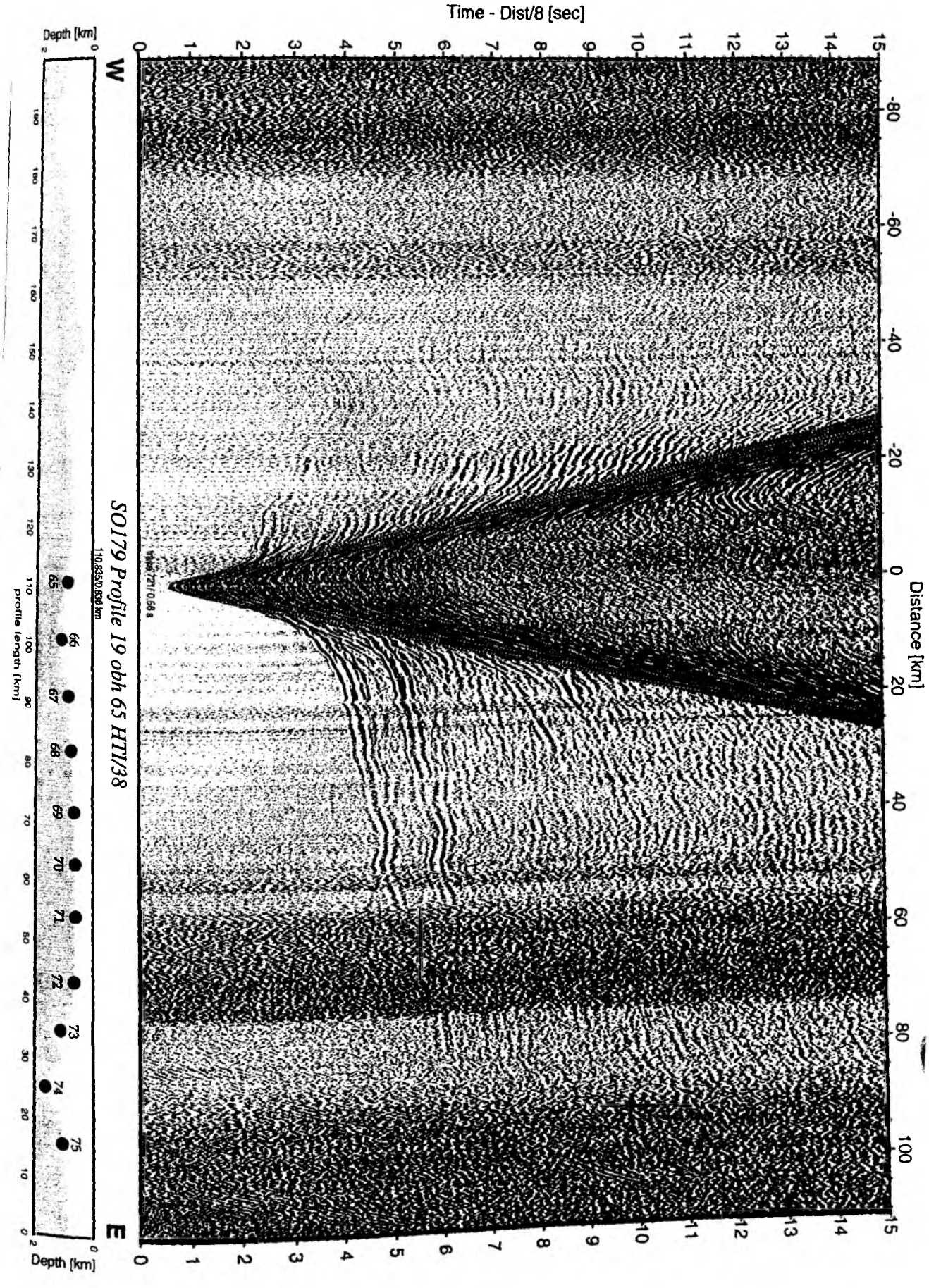

Figure 6.4.4.3: Record section from obh 65 HTI/38, Profile 19.

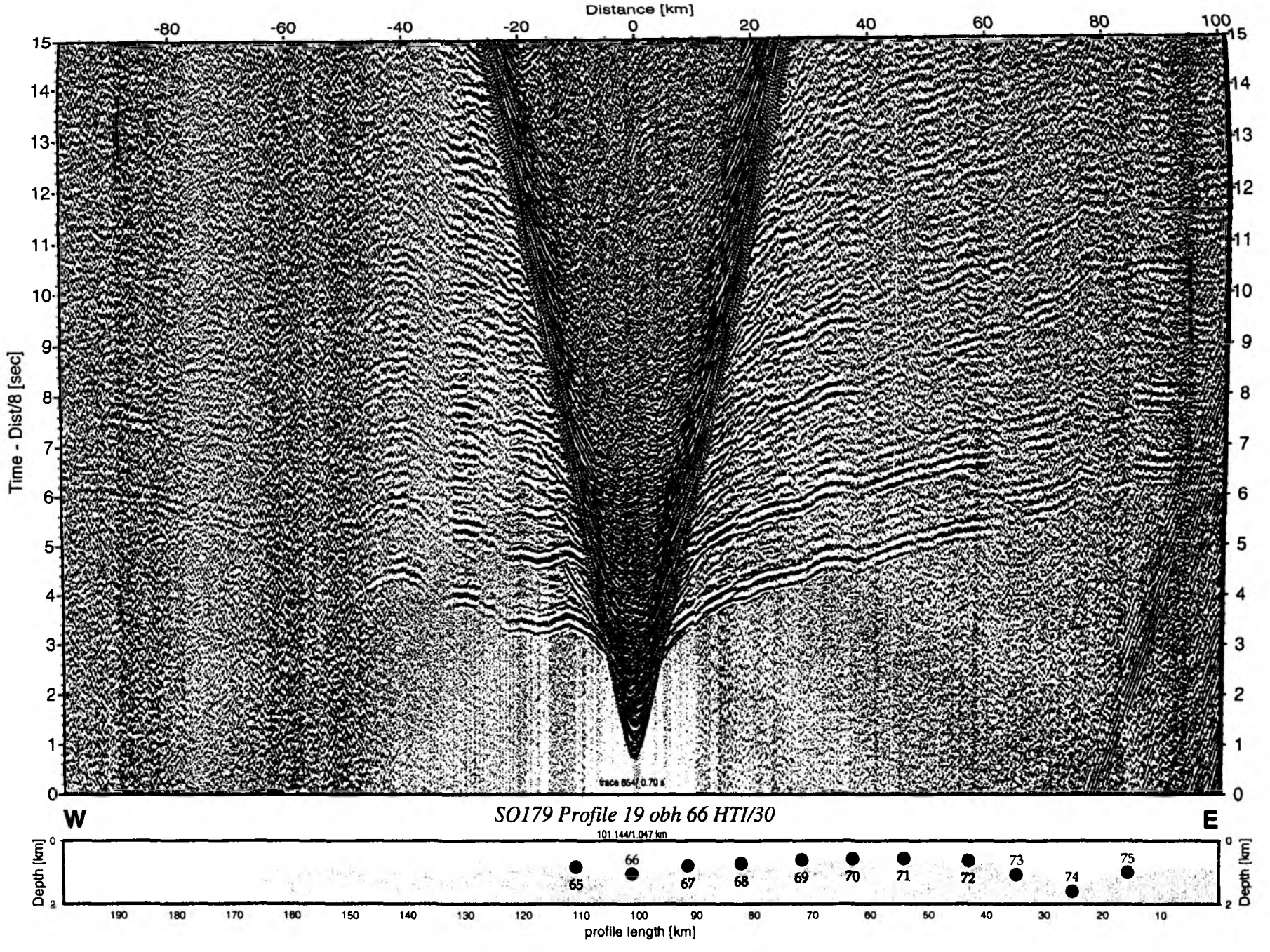

Figure 6.4.4.4: Record section from obh 66 HTI/30, Profile 19.

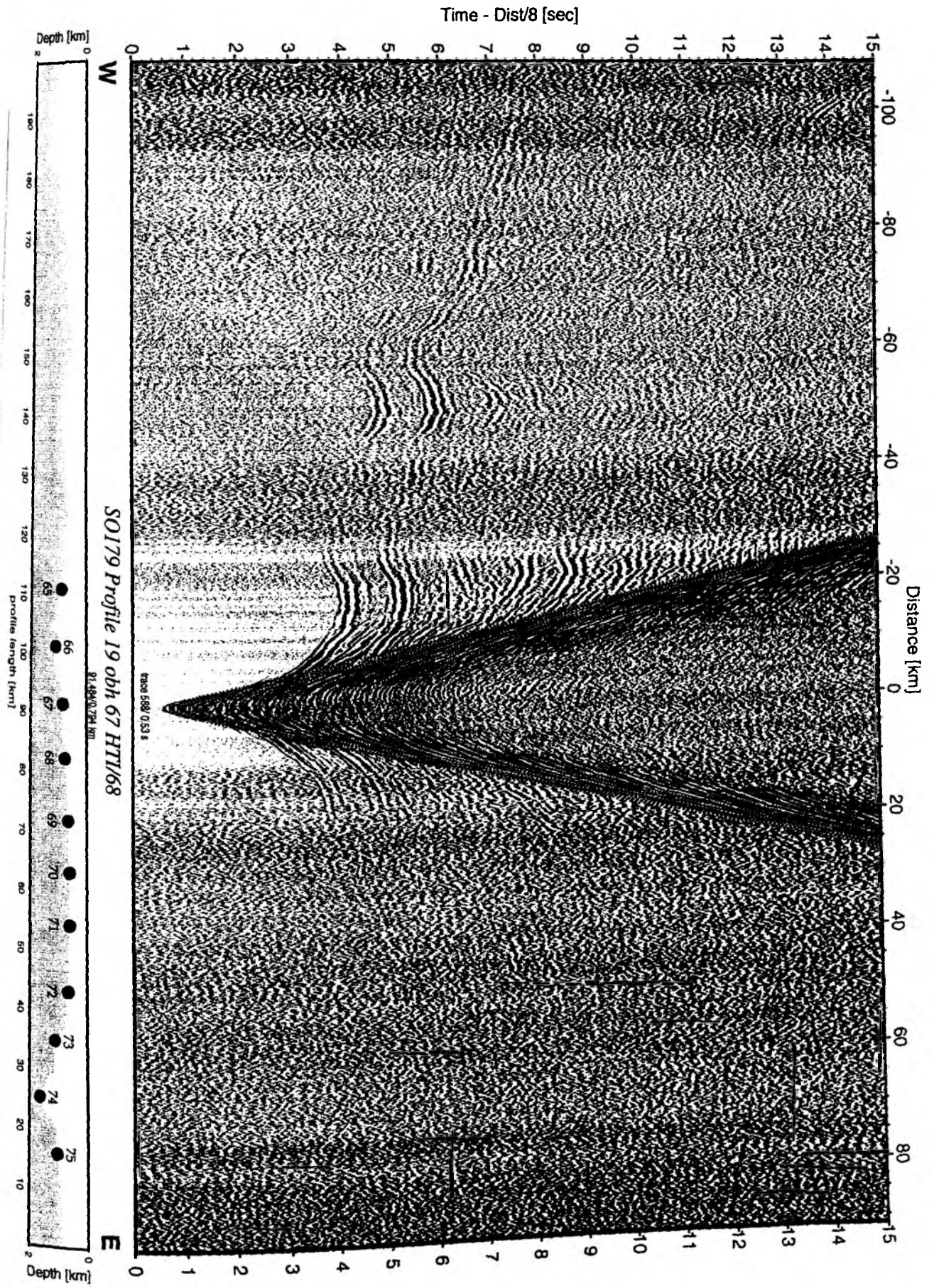

Figure 6.4.4.5: Record section from obh 67 HTI/68, Profile 19.

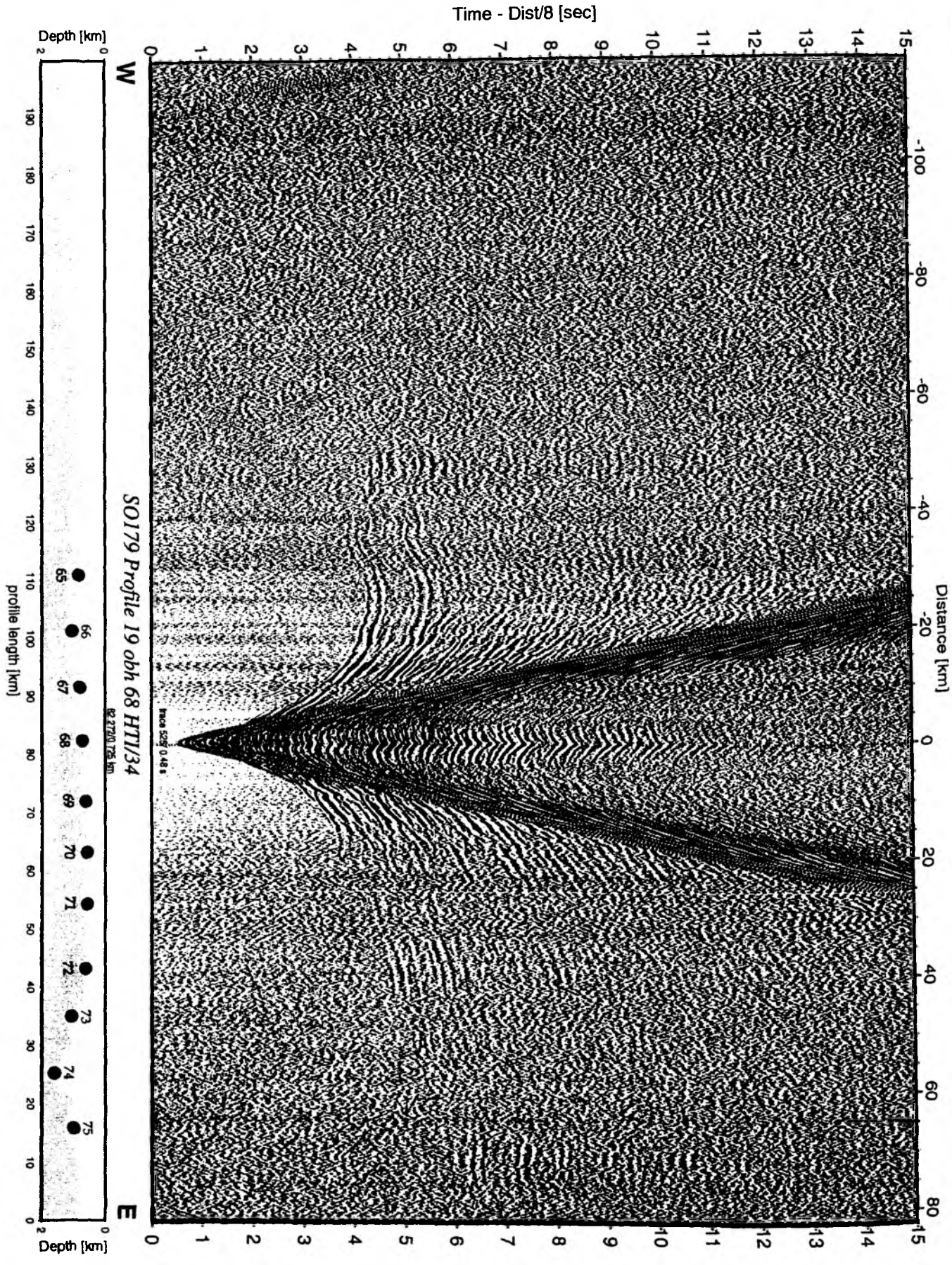

Figure 6.4.4.6: Record section from obh 68 HTI/34, Profile 19.

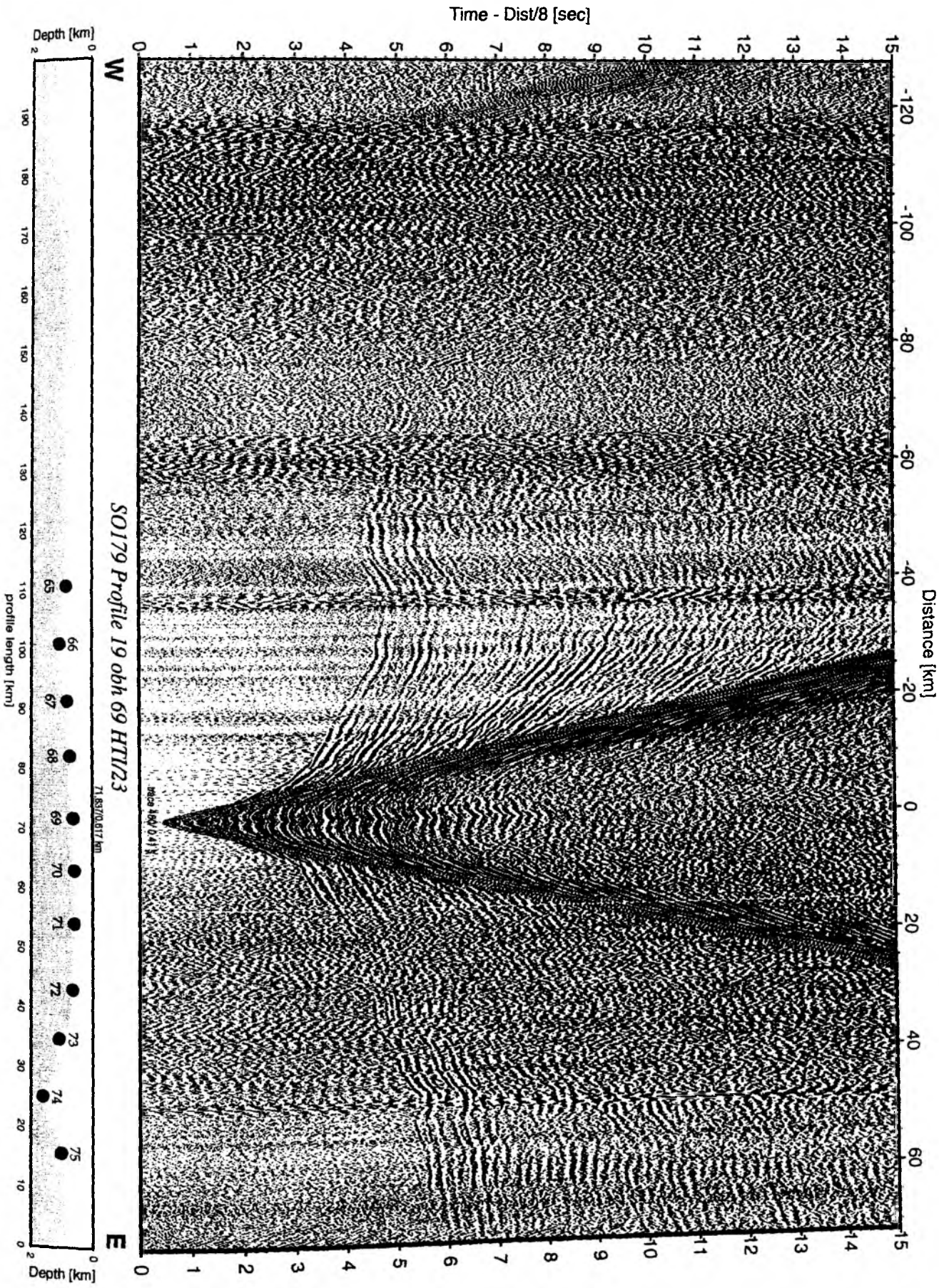

Figure 6.4.4.7: Record section from obh 69 HTI/23, Profile 19.

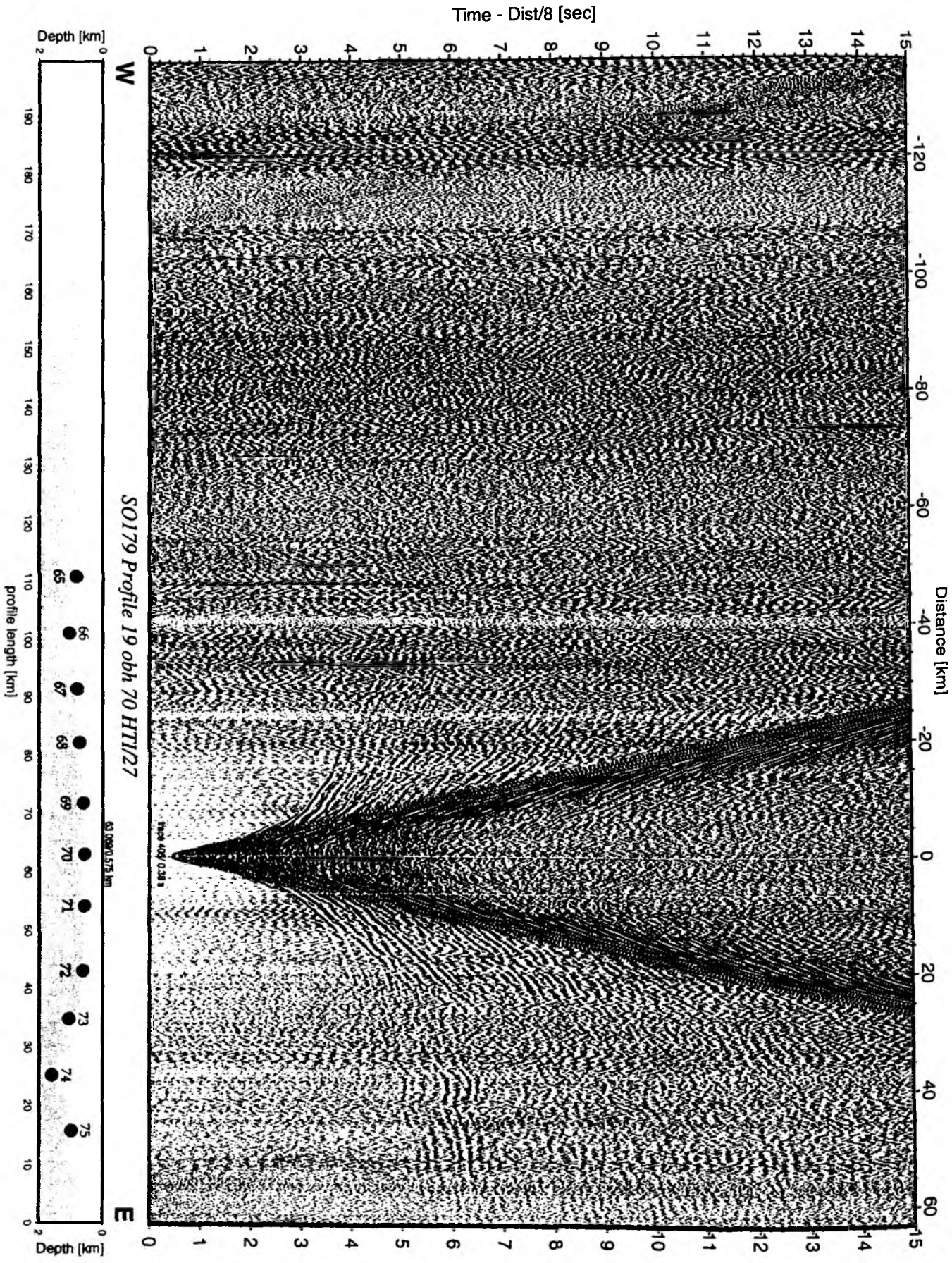

Figure 6.4.4.8: Record section from obh 70 HTI/27, Profile 19.

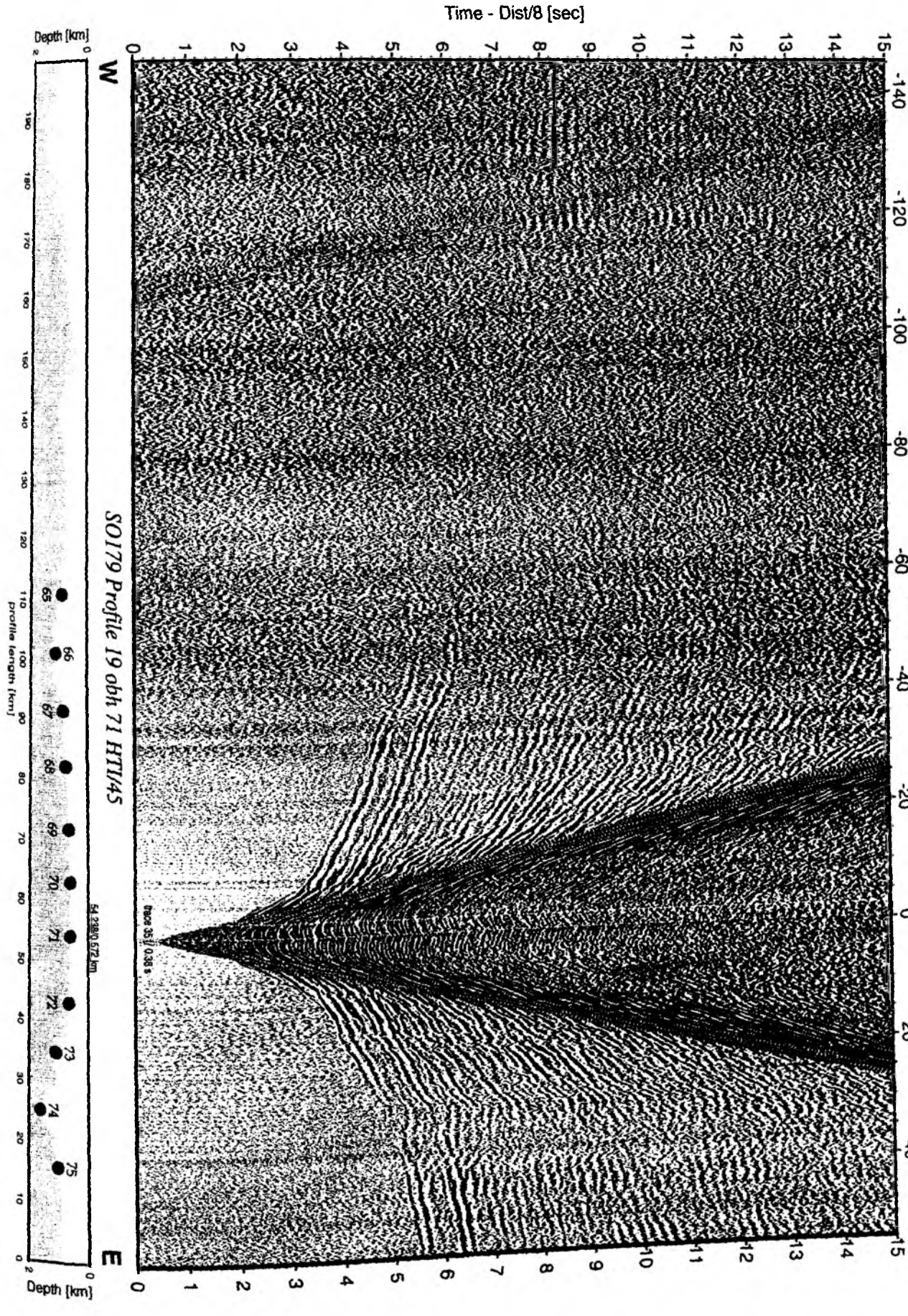

Figure 6.4.4.9: Record section from obh 71 HTI/45, Profile 19.

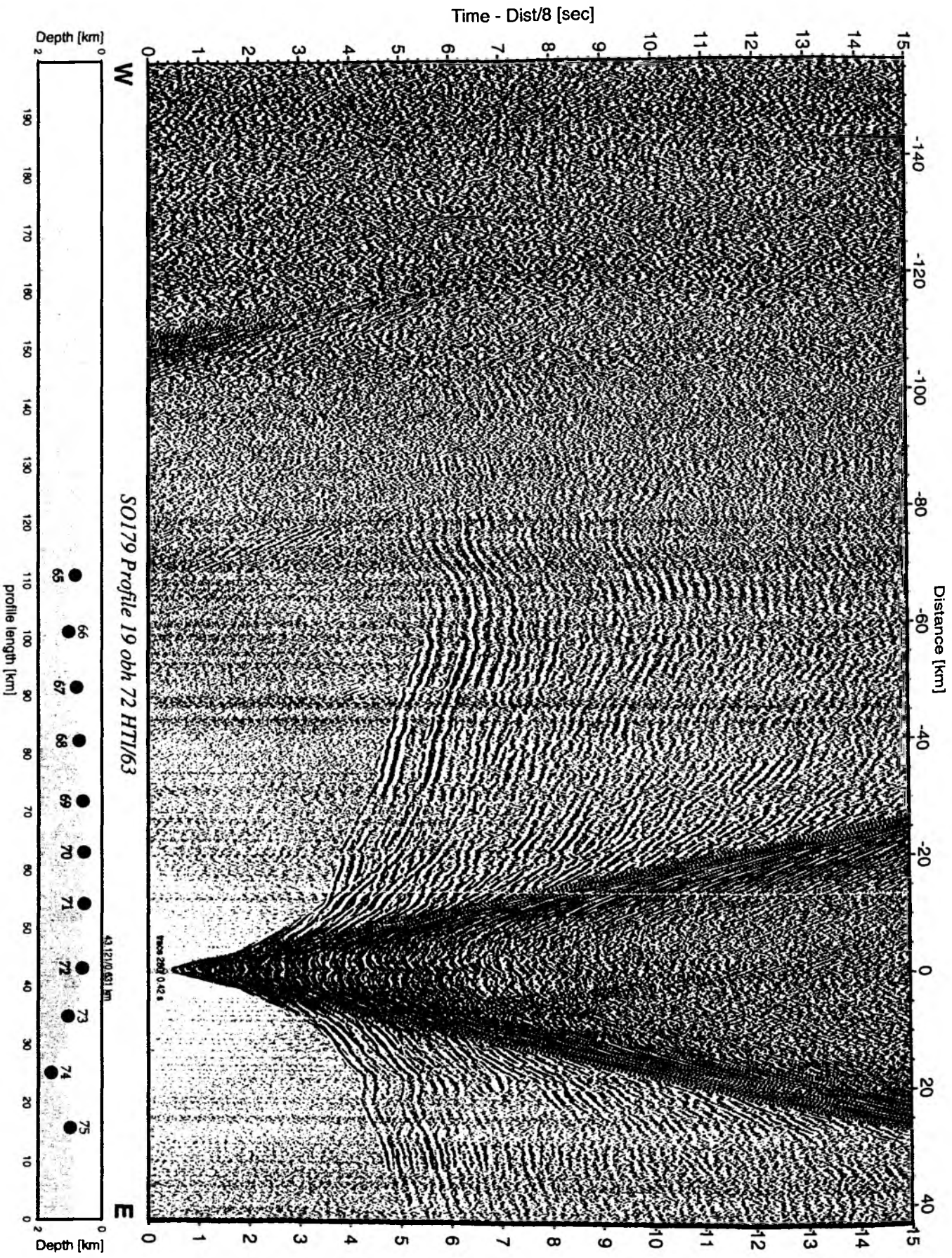

Figure 6.4.4.10: Record section from obh 72 HTI/63, Profile 19.

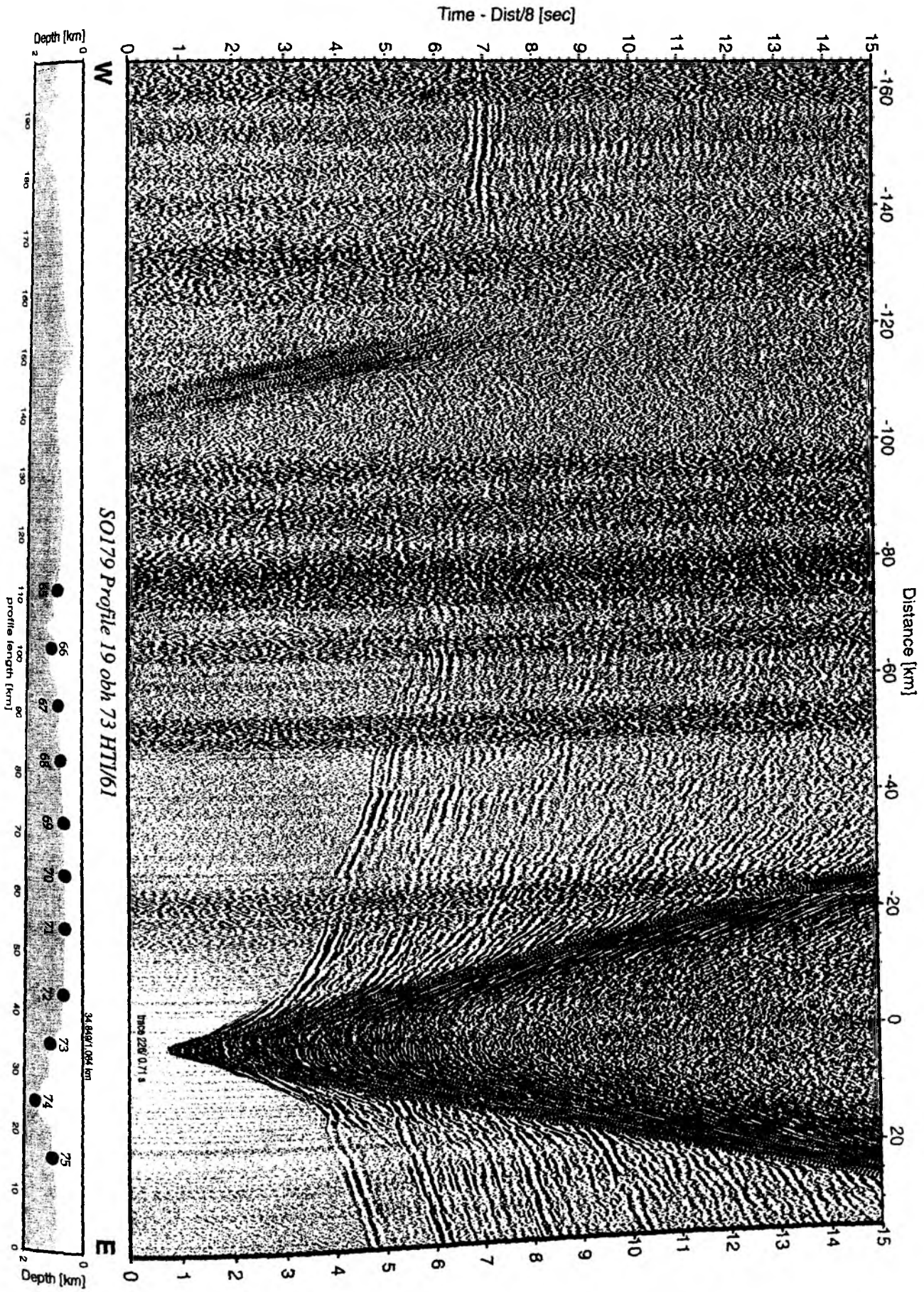

Figure 6.4.4.11: Record section from obh 73 HTI/61, Profile 19.

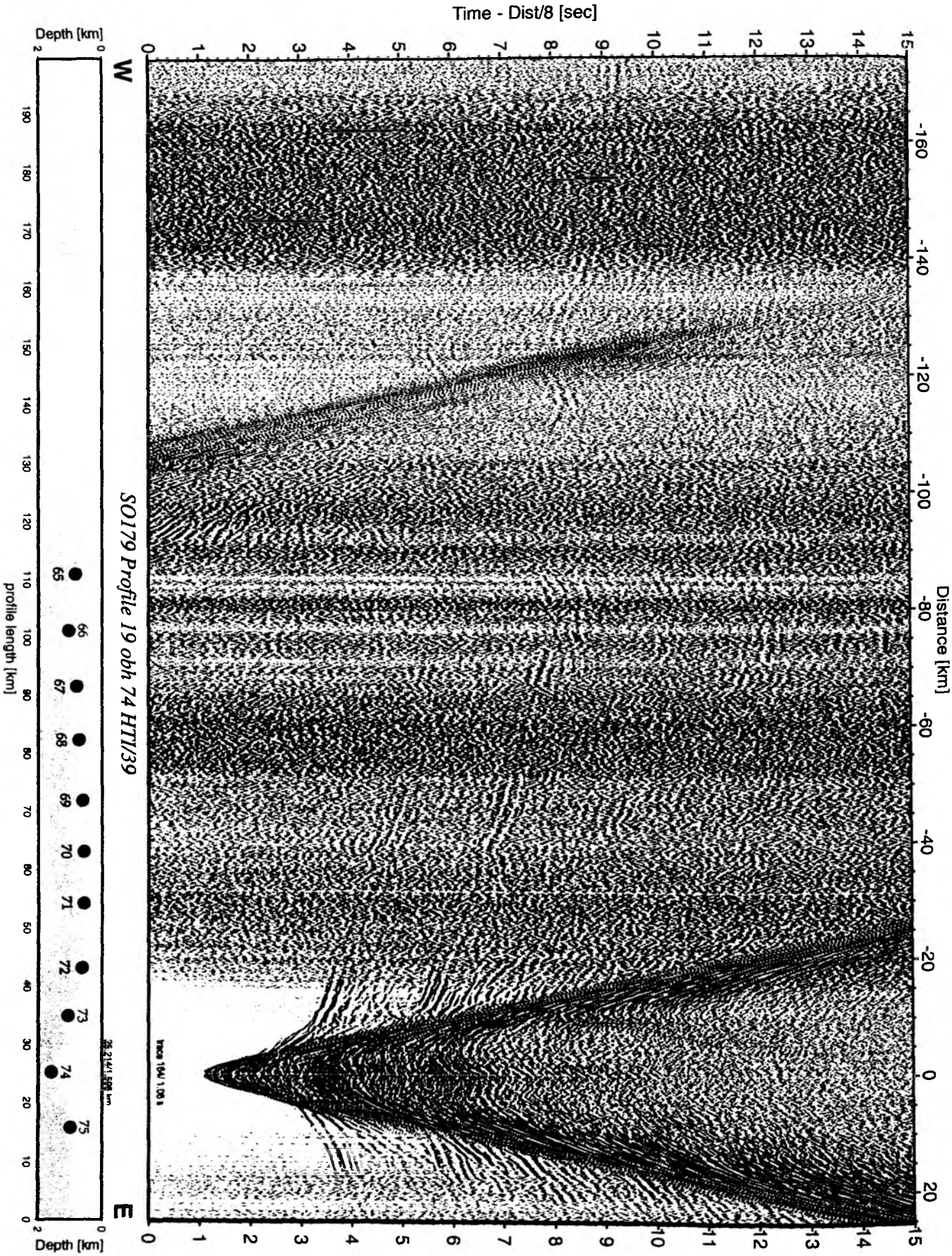

Figure 6.4.4.12: Record section from obh 74 HTI/39, Profile 19.

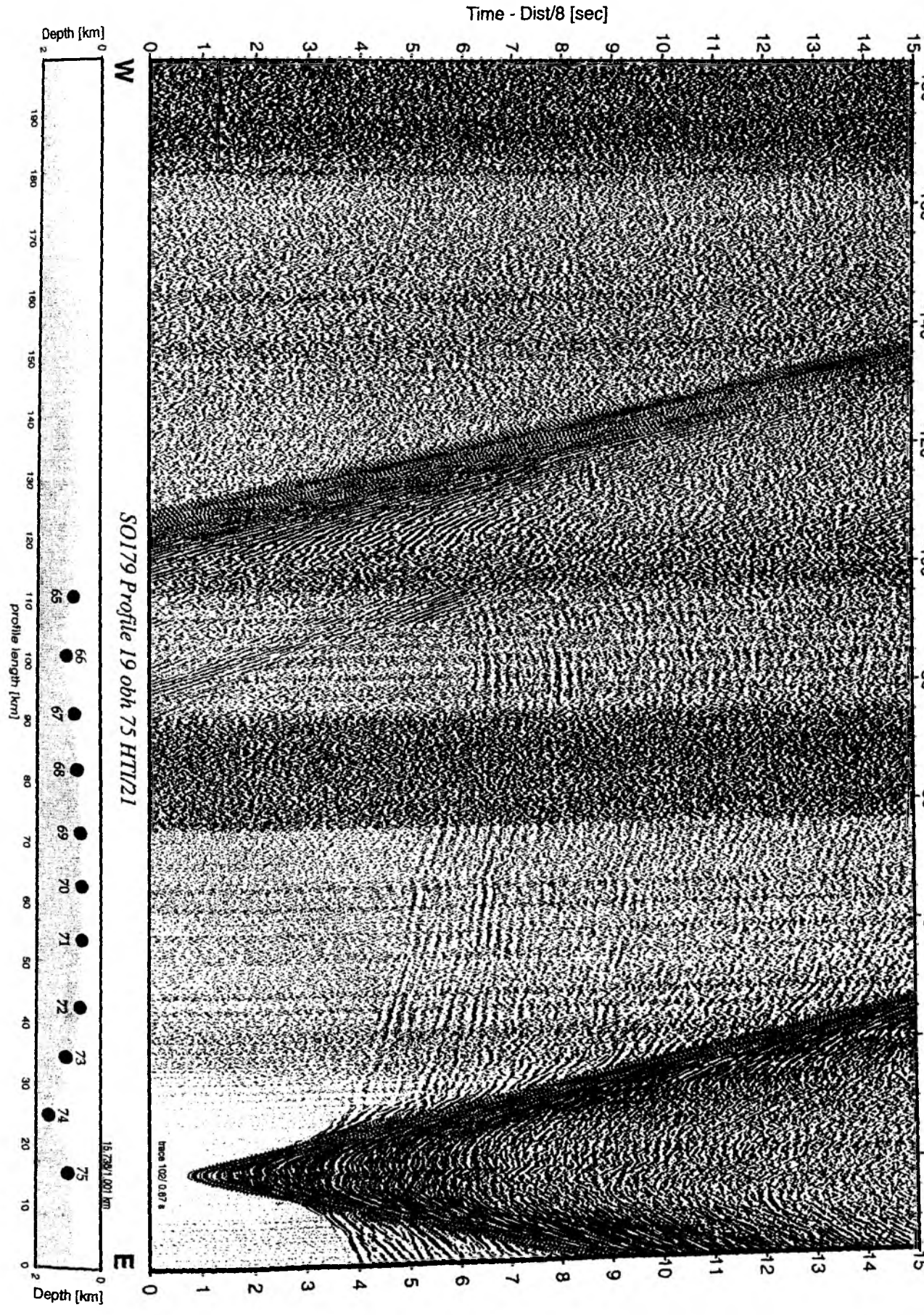

Figure 6.4.4.13: Record section from obh 75 HTI/21, Profile 19.

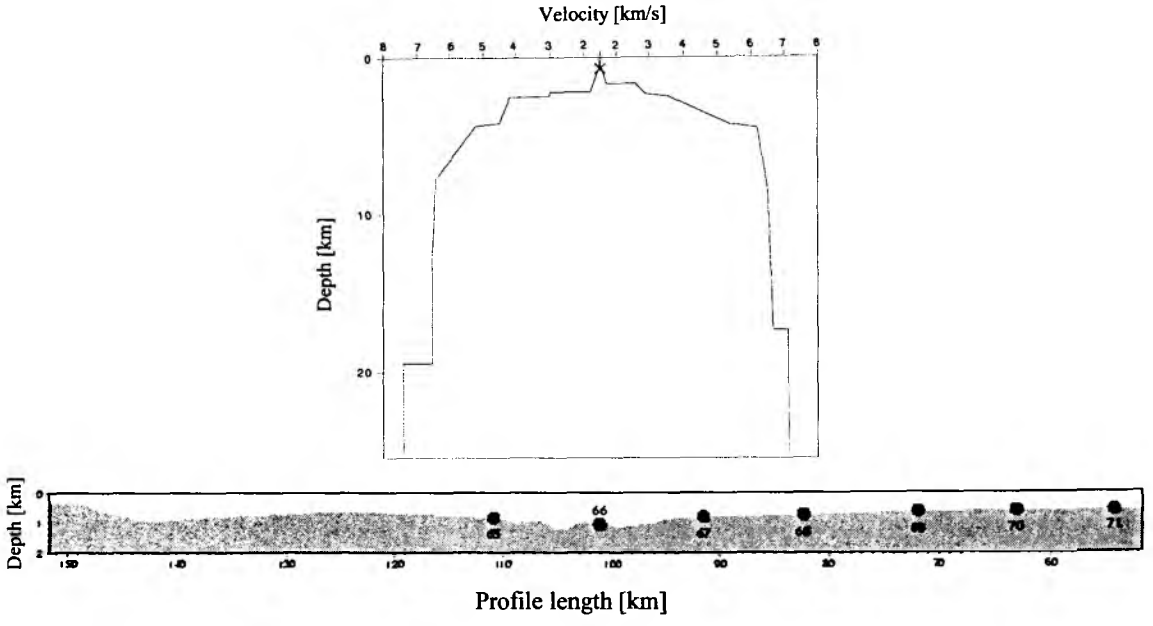

Figure 6.4.4.14: 1-D velocity model of OBH66.

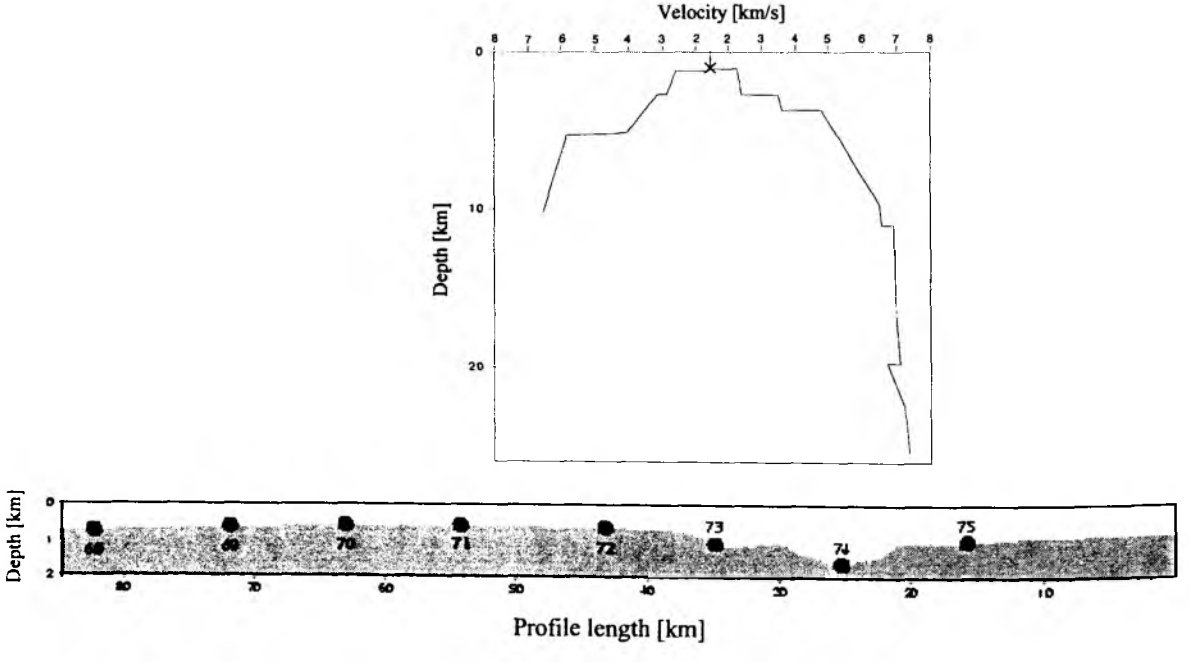

Figure 6.4.4.15: 1-D velocity model of OBH73.

7. Acknowledgements

Cruises SO 176 and 179 were funded by the German Ministery of Education and Research (BMBF) under project No. 03G0176A to IFM-GEOMAR within the continued and generous most commendable support for marine sciences with an outstanding research vessel such as SONNE.
These cruises are part of the SUNDAARC Initiative within the special programme Geotechnology of the BMBF, which provides additional funding for further work and interpreation of the data collected to BGR, Hannover, CAU, Kiel, GFZ, Potsdam and IFM-GEOMAR, Kiel.
We warmly thank masters H. Papenhagen and L. Mallon and their crew for their excellent support in all work done and for the splendid working atmosphere throughout the entire cruise and the ambitious working program.

8. References:

Abercrombie, R., Antolik, M., Felzer, K., and Ekström, G.: The 1994 Java tsunami earthquake: Slip over a subducting seamount, J. Geophys. Res., 106, 6595-6607, 2001.

Audley-Charles, M.G., Evolution of the southern margin of Thethys (North Australian region) from early Permian to late Cretaceous, in: Gondwana and Thethys, Audley-Charles, M.G., and A. Hallam (eds), Geological Society Special Publication 37, 79-100, 1988.

Bangs, N. L. B., G. K. Westbrook, J. W. Ladd, and P. Buhl, Seismic velocities from the Barbados Ridge Complex: Indicators of high pore fluid pressures in an accretionary complex, J. Geophys. Res., 95, 8767-8782, 1990.

Beaudry, D. and G. F. Moore: Seismic-stratigraphic frame work off Central Sumatra, Sunda Arc, Earth and Plan. Sc. Letts., 54, 17-28, 1981.

Beaudry, D. and G. F. Moore: Seismic stratigraphy and Cenozoic evolution of the West Sumatra forearc basin, Am. Assoc. Petr. Geol. Bull., 69, 5, 742-759, 1985.

Beck, R. H. und P. Lehner: Oceans, new frontier in exploration. Am. Assoc. Petr. Geol. 58, 376-395, 1974.

Benaron, N, A geophysical study of the forearc region south of Java, Indonesia, Master Thesis, University of San Diego, CA, 1982, 83 pp.

Bostock, M. G., R. D. Hyndman, S. Rondenay, and S. M. Peacock, An inverted continental Moho and serpentinization of the forearc mantle, Nature, 417, 536-538, 2002

Brouwer, H. A.: The Geology of the Netherlands East Indies, Macmillan, New York, 1-160, 1925.

Byrne, D. E., W.-H. Wang, and D. M. Davis, Mechanical role of backstops in the growth of forearcs, Tectonics, 12, 1, 123-144, 1993.

Cande, S. C., LaBreque, J. L., Larson, R. L., Pitman, W. C. Golovchenko, X., and Hafby, W. F., Magnetic lineations of the world's ocean basins, LDGO contribution 4367, AAPG, Tulsa, Oklahoma, 1989.

Carlson, R. L., and D. J. Miller, Mantle wedge water contents estimated from seismic velocities in partially serpentinized peridotites, Geophys. Res. Lett.,30(5), 1250, doi:10.1029/2002GL016600, 2003

Curray, J.R., Shor, G.G.Jr., Raitt, R.W., and Henry M., Seismic refraction and reflection studies of crustal structure of the Eastern Sunda and Western Banda arcs, Journal of Geophysical Research, 82, 17, 2479-2489, 1977.

Curray, J. R.: The Sunda Arc: A model for oblique plate convergence, Proc. Snellius-II Symp., Neth. Jl. Sea Res., 24, 131-140, 1989.

Dahlen, F. A., Critical taper model of fold-and-thrust belts and accretionary wedges, Annu. Rev. Earth Planet. Sci., 18, 55-99, 1990.

Davis, D. M., J. Suppe, and F. A. Dahlen, Mechanics of Fold-and-Thrust Belts and Accretionary Wedges, J. Geophys. Res., 88, 1153-1172, 1983.

Davis, D.M., and R.von Huene, Inferences on sediment strength and fault friction from structures at the Aleutian Trench, Geology, 15, 517-522, 1987.

Davis, D. M., Accretionary mechanics with properties that vary in space and time, in: Subduction top to bottom, Geophysical Monograph 96, 39-48, 1996.

Davis, E. E., and R. Hyndman, Accretion and recent deformation of sediments along the northern Cascadia subduction zone, Int. Geological Society of America Bulletin, 101, 1465-1480, 1989.

De Mets, Gordon, R. G., Argus, D. F., and Stein, S. Current plate motions, Geophysical Journal International, 101, 425-478, 1990.

Diament, M., H. Harjono, K. Karta, C. Deplus, D. Dahrin, M. T. Zan, Jr., M. Gerard, O. Lassal, A. Martin, J. Malod, Mentawai fault zone off Sumatra: a new key to the geodynamics of western Indonesia, Geology, 20, 259-262, 1992.

Fitch, T. J., Plate convergence, transcurrent faults and internal deformation adjacent to Southeast Asia and the Western Pacific, Int. Journal of Geophysical Research, 77, 4432-4460, 1972.

Flueh, E.R. (edt) and Shipboard Science Party, GINCO2 (SONNE Cruise SO-138): Geo-scientific investigations along the active convergence zone between the Eastern Eurasian and Indo-Australian Plates off Indonesia, Cruise Report, Geomar, Kiel, 1999.

Fruehn, J, R. von Huene, and M. A. Fisher, Accretion in the wake of terrane collision: the Neogene accretionary wedge off Kenai peninsula, Alaska, Tectonics, 18, 2, 263-277, 1999.

Ganie, B., Syafuddin, Superman, A. and Honza, E., 1987: Geomorphological features in the eastern Sunda Trench, CCOP Technical Bulletin, 19, 7-12.

Gasparon, M., and R. Varne, Sumatran granitoids and their relationship to Southeast Asian terranes, Tectonophysics, 251, 277-299, 1995.

Ghose, R., Yoshioka, S., and Oike, K., 1990: Three-dimensional numerical simulation of the subduction dynamics in the Sunda arc region, Southeast Asia, Tectonophysics, 181, 223-255.

Graeber, F. M., and G. Asch, Three-dimensional models of P wave velocity and P-to-S ratio in the southern central Andes by simultaneous inversion of local earthquake data, J. Geophys. Res., 104, 20,237-20,256, 1999

Gutscher, M.A., N. Kukowski, J. Malavieille, and S. Lallemand, Cyclical behavior of thrust wedges: insights from high basal friction sandbox experiments, Geology, 24 (2), 135-138, 1996.

Hamilton, W.B., Tectonics of the Indonesian Region, USGS Professional Paper, 1078, 1979.

Hamilton, W., Plate tectonics and island arcs, Geological Society of America Bulletin, 100, 1503-1527, 1988.

Huchon, P. and Le Pichon, X.: Sunda Strait and Central Sumatra fault, Geology, 12, 668-672, 1984.

Hutagaol, J. P., Report on gravity tying DG.0(Bandung) – BGR-station(Cilacap), Marine Geological Institute (MGI), Bandung, Indonesia, 1999.

Hutchinson, C.S., Geological Evolution of South-East Asia, Claredon Press, Oxford, 1989.

Izart, A., B. Mustafa Kemal, J. A. Malod, Seismic stratigraphy and subsidence evolution of the northwest Sumatra fore-arc basin, Marine Geology, 122, 109-124, 1994.

Ishihara, T., and Kisimoto, K., Magnetic anomaly map of East Asia 1:4.000.000 [CD-ROM], Geological Survey of Japan and Coordinating Committee for Coastal and Offshore Geoscience Programmes in East and Southeast Asia (CCOP), 1996.

Jiao, W., P. G. Silver, Y. Fei, and C. T. Prewitt, Do intermediate- and deep-focus earthquakes occur on preexisting weak zones? An examination of the Tonga subduction zone, J. Geophys. Res., 105, 28,125-28,138, 2000

Kamiya, S., and Y. Kobayashi, Seismological evidence for the existence of serpentinized wedge mantle, Geophys. Res. Lett., 27, 819-822, 2000

Karig, D. E., Suparka, S., Moore, G. F., Hehunassa, P. E.: Structure and Cenozoic evolution of the Sunda Arc in the central Sumatra region, Am. Assoc. Petr. Geol. Mem., 29, 223-237, 1979.

Karig, D. E., Lawrence, M. B., Moore, G. F., Curray, J. R.: Structural framework of the forear-arc basin, NW Sumatra, Jl. Geol. Soc. Lon., 137, 77-91, 1980.

Karig, D. E., Moore, G. F., Curray, J. R., Lawrence, M. B.: Morphology and shallow structure of the lower trench slope off Nias island, Sunda Arc, in: D. E. Hays (ed)., The tectonic and geologic evolution of Southeast Asian Seas and Islands, Geoph. Mon., 23, 179-208, 1980.

Kirby, S., E. R. Engdahl, and R. Denlinger, Intermediate-depth intraslab earthquakes and arc volcanism as physical expressions of crustal and uppermost mantle metamorphism in subducted slabs, in: Subduction Top to Bottom, Geophys. Monogr. Ser., vol. 96, edited by G. Bebout et al., pp. 195-214, AGU, Washington, DC, 1996

Kobayashi, K., Nakanishi, M., Tamaki, K., Ogawa, Y.: Outer slope faulting associated with the western Kuril and Japan trenches, Geophys. J. Int., 134, 356-372, 1998.

Kopp, H., Crustal Structure Along the Central Sunda Margin, Indonesia, PhD Thesis, University of Kiel, 2001.

Kopp, H., BSR occurrence along the Sunda margin: evidence from seismic data, Earth and Planetary Science Letters, 197, 225-235, 2002.

Kopp, H., D. Klaeschen, E. R. Flueh, J. Bialas, C. Reichert, Crustal structure of the Java margin from seismic wide-angle and multichannel reflection data, Journal of Geophysical Research, 107, B2, 10.1029/2000JB000095, 2002.

Kopp, H. und N. Kukowski, Backstop geometry and accretionary mechanics of the Sunda margin, Tectonics, 6, 22, 10.1029/2002TC001420, 2003.

Kopp, H., Flueh, E., Papenberg, C., Klaeschen, D., SPOC Scientists: Seismic Investigations of the O'Higgins Seamount Group and Juan Fernández Ridge: Aseismic Ridge Emplacement and Lithosphere Hydration, Tectonics, 2, 23, TC2009, 10.1029/2003TC001590, 2004.

Kuenen, P. H.: Geological interpretation of bathymetrical results. The Snellius expedition, 5, 1, 1-124, Brill, Leiden, 1935.

Lallemand, S. E., P. Schnuerle, and J. Malavieille, Coulomb theory applied to accretionary and nonaccretionary wedges: Possible causes for tectonic erosion and/or frontal accretion, J. Geophys. Res., 99, 12033-12055, 1994.

Lohrmann, J., N. Kukowski, J. Adam, and O. Oncken, The impact of analogue material properties on the geometry, kinematics, and dynamics of convergent sand wedges, Journal of Structural Geology, 25 (10), 1691-1711, 2003.

Malod, J. A., K. Karta, M.O. Beslier, M.T. Zen Jr., From normal to oblique subduction: Tectonic relationships between Java and Sumatra, Journal of Southeast Asian Earth Sciences, 12, 85-93, 1995.

Malod, J. A., and B. M. Kemal, The Sumatra margin: oblique subduction and lateral displacement of the accretionary prism, in: Tectonic evolution of Southeast Asia, R. Hall and D. Blundell (edts), Geological Society Special Publication, 106, 19-28, 1996.

Masson, D. G., Parson, L. M., Milsom, J., Nichols, G., Sikumbang, N., Dwiyanto, B., Kallagher, H.: Subduction of seamounts at the Java Trench: a view with long-range sidescan sonar, Tectonophysics, 185, 51-65, 1990.

Masson, D. G.: Fault patterns at outer trench walls, Marine Geophys. Res., 13, 209-225, 1991.

McCaffrey, R., Oblique plate convergence, slip vectors, and forearc deformation, Journal of Geophysical Research, 97, B6, 8905-8915, 1992.

McCaffrey, R., P. C. Zwick, Y. Bock, L. Prawirodirdjo, J. F. Genrich, C. W. Stevens, S. S. O. Puntodewo, C. Subarya, Strain partitioning during oblique plate convergence in northern Sumatra: Geodetic and seismologic constraints and numerical modeling,J ournal of Geophysical Research, 105, 28363-28376, 2000.

McCourt, W., M. J. Crow, E. J. Cobbing, and T. C. Amin, Mesozoic and Cenozoic plutonic evolution of SE Asia: evidence from Sumatra, Indonesia, in: Tectonic Evolution of Southeast Asia, R. Hall (edt), Geological Society of London Spec. Publication 106, 321-335, 1996.

Metcalfe, I., Pre-Cretaceous evolution of Se Asian terranes, in: Tectonic Evolution of Southeast Asia, R. Hall (edt), Geological Society of London Spec. Publication 106, 97-122, 1996.

Moore, G. F., J. R. Curray, D. G. Moore, D. E. Karig, Variations in geologic structure along the Sunda fore arc, Northeastern Indian Ocean, in: The tectonic and geologic evolution of Southeast Asian seas and islands, D. Hayes (edt), Geophysical Monograph, 23,145-160, 1980.

Müller, D., W. R. Roest, J. Y. Royer, L. M.Gahagan, and J. G. Sclater, Digital isochrons of the world's ocean floor, Journal of Geophysical Research, 102, 3211-3214, 1997.

National Geophysical Data Center, *Marine Geophysical Data* [CD-ROM], National Oceanic and Atmospheric Administration, Boulder, Col., 2002.

Newcomb, K.R., and McCann, W.R., 1987: Seismic history and seismotectonics of the Sunda Arc, Journal of Geophysical Research, 92: 421-439.

Nishimura, S., and S. Suparka, Tectonic approach to the Neogene evolution of Pacific-Indian Ocean seaways, Tectonophysics, 281, 1-16, 1997.

Peacock, S., Fluid processes in subduction zones, Science, 248, 329-337, 1990

Peacock, S., Large-scale hydration of the lithosphere above subducting slabs, Chem. Geol., 108, 49-59, 1993

Peacock, S., Are the lower planes of double seismic zones caused by serpentine dehydration in the subducting oceanic mantle?, Geology, 29, 299-302, 2001

Pubellier, M., C. Rangin, J.-P. Cadet, I. Tjashuri, J. Butterlin and C. Mueller, L'ile de Nias, un edifice polyphase sur la bordure interne de la fosse de la Sonde (Archipel de Mentawai, Indonesie), Comptes rendus de l'Academie des sciences, Serie II, 8, 1019-1026, 1992.

Ranero, C. R. and R. von Huene, Subduction erosion along the Middle America convergent margin, Nature, 404, 748-752, 2000.

Ranero, C. R., J. Phipps Morgan, K. McIntosh, and C. Reichert, Bending-related faulting and mantle serpentinization at the Middle America trench, Nature, 425, 367-373, 2003.

Reichert, C. (edt) and Shipboard Science Party, GINCO1 (SONNE Cruise SO-137): Geo-scientific investigations along the active convergence zone between the Eastern Eurasian and Indo-Australian Plates off Indonesia, Cruise Report, BGR, Hannover, 1999.

Ryan, H. F., and D. W. Scholl, The evolution of forearc structures along an oblique convergent margin, Central Aleutian arc, Tectonics, 8, 3 497-516, 1989.

Samuel, M. A.: The Structural and Stratigraphic Evolution of Islands of the Active Margin of the Sumatra Forearc, Indonesia. PhD-Thesis University of London, pp. 345, 1994.

Samuel, M. A., and N. A. Harbury, The Mentawai fault zone and deformation of the Sumatran forearc in the Nias area, in: Tectonic evolution of Southeast Asia, R. Hall and D. Blundell (edts), Geological Society Special Publication, 106, 337-351, 1996.

Schlueter, H. U., C. Gaedicke, H. A. Roeser, B. Schreckenberger, H. Meyer, C. Reichert, Y. Djajadihardja, and A. Prexl, Tectonic features of the southern Sumatra-western Java forearc of Indonesia-, Tectonics, 21(5), 1047, doi:10.1029/2001TC901048, 2002.

Scholl, D. W., Stuffing continental crustal material into the mantle at subduction zones—evidence, quantities, consequences, http://pangaea.stanford.edu/GP/Scholl.html, 2002.

Schott, B., and H.A. Koyi, Estimating basal friction in accretionary wedges from the geometry and spacing of frontal faults, Earth and Planetary Science Letters, 194, 221-227, 2001.

Schweitzer, J., An enhanced routine to locate seismic events, Pure & Applied geophysics, 158, 2001.

Seno, T., and Y. Yamanaka, Double seismic zones, compressional deep trench-outer rise events, and superplumes, in: Subduction Top to Bottom, Geophys. Monogr. Ser., vol. 96, edited by G. Bebout et al., pp. 347-355, AGU, Washington, DC, 1996

Seno, T., D. Zhao, Y. Kobayashi, and M. Nakamura, Dehydration of serpentinized mantle: Seismic evidence from southwest Japan, Earth Planets Space, 53, 861-871, 2001

Sieh, K., and D. Natawidjaja, Neotectonics of the Sumatran fault, Indonesia, Journal of Geophysical Research, 105, 12 28295-28326, 2000.

Tapponnier, P., G. Peltzer, A. Y. Le Dain, Armijo-Rolando, and P. Cobbold, Propagating extrusion tectonics in Aisa: new insights from simple experiments with plasticine, Geology, 10, 12, 611-616, 1982.

Tregoning et al., 1994

Van Bemmelen, R. W.: The geology of Indonesia, Vol. IA, General Geology, IB Portfolio. Government Printing Office, Nijhoff, The Hague, 1-732, 1949.

Van Weering, T. C. E., Kusnida, D., Tjokrosapoetro, S., Lubis, S., Kridoharto, P., Munadi, S.: The seismic structure of the Lombok and Savu forearc basins, Indonesia, Neth. J. Sea Res., 24, 251-262, 1989.

Vening Meinesz, F. A.: The earth's crust deformtion in the East Indies, Proc. K. Ned. Akad. Wet., 43, 2778-293, 1940.

von Huene, R., and D. W. Scholl, Observations at convergent margins concerning sediment subduction, subduction erosion and the growth of continental crust, Reviews of Geophysics, 29, 279-316, 1991.

von Huene, R., and D. Klaeschen, Opposing gradients of permanent strain in the aseismic zone and elastic strain across the seismogenic zone of the Kodiak shelf and slope, Alaska, Tectonics,18,2, 248-262, 1999.

Von Huene, R., Ranero, C.R. und Watts, P.:Tsunamigenic slope failure along the Middle America Trench in two tectonic settings, Marine Geology, 203, 303-317, 2004.

Widiyantoro, S., and R. van der Hilst, Structure and Evolution of Lithospheric Slab Beneath the Sunda Arc, Indonesia, Science, 271, 1566-1570, 1996.

Zhao, D., F. Ochi, A. Hasegawa, and A. Yamamoto, Evidence for the location and cause of large crustal earthquakes in Japan, J. Geophys. Res., 105, 13,579-13,594, 2000

9. Appendices
9.1 Magnetic and gravity profiles

Table 9.1.1: *List of magnetic profiles SO-179*

line number	date	time	latitude	longitude	course	
SO179-100	18.09.2004	14:25:00	8° 31.103 W	108° 2.348 E		
SO179-100	18.09.2004	23:01:00	9° 6.823 W	109° 24.788 E	114°	164.71 km
SO179-01	18.09.2004	23:44:00	9° 7.846 W	109° 27.133 E		
SO179-01	20.09.2004	01:05:00	9° 28.022 W	111° 16.566 E	101°	203.43 km
SO179-101	20.09.2004	11:16:20	9° 3.295 W	111° 22.274 E		
SO179-101	20.09.2004	16:22:40	8° 57.371 W	110° 24.709 E	276°	105.85 km
SO179-102	21.09.2004	01:17:20	8° 37.763 W	110° 20.632 E		
SO179-102	21.09.2004	05:11:20	8° 30.181 W	109° 29.233 E	278°	95.15 km
SO179-103	21.09.2004	08:54:00	8° 29.643 W	109° 26.511 E		
SO179-103	21.09.2004	09:44:40	8° 34.788 W	109° 33.757 E	126°	16.33 km
SO179-103a	21.09.2004	09:45:00	8° 34.829 W	109° 33.801 E		
SO179-103a	21.09.2004	12:39:00	9° 8.470 W	109° 34.021 E	180°	62.29 km
SO179-104	21.09.2004	16:58:00	9° 11.163 W	109° 32.955 E		
SO179-104	21.09.2004	19:25:40	9° 7.565 W	109° 59.881 E	82°	49.67 km
SO179-105	22.09.2004	12:40:20	9° 6.833 W	110° 30.001 E		
SO179-105	22.09.2004	14:35:20	8° 41.892 W	110° 29.988 E	360°	46.18 km
SO179-16	24.09.2004	00:00:20	10° 49.811 W	110° 24.265 E		
SO179-16	25.09.2004	22:54:20	8° 18.266 W	110° 51.383 E	10°	284.94 km
SO179-106	26.09.2004	14:49:20	9° 42.386 W	110° 39.692 E		
SO179-106	26.09.2004	16:49:40	9° 45.243 W	111° 3.698 E	97°	44.13 km

SO179-107	26.09.2004	19:04:20	9° 46.720 W	111° 8.563 E		
SO179-107	26.09.2004	19:19:40	9° 49.603 W	111° 9.833 E	157°	5.82 km
SO179-107a	26.09.2004	19:20:00	9° 49.666 W	111° 9.860 E		
SO179-107a	26.09.2004	21:05:00	9° 59.812 W	110° 49.773 E	243°	41.18 km
SO179-107b	26.09.2004	21:05:20	9° 59.751 W	110° 49.748 E		
SO179-107b	26.09.2004	21:35:40	9° 54.087 W	110° 47.509 E	339°	11.26 km
SO179-108	27.09.2004	03:21:40	10° 11.781 W	110° 33.029 E		
SO179-108	27.09.2004	04:19:40	10° 14.955 W	110° 44.723 E	105°	22.11 km
SO179-108a	27.09.2004	04:20:00	10° 14.993 W	110° 44.776 E		
SO179-108a	27.09.2004	07:30:00	10° 55.130 W	110° 44.741 E	180°	74.32 km
SO179-108b	27.09.2004	07:30:20	10° 55.179 W	110° 44.686 E		
SO179-108b	27.09.2004	09:01:20	10° 57.663 W	110° 25.302 E	263°	35.54 km
SO179-109	27.09.2004	15:15:40	10° 40.001 W	110° 23.983 E		
SO179-109	27.09.2004	18:41:40	10° 39.997 W	109° 37.885 E	270°	83.88 km
SO179-110	27.09.2004	21:25:00	10° 57.439 W	109° 35.496 E		
SO179-110	28.09.2004	00:34:40	10° 46.605 W	110° 13.487 E	74°	71.94 km
SO179-110a	28.09.2004	00:35:00	10° 46.586 W	110° 13.556 E		
SO179-110a	28.09.2004	01:18:20	10° 50.609 W	110° 21.482 E	117°	16.23 km
SO179-111	28.09.2004	05:09:20	10° 47.843 W	110° 13.245 E		
SO179-111	28.09.2004	08:37:40	10° 12.079 W	109° 40.727 E	318°	88.83 km
SO179-18	28.09.2004	23:45:00	7° 59.824 W	109° 50.230 E		

SO179-18	30.09.2004	17:00:00	11° 5.743 W	109° 33.558 E	185°	345.60 km
SO179-112	30.09.2004	17:00:20	11° 5.754 W	109° 33.551 E		
SO179-112	30.09.2004	17:40:00	11° 0.589 W	109° 33.889 E	4°	9.58 km
SO179-112a	30.09.2004	17:40:20	11° 0.564 W	109° 33.883 E		
SO179-112a	30.09.2004	18:10:00	10° 55.824 W	109° 30.973 E	329°	10.25 km
SO179-112b	30.09.2004	18:10:20	10° 55.797 W	109° 31.033 E		
SO179-112b	30.09.2004	18:22:20	10° 54.986 W	109° 33.202 E	69°	4.22 km
SO179-113	30.09.2004	23:26:40	10° 38.554 W	109° 35.214 E		
SO179-113	01.10.2004	00:10:00	10° 30.141 W	109° 30.102 E	329°	18.15 km
SO179-113a	01.10.2004	00:10:20	10° 30.076 W	109° 30.065 E		
SO179-113a	01.10.2004	01:15:00	10° 15.651 W	109° 29.951 E	360°	26.71 km
SO179-113b	01.10.2004	01:15:20	10° 15.577 W	109° 29.949 E		
SO179-113b	01.10.2004	01:41:40	10° 12.165 W	109° 34.516 E	53°	10.45 km
SO179-114	01.10.2004	22:44:40	8° 3.149 W	109° 50.723 E		
SO179-114	02.10.2004	00:54:40	8° 23.125 W	110° 8.200 E	139°	48.93 km
SO179-19	02.10.2004	08:38:20	8° 43.003 W	111° 6.780 E		
SO179-19	03.10.2004	06:30:00	8° 10.437 W	109° 21.981 E	287°	201.20 km
SO179-115	03.10.2004	06:54:00	8° 11.777 W	109° 21.101 E		
SO179-115	03.10.2004	10:39:40	8° 26.160 W	110° 5.422 E	108°	85.46 km
SO179-116	03.10.2004	21:03:20	8° 42.738 W	111° 0.081 E		
SO179-116	03.10.2004	22:10:00	8° 55.033 W	111° 4.534 E	160°	24.18 km
SO179-117	03.10.2004	22:10:20	8° 55.025 W	111° 4.471 E		
SO179-117	03.10.2004	23:05:00	8° 50.328 W	110° 52.939 E	292°	22.82 km

SO179-118	03.10.2004	23:05:20	8° 50.391 W	110° 52.921 E		
SO179-118	04.10.2004	02:00:00	9° 27.439 W	110° 46.363 E	190°	69.64 km
SO179-119	04.10.2004	02:00:20	9° 27.456 W	110° 46.290 E		
SO179-119	04.10.2004	02:55:00	9° 25.204 W	110° 34.268 E	281°	22.35 km
SO179-120	04.10.2004	02:55:20	9° 25.247 W	110° 34.208 E		
SO179-120	04.10.2004	04:05:00	9° 39.802 W	110° 34.592 E	179°	26.96 km
SO179-121	04.10.2004	04:05:20	9° 39.782 W	110° 34.651 E		
SO179-121	04.10.2004	06:00:00	9° 33.675 W	110° 56.476 E	74°	41.42 km
SO179-122	04.10.2004	06:00:20	9° 33.736 W	110° 56.498 E		
SO179-122	04.10.2004	08:40:00	10° 4.642 W	110° 40.182 E	207°	64.51 km
SO179-123	04.10.2004	08:40:20	10° 4.711 W	110° 40.171 E		
SO179-123	04.10.2004	09:40:00	10° 5.126 W	110° 51.829 E	92°	21.27 km
SO179-124	04.10.2004	09:40:20	10° 5.174 W	110° 51.877 E		
SO179-124	04.10.2004	11:05:00	10° 22.499 W	110° 52.394 E	178°	32.09 km
SO179-125	04.10.2004	11:05:20	10° 22.510 W	110° 52.325 E		
SO179-125	04.10.2004	12:10:00	10° 23.041 W	110° 37.363 E	268°	27.27 km
SO179-126	04.10.2004	12:10:20	10° 23.053 W	110° 37.289 E		
SO179-126	04.10.2004	14:15:00	10° 49.927 W	110° 32.816 E	189°	50.42 km
SO179-127	04.10.2004	14:15:20	10° 49.972 W	110° 32.753 E		
SO179-127	04.10.2004	15:10:20	10° 51.897 W	110° 24.759 E	256°	14.97 km
SO179-128	04.10.2004	16:24:40	10° 52.757 W	110° 22.740 E		
SO179-128	04.10.2004	21:40:00	11° 14.697 W	109° 14.981 E	252°	129.66 km
SO179-129	04.10.2004	21:40:20	11° 14.636 W	109° 14.952 E		
SO179-129	05.10.2004	02:50:00	10° 3.779 W	109° 15.004 E	0°	131.20 km

SO179-130	05.10.2004	02:50:20	10° 3.704 W	109° 15.005 E		
SO179-130	05.10.2004	08:00:00	10° 9.929 W	110° 20.608 E	96°	120.14 km
SO179-131	05.10.2004	08:00:20	10° 9.918 W	110° 20.674 E		
SO179-131	05.10.2004	10:32:00	9° 42.437 W	110° 31.484 E	21°	54.57 km
SO179-132	05.10.2004	10:32:20	9° 42.416 W	110° 31.417 E		
SO179-132	05.10.2004	11:20:00	9° 48.093 W	110° 22.051 E	238°	20.06 km
SO179-133	05.10.2004	11:20:20	9° 48.160 W	110° 22.024 E		
SO179-133	05.10.2004	13:40:00	10° 19.574 W	110° 15.509 E	192°	59.37 km
SO179-134	05.10.2004	13:40:20	10° 19.649 W	110° 15.493 E		
SO179-134	05.10.2004	14:25:00	10° 21.318 W	110° 7.175 E	258°	15.46 km
SO179-135	05.10.2004	14:25:20	10° 21.254 W	110° 7.201 E		
SO179-135	05.10.2004	16:40:00	9° 53.355 W	110° 12.075 E	10°	52.42 km
SO179-136	05.10.2004	16:40:20	9° 53.375 W	110° 12.006 E		
SO179-136	05.10.2004	18:20:00	9° 59.563 W	109° 50.563 E	254°	40.75 km
SO179-137	05.10.2004	18:20:20	9° 59.541 W	109° 50.492 E		
SO179-137	05.10.2004	21:25:00	9° 19.879 W	109° 49.506 E	359°	73.46 km
SO179-138	05.10.2004	21:25:20	9° 19.883 W	109° 49.439 E		
SO179-138	05.10.2004	23:15:00	9° 19.978 W	109° 25.821 E	270°	43.15 km
SO179-139	05.10.2004	23:15:20	9° 19.977 W	109° 25.749 E		
SO179-139	06.10.2004	03:56:20	8° 18.847 W	109° 13.127 E	348°	115.34 km

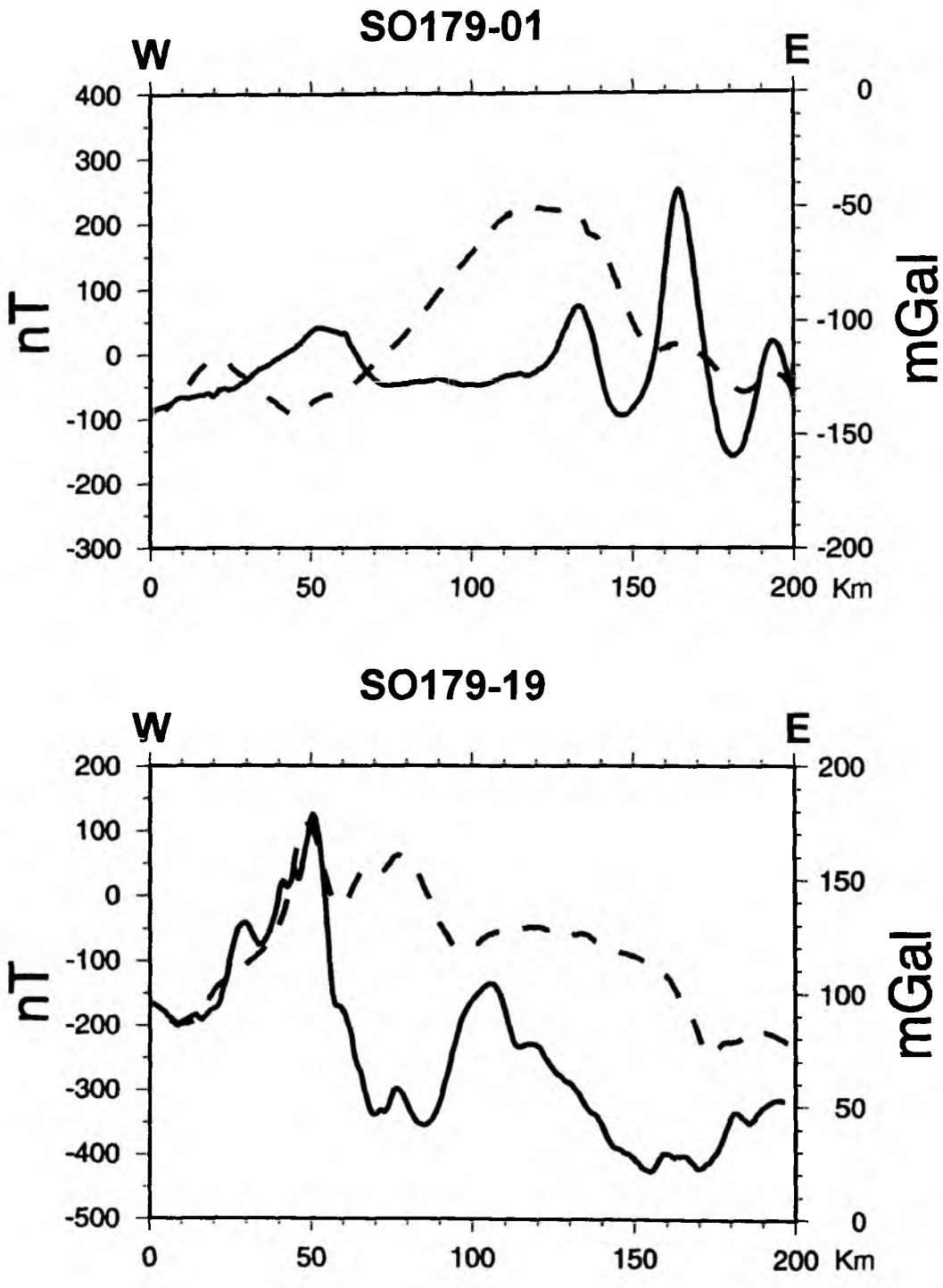

Fig. 9.1.1: Profiles SO179-01 and SO179-19. Solid lines: magnetics, dashed lines: gravity.

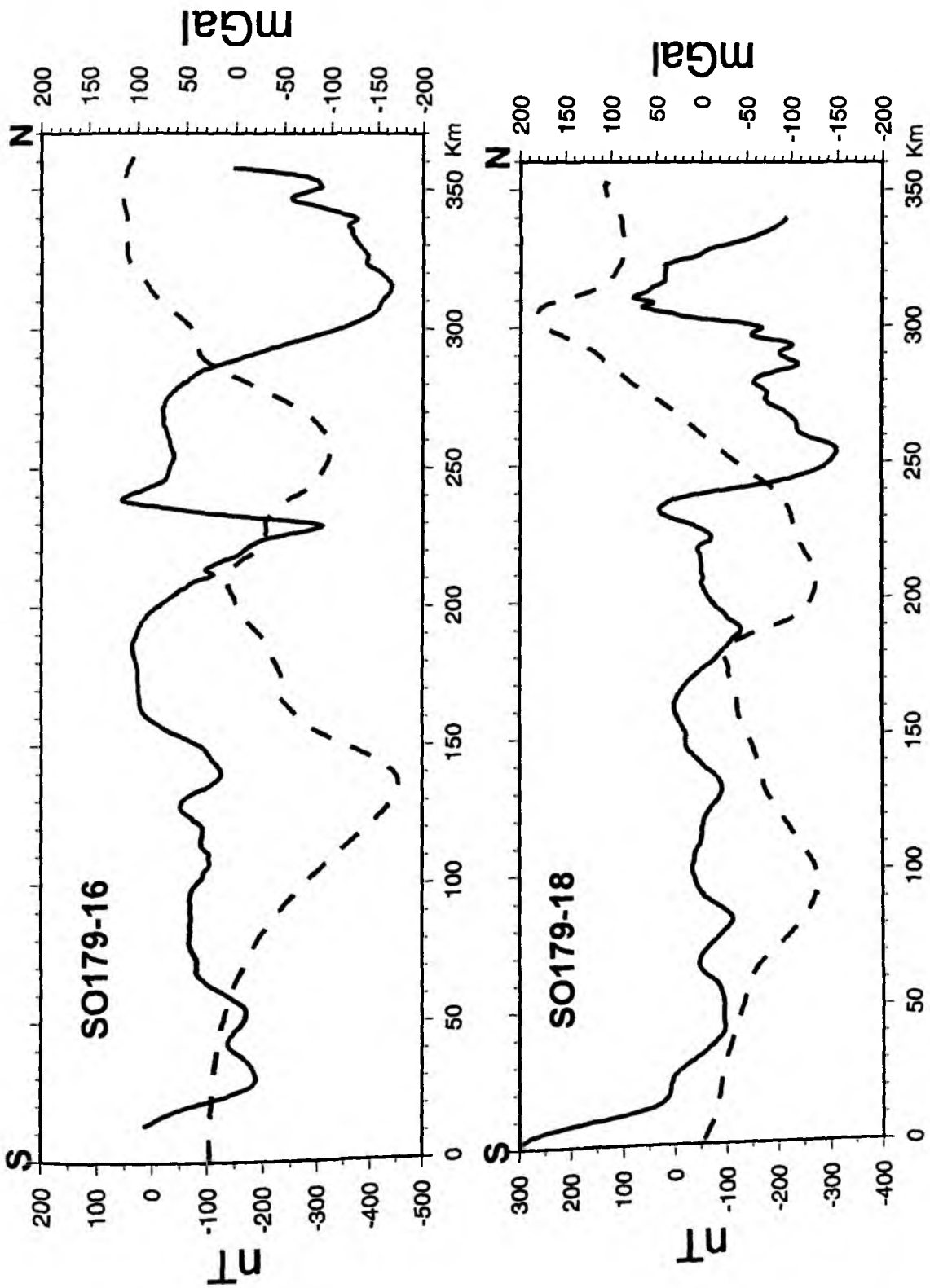

Fig. 9.1.2: Profiles SO179-16 and SO179-18. Solid lines: magnetics, dashed lines: gravity.

INST.	LAT (S)	LON (E)	DIST.	DEPTH	REL.	ANT.	REC	[illegible]	SENSORS	POSITION AFTER RELOBS	
	D:M	D:M	NEXT	(m)	CODE	CH.	NO.	[illegible]		LAT (S) [D:M]	LON (E) [D.M]
OBH 01	08:29,61	109:27,034	42	2213	03BD+0355	C	991243	-991849	HTI 15	8:29.611	109:27.06
OBS 02	09:11,405	109:32,196	49	3135	03B2+0355	C	991256	-209	HTI 73, Webb 2352	9:11.405	109:32.22
OBH 03	09:50,207	110:02,597	43	1853	3674	C	991259	-233	HTI 30	9:50.507	110:25.8
OBH 04	09:51,209	110:46,287	22	2908	03B8+0355	D	990701	342	HTI 42	9:51.209	110:46.26
OBH 05	09:45,771	111:08,159	20	2824	03B5	D	010402	-1158	HTI 28	9:45.771	111:08.16
OBS 06	09:27,112	111:14,596	31	2913	3629	D	991246	-182	HTI 44, Webb 2328	9:27.112	111:14.58
OBS 07	09:30,573	110:43,321	32	987	0386+0355	D	010409	89	DPG 95, Webb 1695	9:30.573	110:43.32
OBS 08	09:26,420	110:10,107	19	1224	3614	C	010403	312	HTI 22, Webb 2352	9:26.420	110:10.08
OBS 09	09:09,131	110:01,722	22	3302	3659	C	991235	317	DPG 75, Webb 2329	9:09.131	110:18
OBH 10	08:58,368	110:21,556	26	1696	03B6+0355	D	000711	-213	HTI 23	8:58.368	110:21.54
OBH 11	09:03,519	110:47,396	35	3224	03B1+0355	B	010405	75	HTI 27	9:03.519	110:47.4
OBH 12	09:03,335	111:22,545	27	2474	03B7+0355	D	991236	3114	HTI 39, horizontal (Send)	9:03.335	111:22.56
OBH 13	08:46,121	111:01,573	39	1133	0387+0355	C	010401	-381	HTI 38	8:46.121	111:15.6
OBH 14	08:38,073	110:22,589		1093	03BC+0355	C	991238	-240	HTI 45	8:38.073	110:22.56
OBH 15	09:27,630	111:14,527		2883	3624 (B)	C	971202	0	OAS 21 ; OAS 22 ; OAS 46 ; HTI 24		
OBH 16	09:03,981	111:23,405		2640	3624 (B)	C	971202	0	OAS 21 ; OAS 22 ; OAS 46 ; HTI 24		
OBH 17	08:58,050	110:21,517		1700	3624 (B)	C	971202	3	OAS 21 ; OAS 22 ; OAS 46 ; HTI 24		
OBH 18	08:37,998	110:22,558		1090	3624 (B)	D	971202	0	OAS 13 ; OAS 74 ; AQ 12 ; HTI 35		
OBH 19	08:29,391	109:26,513		2188	3624 (B)	D	971202	0	OAS 13 ; OAS 74 ; AQ 12 ; HTI 35		
OBH 20	09:8,970	109:30,578		3158	3624 (B)	D	971202	0	OAS 14 ; OAS 26 ; OAS 34 ; HTI 44		
OBH 21	09:09,191	110:01,489		3297	3624 (B)	D	971202	0	OAS 14 ; OAS 26 ; OAS 34 ; HTI 44		

INST.	LAT (S)	LON (E)	DIST.	DEPTH	REL.	ANT.	REC.	SKEW	SENSORS	POSITION AFTER RELOBS	
	D:M	D:M	NEXT	(m)	CODE	CH.	NO.	(ms)		LAT (S) [D:M]	LON (E) [D.M]
OBH 01	08:29,61	109:27,034	42	2213	03BD+0355	C	991243	-991849	HTI 15	8:29.611	109:27.06
OBS 02	09:11,405	109:32,196	49	3135	03B2+0355	C	991256	-209	HTI 73, Webb 2352	9:11.405	109:32.22
OBH 03	09:50,207	110:02,597	43	1853	3674	C	991259	-233	HTI 30	9:50.507	110:25.8
OBH 04	09:51,209	110:46,287	22	2908	03B8+0355	D	990701	342	HTI 42	9:51.209	110:46.26
OBH 05	09:45,771	111:08,159	20	2824	03B5	D	010402	-1158	HTI 28	9:45.771	111:08.16
OBS 06	09:27,112	111:14,596	31	2913	3629	D	991246	-182	HTI 44, Webb 2328	9:27.112	111:14.58
OBS 07	09:30,573	110:43,321	32	987	0386+0355	D	010409	89	DPG 95, Webb 1695	9:30.573	110:43.32
OBS 08	09:26,420	110:10,107	19	1224	3614	C	010403	312	HTI 22, Webb 2352	9:26.420	110:10.08
OBS 09	09:09,131	110:01,722	22	3302	3659	C	991235	317	DPG 75, Webb 2329	9:09.131	110:18
OBH 10	08:58,368	110:21,556	26	1696	03B6+0355	D	000711	-213	HTI 23	8:58.368	110:21.54
OBH 11	09:03,519	110:47,396	35	3224	03B1+0355	B	010405	75	HTI 27	9:03.519	110:47.4
OBH 12	09:03,335	111:22,545	27	2474	03B7+0355	D	991236	3114	HTI 39, horizontal (Send)	9:03.335	111:22.56
OBH 13	08:46,121	111:01,573	39	1133	0387+0355	C	010401	-381	HTI 38	8:46.121	111:15.6
OBH 14	08:38,073	110:22,589		1093	03BC+0355	C	991238	-240	HTI 45	8:38.073	110:22.56
OBH 15	09:27,630	111:14,527		2883	3624 (B)	C	971202	0	OAS 21 ; OAS 22 ; OAS 46 ; HTI 24		
OBH 16	09:03,981	111:23,405		2640	3624 (B)	C	971202	0	OAS 21 ; OAS 22 ; OAS 46 ; HTI 24		
OBH 17	08:58,050	110:21,517		1700	3624 (B)	C	971202	3	OAS 21 ; OAS 22 ; OAS 46 ; HTI 24		
OBH 18	08:37,998	110:22,558		1090	3624 (B)	D	971202	0	OAS 13 ; OAS 74 ; AQ 12 ; HTI 35		
OBH 19	08:29,391	109:26,513		2188	3624 (B)	D	971202	0	OAS 13 ; OAS 74 ; AQ 12 ; HTI 35		
OBH 20	09:8,970	109:30,578		3158	3624 (B)	D	971202	0	OAS 14 ; OAS 26 ; OAS 34 ; HTI 44		
OBH 21	09:09,191	110:01,489		3297	3624 (B)	D	971202	0	OAS 14 ; OAS 26 ; OAS 34 ; HTI 44		

INST.	LAT (S) D:M	LON (E) D:M	DIST. TO NEXT (nm)	DEPTH (m)	REL. CODE	ANT. CH.	REC. NO.	SKEW (ms)	SENSORS	POSITION AFTER RELOBS LAT (S) (D:M)	POSITION AFTER RELOBS LON (E) (D.M)
OBH 22	08:21,032	110:50,891	4,0	204	0387+0355 (B)	C	991236	-2	HTI 38	8:21.032	110:50.88
OBH 23	08:24,975	110:50,169	5,1	281	3674 (B)	D	991238	-3	HTI 30	8:24.975	110:50.16
OBH 24	08:29,967	110:49,314	5,1	428	3624 (B)	D	991246	-3	OAS 26	8:29.967	110:49.32
OBH 25	08:34,928	110:48,414	5,1	541	03BD+0355	C	000711	-4	HTI 34	8:34.919	110:48.42
OBH 26	08:39,949	110:47,484	10,2	954	03B6+0355	D	991243	5	HTI 23	8:39.935	110:47.46
OBH 27	08:50,039	110:45,803	5,1	1780	03B7+0355	C	991259	-6	HTI 39	8:50.008	110:45.78
OBH 28	08:55,011	110:44,866	8,9	2033	3609 (B)	C	010401	-9	HTI 21	8:54.997	110:44.88
OBH 11	09:03,519	110:47,396	6,6	3224	03B1+0355	B	010405	75	HTI 27	9:03.519	110:47.4
OBS 29	09:07,979	110:42,518	7,1	3113	3614 (B)	C	030901	0.875	HTI 22, Geospace	9:07.968	110:42.54
OBH 30	09:15,019	110:41,258	7,1	2561	6969 (A)	D	991235	6	HTI 29	9:14.995	110:41.28
OBH 31	09:22,011	110:40,014	9,2	1806	03BC+0355	C	000706	7	HTI 45	9:21.989	110:43.32
OBS 07	09:30,573	110:43,321	7,1	987	0386+0355	D	010409	89	DPG 95, Webb 1695	9:30.573	110:43.32
OBH 32	09:34,995	110:37,639	7,1	611	D654 (A)	D	030904	-1.375	OAS 36	9:34.944	110:37.62
OBH 33	09:41,999	110:36,406	offline	638	6334 (B)	C	991247	2	HTI 66	9:41.952	110:36.42
OBH 05	09:45,771	111:08,159	offline	2824	03B5+0355	D	010402	-1158	HTI 28	9:45.771	111:08.16
OBH 04	09:51,209	110:46,287	offline	2908	03B8+0355	D	990701	342	HTI 42	9:51.209	110:46.26
OBH 34	09:56,000	110:33,940	5,1	1943	4A49 (B)	D	040101	0	HTI 60	9:55.964	110:33.96
OBH 35	10:00,997	110:33,032	7,1	2332	C444 (A)	C	991256	-5	HTI 63	10:00.954	110:33.06
OBH 36	10:08,015	110:31,786	3,3	4260	B495 (A)	D	010403	10	HTI 67	10:07.962	110:31.8
OBH 37	10:11,293	110:31,208	29,1	5803	C454 (A)	C	971202	-12	HTI 59, HTI 61, HTI 65, HTI 68	10:11.292	110:31.2
OBS 38	10:39,932	110:25,987	6,1	5752	03B2+0355 (B)	C	031002	-12.75	HTI 43, OWEN 63	10:39.93	110:25.98
OBS 39	10:45,979	110:24,953	6,1	5551	3659 (B)	D	030902	3	HTI 37, OWEN 62	10:45.978	110:24.96
OBH 40	10:52,013	110:23,876	6,1	5317	A314 (A)	D	980402		HTI 62	10:52.014	110:23.88
OBS 41	10:58,018	110:22,791		5220	3629 (B)	D	31001	6.2	OAS 04, OWEN 59	10:58.02	110:22.8

INST.	LAT (S)	LON (E)	DIST. TO	DEPTH	REL.	ANT.	REC.	SKEW	SENSORS	POSITION AFTER RELOBS	
	D:M	D:M	NEXT (nm)	(m)	CODE	CH.	NO.	(ms)		LAT (S) (D:M)	LON (E) (D.M)
OBS 42	10:57,829	109:34,585	5,9	5611	3659	D	980401	-15	HTI 37, OWEN 62	10:57.828	109:34.56
OBH 43	10:51,996	109:35,145	6,1	5666	C454 (A)	C	991236	-2	HTI 59	10:51.996	109:35.16
OBS 44	10:45,935	109:35,649	6,0	5725	3614	C	030904	-2.209	HTI 22, Geospace	10:45.936	109:35.64
OBS 45	10:39,982	109:36,151	30,7	5875	03B2+0355	C	030902	-2.625	HTI 43, OWEN 63	10:39.984	109:36.18
OBH 46	10:09,454	109:38,877	6,6	5875	B495 (A)	C	971202	-10	HTI 44 , HTI 67 , OAS HH , AQ 12	10:09.456	109:38.88
OBH 47	10:02,904	109:39,472	7,1	4907	C444 (A)	D	010403	+7	HTI 63	10:02.904	109:39.48
OBH 48	09:55,781	109:40,088	7,0	3824	4A49 (B)	C	010405	3	HTI 94	9:55.781	109:40.08
OBH 49	09:48,743	109:40,684	7,1	3104	03B8+0355	D	010401	-7	HTI 61	9:48.743	109:40.68
OBH 50	09:41,734	109:41,329	7,2	2231	03B5+0355	C	991259	-5	HTI 28	9:41.734	109:41.34
OBH 51	09:34,507	109:41,973	7,1	1666	6334 (B)	A	991243	4	HTI 66	9:34.507	109:42
OBH 52	09:27,418	109:42,598	7,1	1556	D654 (A)	D	000711	-4	HTI 36	9:27.418	109:42.6
OBH 53	09:20,341	109:43,244	7,1	2748	03BC+0355	B	991246	-4	HTI 45	9:20.341	109:43.26
OBH 54	09:13,245	109:43,825	7,2	3143	6969	D	991238	-2	HTI 29	9:13.245	109:43.8
OBH 55	09:06,095	109:44,426	7,1	3209	03B1+0355	C	010402	-24	HTI 27	9:06.095	109:44.4
OBS 56	08:59,011	109:45,052	7,1	3270	0386+0355	D	031002	-16.084	HTI 65, OWEN	8:59.011	109:45.06
OBS 57	08:51,926	109:45,722	7,1	3303	3629	D	030901	0.625	HTI 04, OWEN 60	8:51.926	109:45.72
OBH 58	08:44,787	109:46,345	7,1	3233	3609	C	991235	4	HTI 21	8:44.787	109:46.32
OBH 59	08:37,714	109:46,957	7,1	2407	03B7+0355	D	031001	+5.458	HTI 39	8:37.714	109:46.98
OBH 60	08:30,669	109:47,574	7,1	1594	03B6+0355	D	991247	+3	HTI 23	8:30.669	109:47.58
OBH 61	08:23,616	109:48,174	7,2	474	0387+0355	A	000706	5	HTI 34	8:23.616	109:48.18
OBH 62	08:16,394	109:48,812	7,0	635	3624	D	990701	+7	HTI 68	8:16.394	109:48.84
OBH 63	08:09,457	109:49,414	7,2	590	3674	B	040101	XXXXX	HTI 30	8:09.457	109:49.44
OBH 64	08:02,229	109:50,060		283	03BD+0355	D	991256	-7	HTI 38	8:02.229	109:50.04

INST.	LAT (S)	LON (E)	DIST. TO	DEPTH	REL.	ANT.	REC.	SKEW	SENSORS	POSITION AFTER RELOBS	
	D:M	D:M	NEXT (nm)	(m)	CODE	CH.	NO.	(ms)		LAT (S) (D:M)	LON (E) (D.M)
OBH 65	08:24,999	110:09,829	5,2	841	03BD+0355	D	991256	-3	HTI 38	8:24.500	110:09.84
OBH 66	08:26,584	110:14,863	5,2	1052	3674	C	0706	2	HTI 30	8:26.591	110:14.88
OBH 67	08:28,174	110:19,878	5,0	812	0387+0355	D	010401	-4	HTI 68	8:28.178	110:19.92
OBH 68	08:29,677	110:24,665	5,6	727	03B6+0355	C	991259	-2	HTI 34	8:29.676	110:24.66
OBH 69	08:31,359	110:30,076	4,8	618	03B1+0355	D	991247	-8	HTI 23	8:31.340	110:30.12
OBH 70	08:32,786	110:34,624	4,7	576	3624	C	991243	1	HTI 27	8:32.794	110:34.62
OBH 71	08:34,237	110:39,227	6,0	573	03BC+0355	D	000711	XXXXX	HTI 45	8:34.240	110:39.24
OBH 72	08:36,040	110:45,023	4,5	631	03B5+0355	B	990701	3	HTI 63	8:36.040	110:45
OBH 73	08:37,383	110:49,322	5,2	1055	03B8+0355	C	991238	-2	HTI 61	8:37.385	110:49.32
OBH 74	08:38,969	110.54,330	5,1	1599	03B7+0355	D	010402	-14	HTI 39	8:38.969	110:54.30
OBH 75	08:40,519	110:59,253		1001	3609	C	991236	-1	HTI 21	8:40.519	110:59.28

Appendix 9.3 AIRGUN SHOTS

PROFILE NO.	SHOT NO.	DATE UTC	TIME UTC	LON (E) D:M	LAT (S) D:M	PULSE INT.	GUN POSITION	PROFILE LENGTH [nm]	REMARKS
SO179-01	1	18/09/2004	23:44	9:7.925	109:27.315	60 s	S, M	109	
	98	19/09/2004	01:22	9:9.187	109:33.992	60 s	M		lost floats
	262	19/09/2004	03:08	9:10.613	109:41.751	60 s	S, M		
	580	19/09/2004	08:10	9:14.491	110:2.918	60 s	S, M, P		
	890	19/09/2004	13:00	9:18.468	110:24.558	60 s	S, M, P		lost floats
	1430	19/09/2004	22:00	9:25.577	111:3.210	60 s	M, P		
	1615	20/09/2004	01:05	9:28.035	111:16.651	60 s	M		EOL
SO179-02	1	20/09/2004	02:05	9:29.385	111:15.302	30 s	M	3	near OBS 06
	70	20/09/2004	02:40	9:25.325	111:14.995	30 s	M		EOL
SO179-03	1	20/09/2004	08:06	9:2.729	111:22.465	30 s	M	2.5	near OBH 15
	48	20/09/2004	08:30	9:4.550	111:22.503	30 s	M		EOL
SO179-04	1	20/09/2004	09:02	9:02.96	111:23.96	30 s	M	3	near OBH 16
	70	20/09/2004	09:37	9:3.002	111:20.977	30 s	M		EOL
SO179-05	1	20/09/2004	17:30	110:23.102	8:57.792	30 s	S	3	near OHB 10
	76	20/09/2004	18:08	110:20.390	8:57.993	30 s	S		EOL
SO179-06	1	20/09/2004	18:39	110:20.993	8:57.497	30 s	S	3	near OHB 10
	62	20/09/2004	19:10	110:21.00	8:59.740	30 s	S		EOL
SO179-07	1	20/09/2004	22:37	110:21.480	8:38.008	30 s	S	4	near OBH 18
	70	20/09/2004	23:12	110:23.920	8:37.996	30 s	S		EOL
SO179-08	1	20/09/2004	23:33	110:22.897	8:37.396	30 s	S	3	near OBH 18
	64	21/09/2004	00:05	110:22.995	8:39.984	30 s	S		EOL
SO179-09	1	21/09/2004	05:35	109:27.378	8:29.859	30 s	S	3	near OBH 19
	20	21/09/2004	06:00	109:25.96	8:29.11	30 s			Kompressor break down

Appendix 9.3 AIRGUN SHOTS

PROFILE NO.	SHOT NO.	DATE UTC	TIME UTC	LON (E) D:M	LAT (S) D:M	PULSE INT.	GUN POSITION	PROFILE LENGTH [nm]	REMARKS
SO179-10	1	21/09/2004	06:23	109:25.651	8:29.183	30 s	S	3	near OBH 19
	78	21/09/2004	07:02	109:28.212	8:28.963	30 s	S		EOL
SO179-11	1	21/09/2004	13:05	109:33.91	9:9.634	30 s	S	6.7	near OBH 20
	182	21/09/2004	14:36	109:27.503	9:8.021	30 s	S		EOL
SO179-12	1	21/09/2004	19:57	110:1.379	9:7.873	30 s	S	3.2	near OBS 07
	144	21/09/2004	20:45	110:1.500	9:11.059	30 s	S		EOL
SO179-13	1	22/09/2004	00:22	110:11.533	9:24.340	30 s	S	2	near OBS 08
	132	22/09/2004	01:28	110:7.468	9:28.018	30 s	S		EOL
SO179-14	1	22/09/2004	04:46	110:2.937	9:47.964	30 s	S	3.5	near OBH 02
	114	22/09/2004	05:43	110:03.01	9:51.18	30 s	S		EOL
SO179-15	1	22/09/2004	00:58	111:1.977	8:45.121	30 s	S	2	near OBH 13
	58	22/09/2004	01:27	111:1.956	8:47.642	30 s	S		EOL
SO179-16	1	24/09/2004	04:56	110:17:015	11:28.516	60s	S, M, P	191	
	1629	25/09/2004	07:05						Detour: 0,3nm STB
	1684	25/09/2004	08:00	110:40.366	9:22.881	60s	M, P		lost floats
	1703	25/09/2004	08:19	110:40.141	9:21.387	60s	M, P		lost floats
	1767	25/09/2004	09:23	110:41.016	9:16.575	60s	S, M, P		
	1800	25/09/2004	09:50	110:41.337	9:14.629	60s	M, P		lost floats
	1930	25/09/2004	12:00	110:43.038	9:5.192	60s	M, P		no shots (11:50-12:00)
	1960	25/09/2004	12:30	110:43.417	9:3.058	60s	S, M, P		no shots (12:30-12:34)
	2599	25/09/2004	23:09	110:51.605	8:17.130	60s	S, P		change course 90°
	2630	25/09/2004	23:40	110:51.045	8:15.476	60s	S, P		EOL
SO179-17	1	26/09/2004	17:14	111:5.815	9:45.480	30 s	S	3	near OBH 05
	107	26/09/2004	18:07	111:9.800	9:45.495	30 s	S		EOL

Appendix 9.3 AIRGUN SHOTS

PROFILE NO.	SHOT NO.	DATE UTC	TIME UTC	LON (E) D:M	LAT (S) D:M	PULSE INT.	GUN POSITION	PROFILE LENGTH [nm]	REMARKS
SO179-18	1	28/09/2004	22:11	109:49.019	7:54.754	60s	S, P	236	
	32	28/09/2004	22:48	109:50.576	7:55.824	60s	S, M, P		5 min no shots (43-48)
	40	28/09/2004	22:56	109:50.544	7:56.413	60s	M, P		lost floats
	82	28/09/2004	23:38	109:50.301	7:59.266	60s	S, M, P		
	824	29/09/2004	12:00	109:45.485	8:54.435	60s	S, M, P		gun deeper
	1649	30/09/2004	01:45	109:39.931	9:57.349	60s	S, M, P		triggerline broken
	1851	30/09/2004	05:07	109:38.691	10:11.705	60s	M		lost floats
	1909	30/09/2004	06:05	109:38.218	10:16.086	60s	S, M		
	2179	30/09/2004	10:35	109:36.505	10:36.735	60s	S, M, P		
	2354	30/09/2004	13:30	109:35.262	10:51.510	60s	S, P		lost floats
	2542	30/09/2004	16:38	109:34.010	11:4.431	60s	S, P		EOL
SO179-19	1	02/10/2004	08:31	111:07.273	8:43.144	60s	S, M, P	100	
	1290	03/10/2004	06:01	109:23.671	8:10.516	60s	S, M, P		EOL

Appendix 9.4.1

Captain's report SO176

R. F. Reedereigemeinschaft
Forschungsschiffahrt GmbH

Kapitänsbericht Nr. 02/04 SO 176

Kapitän : H.Papenhagen
Reise : 374 von : Cilacap nach : Hongkong

Tiefgang bei Abfahrt : V= 6,32 m H=6,90 m
Tiefgang bei Ankunft : V= 6,44 m H=6,56 m
Abfahrt : Cilacap am 18.05.04 um 1612 Uhr
Ankunft : Hongkong am 30.05.04 um 1500 Uhr
Zeitunterschied: -1,0 Std
Reisedauer (Hafen zu Hafen): 11 Tage 21,8 Std.
Revierdauer: 00 Tage 02,1 Std.
Reiseunterbrechung : 00 Tage 07,6 Std.
Reisedauer (See): 11 Tage 07,8 Std.
Ankerzeit 00 Tage 01,5 Std
Distanzen: See: 3095 sm, Reviere: 17 sm, Gesamt: 3112 sm
Durchschnittsfahrt (See): 11,2 kn

Reisedaten :

18.05.04

1612	Beginn der Reise
1712	Beginn der Seereise
2043	Beginn der wiss. Arbeiten

21.05.04

0600	Unterbrechung der wiss. Aufzeichnungen
0830	Unterbrechung der Seereise
1000	Schiff fest mit Stb-Seite , Unterbrechung der Reise
1524	Alles los, Fortsetzung der Reise
1612	Fortsetzung der Seereise und der wiss.Aufzeichnungen
2400	Ende der wiss. Aufzeichnungen

30.05.04

1130	Ende der Seereise
1206	Lotse an Bord
1248 – 1418	ankern auf Western Quarantäne Reede
1350 – 1416	Einklarierung durch Immigration
1500	Schiff fest mit Stb-Seite China Merchant Wharf
	Ende der Reise

Nautisches, Schiffseinrichtungen:

RF Reedereigemeinschaft
Forschungsschiffahrt GmbH

Maschine: Siehe Bericht Ltd. Ingenieur

Mannschaftsangelegenheiten:
Keine besonderen Vorkommnisse

Forschungsprogramm: MERAMEX I

Fahrtleiter Prof. Dr. Ernst Flueh GEOMAR

***Teilnehmer* außer *Besatzung*:** Cilacap – Cilacap 12
Cilacap – Hongkong keine

Eingesetztes Instrumentarium: ***SIMRAD Fächerlot EM 120***
11 OBH und 3 OBS
CTD-Sonde

Reiseverlauf

18.05.04

1612	Alles los, Beginn der Reise		
1626 – 1635	Stellmanöver für Wissenschaftler		
1655	Lotse von Bord		
1712	Beginn der Seereise		
2043 – 2223	Station 01CTD	LT = 2056 m	08 21,93 S 109 23,25 E

2312 – 2325	Station 02OBH 1	LT = 2209 m	08 29,62 S 109 27,05 E
2325	Beginn Profilfahrt		

19.05.04

1200	09 50,8 S 110 30,4 E SE 6 ; 5 ; c,p ; 1009,3 ; 27,0 ; 30 ;	
0126	Beginn Kalibrierung SIMRAD-EM 120	08 51,84 S 109 29,64 E
0224	Ende Kalibrierung	08 54,06 S 109 29,90 E
0427	Station 03OBH 02 z.W. LT = 3138 m	09 11,40 S 110 32,18 E
0911	Station 04OBH 03 z.W. LT = 1856 m	09 50,20 S 110 02,59 E
1333	Station 05OBH 04 z.W. LT = 2916 m	09 51,06 S 110 46,28 E
1538	Station 06OBH 05 z.W. LT = 2822 m	09 45,77 S 111 08,16 E
1729	Station 07OBS 06 z.W. LT = 2917 m	09 27,11 S 111 14,60 E
2026	Station 08OBS 07 z.W. LT = 0986 m	09 30,57 S 110 43,33 E
2329	Station 09OBS 08 z.W. LT = 1224 m	09 26,42 S 110 10,11 E

20.05.04

1200	08 43,7 N 110 48,3 E E 4 ; 3 ; c ; 1010,9 ; 29,2 ; 30	
0116	Station 10OBH 09 z.W. LT = 3302 m	09 09,12 S 110 01,75 E
0311	Station 11OBH 10 z.W. LT = 1695 m	08 58,37 S 110 21,55 E
0519	Station 12OBH 11 z.W. LT = 3224 m	09 03,51 S 110 47,39 W
0804	Station 13OBH 12 z.W. LT = 2473 m	09 03,33 S 111 22,54 E
1041	Station 14OBH 13 z.W. LT = 1133 m	08 46,12 S 111 01,59 E
1444	Station 15OBH 14 z.W. LT = 1033 m	08 38,07 S 110 22,59 E
1445	Beginn EM 120 – Vermessung Kurs 180 Grad v = 11 kn	09 35,0 S 110 22,4 E
1953	ä.K. auf 325 Grad	09 35,0 S 110 23,0 E
2400		08 59,5 S 110 58,0 E

21.05.04

1200	Cilacap SE`I 2 ; 1 ; c ; 1010,2 ; 30,1 ; 30 ;	
0623	Ende der EM 120 – Vermessung	08 04,2 S 109 19,4 E
0830	Unterbrechung der Seereise	
0915	passieren TN Fairway	
0928	Lotse an Bord	
1000	Schiff fest mit Stb-Seite 2+1 Pier Nr. 2 in Cilacap Lotse von Bord	

21.05.04 ff

1030 – 1120	Agentur und Behörden an Bord
1030	RF-Luftfracht an Bord Schiffswäsche zurück
1040	7 indonesische Gastwissenschaftler von Bord
1205	5 Wissenschaftler GEOMAR von Bord
1210	Geomar-Luftfracht von Bord
1450	Schiff klar zum Auslaufen
1509	Lotse an Bord
1520	Heckschlepper fest
1524	Alles los, Fortsetzung der Reise SO 176
1527	Heckschlepper los
1549	Lotse von Bord

1600 – 1635	Durchsuchung des Schiffes nach stowaways, ohne Befund
1610	passieren Tn Fairway
1612	Fortsetzung der Seereise, Beginn der Aufzeichnungen EM 120
2350	Ende der Aufzeichnungen 08 29,9 S 108 00,0 E

22.05.04

1200	07 49,1 S 106 11,7 E SSE 4 ; 3 ; c ; 1010 ; 30 ; 30 ;
0000 – 2400	Anreise Hongkong
2400	07 08,0 S 104 08,9 E

23.05.04

1200	05 30,5 S 106 03,0 E ESE 2 ; 1 ; c ; 1009,4 ; 28,5 ; 30 ;
0600	Aufgrund Gefahr von Piraterie werden die Wachen umgestellt : Bücke : 2 Nautiker Maschine : 1 Patentinhaber Deck : tags = 1 Mann Wache nachts : 2 Mann Wache Verschlusszustand und Ronden wie sec level 2
2400	04 21,6 S 108 28,4 E

24.05.04

1200	02 16,6 S 109 19,5 E E 3 ; 2 ; o ; 1011 ; 29 ; 31 ;
0000 – 2400	Anreise Hongkong
2400	00 27,5 S 106 58,5 E

25.05.04

1200	02 08,3 N 107 26,8 E Umlfd. 1 ; 1 ; c ; 1011,5 ; 29 ; 32
0000 – 2400	Anreise Hongkong
2100	Schiff geht wieder auf normalen Reisebetrieb

26.05.04

1200	06 37,1 N 110 22,2 E N`l 2 ; 1 ; c ; 1009,2 ; 28,3 ; 31 ;
0000 – 2400	Anreise Hongkong
2400	08 52,5 N 111 16,2 E

27.05.04

1200	10 31,9 N 111 39,3 E S`l 2 ; 1 ; b ; 1010,7 ; 27,6 ; 29 ;
0000 – 0800	Anreise Hongkong
0800 – 1630	Teststation mit : CTD-ROS ; OFOS ; GTV ; mit SSBL
1630	Anreise Hongkong stellen Borduhren 1 Std voraus (UTC + 8 h)

28.05.04

1200	14 09,9 N 112 30,4 E S 3 ; 2 ; c ; 1009,6 ; 28,8 ; 30 ;
0000 – 2400	Anreise Hongkong
2400	16 21,8 N 113 00,3 E

29.05.04

1200	18 32,9 N 113 20,3 E SzW 4 ; 3 ; c ; 1008 ; 29,7 ; 30 ;
0000 – 2400	Anreise Hongkong
2400	20 38,2 N 113 40,2 E

30.05.04

1200	22 12,8 N 114 10,3 E SzW 2 ; 2 ; c ; 1008 ; 28,2; 29
0000 – 1130	Anreise Hongkong
1206	Lotse an Bord
1233	pass. Green Island
1248 – 1418	ankern Westem Quarantäne Reede
1350 – 1416	Boot der Immigration längseits, Einklarierung
1429	Heckschlepper Quan Zhou fest
1454	fest 1 + 1 ; Schlepper los
1500	Schiff fest mit Stb-Seite China Merchant Wharf Ende der Reise ; Lotse von Bord

Es wurden 11 OBH und 3 OBS ausgelegt.
Mit EM 120 wurden in 61,4 Std 676 sml vermessen
Das Wetter war gut.

Appendix 9.4.2

Captain's report SO179

Abkürzungen / Abbreviation

z.W	zu Wasser
a.D.	an Deck
SL (max.)	(maximale)Seillänge
LT	Lottiefe nach Hydrosweep
W x	eingesetzte Winde
SM	Simrad - Multibeam - Lot
PS	Parasound
rwk:	Rechtweisender Kurs
d:	Distanz
v:	Geschwindigkeit in Knoten

Eingesetzte Geräte

CTD	CTD zum Releasertest
Airgun	Air-Gun
Stream.	Streamer
Magn.	Magnetometer
OBH / S	Auslage
OBH / S	Aufnahme

Einsätze

01
27
19
22
61
74

Geräteverluste: 1 OBH ist nicht aufgefunden worden

Winde	D/M	Typ	RF-Nr	SO 179 Einsatz	Gesamt Einsatz	SO 179 S`länge	Gesamt S`länge	Zust.	SO 179 geflerte max. L	jemals geflerte max. Länge
W 1	18,2	LWL	812001	0 h	0343 h	0 m	0188485 m	3-4	0 m	8022 m
W 2	18,2	LWL	815286	0 h	0 h	0 m	0 m	1	0 m	0 m
W 4	11	NSW	818045	3 h	268 h	57333 m	220273 m	3	3400 m	8081 m
W 5	11,2	NSW	812106	0 h	0 h	0 m	0 m	1	0 m	0 m
W 6	18,2	DRAKO	818238	0 h	1093 h	63310 m	1009569 m	3-4	0 m	7609 m

Station	Datum	UTC Zeit	PositionLat	PositionLon	Tiefe [m]	Windstärke [m/s]	Kurs [°]	v [kn]	Gerät	Gerätekürzel	Aktion	Bemerkung
SO179/001-1	18.09.2004	11:00	8° 30,34' S	108° 0,57' E	3539	NNE 10	85,9	0,8	CTD	CTD	Beginn Station	Releaser test, W 4
SO179/001-1	18.09.2004	11:01	8° 30,34' S	108° 0,58' E	3540	NNE 9	256,6	0,2	CTD	CTD	zu Wasser	
SO179/001-1	18.09.2004	12:02	8° 30,42' S	108° 0,97' E	0	NNE 8	35,2	1,2	CTD	CTD	auf Tiefe	SL = 3400 m
SO179/001-1	18.09.2004	14:01	8° 30,57' S	108° 1,34' E	3542	NNE 8	11,1	1,4	CTD	CTD	an Deck	
SO179/001-1	18.09.2004	14:09	8° 30,59' S	108° 1,34' E	3538	N 8	133	0,8	CTD	CTD	Ende Station	
Transit												Magnetometer, d = 93 sm
SO179/002-1	18.09.2004	23:49	9° 7,91' S	109° 27,30' E	3166	N 10	118,4	1,9	Vermessung	PROFIL	Beginn Profil	rwk: 101°, d: 109 nm, Seismik
SO179/002-1	20.09.2004	01:06	9° 28,03' S	111° 16,63' E	3122	NNE 10	106,2	3,9	Vermessung	PROFIL	Ende Profil	
SO179/003-1	20.09.2004	02:04	9° 29,03' S	111° 15,02' E	3057	E 6	352,8	4,4	Profil	PR	Beginn Profil	rwk= 360°, d= 3sm, 1 Air-gun
SO179/003-1	20.09.2004	02:40	9° 26,05' S	111° 14,99' E	2988	E 7	3,1	4,9	Profil	PR	Ende Profil	
SO179/003-1	20.09.2004	02:54	9° 25,36' S	111° 14,94' E	2968	E 6	348,6	2,4	Profil	PR	1.Airgun an Deck	

Station	Datum	Zeit	PositionLat	PositionLon	Tiefe [m]	Windstärke [m/s]	Kurs [°]	v [kn]	Gerät	Gerätekürzel	Aktion	Bemerkung
SO179/004-1	20.09.2004	02:56	9° 25,29' S	111° 14,93' E	2967	E 6	353,1	2,6	OBS/OBH	OBS/OBH	Beginn Station	
SO179/004-1	20.09.2004	02:57	9° 25,25' S	111° 14,92' E	2967	E 6	354,7	2,2	OBS/OBH	OBS/OBH	OBH ausgelöst	OBH 15
SO179/004-1	20.09.2004	02:58	9° 25,21' S	111° 14,91' E	2968	E 6	345,9	2,8	OBS/OBH	OBS/OBH	OBS ausgelöst	OBS 06
SO179/003-1	20.09.2004	03:00	9° 25,13' S	111° 14,90' E	2972	E 6	359,2	2,6	Profil	PR	Streamer an Deck	
SO179/003-1	20.09.2004	03:00	9° 25,13' S	111° 14,90' E	2972	E 6	359,2	2,6	Profil	PR	Stationsende	
SO179/004-1	20.09.2004	03:56	9° 27,30' S	111° 14,52' E	0	NNW 9	259,1	0,9	OBS/OBH	OBS/OBH	OBS an Deck	OBS 06
SO179/004-1	20.09.2004	04:06	9° 27,69' S	111° 14,51' E	0	WNW 10	225,3	0,6	OBS/OBH	OBS/OBH	OBH an Deck	OBH 15
SO179/004-1	20.09.2004	04:10	9° 27,70' S	111° 14,45' E	0	WNW 8	273	1	OBS/OBH	OBS/OBH	Ende Station	
Transit												Magnetometer, d = 24 sm
SO179/005-1	20.09.2004	06:23	9° 5,16' S	111° 22,27' E	2851	ENE 7	27	2,9	Profil	PR	Stationsbeginn	
SO179/005-1	20.09.2004	06:27	9° 5,02' S	111° 22,31' E	2833	ENE 9	358,5	1,3	Profil	PR	Streamer zu Wasser	
SO179/005-1	20.09.2004	06:34	9° 4,83' S	111° 22,35' E	2779	ENE 10	21,3	2,5	Profil	PR	1. Airgun zu Wasser	
SO179/005-1	20.09.2004	06:41	9° 4,59' S	111° 22,43' E	2736	ENE 10	19,7	3,1	Profil	PR	Beginn Profil	rwk: 000', d: 2,5 nm
SO179/005-1	20.09.2004	07:02	9° 3,96' S	111° 23,37' E	2645	N 10	132,5	3,5	Profil	PR	OBH zu Wasser	OBH 16
SO179/005-1	20.09.2004	08:30	9° 4,50' S	111° 22,50' E	2734	WNW 10	173,7	4,6	Profil	PR	Ende Profil	
SO179/005-1	20.09.2004	08:30	9° 4,50' S	111° 22,50' E	2734	WNW 10	173,7	4,6	Profil	PR	Stationsende	
SO179/006-1	20.09.2004	09:02	9° 2,96' S	111° 24,04' E	2433	E 7	291,4	4,8	Profil	PR	Stationsbeginn	
SO179/006-1	20.09.2004	09:03	9° 2,96' S	111° 23,96' E	2458	SE 5	259,1	5,5	Profil	PR	Beginn Profil	Profil # 4
SO179/006-1	20.09.2004	09:38	9° 3,00' S	111° 20,99' E	2415	SW 7	275,1	4,8	Profil	PR	Ende Profil	
SO179/006-1	20.09.2004	09:43	9° 3,00' S	111° 20,67' E	2426	SW 8	268	2,8	Profil	PR	OBH ausgelöst	OBH 16
SO179/006-1	20.09.2004	09:43	9° 3,00' S	111° 20,67' E	2426	SW 8	268	2,8	Profil	PR	OBH ausgelöst	OBH 12
SO179/006-1	20.09.2004	09:49	9° 3,01' S	111° 20,39' E	2428	SSW 10	262,3	3,4	Profil	PR	1.Airgun an Deck	
SO179/006-1	20.09.2004	09:54	9° 3,03' S	111° 20,17' E	2428	SSW 10	277	2,2	Profil	PR	Streamer an Deck	
SO179/006-1	20.09.2004	10:32	9° 3,47' S	111° 22,63' E	0	N 9	125,8	1	Profil	PR	OBH an Deck	OBH 12
SO179/006-1	20.09.2004	10:53	9° 4,24' S	111° 23,47' E	2672	NNW 9	172	0,1	Profil	PR	OBH an Deck	OBH 16
SO179/006-1	20.09.2004	10:55	9° 4,26' S	111° 23,45' E	2674	NW 8	191,4	0,4	Profil	PR	Stationsende	
Transit												Magnetometer, d = 56 sm

Station	Datum	Zeit	PositionLat	PositionLon	Tiefe [m]	Windstärke [m/s]	Kurs [°]	v [kn]	Gerät	Gerätekürzel	Aktion	Bemerkung
SO179/007-1	20.09.2004	16:32	8° 57,59' S	110° 24,15' E	1623	WSW 10	226,6	1,6	Profil	PR	Stationsbeginn	
SO179/007-1	20.09.2004	16:38	8° 57,65' S	110° 24,02' E	1631	WSW 8	281,8	2,2	Profil	PR	1. Airgun zu Wasser	
SO179/007-1	20.09.2004	17:26	8° 57,64' S	110° 23,25' E	1663	W 8	225,8	3	Profil	PR	Streamer zu Wasser	
SO179/007-1	20.09.2004	17:32	8° 57,87' S	110° 23,04' E	1659	W 9	214,4	3,7	Profil	PR	Beginn Profil	rwk: 270', d: 3,0 nm
SO179/007-1	20.09.2004	17:53	8° 58,05' S	110° 21,54' E	1701	SW 9	277,3	3,1	Profil	PR	OBH zu Wasser	
SO179/007-1	20.09.2004	18:09	8° 57,99' S	110° 20,43' E	1777	SW 8	275,1	4,8	Profil	PR	Ende Profil	
SO179/007-1	20.09.2004	18:10	8° 57,99' S	110° 20,35' E	1780	SW 8	274,7	4,5	Profil	PR	Stationsende	
SO179/008-1	20.09.2004	18:35	8° 57,19' S	110° 20,92' E	1716	N 10	138,5	5,2	Profil	PR	Stationsbeginn	
SO179/008-1	20.09.2004	18:38	8° 57,42' S	110° 20,99' E	1711	NNW 12	185,9	4,4	Profil	PR	Beginn Profil	rwk: 180', d: 3,0 nm
SO179/008-1	20.09.2004	19:11	8° 59,68' S	110° 20,99' E	1941	NW 10	183,9	3,3	Profil	PR	Ende Profil	
SO179/008-1	20.09.2004	19:19	8° 59,99' S	110° 20,95' E	1964	NW 9	202,4	2,4	Profil	PR	1.Airgun an Deck	
SO179/008-1	20.09.2004	19:23	9° 0,10' S	110° 20,92' E	3478	WNW 10	172,5	1,2	Profil	PR	OBH ausgelöst	OBH 10
SO179/008-1	20.09.2004	19:24	9° 0,12' S	110° 20,91' E	3480	WNW 11	160,9	0,8	Profil	PR	OBH ausgelöst	OBH 17
SO179/008-1	20.09.2004	19:27	9° 0,21' S	110° 20,89' E	2610	WNW 10	214,3	1,4	Profil	PR	Streamer an Deck	
SO179/008-1	20.09.2004	20:00	8° 58,36' S	110° 21,43' E	0	WNW 11	353,5	1,2	Profil	PR	OBH an Deck	OBH 10
SO179/008-1	20.09.2004	20:17	8° 57,96' S	110° 21,50' E	1696	WNW 10	257,8	1,1	Profil	PR	OBH an Deck	OBH 17
SO179/008-1	20.09.2004	20:19	8° 57,96' S	110° 21,47' E	1699	W 10	271,1	0,9	Profil	PR	Stationsende	
Transit												Magnetometer, d = 14 sm
SO179/009-1	20.09.2004	22:08	8° 37,99' S	110° 20,05' E	1171	E 9	80,4	3,6	Profil	PR	Stationsbeginn	
SO179/009-1	20.09.2004	22:13	8° 37,98' S	110° 20,23' E	1165	NNE 10	82,7	1,5	Profil	PR	1. Airgun zu Wasser	
SO179/009-1	20.09.2004	22:18	8° 37,97' S	110° 20,43' E	1158	NNE 11	96,8	3,6	Profil	PR	Streamer zu Wasser	
SO179/009-1	20.09.2004	22:19	8° 37,97' S	110° 20,50' E	1158	NNE 11	95,4	4,7	Profil	PR	Beginn Profil	rwk: 90°, d: 3,5 nm
SO179/009-1	20.09.2004	22:55	8° 38,00' S	110° 22,55' E	1092	NNE 11	67,7	2,1	Profil	PR	OBH zu Wasser	OBH 18
SO179/009-1	20.09.2004	23:12	8° 38,01' S	110° 23,79' E	1055	NNE 12	87,5	4,5	Profil	PR	Ende Profil	
SO179/009-1	20.09.2004	23:12	8° 38,01' S	110° 23,79' E	1055	NNE 12	87,5	4,5	Profil	PR	Stationsende	
SO179/010-1	20.09.2004	23:31	8° 37,20' S	110° 22,90' E	1054	SSW 8	208,3	3,7	Profil	PR	Stationsbeginn	
SO179/010-1	20.09.2004	23:32	8° 37,27' S	110° 22,89' E	1058	WSW 8	182,7	4,4	Profil	PR	Beginn Profil	rwk: 180°, d: 3 sm

Station	Datum	Zeit	PositionLat	PositionLon	Tiefe [m]	Windstärke [m/s]	Kurs [°]	v [kn]	Gerät	Gerätekürzel	Aktion	Bemerkung
SO179/010-1	21.09.2004	00:05	8° 39,95' S	110° 23,00' E	1149	WNW 11	176,1	4,9	Profil	PR	Ende Profil	
SO179/010-1	21.09.2004	00:13	8° 40,37' S	110° 22,94' E	1169	WNW 10	185,1	2,6	Profil	PR	1.Airgun an Deck	
SO179/010-1	21.09.2004	00:16	8° 40,49' S	110° 22,90' E	1175	WNW 11	198,7	2,3	Profil	PR	Streamer an Deck	
SO179/010-1	21.09.2004	00:23	8° 40,57' S	110° 22,69' E	0	SSE 6	338,6	2,9	Profil	PR	OBH ausgelöst	OBH 14 / 18
SO179/010-1	21.09.2004	01:00	8° 38,14' S	110° 22,41' E	0	NNW 11	241,3	0,8	Profil	PR	OBH an Deck	OBH 18 / 14
SO179/010-1	21.09.2004	01:00	8° 38,14' S	110° 22,41' E	0	NNW 11	241,3	0,8	Profil	PR	Stationsende	
Transit												Magnetometer, d = 54 sm
SO179/011-1	21.09.2004	05:13	8° 30,15' S	109° 29,06' E	2455	S 5	278,7	6,3	Profil	PR	Stationsbeginn	
SO179/011-1	21.09.2004	05:23	8° 30,05' S	109° 28,28' E	2265	SSW 9	275,4	3,8	Profil	PR	Magnetometer an Deck	
SO179/011-1	21.09.2004	05:28	8° 30,00' S	109° 27,96' E	2279	SSW 7	286,8	3,5	Profil	PR	1. Airgun zu Wasser	
SO179/011-1	21.09.2004	05:32	8° 29,98' S	109° 27,72' E	2261	SSW 14	276,5	4	Profil	PR	Streamer zu Wasser	
SO179/011-1	21.09.2004	05:35	8° 29,90' S	109° 27,53' E	2266	SSE 7	292,5	4,1	Profil	PR	Beginn Profil	rwk: 297', d: 3,0nm
SO179/011-1	21.09.2004	05:50	8° 29,40' S	109° 26,54' E	2188	SSE 7	301,6	3,4	Profil	PR	OBH zu Wasser	OBH 19
SO179/011-1	21.09.2004	06:00	8° 29,11' S	109° 25,96' E	2081	S 6	297	3,8	Profil	PR	Ende Profil	
SO179/011-1	21.09.2004	06:22	8° 29,20' S	109° 25,49' E	2028	NNE 13	74,9	4,5	Profil	PR	Beginn Profil	rwk: 090', d: 3,0nm
SO179/011-1	21.09.2004	07:01	8° 28,96' S	109° 28,11' E	2137	NNE 15	89,2	3,4	Profil	PR	Ende Profil	
SO179/011-1	21.09.2004	07:09	8° 29,00' S	109° 28,39' E	2243	NNE 13	57	1,2	Profil	PR	1.Airgun an Deck	
SO179/011-1	21.09.2004	07:13	8° 29,03' S	109° 28,46' E	2264	N 11	125	1,7	Profil	PR	Streamer an Deck	
SO179/011-1	21.09.2004	07:16	8° 29,12' S	109° 28,50' E	2260	N 11	177,4	4	Profil	PR	OBH ausgelöst	OBH 1
SO179/011-1	21.09.2004	07:16	8° 29,12' S	109° 28,50' E	2260	N 11	177,4	4	Profil	PR	OBH ausgelöst	OBH 19
SO179/011-1	21.09.2004	07:54	8° 29,55' S	109° 26,85' E	2159	N 12	241,9	1,9	Profil	PR	OBH an Deck	OBH 1
SO179/011-1	21.09.2004	08:41	8° 29,20' S	109° 25,56' E	2029	NNW 12	268,2	1,3	Profil	PR	OBH an Deck	OBH 19
SO179/011-1	21.09.2004	08:41	8° 29,20' S	109° 25,56' E	2029	NNW 12	268,2	1,3	Profil	PR	Stationsende	
Transit												Magnetometer, d = 44 sm
SO179/012-1	21.09.2004	12:47	9° 9,01' S	109° 34,02' E	3180	NNW 10	200,1	1,7	Profil	PR	Stationsbeginn	
SO179/012-1	21.09.2004	12:58	9° 9,28' S	109° 33,97' E	3174	NW 9	149,1	1,8	Profil	PR	1. Airgun zu Wasser	
SO179/012-1	21.09.2004	13:02	9° 9,43' S	109° 33,96' E	3175	NW 10	168,5	3,4	Profil	PR	Streamer zu Wasser	

Station	Datum	Zeit	PositionLat	PositionLon	Tiefe [m]	Windstärke [m/s]	Kurs [°]	v [kn]	Gerät	Gerätekürzel	Aktion	Bemerkung
SO179/012-1	21.09.2004	13:06	9° 9,64' S	109° 33,98' E	3171	NNW 10	178	3,3	Profil	PR	Beginn Profil	rwK: 287 d: 6,7nm
SO179/012-1	21.09.2004	13:54	9° 8,98' S	109° 30,63' E	3159	SSW 9	290,9	4,7	Profil	PR	OBH zu Wasser	OBH 20
SO179/012-1	21.09.2004	14:31	9° 8,11' S	109° 27,87' E	3164	SSW 9	270,7	5,5	Profil	PR	Ende Profil	
SO179/012-1	21.09.2004	14:42	9° 7,92' S	109° 27,16' E	3166	SW 10	313,8	3,4	Profil	PR	1.Airgun an Deck	
SO179/012-1	21.09.2004	14:49	9° 7,90' S	109° 26,96' E	2625	W 8	289,9	1,8	Profil	PR	Streamer an Deck	
SO179/012-1	21.09.2004	14:49	9° 7,90' S	109° 26,96' E	2625	W 8	289,9	1,8	Profil	PR	Stationsende	
SO179/013-1	21.09.2004	14:49	9° 7,90' S	109° 26,96' E	2625	W 8	289,9	1,8	OBS/OBH	OBS/OBH	Beginn Station	
SO179/013-1	21.09.2004	14:49	9° 7,90' S	109° 26,96' E	2625	W 8	289,9	1,8	OBS/OBH	OBS/OBH	OBH ausgel.	OBH 20
SO179/013-1	21.09.2004	15:42	9° 8,54' S	109° 30,38' E	2626	N 9	49,6	2,2	OBS/OBH	OBS/OBH	OBH gesichtet	
SO179/013-1	21.09.2004	15:45	9° 8,54' S	109° 30,40' E	2626	N 9	75,1	1,7	OBS/OBH	OBS/OBH	OBS ausgelöst	
SO179/013-1	21.09.2004	16:06	9° 8,69' S	109° 30,70' E	2624	N 10	302,5	0,4	OBS/OBH	OBS/OBH	OBH an Deck	
SO179/013-1	21.09.2004	16:26	9° 10,80' S	109° 31,72' E	2622	NNW 14	149,5	5,8	OBS/OBH	OBS/OBH	OBS gesichtet	
SO179/013-1	21.09.2004	16:42	9° 11,31' S	109° 32,09' E	3133	NW 10	277,3	1,1	OBS/OBH	OBS/OBH	OBS an Deck	
SO179/013-1	21.09.2004	16:43	9° 11,30' S	109° 32,07' E	3135	NW 9	297,4	2,2	OBS/OBH	OBS/OBH	Ende Station	
Transit												Magnetometer, d = 29 sm
SO179/014-1	21.09.2004	19:29	9° 7,48' S	110° 0,33' E	3297	NE 14	85	7,1	Profil	PR	Stationsbeginn	
SO179/014-1	21.09.2004	19:34	9° 7,36' S	110° 0,79' E	3308	NE 13	68,1	5,7	Profil	PR	Magnetometer an Deck	
SO179/014-1	21.09.2004	19:52	9° 7,57' S	110° 1,42' E	3312	NW 10	210,4	3,7	Profil	PR	1. Airgun zu Wasser	
SO179/014-1	21.09.2004	19:54	9° 7,65' S	110° 1,39' E	3305	NW 10	178,3	3,5	Profil	PR	Streamer zu Wasser	
SO179/014-1	21.09.2004	19:56	9° 7,76' S	110° 1,38' E	3302	NNW 12	198,4	5,3	Profil	PR	Beginn Profil	rwk:180', d:3,2 nm
SO179/014-1	21.09.2004	20:17	9° 9,16' S	110° 1,49' E	3302	NNW 12	183,3	4,5	Profil	PR	OBH zu Wasser	OBH 21
SO179/014-1	21.09.2004	20:44	9° 10,98' S	110° 1,51' E	3325	NNW 11	201,5	3,5	Profil	PR	Ende Profil	
SO179/014-1	21.09.2004	20:52	9° 11,26' S	110° 1,41' E	3326	NW 9	217,7	3,4	Profil	PR	1.Airgun an Deck	
SO179/014-1	21.09.2004	20:57	9° 11,38' S	110° 1,32' E	2634	NNW 11	218,2	2,2	Profil	PR	Streamer an Deck	
SO179/014-1	21.09.2004	21:00	9° 11,46' S	110° 1,26' E	2634	NW 10	192,1	1,6	Profil	PR	OBH /OBS ausge	OBS 09 / OBH 21
SO179/014-1	21.09.2004	22:03	9° 8,86' S	110° 1,34' E	3294	NW 9	284,8	1,9	Profil	PR	OBS an Deck	OBS 09
SO179/014-1	21.09.2004	22:12	9° 8,96' S	110° 1,04' E	3292	W 11	289,4	1,5	Profil	PR	OBH an Deck	OBH 21

Station	Datum	Zeit	PositionLat	PositionLon	Tiefe [m]	Windstärke [m/s]	Kurs [°]	v [kn]	Gerät	Gerätekürzel	Aktion	Bemerkung
SO179/014-1	21.09.2004	22:13	9° 8,95' S	110° 1,01' E	3291	W 11	299	2,5	Profil	PR	Stationsende	Anfahrt d = 18 sm
SO179/015-1	22.09.2004	00:13	9° 23,92' S	110° 11,93' E	1508	N 15	200,5	6,1	Profil	PR	Stationsbeginn	
SO179/015-1	22.09.2004	00:17	9° 24,14' S	110° 11,73' E	1429	WNW 11	236,6	3,1	Profil	PR	1. Airgun zu Wasser	
SO179/015-1	22.09.2004	00:20	9° 24,27' S	110° 11,59' E	1366	WNW 12	214,8	5,2	Profil	PR	Streamer zu Wasser	
SO179/015-1	22.09.2004	00:22	9° 24,41' S	110° 11,49' E	1352	WNW 12	221,1	4,5	Profil	PR	Beginn Profil	rwk: 228°, d: 6 nm
SO179/015-1	22.09.2004	01:27	9° 27,97' S	110° 7,53' E	1277	W 11	228,7	3,8	Profil	PR	Ende Profil	
SO179/015-1	22.09.2004	01:35	9° 28,10' S	110° 7,24' E	1289	WNW 10	278	2,3	Profil	PR	1.Airgun an Deck	
SO179/015-1	22.09.2004	01:39	9° 28,07' S	110° 7,11' E	1296	W 10	268,5	2,9	Profil	PR	Streamer an Deck	
SO179/015-1	22.09.2004	01:40	9° 28,06' S	110° 7,08' E	1297	W 9	282,2	2,6	Profil	PR	Stationsende	
SO179/016-1	22.09.2004	01:42	9° 28,05' S	110° 7,01' E	1299	W 9	289,6	2,3	OBS/OBH	OBS/OBH	OBS ausgelöst	OBS 08
SO179/016-1	22.09.2004	02:12	9° 26,39' S	110° 10,13' E	1219	N 12	123,5	2	OBS/OBH	OBS/OBH	OBS gesichtet	
SO179/016-1	22.09.2004	02:28	9° 25,84' S	110° 9,71' E	1189	N 9	281,1	2,1	OBS/OBH	OBS/OBH	OBS an Deck	OBS 08
SO179/016-1	22.09.2004	02:28	9° 25,84' S	110° 9,71' E	1189	N 9	281,1	2,1	OBS/OBH	OBS/OBH	Ende Station	
SO179/017-1	22.09.2004	04:41	9° 47,80' S	110° 3,17' E	1927	NW 10	235,6	3	Profil	PR	Stationsbeginn	
SO179/017-1	22.09.2004	04:45	9° 47,84' S	110° 3,06' E	1911	WNW 9	228,6	1,8	Profil	PR	1. Airgun zu Wasser	
SO179/017-1	22.09.2004	04:49	9° 47,97' S	110° 2,94' E	1873	WNW 9	211,7	3,8	Profil	PR	Streamer zu Wasser	
SO179/017-1	22.09.2004	04:54	9° 48,24' S	110° 2,89' E	1869	NW 9	178	4,2	Profil	PR	Beginn Profil	
SO179/017-1	22.09.2004	05:35	9° 51,18' S	110° 3,01' E	1814	NW 9	164	4,7	Profil	PR	Ende Profil	
SO179/017-1	22.09.2004	05:40	9° 51,38' S	110° 2,96' E	1809	NW 9	250,6	1,8	Profil	PR	1.Airgun an Deck	
SO179/017-1	22.09.2004	05:46	9° 51,50' S	110° 2,85' E	1811	WNW 8	226,8	1,8	Profil	PR	Streamer an Deck	
SO179/017-1	22.09.2004	05:48	9° 51,54' S	110° 2,79' E	1808	WNW 9	259,2	2	Profil	PR	OBH ausgelöst	OBH 3
SO179/017-1	22.09.2004	06:22	9° 49,95' S	110° 2,40' E	0	NNE 8	342,1	1,1	Profil	PR	OBH an Deck	OBH 3
SO179/017-1	22.09.2004	06:26	9° 49,93' S	110° 2,31' E	0	W 9	232,6	1,3	Profil	PR	Stationsende	
SO179/018-1	22.09.2004	06:28	9° 49,99' S	110° 2,27' E	0	WNW 8	200,2	3,4	Magnetometer	MAGN	Beginn Station	
SO179/018-1	22.09.2004	06:29	9° 50,04' S	110° 2,26' E	2520	WNW 8	189,9	3,4	Magnetometer	MAGN	Magnetometer zu Wasser	
SO179/018-1	22.09.2004	09:38	9° 40,10' S	110° 29,69' E	888	NE 12	74,8	4,6	Magnetometer	MAGN	Magnetometer an Deck	
SO179/018-1	22.09.2004	09:43	9° 39,91' S	110° 29,99' E	845	NE 11	351,6	5	Magnetometer	MAGN	Kursänderung	rwk: 360°, d = 70 sm

Station	Datum	Zeit	PositionLat	PositionLon	Tiefe [m]	Windstärke [m/s]	Kurs [°]	v [kn]	Gerät	Gerätekürzel	Aktion	Bemerkung
SO179/018-1	22.09.2004	09:51	9° 38,99' S	110° 29,98' E	796	E 7	360	6,9	Magnetometer	MAGN	Magnetometer zu Wasser	
SO179/018-1	22.09.2004	11:12	9° 24,42' S	110° 29,97' E	1140	E 5	358,6	4,7	Magnetometer	MAGN	Magnetometer an Deck	
SO179/018-1	22.09.2004	11:21	9° 23,41' S	110° 30,00' E	1198	E 8	9,4	11,7	Magnetometer	MAGN	Magnetometer zu Wasser	
SO179/018-1	22.09.2004	15:31	8° 29,90' S	110° 30,36' E	554	NE 12	85,2	10,6	Magnetometer	MAGN	Kursänderung	rwK 090 d:40 nm
SO179/018-1	22.09.2004	16:33	8° 30,02' S	110° 41,18' E	408	NNE 9	81,3	3,7	Magnetometer	MAGN	Magnetometer an Deck	
SO179/018-1	22.09.2004	19:00	8° 30,03' S	111° 9,82' E	348	NNE 13	87,1	11,6	Magnetometer	MAGN	Kursänderung	rwk: 180', d: 5nm
SO179/018-1	22.09.2004	19:25	8° 34,96' S	111° 9,97' E	477	NW 12	194,1	10,7	Magnetometer	MAGN	Kursänderung	rwk: 270', d: 19,8nm
SO179/018-1	22.09.2004	20:56	8° 34,99' S	110° 50,05' E	609	WSW 3	273,5	13,2	Magnetometer	MAGN	Kursänderung	rwk: 000', d: 10nm
SO179/018-1	22.09.2004	21:44	8° 25,04' S	110° 50,01' E	283	ENE 8	8	12,3	Magnetometer	MAGN	Kursänderung	rwk: 90°, d: 20 nm
SO179/018-1	22.09.2004	23:10	8° 24,98' S	111° 6,60' E	256	NNE 11	91,3	12,2	Magnetometer	MAGN	Ende Station	
SO179/019-1	23.09.2004	00:48	8° 44,48' S	111° 2,09' E	1024	WNW 10	192,3	4,8	Profil	PR	Stationsbeginn	
SO179/019-1	23.09.2004	00:54	8° 44,82' S	111° 2,03' E	1051	WNW 10	195,5	3,2	Profil	PR	1. Airgun zu Wasser	
SO179/019-1	23.09.2004	00:57	8° 45,03' S	111° 1,99' E	1058	W 9	188,8	4,9	Profil	PR	Streamer zu Wasser	
SO179/019-1	23.09.2004	01:00	8° 45,30' S	111° 1,97' E	1069	WNW 10	183	6,1	Profil	PR	Beginn Profil	rwk: 180°, d: 2,5 nm
SO179/019-1	23.09.2004	01:25	8° 47,46' S	111° 1,97' E	1167	WNW 9	177,1	4,8	Profil	PR	Ende Profil	
SO179/019-1	23.09.2004	01:36	8° 47,97' S	111° 1,88' E	1199	WNW 8	183,5	1,8	Profil	PR	1.Airgun an Deck	
SO179/019-1	23.09.2004	01:39	8° 48,04' S	111° 1,85' E	1204	WNW 8	205,7	2,2	Profil	PR	Streamer an Deck	
SO179/019-1	23.09.2004	01:40	8° 48,06' S	111° 1,83' E	1204	W 8	217,9	1	Profil	PR	OBH ausgelöst	OBH 13
SO179/019-1	23.09.2004	02:12	8° 46,31' S	111° 1,58' E	1147	NW 8	172,2	1,1	Profil	PR	OBH an Deck	OBH 13
SO179/019-1	23.09.2004	02:13	8° 46,33' S	111° 1,58' E	1147	NW 8	144,5	0,4	Profil	PR	Stationsende	
SO179/020-1	23.09.2004	04:26	8° 21,02' S	110° 51,12' E	203	ENE 5	294,9	9,2	OBS/OBH	OBS/OBH	Beginn Station	d: 191 sm
SO179/020-1	23.09.2004	04:28	8° 21,03' S	110° 50,90' E	204	SW 4	254,8	4,1	OBS/OBH	OBS/OBH	OBH zu Wasser	OBH 22
SO179/020-1	23.09.2004	04:57	8° 24,95' S	110° 50,18' E	279	WNW 10	194,5	3,6	OBS/OBH	OBS/OBH	OBH zu Wasser	OBH 23
SO179/020-1	23.09.2004	05:28	8° 29,95' S	110° 49,33' E	427	NW 10	191,7	3	OBS/OBH	OBS/OBH	OBH zu Wasser	OBH 24
SO179/020-1	23.09.2004	06:02	8° 34,92' S	110° 48,42' E	539	WNW 10	199,5	3,3	OBS/OBH	OBS/OBH	OBH zu Wasser	OBH 25
SO179/020-1	23.09.2004	06:37	8° 39,95' S	110° 47,48' E	955	NW 9	196,2	2,2	OBS/OBH	OBS/OBH	OBH zu Wasser	OBH 26
SO179/020-1	23.09.2004	07:38	8° 50,03' S	110° 45,80' E	1776	NW 7	155,1	0,7	OBS/OBH	OBS/OBH	OBH zu Wasser	OBH 27

Station	Datum	Zeit	PositionLat	PositionLon	Tiefe [m]	Windstärke [m/s]	Kurs [°]	v [kn]	Gerät	Gerätekürzel	Aktion	Bemerkung
SO179/020-1	23.09.2004	08:14	8° 55,01' S	110° 44,87' E	2024	WNW 10	204	2,7	OBS/OBH	OBS/OBH	OBH zu Wasser	OBH 28
SO179/020-1	23.09.2004	09:31	9° 7,97' S	110° 42,53' E	3112	NNW 9	175,5	0,6	OBS/OBH	OBS/OBH	OBS zu Wasser	OBS 29
SO179/020-1	23.09.2004	10:28	9° 15,01' S	110° 41,26' E	2567	WNW 10	188,4	2,6	OBS/OBH	OBS/OBH	OBH zu Wasser	OBH 30
SO179/020-1	23.09.2004	11:11	9° 21,99' S	110° 40,03' E	1805	NW 9	182,9	2	OBS/OBH	OBS/OBH	OBH zu Wasser	OBH 31
SO179/020-1	23.09.2004	12:29	9° 34,98' S	110° 37,64' E	612	NNW 9	169,7	2,1	OBS/OBH	OBS/OBH	OBH zu Wasser	OBH 32
SO179/020-1	23.09.2004	13:17	9° 42,00' S	110° 36,41' E	807	WNW 9	207,1	1,1	OBS/OBH	OBS/OBH	OBH zu Wasser	OBH 33
SO179/020-1	23.09.2004	14:42	9° 56,01' S	110° 33,92' E	1936	WNW 9	217,1	1,6	OBS/OBH	OBS/OBH	OBH zu Wasser	OBH 34
SO179/020-1	23.09.2004	15:18	10° 1,00' S	110° 33,03' E	2324	WNW 10	170	1	OBS/OBH	OBS/OBH	OBH zu Wasser	OBH 35
SO179/020-1	23.09.2004	16:04	10° 8,01' S	110° 31,79' E	4250	WNW 9	195,8	1,1	OBS/OBH	OBS/OBH	OBH zu Wasser	OBH 36
SO179/020-1	23.09.2004	17:05	10° 17,07' S	110° 30,14' E	4966	NW 9	185,2	2,2	OBS/OBH	OBS/OBH	OBH zu Wasser	OBH 37
SO179/020-1	23.09.2004	18:05	10° 17,82' S	110° 27,04' E	5038	NE 11	81,3	5,3	OBS/OBH	OBS/OBH	OBH ausgelöst	OBH 37
SO179/020-1	23.09.2004	19:13	10° 16,84' S	110° 30,09' E	7178	WSW 6	319,2	1,4	OBS/OBH	OBS/OBH	OBH an Deck	OBH 37
SO179/020-1	23.09.2004	19:47	10° 11,31' S	110° 31,20' E	5788	ENE 6	27,6	2	OBS/OBH	OBS/OBH	OBH zu Wasser	OBH 37
SO179/020-1	23.09.2004	22:52	10° 39,94' S	110° 25,99' E	5754	NW 6	57,8	0,4	OBS/OBH	OBS/OBH	OBS zu Wasser	OBS 38
SO179/020-1	23.09.2004	23:35	10° 45,98' S	110° 24,96' E	5542	NNW 7	354,9	1,6	OBS/OBH	OBS/OBH	OBS zu Wasser	OBS 39
SO179/020-1	24.09.2004	00:14	10° 51,99' S	110° 23,89' E	5343	WNW 8	200,8	3,1	OBS/OBH	OBS/OBH	OBH zu Wasser	OBH 40
SO179/020-1	24.09.2004	00:52	10° 58,02' S	110° 22,80' E	5216	WNW 8	256,7	0,8	OBS/OBH	OBS/OBH	OBS zu Wasser	OBS 41
SO179/020-1	24.09.2004	00:53	10° 58,02' S	110° 22,79' E	5214	WNW 7	255,2	0,6	OBS/OBH	OBS/OBH	Ende Station	
SO179/021-1	24.09.2004	04:31	11° 29,86' S	110° 17,00' E	4711	NNE 9	345,8	5	Profil	PR	Stationsbeginn	
SO179/021-1	24.09.2004	04:34	11° 29,69' S	110° 16,99' E	4690	ENE 6	356,6	2,5	Profil	PR	Bb Airgun zu Wasser	
SO179/021-1	24.09.2004	04:48	11° 29,02' S	110° 16,93' E	4706	ENE 6	347,8	3,1	Profil	PR	Mittlere Airgun zu Wasser	
SO179/021-1	24.09.2004	04:53	11° 28,74' S	110° 16,95' E	4714	ENE 8	23	3,7	Profil	PR	Stb Airgun zu Wasser	
SO179/021-1	24.09.2004	04:57	11° 28,46' S	110° 17,03' E	4719	ENE 7	25,7	4,2	Profil	PR	Streamer zu Wasser	
SO179/021-1	24.09.2004	06:02	11° 23,67' S	110° 18,17' E	4760	ENE 8	17,7	4,9	Profil	PR	Beginn Profil	rwk: 010°, d: 191 sm
SO179/021-1	24.09.2004	06:19	11° 22,37' S	110° 18,44' E	4781	ENE 6	19,7	4,2	Profil	PR	Magnetometer zu Wasser	
SO179/021-1	25.09.2004	08:12	9° 21,91' S	110° 40,17' E	1820	E 5	350,6	4,3	Profil	PR	Stb Airgun an De	Schwimmkörper verloren
SO179/021-1	25.09.2004	09:22	9° 16,66' S	110° 41,00' E	2421	E 7	13,8	4,3	Profil	PR	Stb Airgun zu Wasser	

Station	Datum	Zeit	PositionLat	PositionLon	Tiefe [m]	Windstärke [m/s]	Kurs [°]	v [kn]	Gerät	Gerätekürzel	Aktion	Bemerkung
SO179/021-1	25.09.2004	10:01	9° 13,85' S	110° 41,48' E	2702	E 7	8,7	4,4	Profil	PR	Stb Airgun an De	Schwimmkörper verloren
SO179/021-1	25.09.2004	11:56	9° 5,43' S	110° 42,99' E	3179	E 4	9,6	4,3	Profil	PR	Stb Airgun zu Wa	mit Yoko Ono-Fender
SO179/021-1	25.09.2004	12:06	9° 4,74' S	110° 43,12' E	3183	E 5	5,3	4,3	Profil	PR	Stb Airgun an Deck	
SO179/021-1	25.09.2004	12:33	9° 2,87' S	110° 43,45' E	3190	E 4	8	4,1	Profil	PR	Stb Airgun zu Wasser	
SO179/021-1	25.09.2004	23:07	8° 17,29' S	110° 51,58' E	143	ENE 5	8	5,1	Profil	PR	Magnetometer an Deck	
SO179/021-1	25.09.2004	23:15	8° 16,74' S	110° 51,66' E	134	NE 5	3,8	2,8	Profil	PR	Mittlere Airgun an Deck	
SO179/021-1	25.09.2004	23:41	8° 15,47' S	110° 50,97' E	109	SSW 3	276	4,6	Profil	PR	Ende Profil	
SO179/021-1	25.09.2004	23:49	8° 15,44' S	110° 50,51' E	114	SSW 4	273,1	3,1	Profil	PR	Bb airgun an Deck	
SO179/021-1	25.09.2004	23:59	8° 15,42' S	110° 50,06' E	112	SSW 5	255,1	2,4	Profil	PR	Stb Airgun an Deck	
SO179/021-1	26.09.2004	00:05	8° 15,43' S	110° 49,79' E	113	SSW 5	258,8	3,1	Profil	PR	Streamer an Deck	
SO179/021-1	26.09.2004	00:06	8° 15,43' S	110° 49,74' E	113	SSW 5	264,7	3,2	Profil	PR	Stationsende	
SO179/022-1	26.09.2004	00:40	8° 20,73' S	110° 50,55' E	200	NW 9	122,3	2,4	OBS/OBH	OBS/OBH	Beginn Station	
SO179/022-1	26.09.2004	00:41	8° 20,75' S	110° 50,57' E	201	NW 8	155,6	2	OBS/OBH	OBS/OBH	OBH ausgelöst	OBH 22
SO179/022-1	26.09.2004	00:52	8° 20,77' S	110° 50,64' E	201	N 6	172,9	1	OBS/OBH	OBS/OBH	OBH gesichtet	OBH 22
SO179/022-1	26.09.2004	00:58	8° 20,89' S	110° 50,69' E	202	NNW 7	308,6	0,2	OBS/OBH	OBS/OBH	OBH an Deck	OBH 22
SO179/022-1	26.09.2004	01:25	8° 24,69' S	110° 49,90' E	275	WNW 10	176,8	4,8	OBS/OBH	OBS/OBH	OBH ausgelöst	OBH 23
SO179/022-1	26.09.2004	01:29	8° 24,81' S	110° 49,95' E	277	N 8	346,9	1,4	OBS/OBH	OBS/OBH	OBH gesichtet	OBH 23
SO179/022-1	26.09.2004	01:40	8° 25,00' S	110° 50,03' E	282	NW 6	243,5	1,3	OBS/OBH	OBS/OBH	OBH an Deck	OBH 23
SO179/022-1	26.09.2004	02:10	8° 29,71' S	110° 49,01' E	413	WNW 8	141,1	6,7	OBS/OBH	OBS/OBH	OBH ausgelöst	OBH 24
SO179/022-1	26.09.2004	02:17	8° 29,99' S	110° 49,26' E	428	NW 7	352,9	1,5	OBS/OBH	OBS/OBH	OBH gesichtet	OBH 24
SO179/022-1	26.09.2004	02:24	8° 29,99' S	110° 49,29' E	429	NNW 7	216,1	1,1	OBS/OBH	OBS/OBH	OBH an Deck	OBH 24
SO179/022-1	26.09.2004	02:56	8° 34,87' S	110° 48,25' E	535	NNW 8	125,4	2,1	OBS/OBH	OBS/OBH	OBH ausgelöst	OBH 25
SO179/022-1	26.09.2004	03:02	8° 34,95' S	110° 48,29' E	540	N 7	143,3	1,1	OBS/OBH	OBS/OBH	OBH gesichtet	OBH 25
SO179/022-1	26.09.2004	03:11	8° 34,96' S	110° 48,32' E	541	N 7	231,6	1,2	OBS/OBH	OBS/OBH	OBH an Deck	OBH 25
SO179/022-1	26.09.2004	03:35	8° 38,67' S	110° 47,23' E	857	WNW 8	206,8	4,8	OBS/OBH	OBS/OBH	OBH ausgelöst	OBH 26
SO179/022-1	26.09.2004	03:44	8° 39,52' S	110° 47,22' E	908	NW 8	167,8	5,1	OBS/OBH	OBS/OBH	OBH gesichtet	OBH 26
SO179/022-1	2` 09.2004	03:54	8° 39,98' S	110° 47,39' E	953	NW 6	254,7	0,9	OBS/OBH	OBS/OBH	OBH an Deck	OBH 26

Station	Datum	Zeit	PositionLat	PositionLon	Tiefe [m]	Windstärke [m/s]	Kurs [°]	v [kn]	Gerät	Gerätekürzel	Aktion	Bemerkung
SO179/022-1	26.09.2004	04:38	8° 48,12' S	110° 45,53' E	1498	WNW 9	193,9	5,2	OBS/OBH	OBS/OBH	OBH ausgelöst	OBH 27
SO179/022-1	26.09.2004	05:04	8° 49,54' S	110° 45,53' E	1667	N 8	153,7	0,8	OBS/OBH	OBS/OBH	OBH gesichtet	OBH 27
SO179/022-1	26.09.2004	05:15	8° 50,04' S	110° 45,81' E	1774	W 9	232,2	1,3	OBS/OBH	OBS/OBH	OBH an Deck	OBH 27
SO179/022-1	26.09.2004	05:20	8° 50,06' S	110° 45,72' E	1765	W 8	268,7	1,4	OBS/OBH	OBS/OBH	OBH ausgelöst	OBH 28
SO179/022-1	26.09.2004	05:52	8° 54,86' S	110° 44,58' E	2026	WNW 11	122,4	3,2	OBS/OBH	OBS/OBH	OBH gesichtet	OBH 28
SO179/022-1	26.09.2004	05:59	8° 54,98' S	110° 44,88' E	2025	N 10	169,4	0,8	OBS/OBH	OBS/OBH	OBH an Deck	OBH 28
SO179/022-1	26.09.2004	06:31	9° 0,08' S	110° 46,33' E	2896	NW 10	159,8	5,3	OBS/OBH	OBS/OBH	OBH ausgelöst	OBH 11
SO179/022-1	26.09.2004	07:12	9° 3,48' S	110° 47,21' E	6830	NNW 7	41,1	0,8	OBS/OBH	OBS/OBH	OBH gesichtet	OBH 11
SO179/022-1	26.09.2004	07:21	9° 3,60' S	110° 47,48' E	6838	N 8	181,8	1	OBS/OBH	OBS/OBH	OBH an Deck	OBH 11
SO179/022-1	26.09.2004	07:27	9° 3,62' S	110° 47,44' E	6836	WNW 8	281,7	1	OBS/OBH	OBS/OBH	OBS ausgelöst	OBS 29
SO179/022-1	26.09.2004	08:12	9° 7,94' S	110° 42,34' E	3107	WNW 8	164	1,1	OBS/OBH	OBS/OBH	OBS gesichtet	OBS 29
SO179/022-1	26.09.2004	08:21	9° 8,02' S	110° 42,73' E	3115	NNW 8	158,2	0,8	OBS/OBH	OBS/OBH	OBS an Deck	OBS 29
SO179/022-1	26.09.2004	08:27	9° 8,03' S	110° 42,71' E	3114	WNW 8	334,7	0,4	OBS/OBH	OBS/OBH	OBH ausgelöst	OBH 30
SO179/022-1	26.09.2004	09:42	9° 14,93' S	110° 41,17' E	2580	NW 7	164,1	0,8	OBS/OBH	OBS/OBH	OBH gesichtet	OBH 30
SO179/022-1	26.09.2004	09:59	9° 15,00' S	110° 41,53' E	2587	W 8	276,2	0,1	OBS/OBH	OBS/OBH	OBH an Deck	OBH 30
SO179/022-1	26.09.2004	10:22	9° 18,23' S	110° 40,50' E	2335	WNW 9	195	4,2	OBS/OBH	OBS/OBH	OBH ausgelöst	OBH 31
SO179/022-1	26.09.2004	10:47	9° 21,78' S	110° 39,79' E	1795	WNW 9	200,2	3	OBS/OBH	OBS/OBH	OBH gesichtet	OBH 31
SO179/022-1	26.09.2004	10:58	9° 22,01' S	110° 40,13' E	1814	N 8	97,5	1,4	OBS/OBH	OBS/OBH	OBH an Deck	OBH 31
SO179/022-1	26.09.2004	11:48	9° 28,37' S	110° 41,43' E	1051	N 10	131,1	1,4	OBS/OBH	OBS/OBH	OBS ausgelöst	OBS 7
SO179/022-1	26.09.2004	12:03	9° 29,79' S	110° 42,58' E	1052	N 14	144,8	11,1	OBS/OBH	OBS/OBH	OBS gesichtet	OBS 7
SO179/022-1	26.09.2004	12:16	9° 30,62' S	110° 43,23' E	986	NW 9	238,3	1,4	OBS/OBH	OBS/OBH	OBS an Deck	OBS 7
SO179/022-1	26.09.2004	12:45	9° 33,29' S	110° 39,87' E	702	W 9	229	2,3	OBS/OBH	OBS/OBH	OBH ausgelöst	OBH 32
SO179/022-1	26.09.2004	12:54	9° 34,00' S	110° 38,91' E	720	W 9	234,3	11,6	OBS/OBH	OBS/OBH	OBH gesichtet	OBH 32
SO179/022-1	26.09.2004	13:11	9° 34,91' S	110° 37,50' E	614	W 8	284,8	1,5	OBS/OBH	OBS/OBH	OBH an Deck	OBH 32
SO179/022-1	26.09.2004	13:43	9° 39,85' S	110° 36,28' E	695	WNW 10	193	4,6	OBS/OBH	OBS/OBH	OBH ausgelöst	OBH 33
SO179/022-1	26.09.2004	13:54	9° 41,01' S	110° 36,07' E	763	WNW 11	187,9	6	OBS/OBH	OBS/OBH	OBH gesichtet	OBH 33
SO179/022-1	26.09.2004	14:13	9° 41,88' S	110° 36,30' E	791	NNW 8	355,6	0,5	OBS/OBH	OBS/OBH	OBH an Deck	OBH 23

Station	Datum	Zeit	PositionLat	PositionLon	Tiefe [m]	Windstärke [m/s]	Kurs [°]	v [kn]	Gerät	Gerätekürzel	Aktion	Bemerkung
SO179/022-1	26.09.2004	14:16	9° 41,86' S	110° 36,27' E	785	NNW 8	298,8	1,4	OBS/OBH	OBS/OBH	Ende Station	
SO179/023-1	26.09.2004	17:02	9° 45,42' S	111° 5,19' E	2673	NNE 9	76,5	4,1	Profil	PR	Stationsbeginn	
SO179/023-1	26.09.2004	17:08	9° 45,44' S	111° 5,51' E	2676	NNE 9	90,6	2,6	Profil	PR	Stb Airgun zu Wasser	
SO179/023-1	26.09.2004	17:13	9° 45,45' S	111° 5,75' E	2673	NNE 9	96,9	2,3	Profil	PR	Streamer zu Wasser	
SO179/023-1	26.09.2004	17:18	9° 45,49' S	111° 6,00' E	2671	NNE 9	105,8	3,5	Profil	PR	Beginn Profil	Profil 17, rwk: 090', d: 3,2 nm
SO179/023-1	26.09.2004	18:04	9° 45,49' S	111° 9,55' E	2887	NNE 9	98,6	4,1	Profil	PR	Ende Profil	
SO179/023-1	26.09.2004	18:05	9° 45,49' S	111° 9,62' E	2885	NNE 9	109,7	4,9	Profil	PR	OBH ausgelöst	OBH 05
SO179/023-1	26.09.2004	18:13	9° 45,49' S	111° 10,02' E	2910	NNE 8	62,3	2,6	Profil	PR	Stb Airgun an Deck	
SO179/023-1	26.09.2004	18:20	9° 45,48' S	111° 10,28' E	2912	NNE 8	109,5	2,4	Profil	PR	Streamer an Deck	
SO179/023-1	26.09.2004	18:49	9° 45,97' S	111° 7,96' E	2805	SW 8	222,9	1,4	Profil	PR	OBH an Deck	OBH 05
SO179/023-1	26.09.2004	18:50	9° 45,98' S	111° 7,93' E	2803	SW 8	241,5	1,5	Profil	PR	Stationsende	
Transit												Magnetometer, d = 33 sm
SO179/024-1	26.09.2004	21:38	9° 53,93' S	110° 47,45' E	3439	ESE 5	334,2	4,8	OBS/OBH	OBS/OBH	Beginn Station	
SO179/024-1	26.09.2004	21:39	9° 53,86' S	110° 47,41' E	3440	ESE 5	338,5	4,1	OBS/OBH	OBS/OBH	OBH ausgelöst	OBH 4
SO179/024-1	26.09.2004	22:13	9° 51,08' S	110° 45,82' E	0	NNE 7	114,3	2,2	OBS/OBH	OBS/OBH	OBH gesichtet	OBH 4
SO179/024-1	26.09.2004	22:24	9° 51,39' S	110° 46,17' E	2938	NW 7	168,1	0,9	OBS/OBH	OBS/OBH	OBH an Deck	OBH 4
SO179/024-1	26.09.2004	23:19	9° 54,94' S	110° 36,54' E	2182	SSW 4	233,7	4,4	OBS/OBH	OBS/OBH	OBH ausgelöst	OBH 34
SO179/024-1	26.09.2004	23:37	9° 55,61' S	110° 34,21' E	0	SW 5	251,1	5,9	OBS/OBH	OBS/OBH	OBH gesichtet	OBH 34
SO179/024-1	26.09.2004	23:48	9° 56,03' S	110° 33,99' E	0	NW 7	234,8	1,2	OBS/OBH	OBS/OBH	OBH an Deck	OBH 34
SO179/024-1	26.09.2004	23:50	9° 56,05' S	110° 33,98' E	2877	NW 6	247,3	1,7	OBS/OBH	OBS/OBH	OBH ausgelöst	OBH 35
SO179/024-1	27.09.2004	00:16	10° 0,35' S	110° 33,10' E	0	WNW 9	196,4	7,5	OBS/OBH	OBS/OBH	OBH gesichtet	OBH 35
SO179/024-1	27.09.2004	00:19	10° 0,60' S	110° 33,04' E	0	W 8	193,6	4,2	OBS/OBH	OBS/OBH	OBH ausgelöst	OBH 36, ohne Antwort
SO179/024-1	27.09.2004	00:29	10° 0,98' S	110° 33,13' E	0	NW 7	177,5	1,3	OBS/OBH	OBS/OBH	OBH an Deck	OBH 35
SO179/024-1	27.09.2004	01:02	10° 5,48' S	110° 32,22' E	0	W 8	181,8	3,6	OBS/OBH	OBS/OBH	OBH ausgelöst	OBH 36
SO179/024-1	27.09.2004	01:37	10° 7,74' S	110° 31,59' E	0	NW 6	17,5	0,8	OBS/OBH	OBS/OBH	OBH ausgelöst	OBH 37
SO179/024-1	27.09.2004	01:55	10° 7,74' S	110° 31,63' E	0	NNW 7	79,5	2,2	OBS/OBH	OBS/OBH	OBH gesichtet	OBH 36
SO179/024-1	27.09.2004	02:06	10° 8,01' S	110° 32,03' E	0	NW 7	278,3	0,4	OBS/OBH	OBS/OBH	OBH an Deck	OBH 36

Station	Datum	Zeit	PositionLat	PositionLon	Tiefe [m]	Windstärke [m/s]	Kurs [°]	v [kn]	Gerät	Gerätekürzel	Aktion	Bemerkung
SO179/024-1	27.09.2004	02:56	10° 11,26' S	110° 31,13' E	0	N 7	109,8	1,8	OBS/OBH	OBS/OBH	OBH gesichtet	OBH 37
SO179/024-1	27.09.2004	03:05	10° 11,33' S	110° 31,36' E	0	N 7	32,8	0,6	OBS/OBH	OBS/OBH	OBH an Deck	OBH 37
SO179/024-1	27.09.2004	03:06	10° 11,33' S	110° 31,35' E	0	NNW 6	236,8	1,1	OBS/OBH	OBS/OBH	Ende Station	
SO179/025-1	27.09.2004	03:06	10° 11,33' S	110° 31,35' E	0	NNW 6	236,8	1,1	Magnetometer	MAGN	Beginn Station	
SO179/025-1	27.09.2004	03:15	10° 11,46' S	110° 31,81' E	5681	N 8	108,4	7,3	Magnetometer	MAGN	Magnetometer zu	rwk: 105°, d : 14 sm
SO179/025-1	27.09.2004	04:22	10° 15,35' S	110° 44,93' E	4747	NNW 12	174,3	12,1	Magnetometer	MAGN	Kursänderung	rwk: 180°, d: 40 sm
SO179/025-1	27.09.2004	07:27	10° 54,54' S	110° 44,98' E	5107	NW 9	183,5	12,6	Magnetometer	MAGN	Kursänderung	rwk: 262°, d: 22 sm
SO179/025-1	27.09.2004	09:10	10° 57,52' S	110° 24,26' E	5034	SSE 3	271,5	6	Magnetometer	MAGN	Magnetometer an Deck	
SO179/025-1	27.09.2004	09:10	10° 57,52' S	110° 24,26' E	5034	SSE 3	271,5	6	Magnetometer	MAGN	Ende Station	
SO179/026-1	27.09.2004	09:10	10° 57,52' S	110° 24,26' E	5034	SSE 3	271,5	6	OBS/OBH	OBS/OBH	Beginn Station	
SO179/026-1	27.09.2004	09:10	10° 57,52' S	110° 24,26' E	5034	SSE 3	271,5	6	OBS/OBH	OBS/OBH	OBS ausgelöst	OBS 41
SO179/026-1	27.09.2004	09:25	10° 56,05' S	110° 23,50' E	5035	E 6	335	4,8	OBS/OBH	OBS/OBH	OBH ausgelöst	OBH 40 (vermißt !)
SO179/026-1	27.09.2004	10:18	10° 57,93' S	110° 22,65' E	5034	NNE 7	13,4	0,9	OBS/OBH	OBS/OBH	OBS gesichtet	OBS 41
SO179/026-1	27.09.2004	10:30	10° 58,02' S	110° 22,52' E	5036	NW 7	187,8	0,2	OBS/OBH	OBS/OBH	OBS an Deck	OBS 41
SO179/026-1	27.09.2004	11:15	10° 51,32' S	110° 24,10' E	4436	N 8	62,8	1,9	OBS/OBH	OBS/OBH	OBS ausgelöst	OBS 39
SO179/026-1	27.09.2004	12:53	10° 48,91' S	110° 23,97' E	0	ENE 8	4,8	13,1	OBS/OBH	OBS/OBH	OBS gesichtet	OBS 39
SO179/026-1	27.09.2004	13:16	10° 46,16' S	110° 24,35' E	0	WNW 7	243,1	1,1	OBS/OBH	OBS/OBH	OBS an Deck	OBS 39
SO179/026-1	27.09.2004	13:20	10° 46,17' S	110° 24,28' E	0	NW 6	303,1	0,6	OBS/OBH	OBS/OBH	OBS ausgelöst	OBS 38
SO179/026-1	27.09.2004	14:44	10° 39,70' S	110° 25,79' E	0	NNW 7	344,9	0,4	OBS/OBH	OBS/OBH	OBS gesichtet	OBS 38
SO179/026-1	27.09.2004	14:58	10° 39,91' S	110° 25,82' E	5748	NW 7	240,1	0,9	OBS/OBH	OBS/OBH	OBS an Deck	OBS 38
SO179/026-1	27.09.2004	14:58	10° 39,91' S	110° 25,82' E	5748	NW 7	240,1	0,9	OBS/OBH	OBS/OBH	Ende Station	
Transit												Magnetometer, d = 49 sm
SO179/027-1	27.09.2004	18:50	10° 39,97' S	109° 36,94' E	5830	SSW 4	274,2	4,5	OBS/OBH	OBS/OBH	Beginn Station	
SO179/027-1	27.09.2004	19:00	10° 39,99' S	109° 36,17' E	5875	SSW 6	272,5	0,6	OBS/OBH	OBS/OBH	OBS zu Wasser	OBS 45
SO179/027-1	27.09.2004	19:43	10° 45,93' S	109° 35,65' E	5722	WNW 8	343,1	0,8	OBS/OBH	OBS/OBH	OBS zu Wasser	OBS 44
SO179/027-1	27.09.2004	20:25	10° 52,00' S	109° 35,14' E	5668	WNW 8	116	1	OBS/OBH	OBS/OBH	OBH zu Wasser	OBH 43
SO179/027-1	27.09.2004	21:11	10° 57,83' S	109° 34,58' E	5611	WNW 8	268,1	1	OBS/OBH	OBS/OBH	OBS zu Wasser	OBS 42

Station	Datum	Zeit	PositionLat	PositionLon	Tiefe [m]	Windstärke [m/s]	Kurs [°]	v [kn]	Gerät	Gerätekürzel	Aktion	Bemerkung
SO179/027-1	27.09.2004	21:11	10° 57,83' S	109° 34,58' E	5611	WNW 8	268,1	1	OBS/OBH	OBS/OBH	Ende Station	
Suchprofile												suche nach OBH 40, d = 43 sm
Transit												Magnetometer, d = 52 sm
SO179/028-1	28.09.2004	09:00	10° 9,94' S	109° 38,85' E	5971	ESE 6	341,9	3,2	OBS/OBH	OBS/OBH	Beginn Station	
SO179/028-1	28.09.2004	09:09	10° 9,46' S	109° 38,88' E	5891	ENE 6	4,3	2,4	OBS/OBH	OBS/OBH	OBH zu Wasser	OBH 46
SO179/028-1	28.09.2004	09:43	10° 2,93' S	109° 39,47' E	4949	ENE 8	10,2	2	OBS/OBH	OBS/OBH	OBH zu Wasser	OBH 47
SO179/028-1	28.09.2004	10:20	9° 55,83' S	109° 40,08' E	3838	ENE 8	6,1	2,2	OBS/OBH	OBS/OBH	OBH zu Wasser	
SO179/028-1	28.09.2004	10:57	9° 48,79' S	109° 40,68' E	3110	E 7	2	3,6	OBS/OBH	OBS/OBH	OBH zu Wasser	OBH 49
SO179/028-1	28.09.2004	11:39	9° 41,75' S	109° 41,33' E	2246	E 6	3,6	3	OBS/OBH	OBS/OBH	OBH zu Wasser	OBH 50
SO179/028-1	28.09.2004	12:20	9° 34,50' S	109° 41,97' E	1666	E 5	354,6	3,2	OBS/OBH	OBS/OBH	OBH zu Wasser	OBH 51
SO179/028-1	28.09.2004	13:10	9° 27,42' S	109° 42,59' E	1559	ENE 9	38,4	2,9	OBS/OBH	OBS/OBH	OBH zu Wasser	OBH 52
SO179/028-1	28.09.2004	13:49	9° 20,36' S	109° 43,23' E	2758	E 6	21,2	3,5	OBS/OBH	OBS/OBH	OBH zu Wasser	OBH 53
SO179/028-1	28.09.2004	14:27	9° 13,28' S	109° 43,82' E	3139	E 7	14,3	3,5	OBS/OBH	OBS/OBH	OBH zu Wasser	OBH 54
SO179/028-1	28.09.2004	15:06	9° 6,09' S	109° 44,43' E	3210	E 7	340,4	1,6	OBS/OBH	OBS/OBH	OBH zu Wasser	OBH 55
SO179/028-1	28.09.2004	15:45	8° 59,02' S	109° 45,06' E	3269	E 8	323,9	1,4	OBS/OBH	OBS/OBH	OBS zu Wasser	OBS 56
SO179/028-1	28.09.2004	16:28	8° 51,90' S	109° 45,72' E	3304	ENE 8	317,8	1,1	OBS/OBH	OBS/OBH	OBS zu Wasser	OBS 57
SO179/028-1	28.09.2004	17:07	8° 44,80' S	109° 46,34' E	3235	E 5	14,8	2,3	OBS/OBH	OBS/OBH	OBH zu Wasser	OBH 58
SO179/028-1	28.09.2004	17:47	8° 37,73' S	109° 46,95' E	2413	E 6	12,2	2,6	OBS/OBH	OBS/OBH	OBH zu Wasser	OBH 59
SO179/028-1	28.09.2004	18:27	8° 30,68' S	109° 47,57' E	1597	E 6	354	3,5	OBS/OBH	OBS/OBH	OBH zu Wasser	OBH 60
SO179/028-1	28.09.2004	19:07	8° 23,61' S	109° 48,18' E	474	E 8	16,9	2,5	OBS/OBH	OBS/OBH	OBH zu Wasser	OBH 61
SO179/028-1	28.09.2004	19:46	8° 16,41' S	109° 48,81' E	630	ENE 6	3	2,8	OBS/OBH	OBS/OBH	OBH zu Wasser	OBH 62
SO179/028-1	28.09.2004	20:25	8° 9,48' S	109° 49,41' E	591	ENE 7	6,8	3	OBS/OBH	OBS/OBH	OBH zu Wasser	OBH 63
SO179/028-1	28.09.2004	21:08	8° 2,24' S	109° 50,06' E	284	E 3	1,8	3	OBS/OBH	OBS/OBH	OBH zu Wasser	OBH 64
SO179/028-1	28.09.2004	21:08	8° 2,24' S	109° 50,06' E	284	E 3	1,8	3	OBS/OBH	OBS/OBH	Ende Station	
SO179/029-1	28.09.2004	21:45	7° 55,31' S	109° 48,27' E	59	NNE 6	358,7	8,7	Profil	PR	Stationsbeginn	Profil 18
SO179/029-1	28.09.2004	22:03	7° 54,73' S	109° 48,65' E	55	NNW 3	99,4	2,6	Profil	PR	Bb Airgun zu Wasser	
SO179/029-1	28.09.2004	22:10	7° 54,74' S	109° 48,94' E	54	NNW 3	92,6	2,5	Profil	PR	Stb Airgun zu Wasser	

Station	Datum	Zeit	PositionLat	PositionLon	Tiefe [m]	Windstärke [m/s]	Kurs [°]	v [kn]	Gerät	Gerätekürzel	Aktion	Bemerkung
SO179/029-1	28.09.2004	22:35	7° 54,96' S	109° 50,63' E	56	NNW 5	169,8	4,6	Profil	PR	Beginn Profil	rwk: 185°, d: 206 nm
SO179/029-1	28.09.2004	22:48	7° 55,79' S	109° 50,58' E	63	WSW 3	180,9	3,3	Profil	PR	Mittlere Airgun zu Wasser	
SO179/029-1	28.09.2004	23:05	7° 56,90' S	109° 50,52' E	79	WSW 2	190,6	3,1	Profil	PR	Stb Airgun an Deck	
SO179/029-1	28.09.2004	23:38	7° 59,25' S	109° 50,31' E	172	W 2	188,7	4,3	Profil	PR	Stb Airgun zu Wasser	
SO179/029-1	28.09.2004	23:44	7° 59,74' S	109° 50,24' E	198	WNW 4	186,1	5,4	Profil	PR	Streamer zu Wasser	
SO179/029-1	29.09.2004	00:04	8° 1,40' S	109° 50,14' E	258	W 5	184,3	5	Profil	PR	Magnetometer zu Wasser	
SO179/029-1	29.09.2004	14:19	9° 5,02' S	109° 44,45' E	3214	NW 8	181,4	4,4	Profil	PR	Bb airgun an Deck	
SO179/029-1	29.09.2004	14:53	9° 7,44' S	109° 44,27' E	3211	WNW 10	202,6	2,6	Profil	PR	Bb Airgun zu Wasser	
SO179/029-1	30.09.2004	02:11	9° 59,11' S	109° 39,77' E	4387	NW 9	181,4	3,9	Profil	PR	Bb airgun an Deck	
SO179/029-1	30.09.2004	04:59	10° 11,29' S	109° 38,75' E	6186	NW 9	189,6	2,7	Profil	PR	Stb Airgun an Deck	
SO179/029-1	30.09.2004	06:02	10° 15,32' S	109° 38,27' E	6208	NW 9	213,5	2,2	Profil	PR	Stb Airgun zu Wasser	
SO179/029-1	30.09.2004	10:34	10° 35,95' S	109° 36,51' E	5889	NNW 9	183,9	4,1	Profil	PR	Bb Airgun zu Wasser	
SO179/029-1	30.09.2004	13:50	10° 51,47' S	109° 35,15' E	5670	NW 9	184,4	2,1	Profil	PR	Mittlere Airgun an Deck	
SO179/029-1	30.09.2004	16:38	11° 4,97' S	109° 33,95' E	5412	NNW 9	187	3,9	Profil	PR	Ende Profil	
SO179/029-1	30.09.2004	16:51	11° 5,46' S	109° 33,73' E	5396	NNW 8	208,7	2	Profil	PR	Bb airgun an Deck	
SO179/029-1	30.09.2004	16:59	11° 5,71' S	109° 33,58' E	5397	NNW 8	209,2	2,2	Profil	PR	Stb Airgun an Deck	
SO179/029-1	30.09.2004	16:59	11° 5,71' S	109° 33,58' E	5397	NNW 8	209,2	2,2	Profil	PR	Streamer an Deck	
SO179/029-1	30.09.2004	17:00	11° 5,74' S	109° 33,56' E	5387	NW 8	214,4	2,2	Profil	PR	Stationsende	
SO179/030-1	30.09.2004	17:00	11° 5,74' S	109° 33,56' E	5387	NW 8	214,4	2,2	OBS/OBH	OBS/OBH	Beginn Station	
SO179/030-1	30.09.2004	17:38	11° 0,74' S	109° 33,91' E	0	E 4	351,5	4,6	OBS/OBH	OBS/OBH	OBS ausgelöst	OBS 42
SO179/030-1	30.09.2004	18:28	10° 54,77' S	109° 33,64' E	0	NE 8	57,2	3,5	OBS/OBH	OBS/OBH	OBH ausgelöst	OBH 43
SO179/030-1	30.09.2004	19:11	10° 57,80' S	109° 34,54' E	0	NE 7	344,6	2,2	OBS/OBH	OBS/OBH	OBS gesichtet	OBS 42
SO179/030-1	30.09.2004	19:22	10° 57,60' S	109° 34,09' E	5609	SW 5	280,1	1,8	OBS/OBH	OBS/OBH	OBS an Deck	OBS 42
SO179/030-1	30.09.2004	19:46	10° 53,22' S	109° 34,38' E	5666	NE 7	5,5	13,3	OBS/OBH	OBS/OBH	OBH gesichtet	OBH 43
SO179/030-1	30.09.2004	20:07	10° 49,53' S	109° 35,08' E	0	ENE 6	353,9	4,1	OBS/OBH	OBS/OBH	OBS ausgelöst	OBS 44
SO179/030-1	30.09.2004	20:34	10° 51,61' S	109° 33,94' E	5677	W 6	265,9	1,7	OBS/OBH	OBS/OBH	OBH an Deck	OBH 43
SO179/030-1	30.09.2004	21:35	10° 43,93' S	109° 35,86' E	0	ENE 6	263,2	1,1	OBS/OBH	OBS/OBH	OBS ausgelöst	OBS 45

Station	Datum	Zeit	PositionLat	PositionLon	Tiefe [m]	Windstärke [m/s]	Kurs [°]	v [kn]	Gerät	Gerätekürzel	Aktion	Bemerkung
SO179/030-1	30.09.2004	21:37	10° 43,91' S	109° 35,83' E	0	ENE 6	320,4	1,8	OBS/OBH	OBS/OBH	OBS gesichtet	OBS 44
SO179/030-1	30.09.2004	22:06	10° 45,89' S	109° 35,36' E	0	WNW 7	261,6	0,8	OBS/OBH	OBS/OBH	OBS an Deck	OBS 44
SO179/030-1	30.09.2004	22:58	10° 39,73' S	109° 35,52' E	0	NNE 6	58,7	0,9	OBS/OBH	OBS/OBH	OBS gesichtet	OBS 45
SO179/030-1	30.09.2004	23:12	10° 39,71' S	109° 36,00' E	5888	WSW 6	310,1	1,2	OBS/OBH	OBS/OBH	OBS an Deck	OBS 45
SO179/030-1	30.09.2004	23:12	10° 39,71' S	109° 36,00' E	5888	WSW 6	310,1	1,2	OBS/OBH	OBS/OBH	Ende Station	
Transit												Magnetometer, d = 21 sm
SO179/031-1	01.10.2004	01:47	10° 11,76' S	109° 35,13' E	5982	ENE 9	52,6	4,9	OBS/OBH	OBS/OBH	Beginn Station	
SO179/031-1	01.10.2004	01:58	10° 11,49' S	109° 35,48' E	0	ENE 5	9,3	1,5	OBS/OBH	OBS/OBH	OBH ausgelöst	OBH 46
SO179/031-1	01.10.2004	03:02	10° 7,43' S	109° 39,02' E	0	NW 7	181,6	0,5	OBS/OBH	OBS/OBH	OBH ausgelöst	OBH 47
SO179/031-1	01.10.2004	03:12	10° 8,65' S	109° 38,83' E	0	NNW 11	188,6	11,6	OBS/OBH	OBS/OBH	OBH gesichtet	OBH 46
SO179/031-1	01.10.2004	03:25	10° 9,28' S	109° 39,30' E	0	NNW 7	189,7	0,4	OBS/OBH	OBS/OBH	OBH an Deck	OBH 46
SO179/031-1	01.10.2004	03:57	10° 3,45' S	109° 39,28' E	0	ENE 5	7,4	12,5	OBS/OBH	OBS/OBH	OBH gesichtet	OBH 47
SO179/031-1	01.10.2004	04:05	10° 2,76' S	109° 39,71' E	0	ENE 6	116,1	2,2	OBS/OBH	OBS/OBH	OBH ausgelöst	OBH 48
SO179/031-1	01.10.2004	04:09	10° 2,80' S	109° 39,72' E	0	NNW 7	192,5	0,3	OBS/OBH	OBS/OBH	OBH an Deck	OBH 47
SO179/031-1	01.10.2004	04:49	9° 56,69' S	109° 39,65' E	0	ENE 6	357,4	11,6	OBS/OBH	OBS/OBH	OBH gesichtet	OBH 48
SO179/031-1	01.10.2004	05:01	9° 55,59' S	109° 40,16' E	0	ENE 7	18,1	1,3	OBS/OBH	OBS/OBH	OBH an Deck	OBH 48
SO179/031-1	01.10.2004	05:04	9° 55,54' S	109° 40,20' E	0	ENE 7	43,1	2,8	OBS/OBH	OBS/OBH	OBH ausgelöst	OBH 49
SO179/031-1	01.10.2004	05:40	9° 49,61' S	109° 40,45' E	0	ENE 6	2,6	9,5	OBS/OBH	OBS/OBH	OBH gesichtet	OBH 49
SO179/031-1	01.10.2004	05:58	9° 48,62' S	109° 40,52' E	0	N 7	265,8	1,3	OBS/OBH	OBS/OBH	OBH an Deck	OBH 49
SO179/031-1	01.10.2004	06:25	9° 44,68' S	109° 41,11' E	0	E 5	6,8	4,5	OBS/OBH	OBS/OBH	OBH ausgelöst	OBH 50
SO179/031-1	01.10.2004	06:53	9° 41,54' S	109° 41,21' E	0	N 6	119,3	0,3	OBS/OBH	OBS/OBH	OBH gesichtet	OBH 50
SO179/031-1	01.10.2004	07:01	9° 41,71' S	109° 41,39' E	0	NNW 7	186,8	1,6	OBS/OBH	OBS/OBH	OBH an Deck	OBH 50
SO179/031-1	01.10.2004	07:29	9° 37,00' S	109° 41,73' E	0	E 6	17	3,8	OBS/OBH	OBS/OBH	OBH ausgelöst	OBH 51
SO179/031-1	01.10.2004	07:48	9° 34,21' S	109° 41,93' E	0	NNE 8	153,6	1,8	OBS/OBH	OBS/OBH	OBH gesichtet	OBH 51
SO179/031-1	01.10.2004	07:58	9° 34,41' S	109° 41,99' E	0	N 8	253,1	0,5	OBS/OBH	OBS/OBH	OBH an Deck	OBH 51
SO179/031-1	01.10.2004	08:29	9° 29,41' S	109° 41,76' E	0	E 4	7,6	4,7	OBS/OBH	OBS/OBH	OBH ausgelöst	OBH 52
SO179/031-1	0 .10.2004	08:53	9° 27,17' S	109° 42,48' E	0	N 6	158,9	1,1	OBS/OBH	OBS/OBH	OBH gesichtet	OBH 52

Station	Datum	Zeit	PositionLat	PositionLon	Tiefe [m]	Windstärke [m/s]	Kurs [°]	v [kn]	Gerät	Gerätekürzel	Aktion	Bemerkung
SO179/031-1	01.10.2004	08:59	9° 27,29' S	109° 42,56' E	0	N 8	128	0,3	OBS/OBH	OBS/OBH	OBH an Deck	OBH 52
SO179/031-1	01.10.2004	09:08	9° 27,20' S	109° 42,47' E	0	N 6	315,2	0,9	OBS/OBH	OBS/OBH	OBH ausgelöst	OBH 53
SO179/031-1	01.10.2004	09:50	9° 20,44' S	109° 43,12' E	0	ENE 7	6,2	8,4	OBS/OBH	OBS/OBH	OBH gesichtet	OBH 53
SO179/031-1	01.10.2004	09:59	9° 20,16' S	109° 43,21' E	0	NNW 6	276,8	0,7	OBS/OBH	OBS/OBH	OBH an Deck	OBH 53
SO179/031-1	01.10.2004	10:03	9° 20,14' S	109° 43,18' E	0	N 6	291,6	0,6	OBS/OBH	OBS/OBH	OBH ausgelöst	OBH 54
SO179/031-1	01.10.2004	10:38	9° 14,56' S	109° 43,53' E	0	ENE 6	8,5	12,8	OBS/OBH	OBS/OBH	OBH gesichtet	OBH 54
SO179/031-1	01.10.2004	10:52	9° 13,04' S	109° 43,73' E	0	NW 6	240,3	1,6	OBS/OBH	OBS/OBH	OBH an Deck	OBH 54
SO179/031-1	01.10.2004	10:56	9° 13,01' S	109° 43,68' E	0	WNW 8	300,2	1	OBS/OBH	OBS/OBH	OBH ausgelöst	OBH 55
SO179/031-1	01.10.2004	11:37	9° 6,43' S	109° 43,98' E	0	ENE 7	5,9	12,4	OBS/OBH	OBS/OBH	OBH gesichtet	OBH 55
SO179/031-1	01.10.2004	11:51	9° 5,90' S	109° 44,39' E	0	NW 8	265,1	0,7	OBS/OBH	OBS/OBH	OBH an Deck	OBH 55
SO179/031-1	01.10.2004	12:00	9° 5,78' S	109° 44,26' E	0	W 7	315,2	1,5	OBS/OBH	OBS/OBH	OBS ausgelöst	OBS 56
SO179/031-1	01.10.2004	12:48	8° 58,68' S	109° 44,91' E	0	N 8	70,2	1,5	OBS/OBH	OBS/OBH	OBS gesichtet	OBS 56
SO179/031-1	01.10.2004	13:07	8° 58,81' S	109° 45,13' E	0	NW 6	309,2	1,4	OBS/OBH	OBS/OBH	OBS an Deck	OBS 56
SO179/031-1	01.10.2004	13:15	8° 58,70' S	109° 45,04' E	0	WSW 5	342,6	0,9	OBS/OBH	OBS/OBH	OBS ausgelöst	OBS 57
SO179/031-1	01.10.2004	14:05	8° 51,67' S	109° 45,34' E	0	N 6	339,4	0,9	OBS/OBH	OBS/OBH	OBS gesichtet	OBS 57
SO179/031-1	01.10.2004	14:24	8° 51,84' S	109° 45,80' E	0	NNW 6	217,8	1	OBS/OBH	OBS/OBH	OBS an Deck	OBS 57
SO179/031-1	01.10.2004	14:30	8° 51,82' S	109° 45,73' E	0	NNW 6	316,5	0,9	OBS/OBH	OBS/OBH	OBH ausgelöst	OBH 58
SO179/031-1	01.10.2004	15:10	8° 45,76' S	109° 45,83' E	0	ENE 5	11,9	9,6	OBS/OBH	OBS/OBH	OBH gesichtet	OBH 58
SO179/031-1	01.10.2004	15:34	8° 44,66' S	109° 46,43' E	0	NNW 7	198	0,8	OBS/OBH	OBS/OBH	OBH an Deck	OBH 58
SO179/031-1	01.10.2004	16:30	8° 37,53' S	109° 46,56' E	0	NE 6	353,9	1,1	OBS/OBH	OBS/OBH	OBH ausgelöst	OBH 59
SO179/031-1	01.10.2004	17:06	8° 37,58' S	109° 46,83' E	0	NNW 6	139,5	0,6	OBS/OBH	OBS/OBH	OBH gesichtet	OBH 59
SO179/031-1	01.10.2004	17:14	8° 37,69' S	109° 46,98' E	0	N 6	169,7	0,8	OBS/OBH	OBS/OBH	OBH an Deck	OBH 59
SO179/031-1	01.10.2004	17:54	8° 31,94' S	109° 47,35' E	0	ENE 5	313,5	0,5	OBS/OBH	OBS/OBH	OBH ausgelöst	OBH 60
SO179/031-1	01.10.2004	18:07	8° 30,60' S	109° 47,29' E	1553	ENE 4	356,4	8,6	OBS/OBH	OBS/OBH	OBH gesichtet	OBH 60
SO179/031-1	01.10.2004	18:16	8° 30,67' S	109° 47,49' E	1569	N 5	219,5	0,7	OBS/OBH	OBS/OBH	OBH an Deck	OBH 60
SO179/031-1	01.10.2004	18:55	8° 24,74' S	109° 47,87' E	0	ENE 5	358,5	1,7	OBS/OBH	OBS/OBH	OBH ausgelöst	OBH 61
SO179/031-1	01.10.2004	19:14	8° 23,52' S	109° 48,12' E	455	NW 4	286	1	OBS/OBH	OBS/OBH	OBH gesichtet	OBH 61

Station	Datum	Zeit	PositionLat	PositionLon	Tiefe [m]	Windstärke [m/s]	Kurs [°]	v [kn]	Gerät	Gerätekürzel	Aktion	Bemerkung
SO179/031-1	01.10.2004	19:21	8° 23,57' S	109° 48,11' E	460	NNW 6	71,2	0,5	OBS/OBH	OBS/OBH	OBH an Deck	OBH 61
SO179/031-1	01.10.2004	20:04	8° 16,27' S	109° 48,65' E	642	ENE 4	88,4	2,5	OBS/OBH	OBS/OBH	OBH ausgelöst	OBH 62
SO179/031-1	01.10.2004	20:14	8° 16,35' S	109° 48,75' E	637	N 4	269,5	0,3	OBS/OBH	OBS/OBH	OBH gesichtet	OBH 62
SO179/031-1	01.10.2004	20:19	8° 16,37' S	109° 48,76' E	633	N 4	193,8	0,4	OBS/OBH	OBS/OBH	OBH an Deck	OBH 62
SO179/031-1	01.10.2004	21:00	8° 9,44' S	109° 49,11' E	600	NNE 7	87,3	2,7	OBS/OBH	OBS/OBH	OBH ausgelöst	OBH 63
SO179/031-1	01.10.2004	21:06	8° 9,42' S	109° 49,19' E	594	NNE 4	34,2	0,5	OBS/OBH	OBS/OBH	OBH gesichtet	OBH 63
SO179/031-1	01.10.2004	21:24	8° 9,45' S	109° 49,11' E	596	NW 4	218,2	1,6	OBS/OBH	OBS/OBH	OBH an Deck	OBH 63
SO179/031-1	01.10.2004	22:10	8° 2,20' S	109° 49,24' E	287	N 6	80,7	3,5	OBS/OBH	OBS/OBH	OBH ausgelöst	OBH 64
SO179/031-1	01.10.2004	22:16	8° 2,17' S	109° 49,56' E	283	N 4	94,6	3,8	OBS/OBH	OBS/OBH	OBH gesichtet	
SO179/031-1	01.10.2004	22:27	8° 2,25' S	109° 49,98' E	281	WSW 2	224,9	1,1	OBS/OBH	OBS/OBH	Ende Station	
SO179/031-1	01.10.2004	22:27	8° 2,25' S	109° 49,98' E	281	WSW 2	224,9	1,1	OBS/OBH	OBS/OBH	OBH an Deck	
Transit												Magnetometer, d = 30 sm
SO179/032-1	02.10.2004	01:25	8° 24,98' S	110° 9,82' E	836	N 5	151	2,3	OBS/OBH	OBS/OBH	OBH zu Wasser	OBH 65
SO179/032-1	02.10.2004	02:00	8° 26,58' S	110° 14,84' E	1051	NE 5	91	1,7	OBS/OBH	OBS/OBH	OBH zu Wasser	OBH 66
SO179/032-1	02.10.2004	02:33	8° 28,16' S	110° 19,85' E	797	NE 6	131,8	2,3	OBS/OBH	OBS/OBH	OBH zu Wasser	OBH 67
SO179/032-1	02.10.2004	03:05	8° 29,67' S	110° 24,65' E	726	NNE 6	124,5	2,6	OBS/OBH	OBS/OBH	OBH zu Wasser	OBH 68
SO179/032-1	02.10.2004	03:40	8° 31,35' S	110° 30,05' E	619	NNE 5	120,6	2,4	OBS/OBH	OBS/OBH	OBH zu Wasser	OBH 69
SO179/032-1	02.10.2004	04:13	8° 32,78' S	110° 34,62' E	576	NNE 5	112	0,6	OBS/OBH	OBS/OBH	OBH zu Wasser	OBH 70
SO179/032-1	02.10.2004	04:45	8° 34,24' S	110° 39,22' E	574	NNE 5	92,7	2,1	OBS/OBH	OBS/OBH	OBH zu Wasser	OBH 71
SO179/032-1	02.10.2004	05:20	8° 36,04' S	110° 45,01' E	631	NNE 5	107	2,4	OBS/OBH	OBS/OBH	OBH zu Wasser	OBH 72
SO179/032-1	02.10.2004	05:49	8° 37,38' S	110° 49,32' E	1056	NE 6	109,6	2,5	OBS/OBH	OBS/OBH	OBH zu Wasser	OBH 73
SO179/032-1	02.10.2004	06:22	8° 38,98' S	110° 54,33' E	1594	NE 6	136	2,3	OBS/OBH	OBS/OBH	OBH zu Wasser	OBH 74
SO179/032-1	02.10.2004	06:54	8° 40,51' S	110° 59,24' E	1002	NE 6	96,3	2,7	OBS/OBH	OBS/OBH	OBH zu Wasser	OBH 75
SO179/032-1	02.10.2004	06:55	8° 40,52' S	110° 59,27' E	1003	NE 6	134,4	1,7	OBS/OBH	OBS/OBH	Ende Station	
Transit												Magnetometer, d = 12 sm
SO179/033-1	02.10.2004	08:05	8° 43,69' S	111° 9,13' E	846	NW 5	265,6	5,8	Profil	PR	Stationsbeginn	
SO179/033-1	02.10.2004	08:13	8° 43,56' S	111° 8,57' E	844	WSW 3	285,2	3,7	Profil	PR	Bb Airgun zu Wasser	

Station	Datum	Zeit	PositionLat	PositionLon	Tiefe [m]	Windstärke [m/s]	Kurs [°]	v [kn]	Gerät	Gerätekürzel	Aktion	Bemerkung
SO179/033-1	02.10.2004	08:20	8° 43,43' S	111° 8,13' E	841	WSW 4	282	4,6	Profil	PR	Mittlere Airgun zu Wasser	
SO179/033-1	02.10.2004	08:30	8° 43,20' S	111° 7,47' E	840	WSW 3	292,3	4,5	Profil	PR	Stb Airgun zu Wasser	
SO179/033-1	02.10.2004	08:31	8° 43,18' S	111° 7,39' E	838	WSW 3	295,7	4,9	Profil	PR	Beginn Profil	rwk: 288, d = 100 sm
SO179/033-1	02.10.2004	08:36	8° 43,05' S	111° 6,98' E	837	WSW 3	284	5,6	Profil	PR	Streamer zu Wasser	
SO179/033-1	02.10.2004	08:41	8° 42,95' S	111° 6,56' E	838	WSW 3	291,5	4,9	Profil	PR	Magnetometer zu	L = 750 m
SO179/033-1	03.10.2004	06:00	8° 10,55' S	109° 23,81' E	824	SSW 2	283,2	4,7	Profil	PR	Ende Profil	
SO179/033-1	03.10.2004	06:10	8° 10,38' S	109° 23,14' E	1123	SSW 2	285,4	3,5	Profil	PR	Stb Airgun an Deck	
SO179/033-1	03.10.2004	06:24	8° 10,36' S	109° 22,32' E	813	WSW 3	258,8	3,7	Profil	PR	Mittlere Airgun an Deck	
SO179/033-1	03.10.2004	06:36	8° 10,57' S	109° 21,66' E	677	WSW 3	240,7	3,5	Profil	PR	Bb airgun an Deck	
SO179/033-1	03.10.2004	06:43	8° 10,80' S	109° 21,35' E	716	W 4	233,7	3,2	Profil	PR	Streamer an Deck	
SO179/033-1	03.10.2004	06:43	8° 10,80' S	109° 21,35' E	716	W 4	233,7	3,2	Profil	PR	Stationsende	
Transit												Magnetometer, d = 49
SO179/034-1	03.10.2004	11:00	8° 25,30' S	110° 8,56' E	860	NE 10	72,6	6,6	OBS/OBH	OBS/OBH	Beginn Station	
SO179/034-1	03.10.2004	11:11	8° 25,04' S	110° 9,15' E	0	NE 7	64,4	2,1	OBS/OBH	OBS/OBH	OBH ausgelöst	OBH 65
SO179/034-1	03.10.2004	11:24	8° 24,81' S	110° 9,76' E	0	NE 7	94,4	1,9	OBS/OBH	OBS/OBH	OBH gesichtet	
SO179/034-1	03.10.2004	11:31	8° 24,94' S	110° 9,85' E	0	N 7	200,6	0,3	OBS/OBH	OBS/OBH	OBH an Deck	OBH 65
SO179/034-1	03.10.2004	12:01	8° 26,13' S	110° 13,57' E	0	NNE 11	106,4	7,7	OBS/OBH	OBS/OBH	OBH ausgelöst	OBH 66
SO179/034-1	03.10.2004	12:13	8° 26,39' S	110° 14,52' E	0	NNE 8	100,2	4,1	OBS/OBH	OBS/OBH	OBH gesichtet	
SO179/034-1	03.10.2004	12:24	8° 26,56' S	110° 14,90' E	0	NW 6	187,5	0,7	OBS/OBH	OBS/OBH	OBH an Deck	OBH 66
SO179/034-1	03.10.2004	12:53	8° 27,74' S	110° 18,69' E	0	N 10	97,8	6,7	OBS/OBH	OBS/OBH	OBH ausgelöst	OBH 67
SO179/034-1	03.10.2004	13:04	8° 27,99' S	110° 19,69' E	0	NNE 8	88,2	2,7	OBS/OBH	OBS/OBH	OBH gesichtet	OBH 67
SO179/034-1	03.10.2004	13:17	8° 28,12' S	110° 19,92' E	0	NW 6	265,4	0,2	OBS/OBH	OBS/OBH	OBH an Deck	OBH 67
SO179/034-1	03.10.2004	13:44	8° 29,14' S	110° 23,18' E	0	N 10	105,4	9,4	OBS/OBH	OBS/OBH	OBH ausgelöst	OBH 68
SO179/034-1	03.10.2004	13:53	8° 29,40' S	110° 24,20' E	0	N 8	103,7	6,3	OBS/OBH	OBS/OBH	OBH gesichtet	OBH 68
SO179/034-1	03.10.2004	14:06	8° 29,70' S	110° 24,73' E	0	NW 5	158,1	0,9	OBS/OBH	OBS/OBH	OBH an Deck	OBH 68
SO179/034-1	03.10.2004	14:41	8° 30,66' S	110° 29,21' E	0	N 8	121,8	7,8	OBS/OBH	OBS/OBH	OBH ausgelöst	OBH 69
SO179/034-1	03.10.2004	14:46	8° 31,01' S	110° 29,72' E	0	N 8	120,6	6,5	OBS/OBH	OBS/OBH	OBH gesichtet	OBH 69

Station	Datum	UTC Zeit	PositionLat	PositionLon	Tiefe [m]	Windstärke [m/s]	Kurs [°]	v [kn]	Gerät	Gerätekürzel	Aktion	Bemerkung
SO179/034-1	03.10.2004	14:58	8° 31,33' S	110° 30,17' E	0	NW 5	147,4	0,7	OBS/OBH	OBS/OBH	OBH an Deck	OBH 69
SO179/034-1	03.10.2004	15:25	8° 32,10' S	110° 33,78' E	0	N 10	104,6	7,5	OBS/OBH	OBS/OBH	OBH ausgelöst	OBH 70
SO179/034-1	03.10.2004	15:32	8° 32,27' S	110° 34,37' E	0	N 7	83,3	3,4	OBS/OBH	OBS/OBH	OBH gesichtet	OBH 70
SO179/034-1	03.10.2004	16:35	8° 32,17' S	110° 34,43' E	0	NE 3	228,6	4,1	OBS/OBH	OBS/OBH	OBH an Deck	OBH 70
SO179/034-1	03.10.2004	17:13	8° 33,95' S	110° 38,30' E	0	N 9	108,5	8,7	OBS/OBH	OBS/OBH	OBH ausgelöst	OBH 71
SO179/034-1	03.10.2004	17:22	8° 34,18' S	110° 39,02' E	0	NNW 6	115,8	2,3	OBS/OBH	OBS/OBH	OBH gesichtet	OBH 71
SO179/034-1	03.10.2004	17:31	8° 34,30' S	110° 39,30' E	0	NW 5	195,4	1,2	OBS/OBH	OBS/OBH	OBH an Deck	OBH 71
SO179/034-1	03.10.2004	18:08	8° 35,94' S	110° 43,98' E	0	NNW 8	104,8	8,2	OBS/OBH	OBS/OBH	OBH ausgelöst	OBH 72
SO179/034-1	03.10.2004	18:15	8° 36,00' S	110° 44,76' E	0	NNW 7	104,6	4,7	OBS/OBH	OBS/OBH	OBH gesichtet	OBH 72
SO179/034-1	03.10.2004	18:22	8° 36,07' S	110° 45,06' E	0	NNW 5	157,4	1,5	OBS/OBH	OBS/OBH	OBH an Deck	OBH 72
SO179/034-1	03.10.2004	18:47	8° 37,08' S	110° 48,35' E	0	NNW 8	108,5	9,2	OBS/OBH	OBS/OBH	OBH ausgelöst	OBH 73
SO179/034-1	03.10.2004	18:59	8° 37,37' S	110° 49,34' E	0	NW 5	16,3	1,3	OBS/OBH	OBS/OBH	OBH gesichtet	OBH 73
SO179/034-1	03.10.2004	19:06	8° 37,40' S	110° 49,36' E	0	WNW 5	142,3	0,7	OBS/OBH	OBS/OBH	OBH an Deck	OBH 73
SO179/034-1	03.10.2004	19:31	8° 38,47' S	110° 52,73' E	0	N 8	103,2	9,3	OBS/OBH	OBS/OBH	OBH ausgelöst	OBH 74
SO179/034-1	03.10.2004	19:54	8° 39,01' S	110° 54,35' E	0	NW 4	162,3	0,4	OBS/OBH	OBS/OBH	OBH gesichtet	OBH 74
SO179/034-1	03.10.2004	19:55	8° 39,01' S	110° 54,34' E	0	WNW 4	214,1	1,4	OBS/OBH	OBS/OBH	OBH an Deck	OBH 74
SO179/034-1	03.10.2004	20:25	8° 40,23' S	110° 58,31' E	0	N 9	106,8	8,2	OBS/OBH	OBS/OBH	OBH ausgelöst	OBH 75
SO179/034-1	03.10.2004	20:36	8° 40,49' S	110° 59,10' E	0	N 6	131	3,1	OBS/OBH	OBS/OBH	OBH gesichtet	OBH 75
SO179/034-1	03.10.2004	20:42	8° 40,59' S	110° 59,20' E	0	NW 5	208	1,9	OBS/OBH	OBS/OBH	OBH an Deck	OBH 75
SO179/034-1	03.10.2004	20:42	8° 40,59' S	110° 59,20' E	0	NW 5	208	1,9	OBS/OBH	OBS/OBH	Ende Station	
Magnetometerprofil												d = 743 sm
Ende	**06.10.2004**	**04:03**										**Ende Stationsarbeiten SO 179**

Station SO 179	CTD - ROS	Magnetometer	Streamer	Airgun Bb.	Airgun Mitte	Airgun Stb.	OBH / OBS Auslage	OBH / OBS Aufnehme	W 4 Zeit	Länge W 4	sm / Magnetometer - Prof	sm / Stationsarbeit	sm / EM/PS Vermessung	sm / Seismik - Profil	Bemerkungen
01 (1-1-CTD)	1								3,0	3400					Releasertest
Transit / Anfahrt		1									93				Transit mit Magnetometer
02 (2-1-Profil # 1)		1	1	1	1	1								109,0	
03 (3-1-Profil # 2)			1		1							2		3,0	
04 (4-1-OBS/OBH)							1	2				5			
Transit / Anfahrt		1									24				Transit mit Magnetometer
05 (5-1-Profil # 3)			1			1	1							3,0	
06 (6-1-Profil # 4)			1			1		2				4		3,0	
Transit / Anfahrt		1									56				Transit mit Magnetometer
07 (7-1-Profil # 5)			1			1	1							3,0	
08 (8-1-Profil # 6)			1			1		2				4		3,0	
Transit / Anfahrt		1									14				Transit mit Magnetometer
09 (9-1-Profil # 7)			1			1	1							3,0	
10 (10-1-Profil # 8)			1			1		2				4		3,0	
Transit / Anfahrt		1									54				Transit mit Magnetometer
11 (11-1-Profil # 9)			1			1	1							3,0	
11 (11-1-Profil # 10)			1			1		2				4		3,0	
Transit / Anfahrt		1									44				Transit mit Magnetometer
12 (12-1-Profil # 11)			1			1	1							6,7	
13 (13-1-OBH/S)								2				5			
Transit / Anfahrt		1									29				Transit mit Magnetometer
14 (14-1-Profil # 12)			1			1	1	2						3,0	
Anfahrt													18		
15 (15-1-Profil # 13)			1			1								2,0	
16 (16-1-OBH/S)								1				1			
17 (17-1-Profil # 14)			1			1		1						3,0	
18 (18-1-Magn.)		1									115		76		
19 (19-1-Profil # 15)			1			1		1				2		2,0	

Station SO 179	CTD - ROS	Magnetometer	Streamer	Airgun Bb.	Airgun Mitte	Airgun Stb.	OBH / OBS Auslage	OBH / OBS Aufnehme	W 4 Zeit	Länge W 4	sm / Magnetometer - Prof	sm / Stationsarbeit	sm / EM/PS Vermessung	sm / Seismik - Profil	Bemerkungen
20 OBS/H auslegen							20					210			
21 (21-1-Profil # 16)		1	1	1	1	1		1						191,0	
22 OBH/S aufnehmen								14				95			
23 (23-1-Profil # 17)			1			1								3,0	
Transit / Anfahrt		1									33				Transit mit Magnetometer
24 OBH/S aufnehmen								5				32			
25 (25-1-Magn.)		1									76				
26 OBH/S aufnehmen								3				29			
Transit / Anfahrt		1									49				Transit mit Magnetometer
27 OBH/S auslegen							4					20			
Transit / Anfahrt		1									41				
Suche OBH 40												43			
Transit / Anfahrt		1									52				Transit mit Magnetometer
28 OBH/S auslegen							19					131			
29 (29-1 Profil # 18)		1	1	1	1	1						2		192,0	
30 OBH/S aufnehmen								4				42			
Transit / Anfahrt		1									21				Transit mit Magnetometer
31 OBH/S aufnehmen								19				144			
Transit / Anfahrt		1									30				Transit mit Magnetometer
32 OBH auslegen							11					50			
Transit / Anfahrt		1									12				Transit mit Magnetometer
33 (33-1 Profil # 19)		1	1	1	1	1								128,0	
Transit / Anfahrt		1									49				Transit mit Magnetometer
34 OBH aufnehmen								11				51			
Magnetometerprofil		1									743				
Total:	**1**	**22**	**19**	**4**	**5**	**18**	**61**	**74**	**3**	**3400**	**1535**	**880**	**94**	**666,7**	

maximal gefierte Seillänge SO 179 **3400 m** **0** **0**